Depolymerisation and degradation of olefin and sugar-based polymers

By

Emma Catterson

A thesis submitted to the University of Birmingham for the degree of

DOCTOR OF PHILOSOPHY

School of Chemistry

College of Engineering and Physical Science

University of Birmingham

April 2024

University of Birmingham

Edgbaston Birmingham

B15 2TT

1st supervisor: Prof. Andrew Dove

2nd supervisor: Prof. Rachel O’Reilly

Abstract

The manufacturing of polyolefins has significantly escalated in recent decades thanks to their affordability, durability and vast assortment of chemical and mechanical properties. However, their inherent chemical and thermal stability, owing to their stable all-carbon backbone, presents a major disadvantage, limiting their chemical recyclability. The first section of this thesis focuses on developing a solvent-free and low-temperature chemical recycling strategy for the aerobic oxidation and subsequent depolymerisation of polyolefins. Chapter 1 provides an overview of the current plastic recycling strategies and their shortcomings, biodegradable polymers, circular plastic economies, chemical up-cycling, deep eutectic solvents (DES) and dioxygen oxidations. Chapter 2 explores the synthesis of novel DES containing known oxidative metal centres with a strong focus on their long-term thermal stability. Aerobic oxidation of a model small molecule polyolefin, squalane, was used to determine their oxidation capability before applying them to pristine and post-consumer polyolefins. Chapter 3 is an expansion on Chapter 2 with the added objective of accelerating the rate of polyolefin depolymerisation using organic peroxide radical initiators and molecular oxygen. This chapter investigates the influence of the polymer topology and crystallinity on the rate of depolymerisation.

The second aim of this thesis was to explore the influence of stereoisomerism on the mechanical performance and degradation kinetics of high-performance strong thermoplastics based on renewability soured isohexides. Chapter 4 outlines the thiol-ene “click” polymerisation of isomeric homopolymer polyurethanes as well as their corresponding copolymers and blends. Moreover, their mechanical performance and hydrolytic degradation rates were compared and contrasted.

Acknowledgements

The past three and a half years have been a rollercoaster, to say the least, not to mention starting my PhD and moving amid a global pandemic. I certainly wouldn't have gotten here on my own and I need to thank those that have helped me. Firstly, I want to thank my supervisor Professor Andrew Dove for allowing me the opportunity to pursue my PhD and for his support and guidance over the years. Thank you to Polymateria Ltd. for funding the project. Particular thanks to Dr Christoper Wallis for the constant guidance in the initial stages of the project development and to Dr Gavin Hill for running a silly number of HT-GPC samples for me.

Next, I would like to thank all of the members of the Dove and O'Reilly groups for their constant support. You are all a delight to be around every day and I am lucky to call you all my friends. A particular mention to Dr. Josh Worch, Dr. Natalia Reis, Dr. Arianna Brandolese, Dr Thiago Ouriques Machado, Dr Connor Stubbs and Dr. Ali al Rida Hmayed for all of their help with instruments, proofreading and general scientific advice. Thanks to Rachel, Matt, Ana, Jake and Megan for always being up for a chat and to Ed and Louisa for being the best fume hood partners. I would also like to thank Dan for helping me to fix many broken instruments.

Of course, I also want to express my sincere appreciation to my friends and family. Orla, for moving to Birmingham with me and making this entire process a lot less scary. To my twin brother Paul for always picking up the phone and listening to me stress out and of course to my parents. Mum and Dad, you have always been my biggest supporters and your belief in my abilities has always encouraged me to prove you right, I honestly couldn't have done it without you, and I am thankful for you both. An honourable mention has to be made to my horse Mindy whom I moved from Scotland to be my emotional support animal while also providing me with a countryside escape and despite all of the early morning and late night mucking out it was completely worth it.

Finally, to Oliver for supporting me unconditionally, making me happy every day and of course for cooking me delicious food when I am too busy to eat.

Contents

List of abbreviations

GHG	Greenhouse gas
PE	Polyethylene
LLDPE	Linear low-density polyethylene
LDPE	Low-density polyethylene
HDPE	High-density polyethylene
PP	Polypropylene
GPC	Gel permutation chromatography
HT-GPC	High-temperature gel permutation chromatography
DES	Deep eutectic solvent
DSC	Differential scanning calorimetry
TGA	Thermogravimetric analysis
ChCl	Choline chloride
Octa	Octadecanamide
M_w	Weight average molecular weight
M_n	Number average molecular weight
$Đ_M$	Dispersity
Al	Aluminium metal
IR	Infrared
UV	Ultraviolet
PVC	Poly(vinyl chloride)
PET	Polyethylene terephthalate
BHET	Bis(2-hydroxyethyl) terephthalate
PS	Polystyrene

CAM	Cross-alkane metathesis
EDA	Ethyl diazoacetate
PH	Poly(1-hexene)
PEP	Polyethylene-*alt*-propylene
HBA	Hydrogen bond acceptor
HBD	Hydrogen bond donor
IL	Ionic liquid
EG	Ethylene glycol
PEF	Poly(ethylene 2,5-furandicarboxylic acid)
PC	Polycarbonates
BPA	Bisphenol A
BHEFDC	Bis(hydroxyethyl 2,5-furandicarboxylate)
CI	Carbonyl index
NMR	Nuclear magnetic resonance
^{m}CPBA	Meta-chloroperoxybenzoic acid
CO_2	Carbon dioxide
CH_4	Methane
VOC	Volatile organic compound
Mn	Manganese
Co	Cobalt
Fe	Iron
Ni	Nickel
CoSt	Cobalt stearate
CaSt	Calcium stearate

DMU	1,3-dimethylurea
TDCPP	*meso*-tetra-2,6-dichlorophenylporohyrin
TBHP	*Tert*-butyl hydroperoxide
K_d	Decomposition rate
$t_{1/2}$	Half-life
VOC	Volatile organic compound
Wt. %	Weight percentage
MPa	Mega pascal
mg	Milligram
mL	Millilitre
TCB	Trichlorobenzene
TCE	Tetrachloroethane
MeOH	Methanol
J	Joule
°C	Degrees Celsius
ΔH_m	Enthalpy of melting
ΔH_c	Enthalpy of crystallisation
T_m	Melting temperature
T_c	Crystallisation temperature
T_g	Glass transition temperature
T_{onset}	Onset decomposition temperature
$CHCl_3$	Chloroform
$CDCl_3$	Deuterated chloroform
d	Days

ppm	Parts per million
δ	Chemical shift
Da	Dalton
p*K*a	Acid dissociation constant
ε_b	Strain at break
ε_y	Strain at yield
σ_b	Stress at break
σ_y	Stress at yield
µW	Micro Watts
FG	Functional group
TPE	Thermoplastic elastomers
MJ	Mega Joules
BHT	Butylated hydroxytoluene
TLC	Thin layer chromatography
DMPP	Dimethylphenylphosphine
UV-Vis	Ultraviolet-visible

List of figures

List of schemes

List of tables

Declaration of authorship

This thesis is submitted to the University of Birmingham in support of my application for the degree of Doctor of Philosophy. This thesis has been solely composed by myself and no material contained within has been submitted for any other publication, degree or at any other institution. The work presented here was carried out by myself between September 2020 and March 2024 and the thesis has been composed by myself except in the case outlined below:

Wide-angle X-ray scattering (WAXS) studies in **Chapter 4** were performed by Joshua Deakin.

Some of the high-temperature gel permeation chromatography (HT-GPC) was performed by Dr Gavin Hill at Polymateria Ltd.

The initial idea and preliminary investigation into **Chapter 4** were performed by Dr. Connor Stubbs and Dr. Josh Worch; however, all the work reported in Chapter 4 was performed by myself.

Chapter 1

Introduction

1.1 Introduction

Polymers are very large molecules composed of many smaller molecules called monomers. Polymers play a fundamental role in life with a broad scope of functions, from proteins in living organisms, and sugars such as cellulose, to clothing and household appliances. One of their main applications is plastics. Plastics are materials comprised of synthetic or semi-synthetic components imparting properties such as malleability, brittleness or strength (or a combination). Plastic's largest market is packaging, which has seen significant growth because of a global shift from reusable to single-use packaging.[1] As the vast majority of plastics are derived from finite petrochemicals they have been under long-term environmental scrutiny for their strain on finite resources and their impact on climate change, therefore, there is a need for more effective recycling.[2, 3]

1.2 Plastic pollution

1.2.1 The environmental impact of plastics

Environmental concerns arise as plastics, which are commonly treated as disposable commodities, accumulate in the earth's landfills and oceans as a consequence of their inefficient recycling and reuse. Their strong durability and chemical inertness towards degradation means they can withstand decades of weathering before decomposing, threatening wildlife and spreading toxins.[4] This longevity further exacerbates landfill space depletion and although useful for disposing of large volumes of waste, burying plastic results in no value recovery and is not a sustainable waste management strategy. Landfills also have unique ecological systems where anaerobic and aerobic decomposition conditions cause the release of harmful acidic leachates and greenhouse gases (GHG) methane (CH_4) and carbon dioxide (CO_2).[5, 6]

1.2.2 Greenhouse gas emissions

GHG emissions are the leading contributor to climate change by creating what is known as the greenhouse effect whereby infrared (IR) radiation is trapped in the atmosphere resulting in increasing atmospheric temperatures causing flooring, desertification of fertile land and extreme weather conditions.[7] Evidence has shown that GHGs are emitted during all stages of plastic production, beginning with the extraction of raw materials.[8, 9] Oil and natural gas are the finite fossil fuel building blocks used for plastic production and extracting them requires the costly and energy-intensive process of hydraulic fracturing (fracking) of the earth. As well as the concerns surrounding the release of GHGs, fracking also causes damage to the local ecosystems. Transportation of raw materials is likewise a contributor to further millions of metric tonnes of carbon dioxide.

1.2.3 Ocean pollution

Waste plastics accumulate in bodies of water becoming subjected to natural weathering. Plastics that have been exposed to ultraviolet (UV) radiation become brittle and fragment into smaller pieces caused by the loss of molecular weight, these fragments are known as microplastics and nanoplastics. Concern has risen surrounding the impact that these plastic fragments have on human health and ecosystems. Studies have shown that micro and nanoplastics accumulate in our food through water supplies and by transfer up the food chain, leading to their build-up in our bodies. Nanoplastics can enter the circulatory system by passage through the intestinal barrier leading to systemic exposure and therefore potentially manifesting into metabolic disorders and local inflammation.[10] Microplastics are persistent and widely dispersed in the

environment having been found at the bottom of the oceans and the summit of Mount Everest (Figure 1.1).

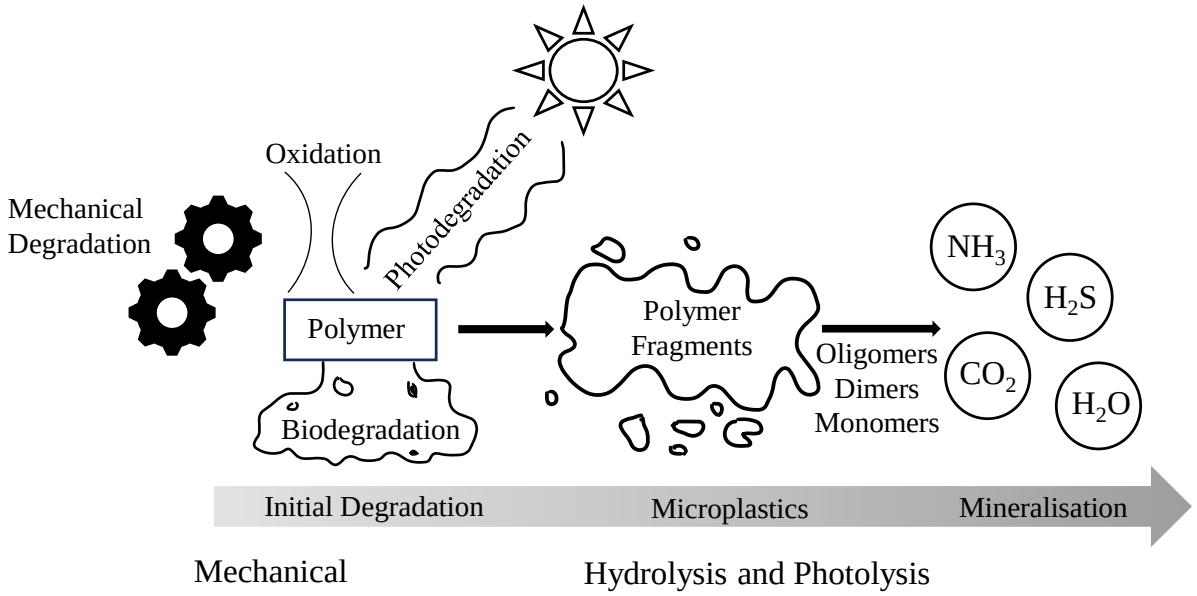

Figure 1.1 Degradation pathway for synthetic polymers

1.3 Plastic waste management

1.3.1 Current recycling methods

To-date recycling, which encapsulates any process concerning the reclamation or reuse of plastics including extracting value in the form of energy or materials, remains the most promising route for reducing plastic accumulation. Efficient recycling of post-consumer plastics decreases demand for virgin materials sourced from finite fossil fuels while lowering production costs and GHG emissions.[11] Traditional primary "closed-loop" recycling directly converts uncontaminated input waste plastic into a new version of the original product, usually by melting and remoulding the sample. Consecutive reprocessing of plastics often causes the molecular weight of the polymer chains to decrease in parallel with a reduction in mechanical and thermal robustness compared to virgin materials. This continued degradation and need for clean waste plastic is a major limiting factor. Mechanical "open-loop" recycling refers to post-

consumer plastics that have been reprocessed (downcycled) by melt extrusion for a new application setting.[12] While mechanical recycling is a frequently employed process, like primary recycling, it ultimately leads to a deterioration in mechanical properties through contamination and thermal degradation. Consequently, the reprocessed or recycled materials are of increasingly lower quality. Energy recycling is a method whereby a portion of energy is recovered in the form of heat through the incineration of complex mixtures of plastic waste. Although this is a valued method for reducing large volumes of plastic in landfills and oceans it is not without its environmental impact. Upon incineration, the process releases GHG emissions and toxins and while some energy is recovered, this energy totals less than the energy conserved by mechanical recycling.[13]

1.3.2 Biodegradable plastics

Biodegradable plastics are defined as plastics that can be broken down by microorganisms into biomass, water or volatile organic compounds (VOC) such as carbon dioxide and methane. The term biodegradable can be divided into two subcategories. The first is materials that are intrinsically biodegradable, whose chemical structure allows enzymes to attack directly, such as sugars, and those which become biodegradable upon an external factor such as light or heat and those that biodegrade by hydrolysis or photolysis.[14] In the latter category sits oxo-degradable plastics.

1.3.3 Oxo-degradable plastics

Oxo-degradable plastics are formed by incorporating a pro-oxidant or pro-degradant into conventional plastics such as polyolefins, poly(vinyl chloride) (PVC), or polyethylene terephthalate (PET). The abiotic oxidation process incorporates oxygen into the carbon backbone creating carboxylic acids, esters, aldehydes or alcohol functionality.[15] The strongly

electronegative oxygen atom creates a polarisable C− O bond that is more susceptible to undergoing chemical reactions as well as imparting hydrophilicity. The internal pro-oxidant encourages consecutive oxidation events, typically by the action of heat or exposure to UV radiation, causing deteriorative chain-scission reactions to occur leading to a loss of molecular weight. The timescale over which the oxidative degradation occurs can be tailored for the application required, ensuring the stability of the product is guaranteed, according to the quantity of additive incorporated. Typical pro-oxidative additives are metal salts of carboxylic acids and dithiocarbatmates with iron (Fe), cobalt (Co), copper (Cu), manganese (Mn) and nickel (Ni) metals.[16, 17] Mandal and co-workers demonstrated that cobalt stearate (CoSt) and calcium stearate (CaSt) pro-oxidant-filled PP films exhibited accelerated thermal degradation compared to unmodified PP. The biodegradability of CoSt and CaSt incorporated PP films were found to be 8.34% and 7.65% respectively after 45 days.[18] Rajagopal *et al.*, investigated the role that the metal stearates oxidation state plays in the thermal and photo-oxidation of low-density polyethylene (LDPE). After incorporating Co^{2+}, Fe^{2+} and Mn^{2+} stearates into LDPE it was revealed that it is the metal's ability to switch between the 2+ and 3+ oxidation states that lead to their oxidative ability by promoting hydroperoxide decomposition. Regarding thermal oxidation Mn and Co exhibit nearly equivalent pro-oxidant performance while iron presents a substantially lower activity, however, all metal stearates showed comparable propensity to initiate photo-oxidation.[19]

Oxo-degradable plastics, although they are an effective method of tackling plastic accumulation, have come under scrutiny for their propensity for generating microplastics. The fragmentation process can terminate before adequate loss of molecular weight, as a result, oxo-degradables have since been banned in some EU countries and the United Arab Emirates.[20] In addition, oxo-degradable plastics have no way of recovering their value once disposed of as all by-products are lost to the environment. The quest to find more eco-friendly plastics has

inadvertently created a linear approach to their end-of-life. As an alternative to downcycling or complete loss of materials, chemical recycling offers both a closed-loop recovery of monomers and an open-loop recovery of value-added products.[21]

1.3.4 Circular plastics economy

Closing the loop creates a circular plastics economy whereby polymers can be chemically recycled back into their original monomers and repolymerised without the loss of mechanical or thermal properties (Figure 1.2). Regenerative in nature, a circular economy maintains the value of the plastic without the need for additional virgin materials with a minimal environmental impact by stemming the production of waste plastics or by-products of degradation.

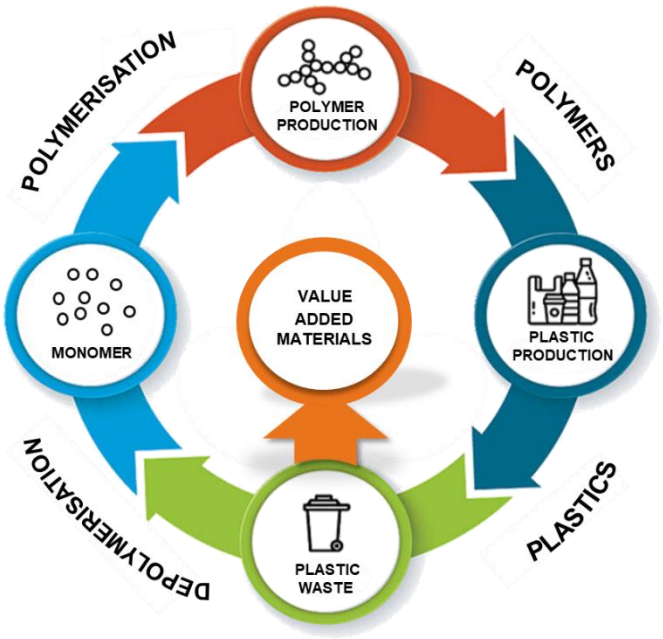

Figure 1.2 The ideal circular plastic economy

The most common example of chemical recycling is pyrolysis, where waste polymers are subjected to elevated temperatures (>500 °C) irreversibly yielding complex mixtures of oils and waxes (Figure 1.3). [22, 23] Pyrolysis provides a flexible pathway in processing a multitude of

feedstocks towards materials such as fuels and lubricants that possess economic value and an overall increased energy density.[23] Although pyrolysis offers some value recovery, it is a chemically non-selective process, often leading to a multitude of reaction products that are not suitable for repolymerisation while also being a very energy-intensive process, demanding temperatures in the range of 300 −800 °C. Catalytic pyrolysis limits some of the negatives surrounding uncatalysed pyrolysis as an acid catalyst reduces energy usage and can be used to tailor the process to yield higher-value products. Modified thermal activation-natural zeolite (TA-NZ) catalysts and acid activation-natural zeolite (AA-NZ) catalysts have proven effective accelerants for the pyrolysis of polystyrene (PS), polyethylene (PE), polypropylene (PP) and polyethylene terephthalate (PET) as single or mixed waste. The percentage of liquid oils produced was highest for PS (70%) compared to PE (42%) and PP (54%). The addition of the catalysts causes PS to degrade via end-chain scission mechanisms as opposed to random chain scission aiding in creating a more selective cracking process.[24] Unfortunately, the technology is in its infant stages and still requires complex purification processes. Gasification is another chemical recycling method which uses extremely high temperatures (1500 °C) in a limited oxygen atmosphere to break polymers down into synthesis gas (syngas) comprised of carbon monoxide (CO) and hydrogen (H_2). Nevertheless, before syngas can be useful, further processing is required to generate hydrocarbons for monomer synthesis. Although gasification is capable of dealing with complex mixed waste it requires large-scale operations, larger than required for pyrolysis, and is still a very energy-demanding process.

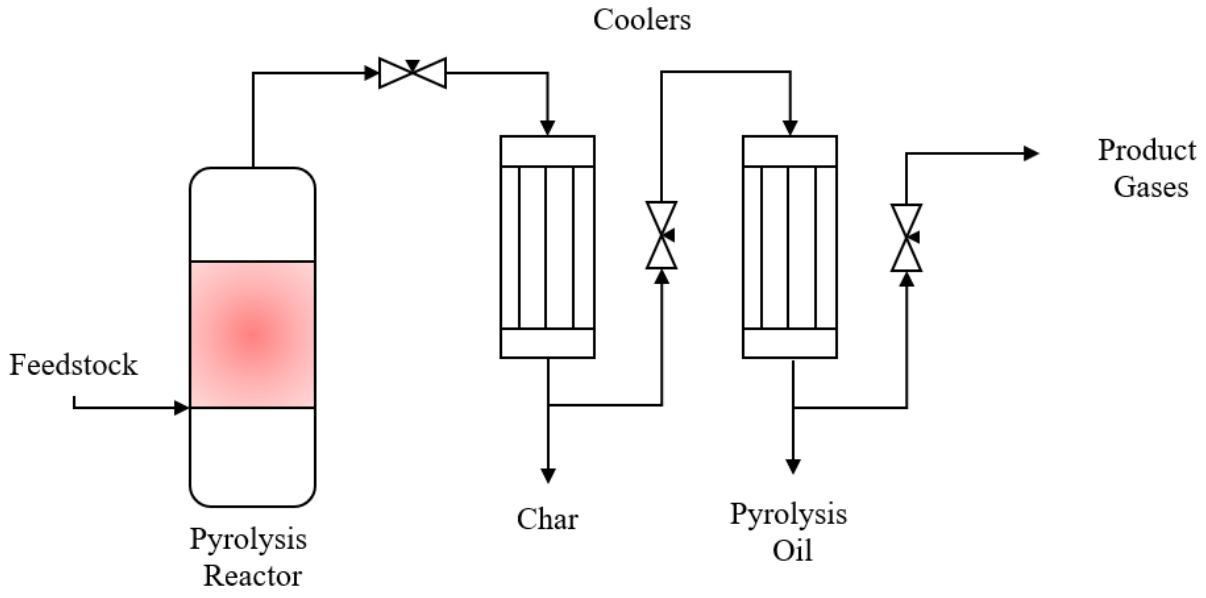

Figure 1.3 General schematic diagram of a pyrolysis reactor

Chemical recycling often suffers from poor reaction site selectivity as a result of homogeneity along polymer backbones creating substantial competition with random chain-scission events. Targeted reactivity typically occurs at the polymer chain end only, giving rise to monomeric units, whereas random chain scission along the backbone can lead to a diverse set of reaction products. Nevertheless, the presence of reactive functional groups (and heteroatoms) on the polymer backbone can greatly increase the chemo-selectivity of the depolymerisation reaction. As such, there are a few polymer classes that are particularly amenable to chemical recycling approaches. For example, the closed-loop chemical recycling of PET is achieved through its controlled depolymerisation to monomeric unit bis(2-hydroxyethyl) terephthalate (BHET) by nucleophilic attack of the ester bond followed by re-polymerisation to yield the recycled polymer.[25] Another example includes the depolymerisation of PS through oxidative degradation reactions involving nitrogen oxides and molecular oxygen forming benzoic acid and substituted nitrobenzoic acids.[26] Unfortunately, polymers like polyolefins with a homogeneous all-carbon backbone make targeted depolymerisation more challenging.

1.4 Chemical (up-cycling) recycling of polyolefins

1.4.1 Polyolefins

Olefins, otherwise known as alkenes, are hydrocarbons with at least one carbon-carbon (sp^2 hybridised) double bond. Polyolefins refer to polymers, with the formula $(CH_2)_n$, built from olefin monomer units through a chain-growth mechanism. In the 1940s researchers discovered one of the first polyolefins by reacting ethylene in the presence of oxygen under high pressure forming a linear polymer that is now better known as PE.[27] Since the discovery of PE, its production has been refined to a simple low-pressure heterogeneous catalysis, making PE an inexpensive and largely accessible plastic. Gaseous ethylene, used for the monomer, is generated by the steam-cracking of fossil fuels, otherwise known as pyrolysis, and is deemed the most important petrochemical raw material. The cracking process generates a crude mixture of low molecular weight alkanes and olefins, ethylene is separated by low-temperature-fractional distillation and selective adsorption. The process is the largest emitter of carbon dioxide (CO_2) in the chemical industry, however, ethylene's reactive carbon-carbon double bond makes it readily chemically accessible driving manufacturers to overlook its environmental impact.[28] The abundance of ethylene and other inexpensive olefins means the low-cost production of polyolefins is suitable for short-term or single-use applications making polyolefins an indispensable plastic in our modern life.[29]

Researchers then developed a methodology for the production of PE with short-chain branching, creating low-density polyethylene (LDPE) (Figure 1.4). The branches restrict LDPE's ability to pack tightly together fabricating a soft, flexible plastic suitable for lightweight packaging and films. PP is similarly formed by the chain-growth polymerisation of propylene with a repeating unit of $[CH_2\text{-}CH(CH_3)]_n$. The methyl group on the backbone allows PP to take on isotactic, syndiotactic and atatic conformations. Isotactic PP has the most commercial application and refers to the stereoregular conformation of the methyl groups located on the same side of the backbone creating a stiff material with a high degree of crystallinity.[30]

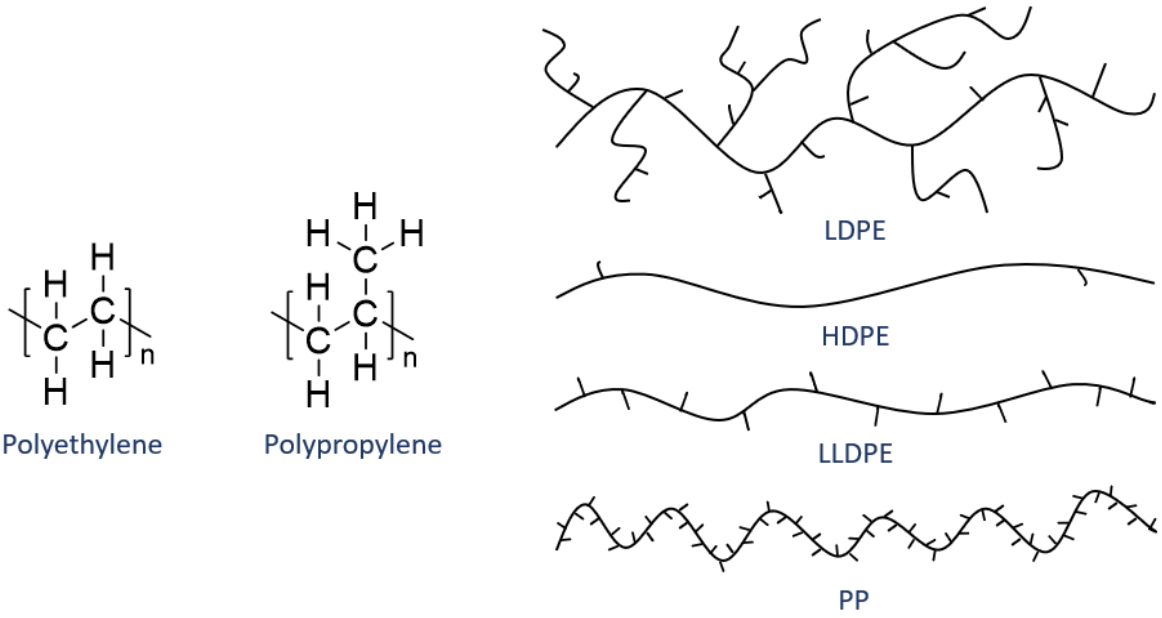

Figure 1.4 The structure of polyethylene and polypropylene

Polyolefins account for approximately 57% of global plastics production with a mere 16% being recycled. The chemical recycling challenges associated with polyolefins make it difficult to recover monomeric materials due to their high ceiling temperatures, which are above their decomposition temperatures.[31] Their non-polar homogeneous carbon-carbon backbone enables them to withstand degradation by hydrolytic cleavage, and although this is advantageous to their valued durability, it makes dyeing, polymer blending or adhesion problematic as well as

making facile oxidation by heat or ultraviolet radiation ineffective.[25,32] Mixed polyolefin waste streams are extremely difficult to separate as a consequence of their similar densities and immiscibility, therefore requiring refined energy-intensive processes to overcome such limitations. During the mechanical recycling of polyolefins, when melted together phase separation can occur creating distinct polymer regions. This non-uniformity of the generated material leads to a lack of control of the properties and a deterioration in value.[33] Despite this, their simple composition, affordability, durability, and vast assortment of chemical and mechanical properties make them integral in all aspects of modern society.[34]

1.4.2 Pyrolysis

As described above, pyrolysis involves the heating (> 500 °C) of plastic waste in the absence of oxygen to yield complex mixtures of oils and waxes. The thermal decomposition of PE is a multistep process and proceeds by a free radical chain mechanism and begins with the homolysis of its C-C backbone via deleterious β-scission reactions.[35] Consecutive intramolecular hydrogen abstraction (backbiting), random β-scission and intermolecular hydrogen shifts cause the eventual decomposition into hydrocarbons.[36] Although pyrolysis successfully deals with large volumes of polyolefin waste it lacks reaction site selectivity.

1.4.3 Alternative chemical recycling of polyethylene

Recently there has been scope for the chemical upcycling of polyolefins by selective depolymerisation or functionalisation to value-added materials and/or via chemo-selective functionalisation of the polymer backbone. The derivatisation of polyolefins may be achieved directly from the incorporation of functionalised monomeric units or by post-polymerisation incorporation of catalyst-tolerant functionalities.[37] The scope of their upcycling has been demonstrated by processes such as alkane metathesis and catalytic cracking.[38] The possibility of generating a number of well-defined alkane products from polyolefins through

interconversion via cross-alkane metathesis (CAM) make them suitable as a fuel source.[39] Goldman and Hunang developed such a tandem catalytic cross-metathesis process inclusive for LDPE, linear low-density polyethylene (LLDPE) and high-density polyethylene (HDPE) utilising simple light alkane reagents alongside a pincer-type iridium complex as a dehydrogenation catalyst (Scheme 1.1).[39,40] Initial CAM reactions decrease the chain length of PE and can be performed in succession to further reduce molecular weight.[32] These dual catalytic CAM reactions avoid heat and mass transfer, a common problem associated with the more traditional recycling process of pyrolysis.

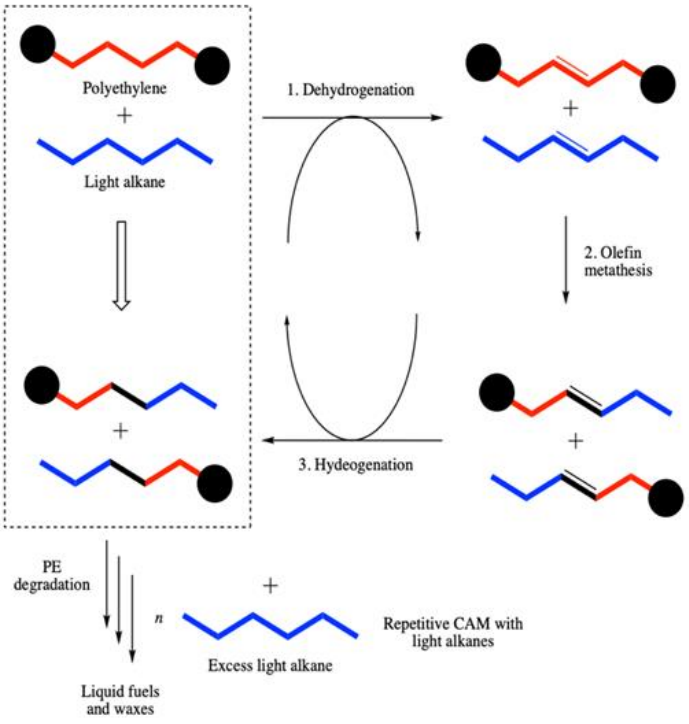

Scheme 1.1 Cross alkane metathesis (CAM) between polyethylene and a light alkane (n-hexane)

Another form of polyolefin chemical recycling is catalytic cracking involving the catalytic degradation of the polymer chain under high temperatures to yield value-added gaseous and/or liquid hydrocarbons. Importantly, the catalyst accelerates the depolymerisation reaction but also serves to narrow the product distribution generating greater selectivity for desired product characteristics while tailoring reaction time and temperature.[41] Cracking of polyolefins, in

particular PE, into small molecular weight alkanes using ionic liquid (IL) systems was investigated by Adams and co-workers where it was established that the chloroaluminate(III) ionic system with the addition of an acidic co-catalyst at 200 °C yielded upwards of 85% low molecular weight alkanes.[42] Lerici and co-workers investigated the cracking of LDPE, HDPE, PP and PS utilising an H-Y zeolite catalyst. The process was moderately efficient when employing HDPE however the same reaction using LDPE or PP afforded 30% less recovered products, which highlights unique challenges for depolymerising different polyolefin compositions.[41]

1.4.4 Post-polymerisation modification of polyolefins

Post-polymerisation modification of polyolefins has become an area of recent interest owing to the potential generation of value-added materials by leveraging the high volume of polyolefin production. Commercially, post-functionalisation processes are heavily reliant on reactive carbon-based radicals as a consequence of polyolefins homogeneity.[43] Chemical modifications of polymer backbones classically compete alongside a series of deleterious side reactions compromising molecular weight distribution and, thus, desired polymer properties, such side reactions include beta-scission, coupling reactions and chain transfer reactions.[44] Although post-polymerisation is challenging on account of the absence of reactive functional groups, significant progress in the search for a viable route to chemically modify polyolefins has led to functionalisation being explored through polymerisation involving chain transfer agents including; silane[45], borane[46] and vinyl chloride.[47] Although the functionalisation was regioselective, it was exclusively limited to the installation of the reactive group in the primary carbon at the polymer chain end. Leibfarth and co-workers reported the tuneable functionalisation of polyolefins via intermolecular metal-free and regioselective xanthylation.[48] Unlocking usually inaccessible C-H transformations for branched polyolefins, the insertion of the xanthate functional groups is achieved without the deleterious chain-scission side reactions

and provides the appropriate platform for further functionalisation to a diverse range of functional materials. For example, Shen and co-workers showed that a one-step reaction at a xanthate group can introduce a trifluoromethylthiol group.[49] Diversification of the aliphatic C-H bond of polyolefins through radical chain transfer was reported by Alexanian and co-workers.[50] Upon mild heating, an O-alkenylhydroamate reagent facilitated the installation of bromide, iodide, thiophenyl, azido, fluoride and trifluoromethylthiol groups into the backbone of LLDPE without loss of molecular weight. Cyanation, thiophenylation and iodination were proven to be successful for crystalline HDPE, LDPE and post-consumer waste PE without discernible chain scission.

1.4.4.1 Oxidation

The successful functionalisation of polyolefins has proven its effectiveness as the foundation for a more sustainable plastics economy leading scientists to look at the direct synthesis of functionalised polyolefin-like materials. Hartwig *et al.* used a library of elementary vinyl monomers to selectively synthesise polyolefins with controlled molecular weights and architectures. Selective oxidation of the polyolefins C-H bonds using a polyfluorinated ruthenium porphyrin and 2,6-dichloropyridine N-oxide catalyst system allowed for oxidation to form alcohols without the overoxidation to form esters, which are more easily degraded by mechanisms such as transesterification and hydrolysis. The oxidised polyolefins exhibit superior properties compared to the unmodified polyolefin with improved tensile strength, stronger adhesion forces and the ability to be painted.[51] Using single-lap-shear testing the adhesion strength of the ox-LDPE species and LDPE to aluminium metal (Al) was compared and the ox-LDPE was found to adhere 20 times stronger than LDPE. This result shows that the limitations faced by unmodified PE, such as lack of adhesion and low surface wetting, can be

overcome by incorporating oxygen-containing functional groups onto the polymer backbone creating opportunities for upcycling.

Modification of polyolefins via hydroxylation opens up potential routes to secondary and tertiary oxidation (Scheme 1.2). Hartwig and co-workers reported the successful regiospecific functionalisation of a variety of commercial polypropylenes utilising a rhodium-catalysed borylation of the methyl C-H bonds followed by oxidation to their hydroxyl groups exclusively at the terminus of the polymer side chains. Using 5 mol% Cp*(Rhη^4-C_6Me_6) and 10 equiv of monomer at 200 °C for 30 h achieved OH% functionalisation of iPP-1 at 1.5% conversion.[52] Hartwig and co-workers also accomplished hydroxylation of PE using a nickel-based catalyst in the presence of meta-chloroperoxybenzoic acid (^{m}CPBA) as an oxidant. Between 2.0 and 5.5 functional groups (alcohol, ketone and alkyl chloride) were introduced per 100 monomer units, with alcohols showing higher selectivity over ketones or chloride moieties.[53] The significance of these methods arises because of the little to no change in the molecular weight parameters for the functionalised polymers, indicating negligible instances of chain scission or cross-linking side reactions.

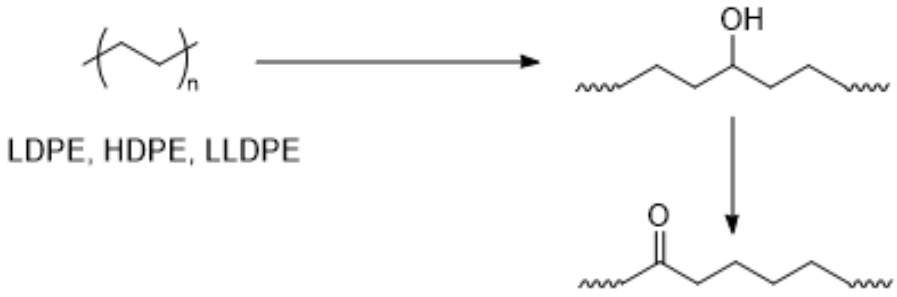

Scheme 1.2 General scheme for the hydroxylation of polyethylene followed by secondary oxidation

As previously stated, the selective depolymerisation of polyolefins is challenging as a result of the polymer's homogeneity. However, microwave-assisted oxidation of LDPE, tuneable through time duration and nitric acid concentration has been found to generate a plethora of dicarboxylic acids, but greater selectivity was demonstrated for succinic acid owing to a

favourable transition state in the proposed mechanism.[54] The regio-selective insertion of ester groups into tertiary C− H bonds of PP has been achieved by a copper-based catalytic functionalisation involving ethyl diazoacetate (EDA). Importantly, the authors determined that the extent of ester group incorporation could be manipulated by altering the EDA: PP ratio.[55] The introduction of C−C double bonds through catalytic dehydrogenation of polyolefins has been demonstrated by Goldman and co-workers using *p*-methoxy-substituted PCP-pincer catalysts which prove effective for both PE and poly(1-hexene) (PH). Although PH showed greater reactivity than PE. This simple homogeneous catalytic system creates scope for further controlled functionalisation of polyolefins.[37] Although these examples are encouraging, the use of transition metal or precious metal catalysts is not ideal owing to scarcity and economic issues, therefore, utilising earth-abundant metals would be a more economically attractive option for industrial application.

1.4.4.2 Functionalisation using earth-abundant metals

Catalysis using earth-abundant metals offers a more cost-effective and sustainable alternative to traditional transition metal catalysts.[56] Hillmyer and co-workers reported the direct oxyfunctionalisation of polyethylene-*alt*-propylene (PEP) and squalane utilising a manganese(II) *meso*-tetra-2,6-diclorophenylporphyrin acetate M_n(TDCPP)OAc/imidazole system combined with a phase transfer agent and oxygen donor. Results found the successful incorporation of ketones and tertiary alcohols without variation in molecular weight.[57] Similarly, the catalytic oxidative decomposition of PE with oxygen in an aqueous dispersion was studied by Marek and co-workers. Revealing Co(II) and Mn(II) acetylacetonates effectiveness for incorporating polar functionalities into the polymer backbone.[58] Despite these

encouraging reports that employ manganese catalysts, the metal remains largely understudied and thus presents a great opportunity for innovation in this area.

1.5 Deep eutectic solvents (DES)

1.5.1 DES composition

Throughout the past decade, deep eutectic solvents (DES) have emerged as a promising class of solvents for chemical synthesis. These innovative eutectic solvents are formed by the complexation of a hydrogen bond donor (HBD) with a hydrogen bond acceptor (HBA). The HBD is notably an organic compound with hydrogen bonding capability, such as urea, ethylene glycol or glycerol, whereas the HBA is typically a quaternary ammonium salt, metal salt or hydrated metal salt (Figure 1.5). DES are widely acknowledged as an alternative to ionic liquids and can be formed by simply mixing both components at an elevated temperature (approximately 80 °C) until a homogeneous liquid forms, often requiring no further purification.[59, 60] Other methods for their preparation include direct mixing in an extruder[61] and manually grinding in a mortar[62]. The eutectic point refers to the system's minimum melting temperature (the point of intersection along the two components melting profiles) (Figure 1.6).[63] A lowered lattice energy, a result of delocalisation through hydrogen bonding, lowers the solvent's melting temperature relative to its individual components. This negative deviation from the thermodynamic ideality arises as the solid-liquid equilibria of the DES are affected by a combination of factors such as the melting points of each component, intramolecular attractions and enthalpies of fusion.[64] Previous work has attempted to rationalise this depression in melting temperature; the HBA anion complexes through ionic hydrogen bonding to the HBD delocalising the negative charge, generating a weaker interaction with the cationic HBA. Therefore, the HBD delocalises the molecular lattice of the HBA.[65, 66]

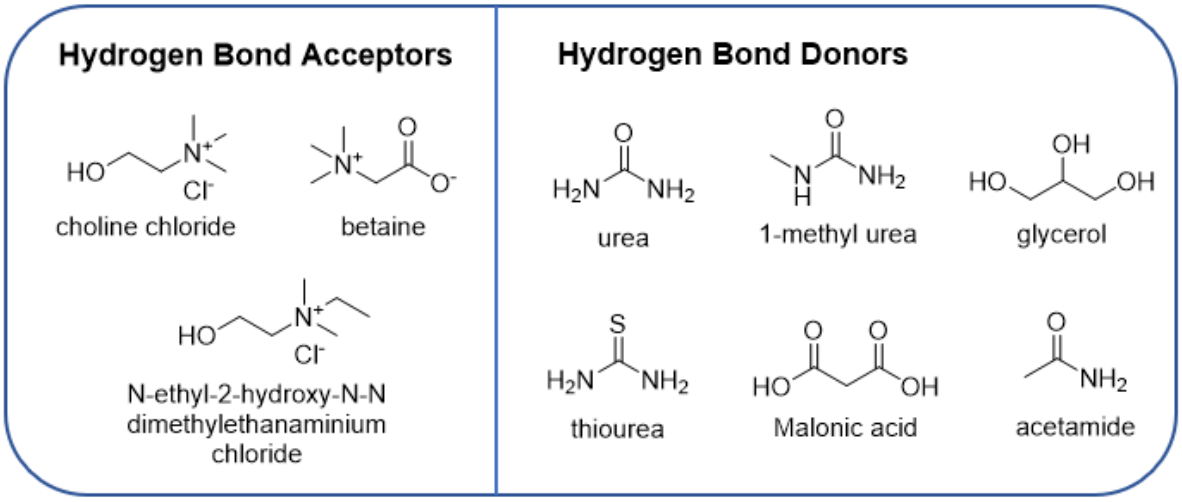

Figure 1.5 Examples of some common hydrogen bond donors and hydrogen bond acceptors for DES

Organic solvents have self-evident advantages in chemical processes; however, they are often volatile, highly flammable, harmful to humans and the environment and explosive. Solvents account for up to 90% of the total mass of an organic reaction with the majority being ineffectively discarded as waste, therefore, careful consideration must be taken to find an alternative approach.[67] DES can be employed as a cost-effective and easily synthesised alternative to conventional organic solvents with tuneable physical and chemical properties. As most DES originate from a renewable source their ecological footprint is low. Unique Lewis/Bronsted acidic character of DES makes for distinctive catalytic activity in addition to their excellent recoverability, biodegradability, low volatility and non-toxicity.[68] Since their discovery, numerous DES have been synthesised, and are generally categorised based on the nature of their complexing agent. Type I eutectics include a quaternary salt with non-hydrated metal chloride, type II eutectics feature a quaternary salt and a hydrated metal salt, type III eutectics are composed of a HBD and a quaternary HBA salt and finally, type IV include a organic HBD combined with a metal chloride. By tailoring the stoichiometric ratios of the HBD:HBA the physical and chemical properties of the DES can be altered. The density of the

DES can be altered for a particular application, for example, the greater the choline chloride (ChCl) concentration the lower the DES density and vice versa.

1.5.2 Viscosity of DES

Viscosity can be defined as the resistivity of a fluid and for industrial applications solvents with low viscosities are desirable as high viscosities can impede flow and decrease the rate of solute mass transfer leading to slow or incomplete reactions. Certain HBD:HBA combinations produce eutectic mixtures with high viscosities, therefore, tunability through stoichiometric ratio and temperature are key in controlling the DES reactivity. Zhang *et al.* reported that the viscosity of the DES is governed by hydrogen bonding, van der Waals and electrostatic interactions, moreover, ChCl-based eutectic solvents have a large dependency on the nature of the HBD.[69] DES are essentially a mixture of anions and cations and when water is added, all of the species become hydrated, the small anions (halides) become more closely connected to the water molecules, and the small halides, even in very dilute solutions, are fully saturated.[66, 70] Many of the advantageous properties of DES are significantly affected by the presence of water, therefore, dilutions must be performed cautiously. DES are often hygroscopic and readily absorb water from the air also influencing their properties.

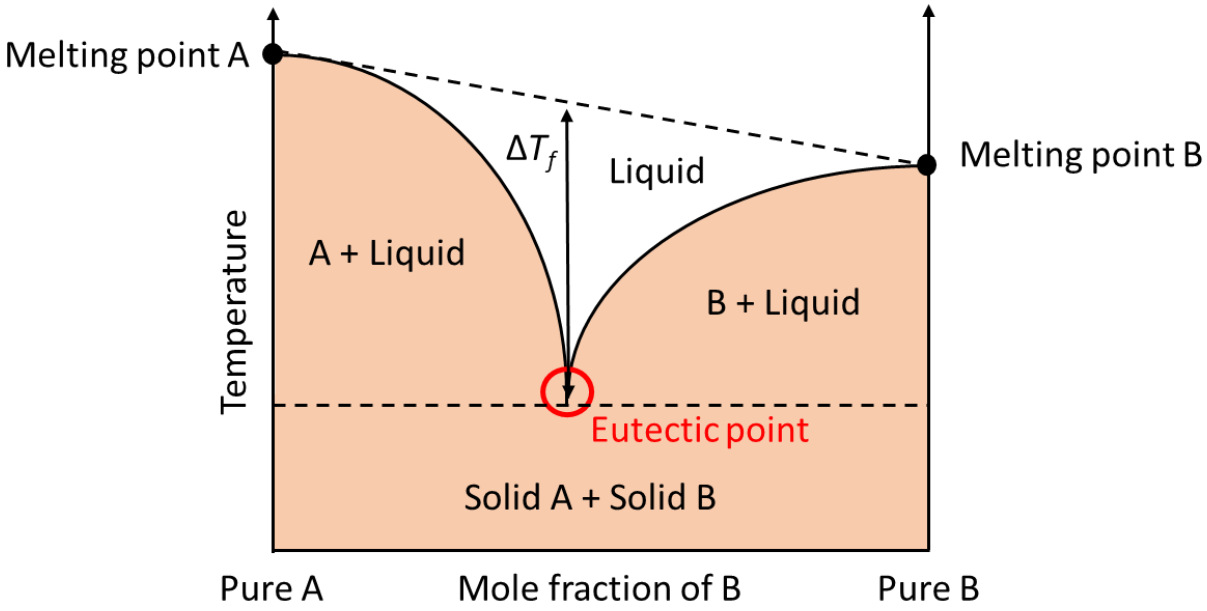

Figure 1.6 Eutectic solvent formation in a two-component phase diagram

1.5.3 Common DES applications

ChCl ($C_5H_{14}ClNO$) functions as one of the most commonly used HBA occurring naturally with a bifunctional structure containing an ammonium salt and alcohol group. Given that most ChCl-based DES are water soluble they make for excellent extraction solvents with the removal of analytes being as simple as the addition of an aprotic solvent to the homogeneous aqueous sample.[71] This creates self-aggregation and is a result of the strong interaction between water and the aprotic solvent compared to the weaker interactions between the water and the DES creating a fast and effective method for extraction.[72] Additionally, water-soluble DES provide a solvent-free alternative to traditional solvents as reaction products can be easily precipitated out upon the addition of water, avoiding the need for solvent extraction. DES have many reported applications, for instance, metal plating,[73, 74] gas adsorption,[75] protein extraction[76], esterification,[77] and biotransformations[78]. They have been used to modify graphene for their use in drug delivery systems, wastewater treatment and catalysis.[79]

1.5.4 DES for depolymerisation

By fulfilling many green chemistry principles DES are an attractive media for plastic depolymerisation. By incorporating a metal salt into the eutectic solvent, the DES can act as both the solvent and the catalyst, maximising catalyst loading. The versatility of DES allows for tailorable physical and chemical properties to achieve the most cost and energy-efficient depolymerisation. The depolymerisation of PET into high-value products is well documented in the literature with common solvents methanol, ethylene glycol and amines, however, there has been scope to use DES. Electron-deficient metals when paired with an electron-rich substrate gain Lewis acidic character suitable for catalysis.[80] Zhou and co-workers explored this idea with the synthesis of dioctyl terephthalate through the alcoholysis of PET using choline chloride-based DES alongside a range of metal salts, obtaining 100% PET conversion in 5 h with $Zn(OAc)_2$.[81]

Scheme 1.3 General scheme for the depolymerisation of polyethylene terephthalate (PET) into its monomer Bis(2-hydroxyethyl) terephthalate (BHET) catalysed by a DES

Wang *et al.* reported the glycolysis by ethylene glycol of PET catalysed by a [Urea][$ZnCl_2$] 4:1 DES achieving full PET conversion with an 83% yield of the BHET monomer under mild reaction conditions (170 °C for 30 mins) (Scheme 1.3).[82, 83] Similarly, Lui B. *et al.* reported the > 99% conversion of PET with an > 80% yield of BHET using 1,3-dimethylurea (1,3-

DMU)/$Zn(OAc)_2$ DES after only 20 minutes at 190 °C. [84, 85] The recyclability of the DES was investigated: six consecutive depolymerisation cycles were performed revealing that the levels of zinc and nitrogen (from the 1,3-DMU) decreased with each cycle and although the catalyst still worked effectively the catalytic efficiency was lower with each cycle. Lui *et al.* demonstrated that PET can be selectively depolymerised from a polycotton blend with complete recovery of undamaged cotton using Betaine/$Zn(OAc)_2$ 1:1 at 190 °C after 60 minutes. [86] Polycarbonates (PC) have shown to successfully depolymerised *via* methanolysis using the highly active ChCl/Urea DES at 130 °C for 2.5h. PC conversion yielded > 99% of bisphenol A (BPA), a value-added molecule. BPA was easily isolated and the DES was reused for a further five cycles without any notable reduction in PC conversion or BPA yield.[87] DES have also been proven to depolymerise bio-based polymers. Poly(ethylene 2,5-furandicarboxylic acid) (PEF) is derived from D-glucose or D-fructose feedstocks and is a potential competitor for the less degradable PET. Employing the same urea/$Zn(OAc)_2$ DES as discussed above for PET depolymerisation, PEF can be converted into its bis(hydroxyethyl 2,5-furandicarboxylate) (BHEFDC) monomer *via* glycolysis. The same DES can be used to repolymerise this monomer back into PEF via a polyesterification reaction at 180 − 210 °C, 7h under vacuum creating a circular economy.[88] There have been no reports in the literature where DES have been applied for the environmentally friendly depolymerisation of polyolefins.

1.6 Radical oxidation reactions

1.6.1 Molecular oxygen oxidations

Molecular oxygen, also known as dioxygen, (O_2) serves as the simplest oxidant, its abundance, low cost, versatility and lack of harmful byproducts make it an attractive reagent for chemical synthesis while aligning with key "chemistry" strategies. Constituting 20% of the earth's atmosphere, molecular oxygen is naturally occurring, highly available and can be harnessed without exhausting finite resources.[89] Oxygen's potent oxidising ability arises as it possesses a high reduction potential and can accept electrons into the vacant sites of its valence shell undergoing a reduction. Aerobic oxidation (oxidation performed using molecular oxygen) has shown previous success in C–H activation and alkene oxidation but often requires transition metals or co-oxidants.[90, 91] The direct C(sp^2)–H hydroxylation by dioxygen is a useful pathway to a series of phenol derivatives [92] while Fukuzumi and co-workers demonstrated the use of molecular oxygen for the oxygenation of anthracene and indoles.[89]

1.6.2 Organic peroxides

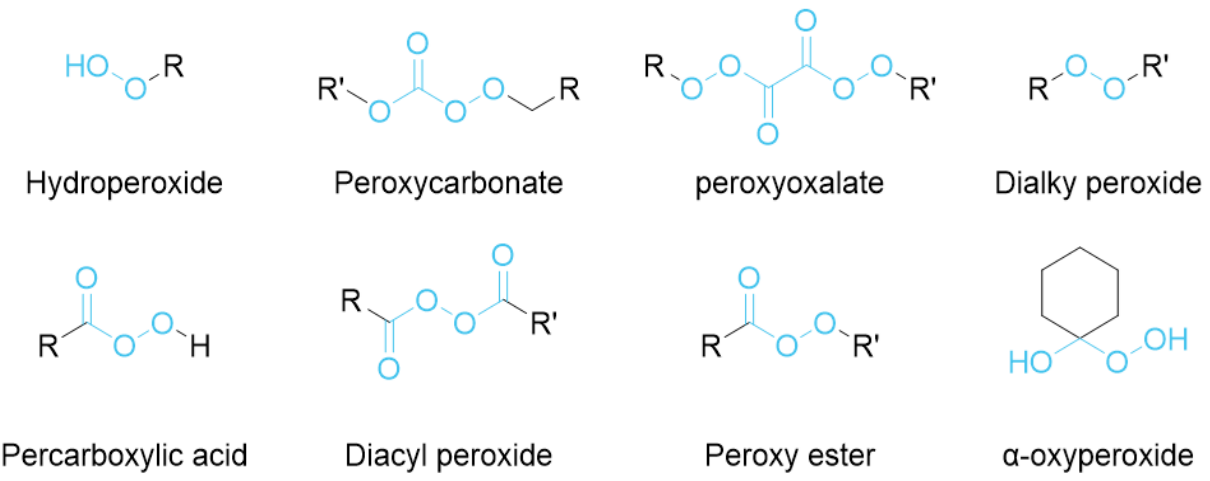

Figure 1.7 Examples of molecules containing peroxide functionality

Despite the potential benefits, the direct reaction of molecular oxygen with hydrocarbons for C–H activation is a high-energy pathway causing slow reactions or failure to initiate. This high energy barrier can be bypassed with the use of radicals and radical initiators. Radical initiators possess weak bonds with low dissociation energies that under mild reaction conditions cleaves giving rise to two radical centres, the most common of which are halogens, azo compounds organic and inorganic peroxides (Figure 1.7).

Organic peroxides possess a peroxide functional group (R–O–O–R), when R is hydrogen, they are called hydroperoxides. The low bond dissociation energy of the peroxide O–O bond means the molecule is capable of undergoing homolytic cleavage under mild heating, light-irradiation or transition metal catalysis (Scheme 1.4). This process results in the formation of two oxygen-centred radicals, which act as radical initiators or as one-electron oxidants.[93] The acyloxyl radical generated from this reaction can further lose CO_2, thus forming the corresponding alkyl radical.[94] Peroxides have applications within oxidation[95] chemistry.

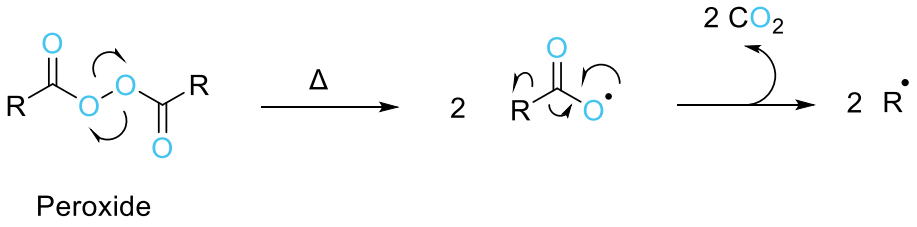

Scheme 1.4 The general radical mechanism for the thermal decomposition of a peroxide radical initiator

The thermal stability of peroxides is defined by the low dissociation energy of the O–O bond, a consequence of the inductive effect of the two oxygens creating an acidic character (pK_a 10 – 3), and therefore decompose easily upon external stimulation. The rate of peroxide decomposition is affected by the solvent and the activity of the initiator is defined by its half-life ($t_{1/2}$), the time it takes for the original initiator content to decrease by 50%. Assuming first-

order kinetics, which is evident in most organic radical initiators, the $t_{1/2}$ is related to the initiator decomposition rate (K_d) by the following equation:

$$t_{1/2} = \frac{ln2}{K_d} \qquad (1)$$

1.6.3 Oxidation using radicals

Literature states that the rate-limiting step of oxidations is the accumulation of hydroperoxides which form as oxygen penetrates the hydrocarbon chain via C-H abstraction, forming free radicals that chain grow to form the corresponding hydroperoxide.[96] Without the assistance of external radicals, this reaction rarely occurs in hydrocarbons, thus, radical initiators are added. Next is the formation of oxidation products by the destruction of the free radicals. Hydroperoxides thermal decompose through a monomolecular mechanism by first-order kinetics. Subsequent alcohol, ketone and ester formation have sufficiently low activation energies (4 kJ·mol) thus they occur immediately upon peroxide decomposition.

1.6.4 Transition metals with peroxides

Redox-active ligands are named as such because they contain energetically accessible levels that allow redox reactions to alter their oxidation state. Transition metals seldom exhibit high activity for oxidation, however, when bound to redox-active ligands they show extensively improved catalytic activity as the ligand can delocalise and/or provide electrons to the complexed metal centre. Such complexes have been applied to the aerobic oxidation of alcohols to aldehydes.[97]

Peroxides can oxidise in the absence of metal catalysts but affords only low yields of oxygen-containing products, nevertheless, peroxides in the presence of transition metals exhibit an

increased effectiveness towards oxidation. Transition metals are known to catalyse the decomposition of peroxides via the cleavage of their RO-OR bond, in particular, transition metals that can undergo a one-electron redox switch, such as cobalt, manganese, iron, copper, ruthenium and platinum. The newly formed RO• radical acts as a hydrogen extractor for C-H activation for alkanes deriving an unstable alkyl radical that can go on to form C-O bonds.[98]

Hydrogen peroxide (H_2O_2) is the ideal oxidant owing to its high activity and its only by-products are water and oxygen (O_2), therefore, in combination with a metal catalyst hydrogen peroxide exhibits an increased effectiveness for oxidation. The decomposition of H_2O_2 catalysed by ferrous ions (Fenton's reagent) in low pH environments is a well-established procedure for its use as an analytical reagent.[99] H_2O_2 decomposition was also utilised to successfully incorporate carbonyl groups into kraft pulp[100, 101] Hydrogen peroxides unique activity originates from its highly reactive HO• radical.

Hydroperoxides with the formula RO−OH all have the capability of forming this reactive species and are expected to show near to no reaction site selectively. Less reactive radicals such as peroxyl radicals preferentially react with tertiary hydrogens compared to secondary and primary, restricting their application for HDPE degradation initiators (Figure 1.8).[102] Despite their effectiveness many of the metals employed for peroxide-coupled oxidations are toxic and expensive, thus, necessitating the development of catalytic systems that utilise earth-abundant and less harmful metals.

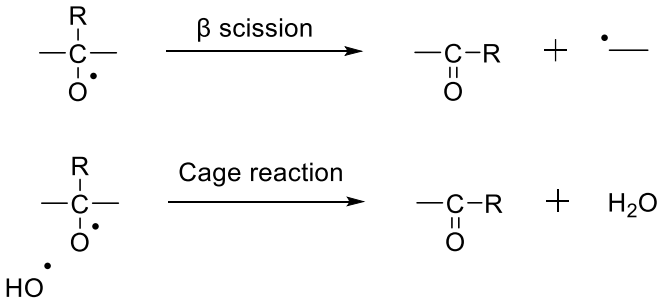

Figure 1.8 Radical decomposition of secondary and tertiary carbon atoms

1.7 Summary

The incorporation of degradable functional groups into polyolefins all carbon backbone is a key challenge in breaking the linearity of their life cycle. This degradable functionality is essential for chemical recycling. This introductory chapter outlines key concepts for creating a circular plastic economy via depolymerisation to monomeric units or value-added products and highlights the potential effectiveness of DES as an alternative dual solvent-catalyst system for the oxidation of polyolefins. Initially, different classes of polymers were introduced with the focus on their recyclability. Following this, the limitations of our current recycling techniques were addressed with specific attention paid to the handling of polyolefin waste. To overcome such limitations the concept of DES has been presented as an alternative to more traditional harmful organic solvents as a tailorable dual solvent-catalyst system for depolymerisation. Finally, the concept of oxidising alkanes via molecular oxygen and radical initiators were summarised as a strategy to accelerate the oxidation of polyolefins through the incorporation of targetable heteroatoms. Overall, the strategies outlined above present the techniques for the environmentally friendly depolymerisation of polyolefins with the aim of studying the incorporation of oxygen-containing functionality on the overall molecular weight of polyolefins.

1.8 Project aims

The primary aim of this thesis comprised the development of catalytically active DES for the accelerated oxidative degradation of polyolefins, while the secondary aim explores the fine manipulation of isohexide stereochemistry within a series of polyurethanes for the investigation into mechanical, thermal and hydrolytic degradation properties. Both projects were performed in parallel as a consequence of the long reaction times required for polyolefin degradation.

The main objective explores DES, composed of hydrated metal salts with a hydrogen bond acceptor, for their use as both the catalyst and the reaction solvent for the oxidation, and subsequent degradation, of model small molecule polyolefin, squalane, as well as LDPE and HDPE. It aims to expand on the suitability of the DES as a dual solvent-catalyst system with a focus on the DES thermal stability, and their oxidation activity towards chemically inert carbon-carbon backbones. It was envisioned that replacing traditional organic solvents with DES would allow the synergy between the HBA:HBD to be manipulated for optional catalytic efficiencies with maximised catalyst loading and lower operating temperatures. Organic peroxides as radical initiators were hypothesised to accelerate polyolefin oxidation through the generation of reactive hydroperoxide species while oxygen atmosphere reactions were thought to maximise the reactive oxygen species available for oxidation.

The second aim of this thesis was to investigate the effect of stereochemistry on a series of sugar-based isohexide containing polyurethanes. Therefore, the first objective was to synthesise strong thermoplastic elastomers via thiol-ene “click” polymerisation. The chemical similarity of the stereoisomers was anticipated to enable easy physical blending and co-polymerisation between the different polyurethanes for potentially tailorable mechanical, thermal and degradation performance.

1.9 References

1. R. Geyer, J. R. Jambeck and K. L. Law, *Sci. Adv.*, 2017, **3**, 1700782-1700787.
2. M. Jefferson, *Energy Res. Soc. Sci.*, 2019, **56**, 101229-101237.
3. M. W. Ryberg, M. Z. Hauschild, F. Wang, S. Averous-Monnery and A. Laurent, *Resour. Conserv. Recycl.*, 2019, **151**, 104459-104469.
4. H. Sardon and A. P. Dove, *Science*, 2018, **17**, 380-381.
5. J. R. Jambeck, R. Geyer, C. Wilcox, T. R. Siegler, M. Perryman, A. Andrady and K. L. Law, *Science*, 2015, **347**, 1234-1242.
6. A. Chamas, H. Moon, J. Zheng, Y. Qiu, T. Tabassum, J. H. Jang, M. Abu-Omar, S. L. Scott and S. Suh, *ACS Sustain. Chem. Eng.*, 2020, **8**, 3494-3511.
7. L. Jeffry, M. Y. Ong, S. Nomanbhay, M. Mofijur, M. Mubashir and P. L. Show, *Fuel*, 2021, **301**, 121017.
8. H. V. Ford, N. H. Jones, A. J. Davies, B. J. Godley, J. R. Jambeck, I. E. Napper, C. C. Suckling, G. J. Williams, L. C. Woodall and H. J. Koldewey, *Sci. Total. Environ.*, 2022, **806**, 150392-150403.
9. M. Shen, W. Huang, M. Chen, B. Song, G. Zeng and Y. Zhang, *J. Clean. Prod.*, 2020, **254**, 120138-120151.
10. H. Bouwmeester, P. C. Hollman and R. J. Peters, *Environ. Sci. Technol.*, 2015, **49**, 8932-8947.
11. J. D. Hamilton, K. H. Reinert, J. V. Hagan and W. V. Lord, *J. Air Waste Manag. Assoc.*, 1995, **45**, 247-251.
12. I. A. Ignatyev, W. Thielemans and B. V. Beke, *Chem. Sus. Chem*, 2014, **7**, 1579-1593.
13. J. Morris, *J. Hazard. Mater.*, 1996, **47**, 277-293.
14. T. F. M. Ojeda, E. Dalmolin, M. M. C. Forte, R. J. S. Jacques, F. M. Bento and F. A. O. Camargo, *Polym. Degrad. Stab.*, 2009, **94**, 965-970.
15. X. Liu, C. Gao, P. Sangwan, L. Yu and Z. Tong, *J. Appl. Polym. Sci.*, 2014, **131**, 40750-40765.
16. J. C. Salcedo Reyes, O. A. Castañeda Uribe, L. D. Gomez Méndez, A. M. Pedroza Rodríguez and R. A. Poutou Piñales, *Univ. Sci.*, 2023, **28**, 65-139.
17. A. J. Sipinen and R. d. R, *J. Environ. Polym. Degrad.*, 1993, **1**, 193-202.
18. D. K. Mandal, H. Bhunia, P. K. Bajpai, A. Kumar, G. Madhu and G. B. Nando, *J. Polym. Environ.*, 2017, **26**, 1061-1071.

19. P. K. Roy, P. Surekha, R. Raman and C. Rajagopal, *Polym. Degrad. Stab.*, 2009, **94**, 1033-1039.
20. S. Selke, R. Auras, T. A. Nguyen, E. Castro Aguirre, R. Cheruvathur and Y. Liu, *Environ. Sci. Technol.*, 2015, **49**, 3769-3777.
21. C. G. Schirmeister and R. Mulhaupt, *Macromol. Rapid. Commun.*, 2022, **43**, 2200247-2200288.
22. A. S. Burange, M. B. Gawande, F. L. Y. Lam, R. V. Jayaram and R. Luque, *Green. Chem.*, 2015, **17**, 146-156.
23. S. R. Chandrasekaran, B. Kunwar, B. R. Moser, N. Rajagopalan and B. K. Sharma, *Energy Fuels*, 2015, **29**, 6068-6077.
24. R. Miandad, M. Rehan, M. A. Barakat, A. S. Aburiazaiza, H. Khan, I. M. I. Ismail, J. Dhavamani, J. Gardy, A. Hassanpour and A.-S. Nizami, *Front. Energy Res.*, 2019, **7**, 1-17.
25. A. M. Al-Sabagh, F. Z. Yehia, G. Eshaq, A. M. Rabie and A. E. ElMetwally, *Egypt. J. Pet.*, 2016, **25**, 53-64.
26. A. Pifer and A. Sen, *J. Commum.*, 1998, **37**, 3306-3308.
27. X. Zhong, Y. Zhao, Y. Qian and Y. Zou, *Mater. Sci. Mater. Rev.*, 2017, **1**, 1-11.
28. J. Gu, H. Kim and H. Lim, *Energy Convers. Manag.*, 2022, **270**, 116256-116260.
29. Y. Miao, Y. Zhao, G. I. N. Waterhouse, R. Shi, L. Z. Wu and T. Zhang, *Nat. Commun.*, 2023, **14**, 4242-4250.
30. H. A. Maddah, *Am. J. Polym. Sci.*, 2016, **6**, 1-11.
31. G. W. Coates and Y. D. Y. L Getzler, *Nat. Rev. Mater.*, 2020, **5**, 501-516.
32. X. Jia, C. Qin, T. Friedberger, Z. Guan and Z. Huang, *J. Mater. Sci.*, 2016, **2**, 1-7.
33. J. Saleem, Z. K. B. Moghal, R. A. Shakoor, A. S. Luyt and G. McKay, *Polym.*, 2023, **15**, 3072-3085.
34. A. Rahimi and J. M. García, *Nat. Rev. Chem.*, 2017, **1**, 1-11.
35. A. Németh, M. Blazsó, P. Baranyai and T. Vidóczy, *JAAP*, 2008, **81**, 237-242.
36. N. Gascoin, A. Navarro-Rodriguez, P. Gillard and A. Mangeot, *Polym. Degrad. Stab.*, 2012, **97**, 1466-1474.
37. A. Ray, K. Zhu, Y. V. Kissin, A. E. Cherian, G. W. Coates and A. S. Goldman, *ChemComm*, 2005, 3388-3390.
38. F. Zhang, M. Zeng, R. D. Yapert, J. Sun, Y. Lee and A. LaPointe, *Science*, 2020, **23**, 437-441.

39. A. S. Goldman, A. H. Roy, Z. Huang, R. Ahuja, W. Schinski and M. Brookhart, *Science*, 2006, **312**, 257-261.
40. Z. Huang, E. Rolfe, E. C. Carson, M. Brookhart, A. S. Goldman, H. S. El-Khalafy and R. H. MacArthur, *Adv. Synth. Catal.*, 2010, **352**, 125-135.
41. L. C. Lerici, M. S. Renzini and L. B. Pierella, *Procedia Materials Science*, 2015, **8**, 297-303.
42. C. J. Adams, M. J. Earle and K. R. Seddon, *Green Chem.*, 2000, **2**, 21-24.
43. E. J. Borsig, *Pure Appl. Chem.*, 1999, **A36**, 1699-1704.
44. K. E. Russell, *Prog. Polym. Sci.*, 2002, **27**, 1007-1011.
45. K. Koo, P. F. Fu and M. T. J., *Macromolecules*, 1999, **32**, 981-993.
46. G. Xu and T. C. Chung, *J. Am. Chem. Soc.*, 1999, **121**, 6763-6766.
47. H. W. Bonne, P. S. Athey, M. J. Mullins, D. Philipp, M. R. and W. A. Goddard, *J. Am. Chem. Soc.*, 2002, **124**, 8790-8799.
48. J. B. Williamson, W. I. Czaplyski, E. J. Alexanian and F. A. Leibfarth, *Angew. Chem. Int. Ed.*, 2018, **57**, 6261-6265.
49. X. Shao, C. Xu, L. Lu and Q. Shen, *J. Org. Chem.*, 2015, **80**, 3012-3021.
50. T. J. Fazekas, J. W. Alty, E. K. Neidhart, A. S. Miller, F. A. Leibfarth and E. J. Alexanian, *Science*, 2022, **375**, 545-550.
51. L. Chen, K. G. Malollari, A. Uliana, D. Sanchez, P. B. Messersmith and J. F. Hartwig, *Chem*, 2021, **7**, 137-145.
52. C. Bae, J. F. Hartwig, N. K. B. Harris, R. O. Long, K. S. Anderson and M. A. Hillmyer, *J. Am. Chem. Soc.*, 2005, **127**, 767-776.
53. A. Bunescu, S. Lee, Q. Li and J. F. Hartwig, *ACS Cent. Sci.*, 2017, **3**, 895-903.
54. E. Bäckström, K. Odelius and M. Hakkarainen, *Ind. Eng. Chem. Res.*, 2017, **56**, 14814-14821.
55. M. M. Díaz-Requejo, P. Wehrmann, M. D. Leatherman, S. Trofimenko, S. Mecking, M. Brookhart and P. J. Pérez, *Macromolecules*, 2005, 4966-4969.
56. J. B. Eastwood, L. A. Hammarback, T. J. Burden, I. P. Clark, M. Towrie, A. Robinson, I. J. S. Fairlamb and J. M. Lynam, *Organometallics*, 2023, **42**, 1766-1773.
57. N. B. Boaen and M. A. Hillmyer, *Macromolecules*, 2003, **30**, 7027-7034.
58. J. Zawadiak, B. Orlińska and A. A. Marek, *J. Appl. Polym. Sci.*, 2013, **127**, 976-981.
59. Q. Wang, X. Yao, Y. Geng, Q. Zhou, X. Lu and S. Zhang, *Green Chem.*, 2015, **17**, 2473-2479.
60. E. L. Smith, A. P. Abbott and K. S. Ryder, *Chem. Rev.*, 2014, **114**, 11060-11082.

61. D. E. Crawford, L. A. Wright, S. L. James and A. P. Abbott, *Chem. Commun.*, 2016, **52**, 4215-4218.
62. C. Florindo, F. S. Oliveira, L. P. N. Rebelo, A. M. Fernandes and I. M. Marrucho, *ACS Sustain. Chem. Eng.*, 2014, **2**, 2416-2425.
63. M. A. R. Martins, S. P. Pinho and J. A. P. Coutinho, *J. Solution. Chem.*, 2018, **48**, 962-982.
64. R. Amoroso, F. Hollmann and C. Maccallini, *Molecules*, 2021, **26**, 6286-6301.
65. G. García, M. Atilhan and S. Aparicio, *Chem. Phys. Lett.*, 2015, **634**, 151-155.
66. P. Kalhor and K. Ghandi, *Molecules*, 2019, **24**, 4012-4049.
67. C. Seyler, C. Capello, S. Hellweg, C. Bruder, D. Bayne, A. Huwiler and K. Hungerbu1hler, *Ind. Eng. Chem. Res.*, 2006, **45**, 7700-7709.
68. Q. Wang, X. Yao, S. Tang, X. Lu, X. Zhang and S. Zhang, *Green Chem.*, 2012, **14**, 2559-2566.
69. Q. Zhang, K. De Oliveira Vigier, S. Royer and F. Jerome, *Chem. Soc. Rev.*, 2012, **41**, 7108-7146.
70. C. Ma, A. Laaksonen, C. Liu, X. Lu and X. Ji, *Chem. Soc. Rev.*, 2018, **47**, 8685-8720.
71. I. Bashir, A. H. Dar, K. K. Dash, V. K. Pandey, U. Fayaz, R. Shams, S. Srivastava and R. Singh, *Sustain. Chem. Pharm.*, 2023, **33**, 101102-101118.
72. T. Khezeli, A. Daneshfar and R. Sahraei, *J. Chromatogr. A.*, 2015, **1425**, 25-33.
73. E. S. C. Ferreira, C. M. Pereira and A. F. Silva, *J. Electroanal. Chem.*, 2013, **707**, 52-58.
74. A. P. Abbott, J. C. Barron, G. Frisch, S. Gurman, K. S. Ryder and A. Fernando Silva, *Phys. Chem. Chem. Phys.*, 2011, **13**, 10224-10231.
75. X. Li, M. Hou, B. Han, X. Wang and L. Zou, *J. Chem. Eng.*, 2008, **53**, 548-550.
76. H. Bowen, R. Durrani, A. Delavault, E. Durand, J. Chenyu, L. Yiyang, S. Lili, S. Jian, H. Weiwei and G. Fei, *Front. Chem.*, 2022, **10**, 912411-912421.
77. J. Cao, B. Qi, J. Liu, Y. Shang, H. Liu, W. Wang, J. Lv, Z. Chen, H. Zhang and X. Zhou, *RSC Advances*, 2016, **6**, 21612-21616.
78. Y. H. Choi, J. van Spronsen, Y. Dai, M. Verberne, F. Hollmann, I. W. Arends, G. J. Witkamp and R. Verpoorte, *Plant. Physiol.*, 2011, **156**, 1701-1705.
79. M. Hayyan, A. Abo-Hamad, M. A. AlSaadi and M. A. Hashim, *Nanoscale. Res. Lett.*, 2015, **10**, 1004-1015.
80. M. Zhou, O. A. Fakayode, A. E. Ahmed Yagoub, Q. Ji and C. Zhou, *Renew. Sust. Energ. Rev.*, 2022, **156**, 111986-112010.

81. R. Wang, T. Wang, G. Yu and X. Chen, *Polym. Deg. Stab.*, 2021, **183**, 1038-1046.
82. A. E. Ünlü, A. Arıkaya and S. Takaç, *Green Process. Synth.*, 2019, **8**, 355-372.
83. H. Wang, Z. Li, Y. Liu, X. Zhang and S. Zhang, *Green Chem.*, 2009, **11**, 1568-1575.
84. B. Liu, W. Fu, X. Lu, Q. Zhou and S. Zhang, *ACS Sustain. Chem. Eng.*, 2018, **7**, 3292-3300.
85. A. N. Paparella, S. Perrone, A. Salomone, F. Messa, L. Cicco, V. Capriati, F. M. Perna and P. Vitale, *Catalysts*, 2023, **13**, 1035-1054.
86. L. Liu, H. Yao, Q. Zhou, X. Yao, D. Yan, J. Xu and X. Lu, *J. Environ. Chem. Eng.*, 2022, **10**, 107512-107524.
87. X. Song, W. Hu, W. Huang, H. Wang, S. Yan, S. Yu and F. Liu, *J. Chem. Eng.*, 2020, **388**, 124324-124333.
88. K. Loos, R. Zhang, I. Pereira, B. Agostinho, H. Hu, D. Maniar, N. Sbirrazzuoli, A. J. D. Silvestre, N. Guigo and A. F. Sousa, *Front. Chem.*, 2020, **8**, 585-592.
89. H. Liu, J. T. Yu and C. Pan, *Chem. Commun. (Camb)*, 2021, **57**, 6707-6724.
90. D. Barnard, K. R. Hargrave and G. M. C. Higgins, *J. Chem. Soc.*, 1956, 2845.
91. R. L. Luck and N. K. Newberry, *J. Phys. Org. Chem.*, 2022, **35**, 4326-4340.
92. A. Ushakova, V. Zatsepin, M. Varfolomeev and D. Emelyanov, *J. Combust.*, 2017, **2017**, 2526596.
93. S. E. Balaghi, E. Safaei, L. Chiang, E. W. Wong, D. Savard, R. M. Clarke and T. Storr, *Dalton. Trans.*, 2013, **42**, 6829-6839.
94. Z. Ma, K. T. Mahmudov, V. A. Aliyeva, A. V. Gurbanov, M. F. C. Guedes da Silva and A. J. L. Pombeiro, *Coord. Chem. Rev.*, 2021, **437**, 213859-213887.
95. W. G. Barb, J. H. Baxendale, P. George and K. R. Hargrave, *Trans. Faraday Soc.*, 1951, **47**, 462-500.
96. A. Martinsson, M. Hasani, A. Potthast and H. Theliander, *Cellulose*, 2020, **27**, 7191-7202.
97. A. Martinsson, M. Hasani and H. Theliander, *Holzforschung*, 2023, **77**, 318-325.
98. S. M. Mitroka, T. D. Smiley, J. M. Tanko and A. M. Dietrich, *Polym. Degrad. Stab.*, 2013, **98**, 1369-1377.
99. C. Tang, X. Qiu, Z. Cheng and N. Jiao, *Chem. Soc. Rev.*, 2021, **50**, 8067-8101.
100. A. N. CAMPBELL and S. S. STAHL, *Acc. Chem. Res.*, 2011, **45**, 851-863.
101. A. A. Andia, M. R. Miner and K. A. Woerpel, *Org. Lett.*, 2015, **17**, 2704-2707.
102. Y. Yan, P. Feng, Q. Z. Zheng, Y. F. Liang, J. F. Lu, Y. Cui and N. Jiao, *Angew. Chem. Int. Ed. Engl.*, 2013, **52**, 5827-5831.

Chapter 2

Oxidation of model small molecule polyolefin, squalane, and selective depolymerisation of LDPE using deep eutectic solvents

2.1 Abstract

Petroleum-based synthetic polymers in the form of plastics are ubiquitous in modern society, however, there exists an imbalance between their production and end-of-life treatment. This linear approach to resource utilisation, a result of largely inefficient and unsustainable disposal practices, generates 200 million metric tonnes of plastic waste annually.[103, 104] Among the wide range of plastics produced, polyolefins account for nearly half of the global demand on account of their versatility, low cost and exceptional durability.[5] Diverse branching structures, resulting in varying mechanical properties, together with their hydrophobic nature and chemical inertness means polyolefins contribute to a substantial share of environmental plastic waste pollution.[105] With near identical densities mixed polyolefin waste is challenging to separate and as a consequence often leads to downcycling and a loss of value. Chemical recycling techniques are being developed to handle polyolefin waste, but state-of-the-art approaches are energy-inefficient and/or require unsustainable metal-based catalysts. Tuneable DES, formed from various HBD and HBA, are presented as an alternative method to depolymerise polyolefins under mild conditions.[59] The DES substrates form a dual solvent-catalyst system alleviating the need for traditional harmful organic solvents during processing while maximising catalyst loading, both of which increase the scalability and efficiency of the polyolefin oxidation. Initial studies examined the aerobic oxidation of squalane, a model small molecule for polyolefins, before demonstrating the selective depolymerisation of LDPE.

2.2 Introduction

Polyolefins are a versatile and well-established class of polymers known for their affordability and exceptional properties. Derived from olefin monomeric units, such as ethylene and propylene, polyolefins find widespread applications across an array of industries and display a range of properties suitable for flexible lightweight films to durable construction materials.[5] Polyolefins exhibit remarkable stability towards degradation thanks to their non-polar homogeneous carbon-carbon composition meaning they can withstand high levels of UV radiation and thermal exposure before degrading.[31, 106] However, in order to increase the circularity of their lifecycle it is essential to achieve effective recycling techniques. Mechanical recycling is one of the most frequently employed methods of recycling plastics, however, with nearly identical compositions traditional density-based separation methods prove ineffective for polyolefins and result in the downcycling of the recovered polymers.[12] While current chemical recycling methods such as pyrolysis offer some value recovery in the form of complex oils and waxes, ultimately the processes are energy-intensive and require expensive facilities.[11, 23]

The lack of functionality within the polyolefin chain precludes targetable chain scission reactions, limiting the potential to depolymerise back into monomeric units. The depolymerisation of PET into its monomer BHET by glycolysis of the internal ester bond is a prime example of selectively targeting degradable functional groups along the polymer chain.[25, 84, 107]

Post-polymerisation modifications represent an attractive strategy for the preparation of polymers bearing a select range of functionalities that are more susceptible to selective thermal degradation or that are more applicable to upcycling. Notably, several studies have investigated the functionalisation of polyolefins. Radical chain transfer has been employed for the

chemoselective placement of ionic functional groups onto polyolefins in the absence of completing chain scission reactions.[108] Hartwig *et al.* reported the successful regiospecific functionalisation of a variety of commercial PP using a rhodium-catalysed borylation followed by oxidation to form alcohol functionality. Importantly, hydroxyl groups are exclusively positioned at the terminus of the polymer side chains and not on the backbone. [52] Hartwig also employed a nickel-based catalyst in the presence of ^{m}CPBA for the hydroxylation of PE. A maximum of 5.5 mol% oxygen-containing functional groups were incorporated for every 100 monomer units, however, alcohol formation was favoured compared to ketone groups.[53]

DES have emerged as a promising alternative to traditional harmful organic solvents for chemical synthesis.[59] These innovative solvents are created by the complexation of an HBD with a HBA, typically a hydrated metal salt. A lowered lattice energy, a result of delocalisation through hydrogen bonding, creates a depression in the solvent's melting temperature (the eutectic point) relative to its individual components forming the eutectic mixture.[68] DES exhibit tailorable Lewis/Bronsted acidic character making for unique catalytic activity in addition to their excellent recoverability, biodegradability, low volatility and non-toxicity.[68] Interestingly, unlike traditional organic solvents whose sole purpose is to act as the reaction media, DES have the capability to act as both the solvent and the catalysts creating a unique dual solvent-catalyst system that maximises catalyst loading. DES have many reported applications, for instance, metal plating[73, 74] gas adsorption[75] protein extraction[76] and biotransformations[78] as well as depolymerisation catalysts. Zhou and co-workers reported the synthesis of dioctyl terephthalate through the alcoholysis of PET using ChCl-based DES alongside a range of metal salts, obtaining 100% PET conversion in 5 h with $Zn(OAc)_2$.[81] Wang *et al.* reported the glycolysis of PET catalysed by various urea-metal salt DES, achieving full PET conversion with an 83% yield of their targeted BHET monomer under moderate reaction conditions (170 °C).[82, 83] There have been no reports in the literature where DES have been applied for the depolymerisation of

polyolefins. Herein, is the reported oxidation of model polyolefin, squalane, and the selective depolymerisation of LDPE as well as the nonselective depolymerisation of both LDPE and HDPE via aerobic oxidation catalysed by dual solvent-catalyst DES.

2.3 Results and discussion

2.3.1 Type IV DES

All DES were synthesised following procedures adapted from literature.[109] A type IV DES was synthesised by reacting the appropriate ratios of acetamide, with the hydrated metal salt, manganese chloride tetrahydrate. Previous work by X. Lai *et al.* reported the synthesis of novel [Acetamide]$_7$[$MnCl_2 \cdot 4H_2O$] DES exhibiting a freezing point depression of 27.5 °C, noticeably lower than that of its respective starting materials.[109]

2.3.1.1 Preparation of [Acetamide]$_7$[$MnCl_2 \cdot 4H_2O$]

The successful formation of the DES was confirmed through comparative Fourier transform-infrared (FT-IR) analysis against its starting materials. A broad peak was observed near 3000−3500 cm^{-1} which is indicative of hydrogen bonding between the acetamides amide N−H and the O−H group present in the hydrated metal salt. When the spectrum of free acetamide was compared with the [Acetamide]$_7$[$MnCl_2 \cdot 4H_2O$] DES, a shift to lower wavenumbers can be seen in the characteristic signal of the carbonyl group (1670 to 1649 cm^{-1}), this is a consequence of supramolecular complex formation characteristic of DES (Figure 2.1). Acetamide can form resonance structures, therefore, has the potential to donate to the metal through its carbonyl or amine group, hence, the shift in the carbonyl peak to a lower wavenumber can be explained through the formation of metal ion-oxygen complexes reducing Mn^{2+} and Cl^- interactions causing a depression in the DES melting point.

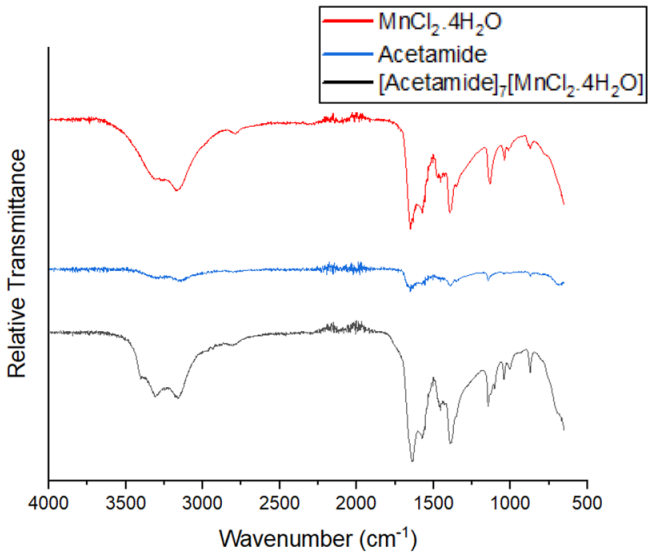

Figure 2.1 Experimental FT-IR of [Acetamide]$_7$[$MnCl_2$·$4H_2O$] and its pure components: Acetamide and $MnCl_2$·$4H_2O$

2.3.1.2 Thermal properties of [Acetamide]$_7$[$MnCl_2$·$4H_2O$]

The thermodynamic characteristics of DES, such as their thermal decomposition temperature, phase transitions and heat capacity, are vital to understanding their potential applications, nevertheless, there is little information documented within the literature.

The thermal behaviour of [Acetamide]$_7$[$MnCl_2$·$4H_2O$] was evaluated using differential scanning calorimetry (DSC) analysis from −80 °C to 180 °C probing thermally induced phase transformations (Figure 2.2a). A glass transition (T_g) is observed at −26.5 °C signifying a change in heat capacity corresponding to the structural change of the DES from a glass-like state to a rubber-like state or vice-versa. The T_g shifts to higher temperatures with an increased number of scans, a result of water evaporating from the DES. Water creates a plasticising effect, therefore causing the T_g to increase upon dehydration. In addition to the glass transition, three complex endothermic peaks are observed corresponding to melting events. The melting peaks at T_m = 47 °C and T_m' = 61 °C are representative of the DES and $MnCl_2$.4H2O respectively,

while the peak at T_m" = 155 °C corresponds to the decomposition of the DES, whose decomposition is also observed by thermogravimetric analysis (TGA). This decomposition resulted in not complementary crystallisation peak being observed upon cooling.

TGA was used to demonstrate the thermal stability of the DES *i.e.* the maximum temperature at which the weight of the DES is maintained without decomposition from its liquid phase and therefore, the active range at which the DES can be used as a solvent. Interestingly, the [Acetamide]$_7$[$MnCl_2$·$4H_2O$] DES decomposition temperature (T_{onset}) is lower than that of its pure components: acetamide (105 °C) and $MnCl_2.4H_2O$ (95 °C) (Figure 2.2b). The premature decomposition may be explained by the evaporation of water, when dehydrated the DES does not have sufficient sites for hydrogen bonding and for that reason breaks down into its individual components, creating the step-like decomposition profile.

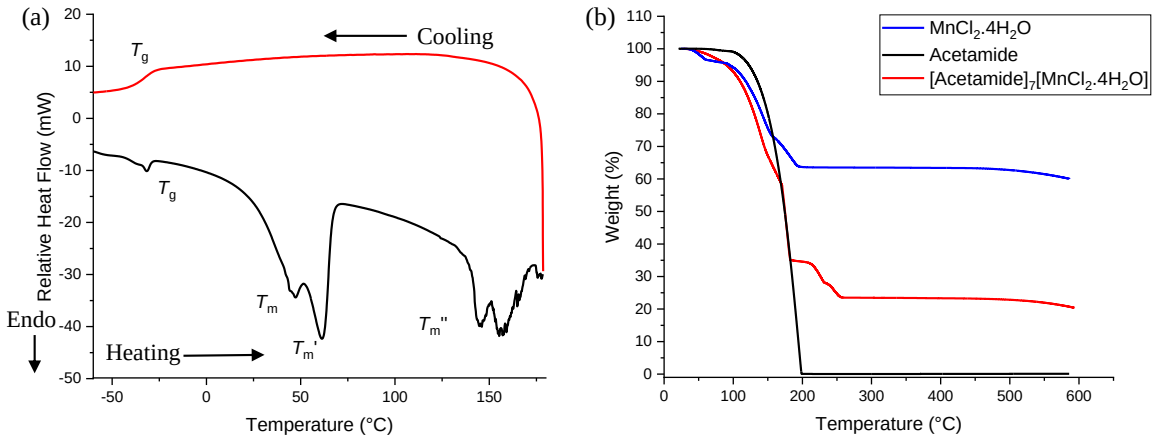

Figure 2.2 (a) DSC thermograms for the first heating cycle (bottom) and the first cooling cycle (top) of [Acetamide]$_7$[$MnCl_2$·$4H_2O$] DES between −80 and 180 °C (b) Dynamic TGA curves of acetamide, $MnCl_2.4H_2O$ and DES [Acetamide]$_7$[$MnCl_2$·$4H_2O$] performed at a heating rate of 10 °C.min^{-1}

2.3.1.3 Thermal properties of $[Octa]_7[MnCl_2{\cdot}4H_2O]$ and $[Octa]_7[FeCl_2{\cdot}4H_2O]$

With the successful formation of the acetamide DES, a comparable octadecanamide DES was synthesised, reasoning that the long non-polar alkyl chain aids in the hydrophobicity of the DES for better interaction with non-polar polyolefins. $[Octa]_7[MnCl_2{\cdot}4H_2O]$ and $[Octa]_7[FeCl_2{\cdot}4H_2O]$ were synthesised following a similar procedure as described for $[Acetamide]_7[MnCl_2{\cdot}4H_2O]$. Octadecanamide ($T_m$ = 102 °C) was combined with $MnCl_2{\cdot}4H_2O$ (T_m = 58 °C), and $FeCl_2{\cdot}4H_2O$ (T_m = 105 ºC) in their respective vessels and gently stirred at 130 °C for 30 min until viscous homogeneous liquids formed.

DSC analysis was used to characterise the phase transformations for $[Octa]_7[MnCl_2{\cdot}4H_2O]$ (Figure 2.3a). A T_g was not observed as seen for $[Acetamide]_7[MnCl_2{\cdot}4H_2O]$ but rather a complex endothermic melting peak from T_m = 74 °C to 108 °C and a corresponding exothermic crystallisation peak (T_c), from 62 °C to 101 °C. The T_m near 108 °C relates to the ambient crystal structure of octadecanamide as confirmed by analysing the peak integrals with respect to the DSC of octadecanamide. On the other hand, the T_m at 62 °C does not relate to a known phase of $MnCl_2{\cdot}4H_2O$ and is thus unique to the DES structure. The similarities shown between the crystallisation and melting peaks are uncommon for such DES systems as melting is a purely thermodynamic process while crystallisation is affected by both thermodynamic and kinetic factors influencing crystal growth. Therefore, such similarities indicate high thermal stability. The primary cooling and heating cycles of $[Octa]_7[FeCl_2{\cdot}4H_2O]$ showed two melting peaks centred at T_m = 66 and T_m' = 104 °C. The second of those peaks relate to the ambient crystal

structure of octadecanamide, however, the first does not relate to any known phase for $FeCl_2{\cdot}4H_2O$ and is, therefore, a product of the DES formation (Figure 2.3).

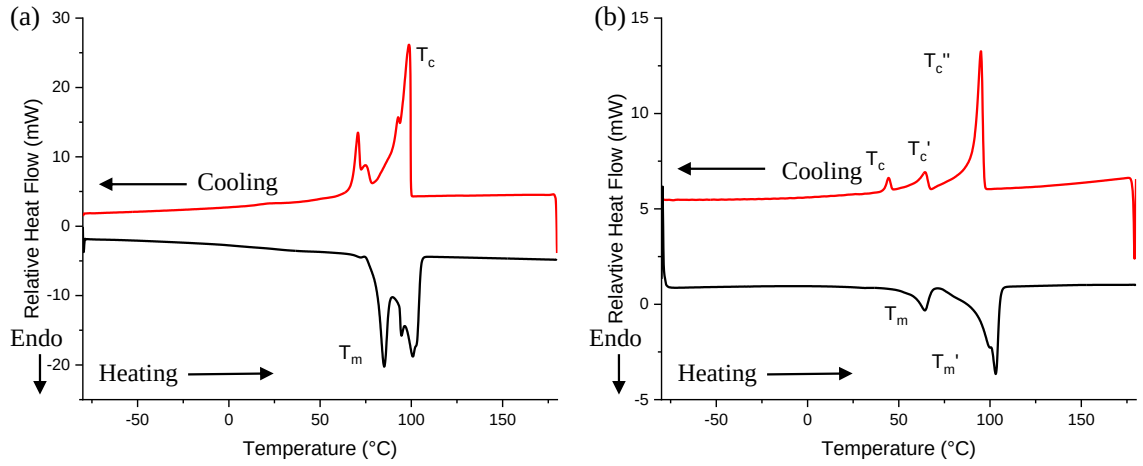

Figure 2.3 DSC thermograms of the first heating (bottom) and cooling (top) cycle between −80 and 180 °C at a heating rate of 10 °C·min^{-1} for (a) $[Octa]_7[MnCl_2{\cdot}4H_2O]$ and (b) $[Octa]_7[FeCl_2{\cdot}4H_2O]$

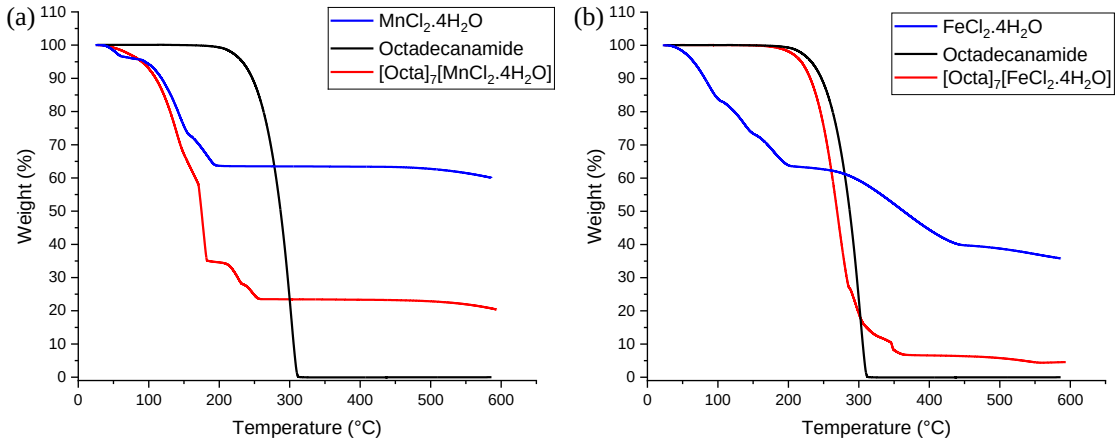

Figure 2.4 Dynamic TGA curves for (a) Octadecanamide, $MnCl_2{\cdot}4H_2O$ and DES $[Octa]_7[MnCl_2{\cdot}4H_2O]$ and (b) Octadecanamide, $FeCl_2.4H_2O$ and DES $[Octa]_7[FeCl_2{\cdot}4H_2O]$ from -80 to 180 °C with a heating rate of 10 °C·min^{-1}

The thermal stability of the $[Octa]_7[MnCl_2{\cdot}4H_2O]$ and its pure constituents were determined by TGA analysis (Figure 2.4a). Mass loss begins immediately upon heating: a lower temperature than for both octadecanamide (207 °C) and $MnCl_2{\cdot}4H_2O$ (95 °C). The step-like nature of the DES decomposition reflects contributions from both components of the eutectic mixture: first

the decomposition of $MnCl_2{\cdot}4H_2O$ followed by octadecanamide. Unlike $[Octa]_7[MnCl_2{\cdot}4H_2O]$, where the onset decomposition temperature of its pure constituents is greater than that of the eutectic liquid, $[Octa]_7[FeCl_2{\cdot}4H_2O]$ onset decomposition temperature (194 °C) is an intermediate between both its starting materials, octadecanamide (207 °C) and $FeCl_2{\cdot}4H_2O$ (37 °C) which is more common for DES (Figure 2.4b). This observation suggests overall good thermal stability.

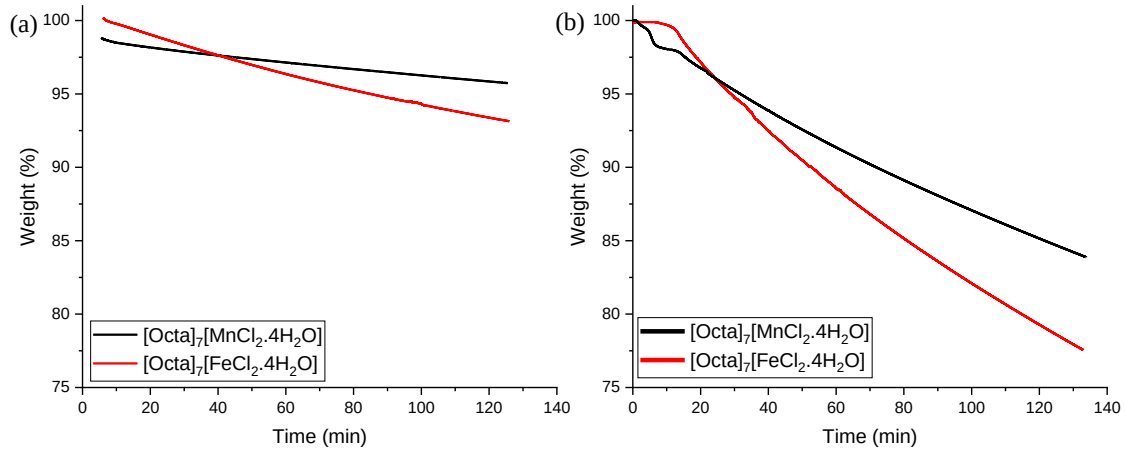

Figure 2.5 Isothermal curve for DES $[Octa]_7[MnCl_2{\cdot}4H_2O]$ and $[Octa]_7[FeCl_2{\cdot}4H_2O]$ over 2 h at (a) 140 °C (b) 160 °C

Isothermal TGA analysis of both octadecanamide-based DES was conducted at 140 °C and 160 °C to assess their long-term thermal stability in high-temperature reactions (Figure 2.5a and 2.5b). Linear weight versus time dependence was observed for both DES over the 2 h run time. At 160 °C 15 and 25% weight loss was recorded while at 140 °C weight loss of 7 and 4% was measured for $[Octa]_7[FeCl_2{\cdot}4H_2O]$ and $[Octa]_7[MnCl_2{\cdot}4H_2O]$ respectively. High levels of weight loss over a short period at temperatures lower than their stated onset decomposition temperatures obtained by dynamic TGA indicate an overestimation of the thermal stability of the DES. This could have negative implications for their use in catalytic reactions by lowering the operational temperature.

2.3.1.4 Amide-based DES catalysed oxidation of squalane

The [Acetamide]$_7$[$MnCl_2 \cdot 4H_2O$] DES was employed to act as both the catalyst and solvent for the oxidation of a model polyolefin substrate (Scheme 2.1). Squalane ($C_{30}H_{62}$) was chosen for its similar chemical and physical properties to PE, alongside its simplicity and low cost. The non-polar properties of squalane compared to the polar nature of [Acetamide]$_7$[$MnCl_2 \cdot 4H_2O$] caused squalane to phase separate as an immiscible layer on top of the DES. Agitation by stirring at 500 RPM was used to help disperse squalane droplets in a continuous liquid phase, creating more favourable conditions to achieve a high interfacial area and therefore interphase mass transfer and improved reaction kinetics. A steady flow of air was bubbled through the reaction mixture at elevated temperatures to both aid in achieving a higher interfacial area and encourage oxygen transfer. A cold trap was also installed to collect any volatiles (i.e., low-mass degradation products) which escape during the process. After reacting for 10 days at 180 °C, the liquid DES solidified, this can be explained by the loss of water from the complex (collected in the cold trap). This corroborates earlier data that suggests the loss of water for the DES at elevated temperatures. FT-IR spectroscopic analysis of the remaining squalane showed no indication of oxidation, but instead unreacted squalane.

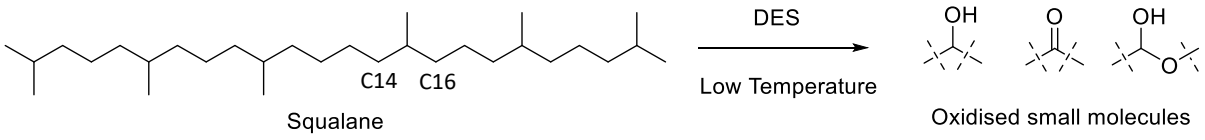

Scheme 2.1 General reaction scheme for the DES catalysed depolymerisation of model polyolefin, squalane, into oxidised small molecules

The same reaction was performed at 70 °C but in the absence of bubbling air to minimise water loss. However, again after 10 days the DES solidified, and FT-IR analysis showed no oxidation

of squalane. The solidification of the DES creates a biphasic mixture which minimises interfacial surface area reducing interactions at catalytically active sites lowering the overall activity. The solidification is not unexpected when considering the previously stated lack of thermal stability the DES face with prolonged heating.

Substituting the small molecule acetamide for a more hydrophobic C_{18}-chain amide octadecanamide lessens the DES polarity overcoming the miscibility issues encountered when mixing [Acetamide]$_7$[$MnCl_2{\cdot}4H_2O$] and squalane. When [Octa]$_7$[$FeCl_2{\cdot}4H_2O$] was combined with squalene, a homogenous mixture formed and the reaction mixture was then heated at 140, 160 and 180 °C in air and after 24 h, 1%, 24.4%. and 17.2% 9-otadecenoic acid (Z)-,2,3-bis(acetyloxy)propyl ester was formed respectively as the sole product. This triester species was isolated through column chromatography and characterised by ^{1}H nuclear magnetic resonance (NMR) spectroscopy (Figure 2.6) and gas chromatography-mass spectrometry (GC-MS) analysis (Figure 2.7). Although the product had already been passed through a silica column and an aluminium plug to remove the DES, residual paramagnetic Mn^{2+} present in the sample caused a significant broadening of proton signals in the ^{1}H NMR spectrum. Furthermore, this prevented the acquisition of a suitable ^{13}C NMR spectrum for the sample.

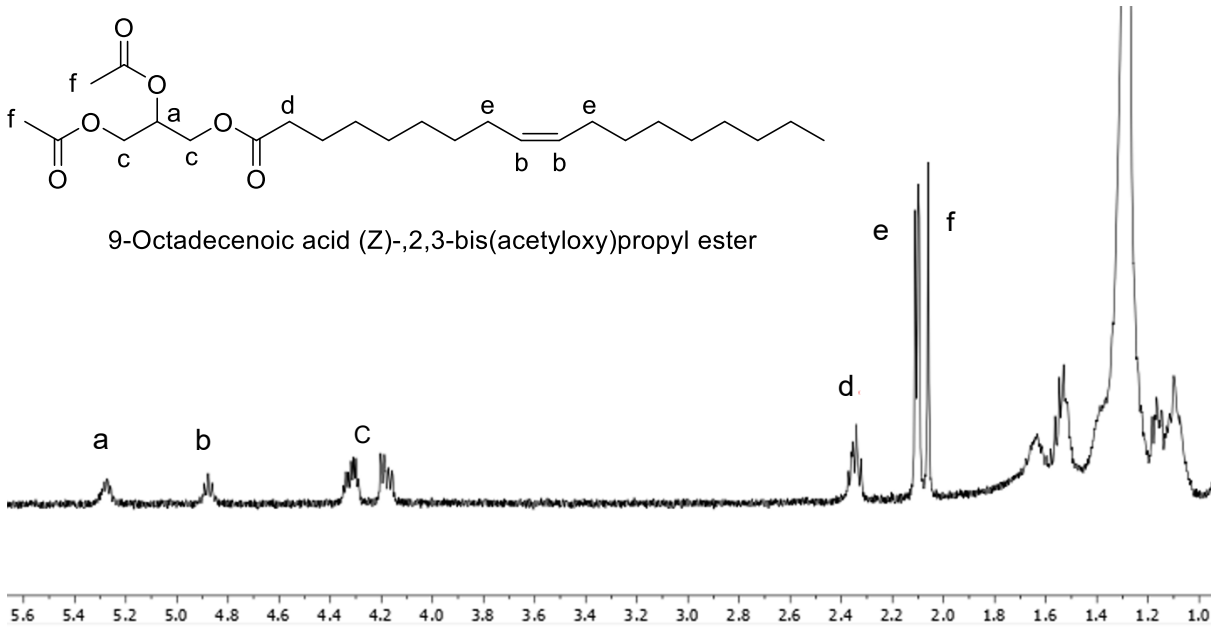

Figure 2.6 ^{1}H NMR spectrum of 9-Octadecenoic acid (Z)-,2,3-bis(acetyloxy)propyl ester product (400 MHz, $CDCl_3$, 298K)

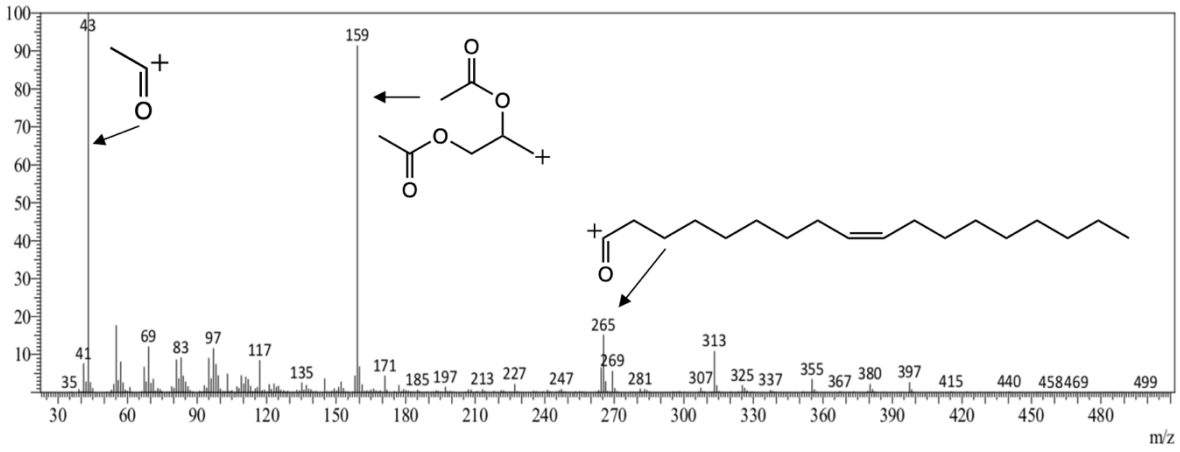

Figure 2.7 Mass spectrum of 9-Octadecenoic acid (Z)-,2,3-bis(acetyloxy)propyl ester

The trend in triester formation was found to be correlated to the mole ratio of octadecanamide present in the DES as the same triester (13.2%) was formed by heating $[Octa]_7[MnCl_2{\cdot}4H_2O]$ and squalane to 160 °C for 24 h. To exclude the possibility that the triester was derived from the DES, a control experiment was performed by heating only the DES under the same reaction conditions. According to GC-MS analysis of the reaction mixture, the triester species is not

formed, however, octadecanamide is dehydrating to its nitrile species and undergoing further reactions to form the corresponding carboxylic acid. Since the decomposition of the DES is not responsible for the triester formation, the octadecanamide is likely reacting with squalane and/or its oxidation products. The lack of thermal stability coupled with the minimum temperature required to keep the DES liquid created an incompatible environment for a successful reaction necessitating a new approach.

2.3.2 Choline chloride-based DES

2.3.2.1 Hydrogen bond donor screen

In an attempt to create a thermally stable DES several ChCl based DES were synthesised (Table 2.1). All DES were synthesised by combining different stoichiometric ratios of the HBA (choline chloride) with the HBD (metal salts) and stirring at 90 °C until a homogeneous mixture was formed. ChCl (2-hydroxyethyl-trimethylammonium chloride) is a naturally occurring bifunctional quaternary ammonium salt and when combined with a HBD density functional theory (DFT) calculations demonstrated its effectiveness at lowering the lattice energy of both homocouples.[110] The electronegative chloride anion provides a greater number of binding sites suitable for hydrogen bonding subsequently creating a delocalisation of charge. The use of ChCl contributes biodegradability, biocompatibility and affordability to the DES system making it of particular interest within “green” sustainable chemistry. Cobalt, manganese and iron metal salts were used as HBD owing to their propensity to catalyse photo and thermal oxidation reactions.[111, 112]

Table 2.1 Series of choline chloride-based DES with varying ChCl: HBD ratios

DES	**ChCl: HBD**	**Physical State at 90 ºC**
ChCl: $MnCl_2{\cdot}4H_2O$	1:2, 1:3, 2:1, 3:1	Viscous pink liquid/yellow liquid
ChCl: $FeCl_2{\cdot}4H_2O$	1:2, 1:3	Brown solid
ChCl: $FeCl_3$	1:2, 1:3	Viscous brown liquid
ChCl: $CoCl{\cdot}6H_2O$	1:2, 1:3	Blue liquid
ChCl: $FeCl_3{\cdot}6H_2O$	1:2, 1:3	Brown liquid

The FT-IR spectra for DES $[ChCl]_2[CoCl_2{\cdot}6H_2O]_3$ and $[ChCl]_2[MnCl_2{\cdot}4H_2O]$ were obtained to better understand their bonding interactions (Figure 2.8a and 2.8b). Broad overlapping bands between 2950 cm^{-1} and 3520 cm^{-1} encompass the O–H and N–H stretching vibrations. The O–H stretch of $[ChCl]_2[CoCl_2{\cdot}6H_2O]_3$ (3521 cm^{-1}) is at a lower wavenumber compared to the 3530 cm^{-1} O–H stretching of pure $CoCl_2{\cdot}6H_2O$. The reason for this shift is likely due to strong hydrogen bonding within the DES causing a decrease in O–H stretching frequencies.

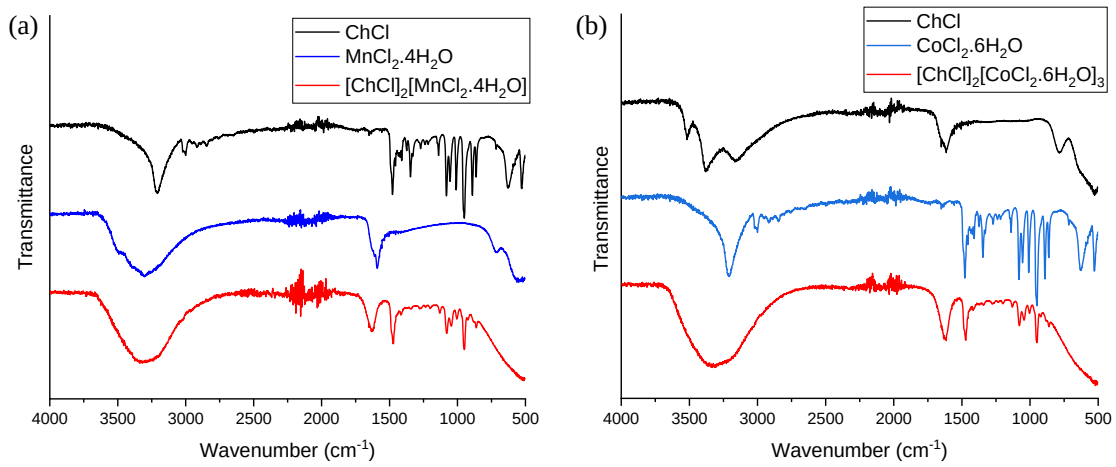

Figure 2.8 (a) FT-IR spectra of $[ChCl]_2[MnCl_2{\cdot}4H_2O]$ and its pure components: ChCl and $MnCl_2{\cdot}4H_2O$ (b) FT-IR spectra of $[ChCl]_2[CoCl_2{\cdot}6H_2O]_3$ and its pure components: ChCl and $CoCl_2{\cdot}6H_2O$

2.3.2.2 Thermal properties of $[ChCl]_2[MnCl_2{\cdot}4H_2O]$ and $[ChCl]_2[CoCl_2{\cdot}6H_2O]_3$

During the first heating and cooling cycle of DES $[ChCl]_2[MnCl_2{\cdot}4H_2O]$ between −80 °C and 180 °C, an endothermic melting peak at 7 °C and an exothermic crystallization peak at −3 °C were observed (Figure 2.9). These transitions are not related to the ambient crystal structure of ChCl or $MnCl_2{\cdot}4H_2O$, indicating the complete formation of the DES and reasonable thermal stability. A DSC curve of $[ChCl]_2[CoCl_2{\cdot}6H_2O]_3$ was not obtained owing to the lack of thermal stability evident by its TGA profile.

DES $[ChCl]_2[CoCl_2{\cdot}6H_2O]_3$ displays a distinct multi-stage decomposition in a step-like pattern, this is not surprising given the low thermal stability of $CoCl_2{\cdot}6H_2O$ (Figure 2.23a). Conversely, $[ChCl]_2[MnCl_2{\cdot}4H_2O]$ exhibits superior thermal stability. $[ChCl]_2[MnCl_2{\cdot}4H_2O]$ losses an initial 5% of its weight, thought to be caused by the evaporation of water, before remaining stable until 281 °C where it undergoes a single weight loss transition (Figure 2.10b).

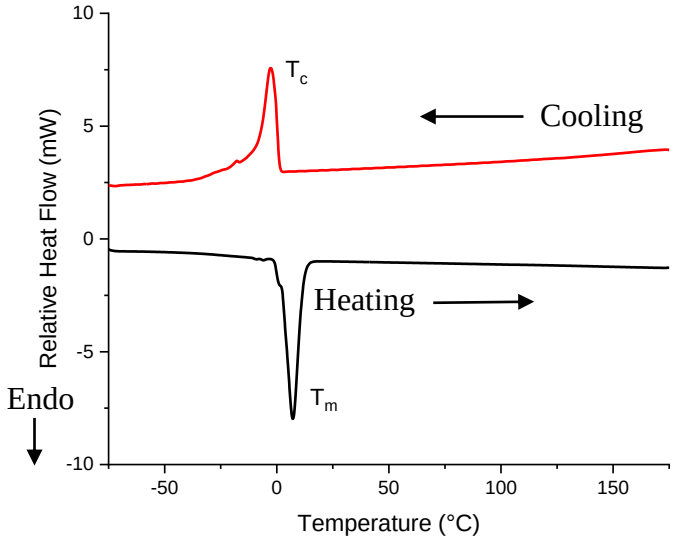

Figure 2.9 DSC thermograms for the first heating (bottom) and cooling (top) cycle of $[ChCl]_2[MnCl_2{\cdot}4H_2O]$ DES

The 90 °C isothermal profile of $[ChCl]_2[CoCl_2{\cdot}6H_2O]_3$ and $[ChCl]_2[MnCl_2{\cdot}4H_2O]$ revealed both DES exhibits divergent stabilities (Figure 2.10a). After an initial 3% weight loss the mass of $[ChCl]_2[MnCl_2{\cdot}4H_2O]$ plateaus for the remainder of the 2 h run time unlike $[ChCl]_2[CoCl_2{\cdot}6H_2O]_3$ whose mass has already lost 6% before reaching 90 °C. Upon reaching 90 °C $[ChCl]_2[CoCl_2{\cdot}6H_2O]_3$ loses a further 16% weight over 2 h. It is possible that because of the hygroscopic nature of choline chloride, the initial sudden weight loss equates to the evaporation of exogenous water. The faster the heating rate the higher the temperature at which water will evaporate, therefore, repeating the TGA analysis at different heating rates would allow for a better understanding of this process. Much like the trends found for the above amide-based DES systems, an overestimation of the thermal stability for the ChCl-based DES was noted.

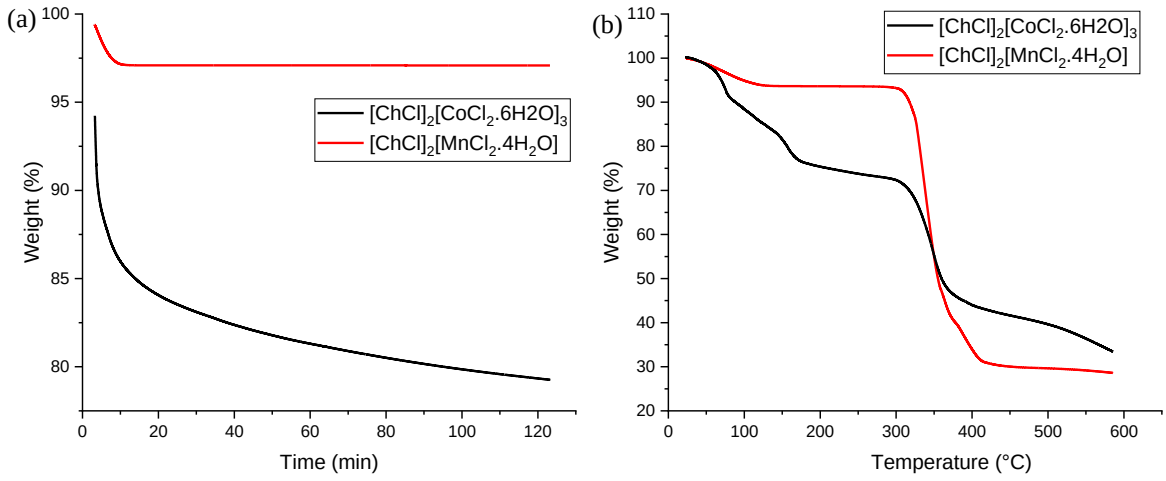

Figure 2.10 (a) Isothermal curve for DES $[ChCl]_2[MnCl_2{\cdot}4H_2O]$ and $[ChCl]_2[CoCl_2{\cdot}6H_2O]_3$ at 90 °C for 2 h. (b) Thermogravimetric analysis of $[ChCl]_2[MnCl_2{\cdot}4H_2O]$ and $[ChCl]_2[CoCl_2{\cdot}6H_2O]_3$ from 0 - 600 °C at a heating rate of 10 °C·min^{-1}

2.3.3.2 Choline chloride-based DES catalysed oxidation

ChCl when employed as an HBA has extensive compatibility with a diverse range of HBDs allowing for tailorable physicochemical properties while remaining environmentally friendly. Iron, manganese and cobalt lewis acids were chosen as HBDs as a consequence of their previously reported propensity to catalyse both photo- and thermal-oxidative processes. Specifically, Fe-based catalysts have shown activity for C-H activation and/or oxidation and Mn and Co-based catalysts have displayed good catalytic activity for both photo- and thermal-oxidative processes.[111]

Since the previous dynamic TGA results indicated a lack of thermal stability, the following oxidation reactions were performed at temperatures less than 100 °C to minimise the evaporation of water and subsequent loss of hydrogen bonding within the DES. Each DES was combined with squalane and heated to 90 °C for 14 days. It is important to note that squalane when heated alone, did not undergo oxidation at this temperature.

The structural changes in squalane subjected to thermal oxidation were monitored by FT-IR spectroscopy, which detects the presence of carbonyl groups not found in the starting material. The carbonyl index (CI) measures the carbonyl absorbance band relative to a reference peak.[113] It is calculated using the generalised SAUBI CI formula:

$$\text{Carbonyl Index (CI)} = \frac{\text{Area under band } 1{,}850 - 1{,}650\ \text{cm}^{-1}}{\text{Area under band } 1{,}500 - 1{,}420\ \text{cm}^{-1}} \quad (2)$$

Specifically, the SAUB CI formula measures the integration of the carbonyl absorbance band between 1,850 – 1,650 cm^{-1} and the methylene scissoring peak between 1,500 – 1,420 cm^{-1}.

Using the SAUBI formula the CI was plotted for the accelerated oxidation of squalane in the presence of various DES over the course of 14 days (Figure 2.11a).

Experiments using catalyst blends of varying composition confirm the synergy between the HBD and HBA, as stoichiometric ratios were found to have a considerable effect on the oxidative ability of the DES. After optimisation, $[ChCl]_2[CoCl_2{\cdot}6H_2O]_3$ and $[ChCl]_2[MnCl_2{\cdot}4H_2O]$ DES lead to the greatest carbonyl group incorporation. After a 14-day reaction at 90 °C, Mn and Co-based DES were found to be the most effective oxidants. $[ChCl]_2[MnCl_2{\cdot}4H_2O]$ resulted in a maximum squalane conversion of 32% and a carbonyl index of 2.01, while $[ChCl]_2[CoCl_2{\cdot}6H_2O]_3$ resulted in a maximum squalane conversion of 37% and a carbonyl index of 2.69 (Figure 2.11c). It is important to note that aerobic oxidation is occurring (oxidation using molecular free oxygen from the air) in the absence of an external oxidant. The same reactions were performed under an inert nitrogen atmosphere and FT-IR analysis gave no indication of oxygen-containing functionality while GC-MS analysis determined that 100% unreacted squalane remained.

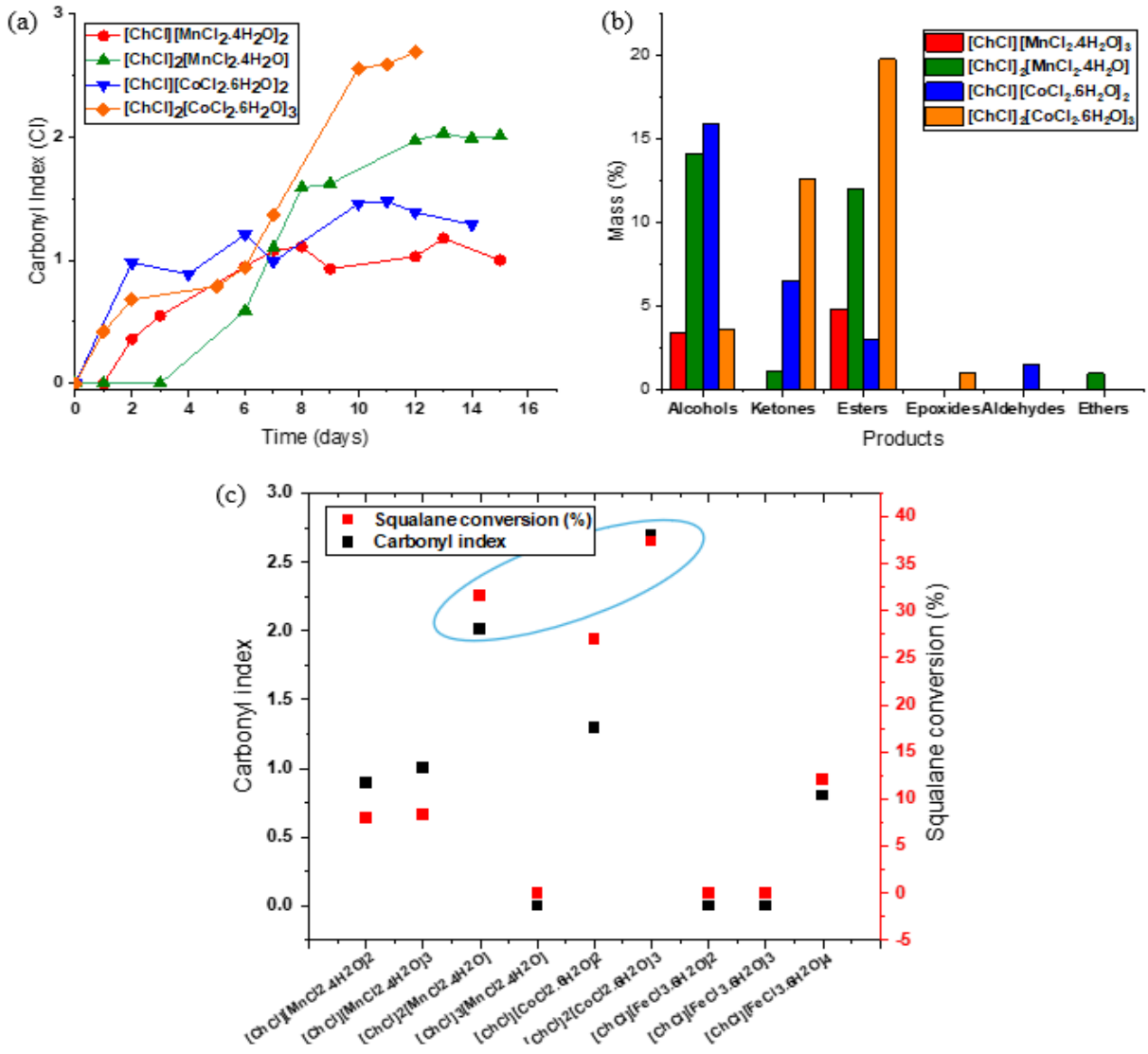

Figure 2.11 (a) Carbonyl index as a function of time for each DES system with squalane over a minimum of 14 days at 90 °C. (b) Oxidised product distributions identified by GC-MS analysis in $CHCl_3$ for each DES with squalane at 90 °C. (c) Comparison of each DES with the percentage of squalane converted and the carbonyl index achieved after 14 days at 90 °C

Interestingly the product distributions vary for each system and there is a notable 5-day induction period for $[ChCl]_2[MnCl_2{\cdot}4H_2O]$ catalysed reactions. Common in certain catalytic reactions, induction periods can occur when the catalytically active species is not initially present. In such cases, the DES acts as a pre-catalyst until it forms the active species, allowing the oxidation or proceed. It is also possible that the induction period is caused by: the direct

reaction of triple oxygen with singlet closed-shell molecules or the presence of (sub)parts per billion of molecules more easily cleaved or because of the competitive $RH + O_2 + RH \rightarrow R^{\bullet}\ H_2O_2 + R^{\bullet}$ reaction.

The large activation time associated with the oxidation may be a consequence of the slow oxidation of Mn^{2+}, Co^{2+} and Fe^{2+} to their less stable and more oxidatively active Mn^{3+}, Co^{3+} and Fe^{3+} oxidation states. All the metals in their 3+ oxidation state can be reduced by gaining an electron from another species, which in exchange is oxidised. Based on this hypothesis it is not surprising that cobalt and manganese DES display superior oxidation activity rivalled by their iron DES monologue when considering the redox potential of the metals. Mn^{3+} and Co^{3+} have high redox potentials (+1.51 V and +1.82 V respectively) while Fe^{3+} has a low redox potential (+0.77 V). The higher the redox potential of the metal the greater the tendency for the species to gain an electron and therefore, the stronger the oxidising agent.

The thermal degradation of squalane in the absence of any catalyst generates a complex product distribution of twenty-five various alcohols, aldehydes, ketones, esters, acids, and light hydrocarbons, of which light hydrocarbons and alcohol are the most dominant species. In contrast, the DES-catalysed reactions display a greater proportion of ketone and ester-containing products (Figure 2.11b). 1-Hexadecanol, 3,7,11,15-tetramethyl and 2-pentadecanone, 6,10,14-trimethyl are the two highest yielding oxidation products (by mass%). Notably, this revealed that the reaction at the secondary carbon positions (C14 and C16) of squalane are favoured despite producing a less stable secondary carbocation intermediate compared to the more favourable and stable tertiary carbocation (Table 2.2). The oxidation of squalane usually proceeds via a radical chain mechanism whereby initiation reactions between squalane and molecular oxygen form an alkyl radical species (Figure 2.12). The free radicals can then undergo chain propagation to form peroxides which then go on to decompose via chain branching reactions. Finally, termination reactions involve the decomposition of the peroxide

radicals alongside further reactions with the hydrocarbon forming their respective alcohols, aldehydes, ketones, and acids.

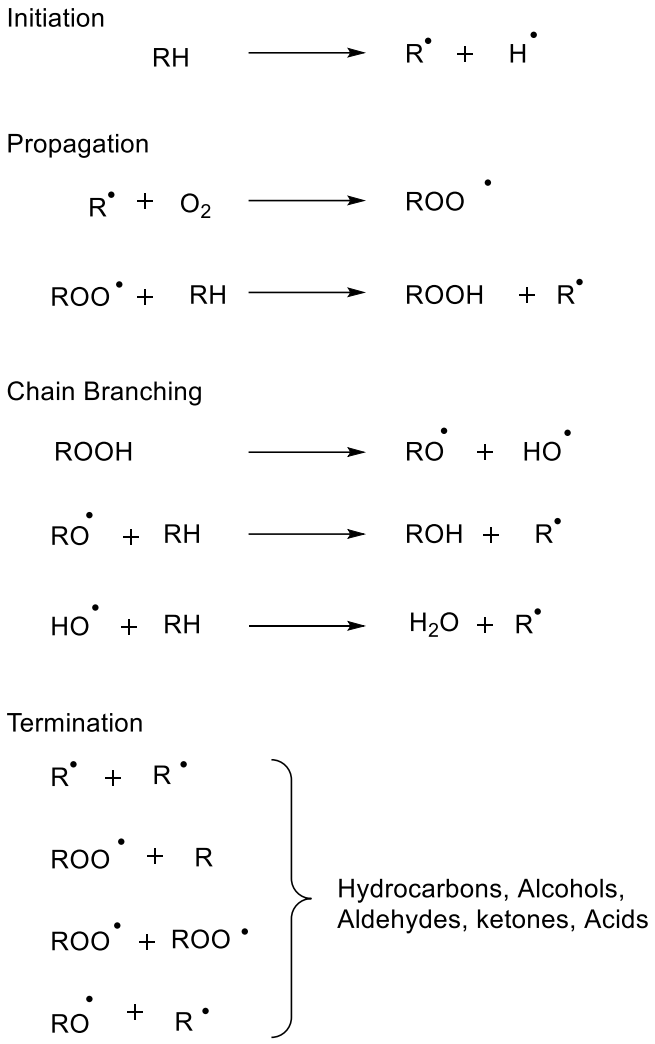

Figure 2.12 General radical chain mechanism for hydrocarbon oxidation

Table 2.2 The primary oxidation products of squalane catalysed by $[ChCl]_2[CoCl_2{\cdot}6H_2O]_3$ identified by GC-MS analysis

Retention time (min)	M_w (g mol^{-1})	Molecular Formula	Proposed Product
Alcohols			
28.7	256	$C_{17}H_{36}O$	1-Hexadecanol, 2-methyl-
41.7	298	$C_{20}H_{42}O$	1-Hexadecanol, 3,7,11,15-tetramethyl-
Aldehydes/Ketones			
29.3/36.0/41.5	268	$C_{18}H_{36}O$	2-Pentadecanone, 6,10,14-trimethyl-
31.9	200	$C_{12}H_{24}O_2$	5-(1-Methylethyl)-8-hydroxynonan-2-one
Esters			
25.2	256	$C_{16}H_{32}O_2$	Tridecanoic acid, 4,8,12-trimethyl-, methyl ester
37.2/42.7	324	$C_{21}H_{40}O_2$	4,8,12,16-Tetramethylheptadecan-4-olide
39.9/40.2	340	$C_{22}H_{44}O_2$	Acetic acid, 3,7,11,15-tetramethyl-hexadecyl ester
41.7	312	$C_{19}H_{36}O_3$	Octadecanoic acid, 2-oxo-, methyl ester
42.0	456	$C_{26}H_{48}O_6$	3,7,11,15-Tetramethylhexadecane-1,2,3-triol triacetate
42.3	226	$C_{14}H_{26}O_2$	Citronellyl isobutyrate
43.8	338	$C_{22}H_{42}O_2$	3,7,11,15-Tetramethylhexadec-2-en-1-yl acetate

The effect of temperature on squalane oxidation using ChCl-based DES was also investigated. An increase to 100 °C reduced $[ChCl]_2[MnCl_2{\cdot}4H_2O]$ DES induction time by one day while

nearly doubling its carbonyl index after 5 days. This trend was not found to be the same for the $[ChCl][CoCl_2{\cdot}6H_2O]_3$ DES. During the first 5 days of the reaction, the number of carbonyl-containing products increased more quickly compared to the 90 °C reaction. But, after 6 days and thereafter, the reaction rate appeared to decrease, and the total conversion of squalene was lower at 100 °C. Although increasing the reaction temperature increased the rate of oxidation, it also accelerated the rate of DES decomposition. Thus, there exists a trade-off between reactivity and total reaction conversion and small changes in reaction temperature can have drastic effects on reaction outcomes.

2.3.3 Efficiency and degree of depolymerisation of polyolefins

Given the DES proclivity to oxidise squalane, their catalytic efficiencies were assessed on polyolefins, HDPE and LDPE. Despite their relatively similar compositions, i.e., sp^3 C-C bonds in the backbone, their diverse branching structures mean their susceptibility to degradation vary significantly. At present, there exists chemical recycling approaches for the combined depolymerisation of HDPE and PP, however, there is no known method to selectively depolymerise LDPE, therefore, tuneable DES systems may have the potential to bridge that technological gap.

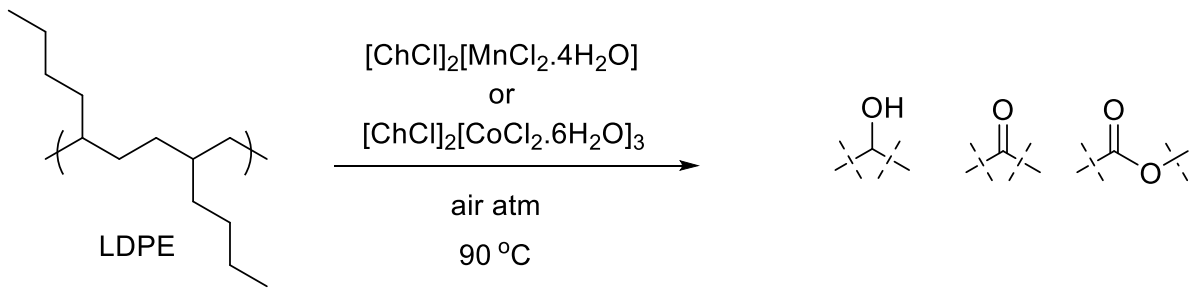

Scheme 2.2 General reaction scheme for the DES catalysed depolymerisation of LDPE

Applying the same $[ChCl]_2[MnCl_2{\cdot}4H_2O]$ DES to LDPE at 90 °C showed moderate carbonyl group incorporation with a CI of 0.76 after 15 days, while the $[ChCl]_2[CoCl_2{\cdot}6H_2O]_3$ DES showed nearly double the incorporation with a CI of 1.40 (Figure 2.13). It is noteworthy that only a C=O stretching band of a ketone is observed by FT-IR spectroscopy (wavenumber 1710 cm^{-1}). It would be appropriate to assume a mix of oxidative groups can be incorporated into the polymer chain ranging from alcohols, ketones, ester, and acids, however, the reaction is selective for ketones. Iron-based complexes have previously been reported to oxidise alkanes thermally and/or photochemically, however, all iron-containing DES tested failed to oxidise the PE samples as evidenced by FT-IR spectroscopy. An induction period of 1−3 days is observed for both systems before any visible incorporation of oxygen containing functional groups onto the polymer backbone, similar to the time frame detected for parallel squalane reactions. Likewise, the DES acts as a pre-catalyst and to test this hypothesis, a control experiment was conducted in which the DES was heated without the polyolefin substrate for a time corresponding to their respective induction periods. Then, the polyolefins were loaded after this pre-heating period. Interestingly, both polyolefins indicated oxidation after 1 day, suggesting that the induction period arises from the DES. FT-IR spectroscopy performed on the DES before and after this pre-heating period showed no distinguishable change in absorbance bands.

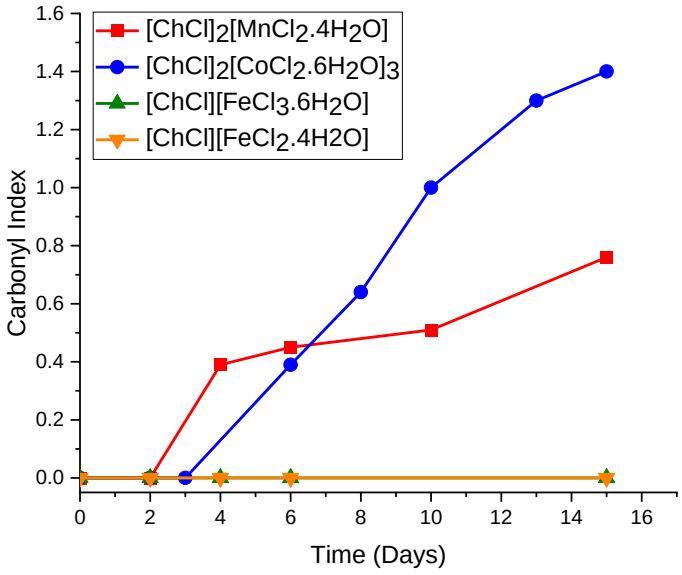

Figure 2.13 Carbonyl Index as a function of time of various DES reacted with low-density polyethylene (LDPE) at 90 °C

2.3.3.1 Selective depolymerisation of LDPE

As a consequence of the heterogeneous reaction conditions, phase transfer agents were introduced to the $[ChCl]_2[CoCl_2{\cdot}6H_2O]_3$ and $[ChCl]_2[MnCl_2{\cdot}4H_2O]$ DES to facilitate the migration of the non-polar polyolefins into the polar DES phase. 1-Butyl-3-methylimidazolium chloride ([BMIm]Cl) was explored because of its low polarity, which should improve interfacial compatibility with the non-polar polyolefin. Studies showed that the presence of [BMIm]Cl increased the carbonyl incorporation in a sample of 500 μm powdered LDPE while also reducing the induction time from 5 to 2 days (Figure 2.14b). In-solution experiments were carried out to consider the effect of phase transfer catalyst loading and showed that higher loading levels did not equate to higher carbonyl incorporation while a modest 10 wt% loading resulted in the highest CI. A humidity chamber was found to be crucial to maintain the DES hydration, without it, the DES dehydrated changing cobalt from its catalytically active Co^{2+} oxidation state while also diminishing favourable hydrogen bond interactions with choline chloride. The lack of hydrogen bonding renders the DES inactive as the catalyst as it loses the

ability to form the eutectic solvent (i.e. the melting point increases). Therefore, it no longer has the potential to act as a dual solvent-catalyst system. In a humidity chamber, the DES was loaded with [BMIm]Cl and powdered LDPE and heated to 90 °C and the reactions examined.

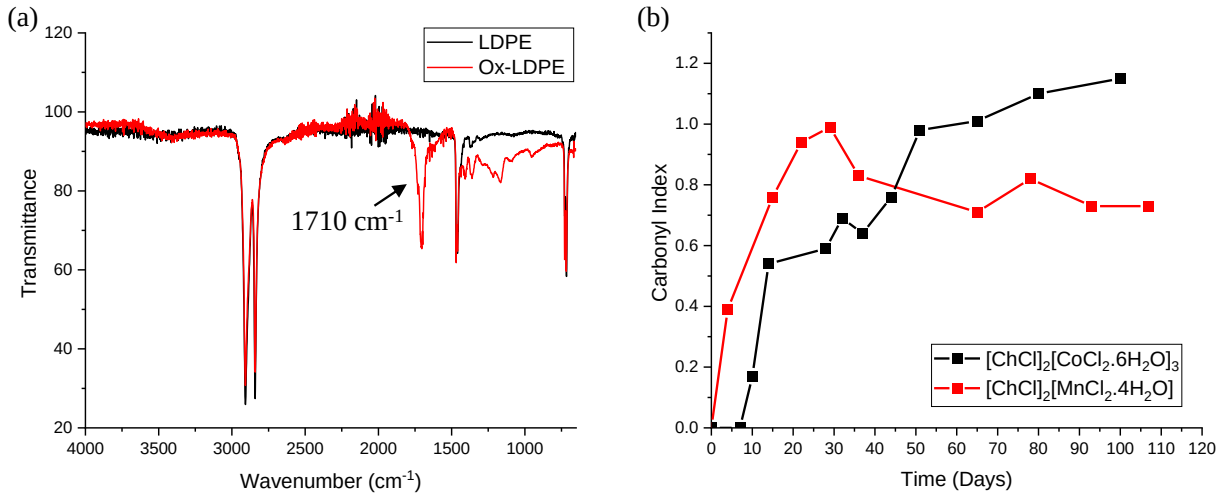

Figure 2.14 (a) FT-IR spectra of squalane and oxidised squalane (b) Carbonyl index as a function of time for the reaction of $[ChCl]_2[MnCl_2{\cdot}4H_2O]$ and $[ChCl]_2[CoCl_2{\cdot}6H_2O]_3$ with LDPE at 90 °C

The depolymerisation of LDPE was monitored by changes in the polymeric structure visible through FT-IR spectroscopy and high temperature-gel permeation chromatography (HT-GPC) analysis. HT-GPC analysis revealed that $[ChCl]_2[CoCl_2{\cdot}6H_2O]_3$ systems experience a non-linear decline in number average molecular weight (M_n) as a function of time, with an initial M_n of 21,000 Da LDPEs M_n reduced to 1,500 Da after 112 days (Figure 2.15a). Interestingly, following the depolymerisation through FT-IR spectroscopy does not display the same linear relationship as a function of time but rather a relative plateau in CI, indicating that incorporated carbonyl functionalities readily undergo consecutive chain scission reactions and are lost as VOCs. Together with the large molecular weight loss, the results are more consistent with backbone cleavage rather than cleavage of the side chains at the branching sites. The influence of polymer topology is evident as this reaction was found to be selective for LDPE (the same

as found for DES-only reactions), as no change in CI or molecular weight was observed for the more linear HDPE sample.

The dispersity ($Đ_M$) of the polymers further aids in understanding the depolymerisation pathway. Specifically, for $[ChCl]_2[CoCl_2{\cdot}6H_2O]_3$ reactions the $Đ_M$ of the LDPE sample increased over the course of 28 days from 5.7 to 17.5 before decreasing back down to 3.0 after 112 days. The increase in $Đ_M$ represents a larger diversity in polymeric chain lengths, broadening the heterogeneity of the sample, a result that is consistent with the polymer undergoing chain scission reactions. In contrast, the decrease in $Đ_M$, from day 28 to 112, signifies a narrowing of molecular weight distributions consistent with the loss of volatile small molecules. Alongside powdered LDPE, 5 mm granules were subjected to the same reaction conditions. The granules showed a 33% greater CI value after 14 days as compared to the powder but showed only 5% molecular weight loss after 14 days. It is hypothesised that the granules undergo greater levels of surface oxidation as compared to the bulk material because of the larger surface area of the granules. In the absence of bulk oxidation, chain scission reactions cannot occur as readily.

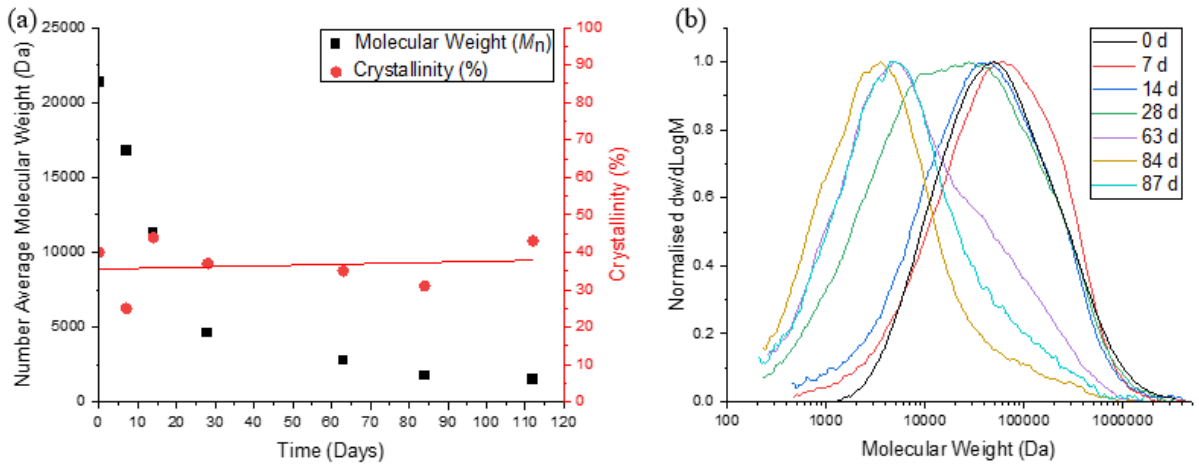

Figure 2.15 (a) Number average molecular weight (M_n) and crystallinity percentage of LDPE as a function of time for the reaction of $[ChCl]_2[CoCl_2{\cdot}6H_2O]_3$ and [BMIm]Cl at 90 °C. (b) Size exclusion chromatogram of the molecular weight distributions of LDPE over the course of its reaction with $[ChCl]_2[CoCl_2{\cdot}6H_2O]_3$ and [BMIm]Cl at 90 °C. Molecular weight was determined against poly(styrene) standards using $C_6H_3Cl_3$. (250 mg·L^{-1} BHT) as eluent at 160 °C

DSC analysis was employed to observe the changes in material properties attributable to the in-chain ketone motifs. The melting temperature for the oxidised LDPE samples remains virtually identical to the unreacted LDPE (112 °C), however, the degradation products can be observed by the development of new secondary crystallisation peaks (Figure 2.16). The first $T_{c,1}$ at 94.6 °C corresponds to unreacted LDPE, while the second crystallisation peak $T_{c,2}$ near 106 °C corresponds to ox-LDPE species/light hydrocarbons. The faster rate of crystallisation for the degradation products is a consequence of their decreased molecular size and therefore increased chain mobility. PE can no longer form the same regular crystal structure. This change in crystallinity is more evidenced in reactions at the PE backbone and not only at the weaker terminal vinyl groups (where minimal changes in crystallinity would have been observed). The percentage crystallinity was calculated based on 293.6 J g^{-1} for 100% crystalline polyethylene material (Figure 2.15a).[114] The amorphous regions within LDPE are more susceptible to degradation compared to the densely packed crystalline regions, therefore, were theorised to depolymerise first thus leaving behind the crystalline regions and therefore observing an

increase in crystallinity. However, this was not the case as the percentage of crystallinity for all ox-LDPE samples over the 112-day study remained consistent at approximately 40% implying that the amorphous and crystalline regions are degrading at an equal rate.

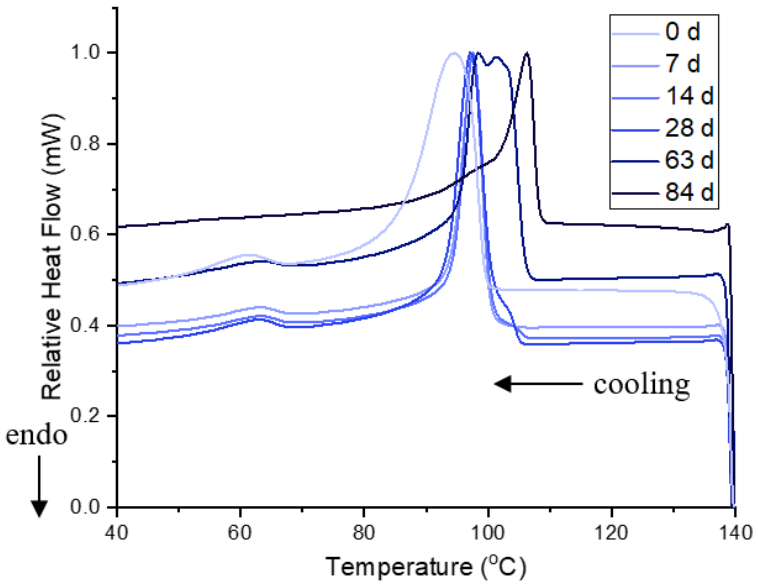

Figure 2.16 DSC thermograms of the cooling cycle for oxidised LDPE at a heating rate of 10 °C·min^{-1} between 40 and 140 °C

The degraded microstructures of LDPE were elucidated by ^{1}H and ^{13}C NMR spectroscopic methods (Figures 2.17 and 2.18 respectively). The ^{1}H NMR revealed a 4.59 mol% C=O group content and a 1.69 mol% C−OH content. Additionally, the ^{13}C NMR spectra identified isolated ester and ketone groups alongside a plethora of light hydrocarbons. However, a 10 mm NMR spectroscopy probe was not available, as such, spectra were collected using a 5 mm probe. Despite maximising the sample concentration and increasing the number of scans, a lack of sensitivity is captured in the spectra by the absence of expected downfield carbonyl signals in the ^{13}C NMR spectra and by the broad peaks in the ^{1}H NMR spectra.

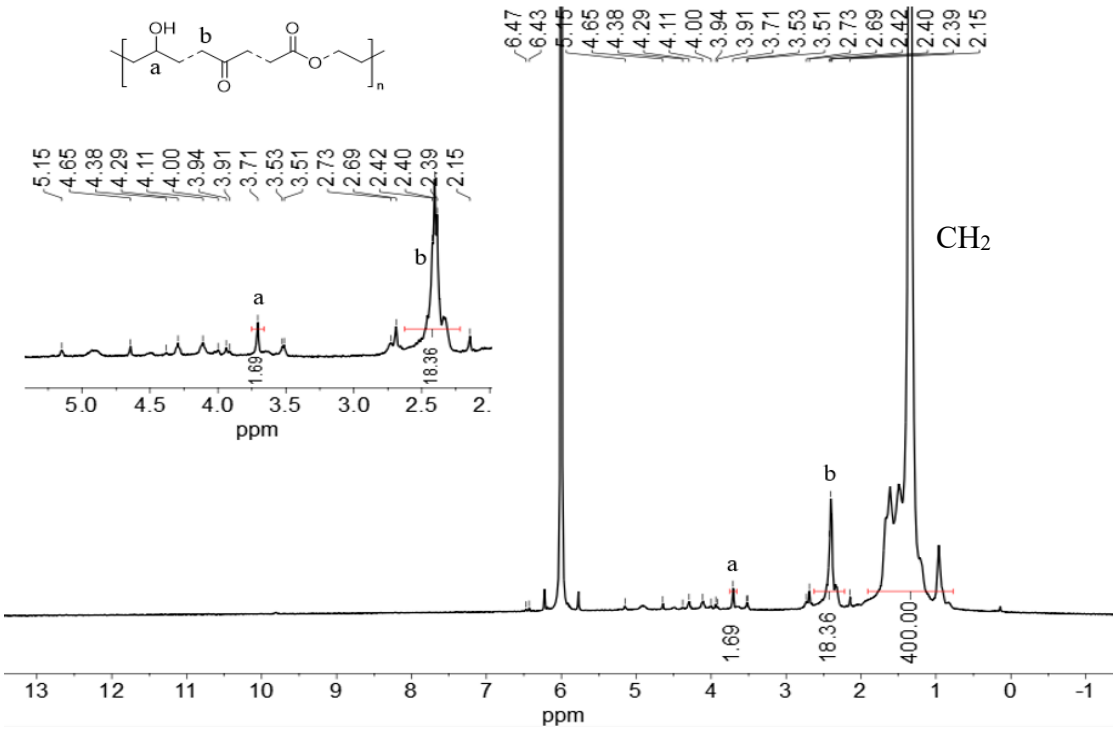

Figure 2.17 ^{1}H NMR spectrum (400 MHz, $C_2D_2Cl_4$ at 100 °C) of oxidised LDPE (FG = 6.28 mol%) after a 112-day reaction with $[ChCl]_2[CoCl_2{\cdot}6H_2O]_3$ [BMIm]Cl at 90 °C

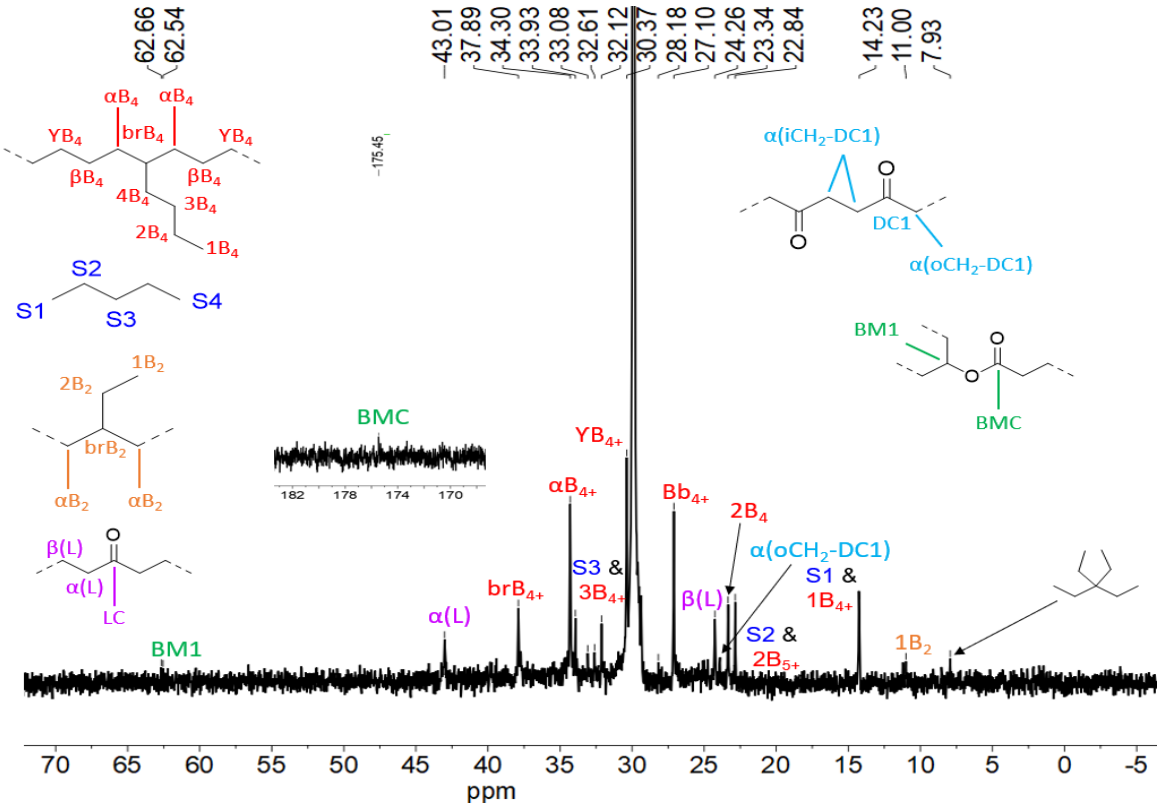

Figure 2.18 ^{13}C NMR spectrum (400 MHz, $C_2D_2Cl_4$ at 100 °C) of oxidised LDPE after a 112-day reaction with $[ChCl]_2[CoCl_2{\cdot}6H_2O]_3$ and [BMIm]Cl at 90 °C

Interestingly, under the same reaction conditions, HDPE remains unchanged over the course of the 100-day reaction. FT-IR analysis shows no presence of carbonyl functionality while the molecular weight and GPC profile of HDPE after 100 days is consistent with the starting polymer (Figure 2.19). The separation of discrete topology polyolefins during chemical recycling has been highlighted as a notorious challenge owing to their chemical similarities and near-identical densities. However, the reactions conditions used in this study have the potential to bridge the technological gap by the selective depolymerisation of LDPE, leaving behind chemically unchanged HDPE.

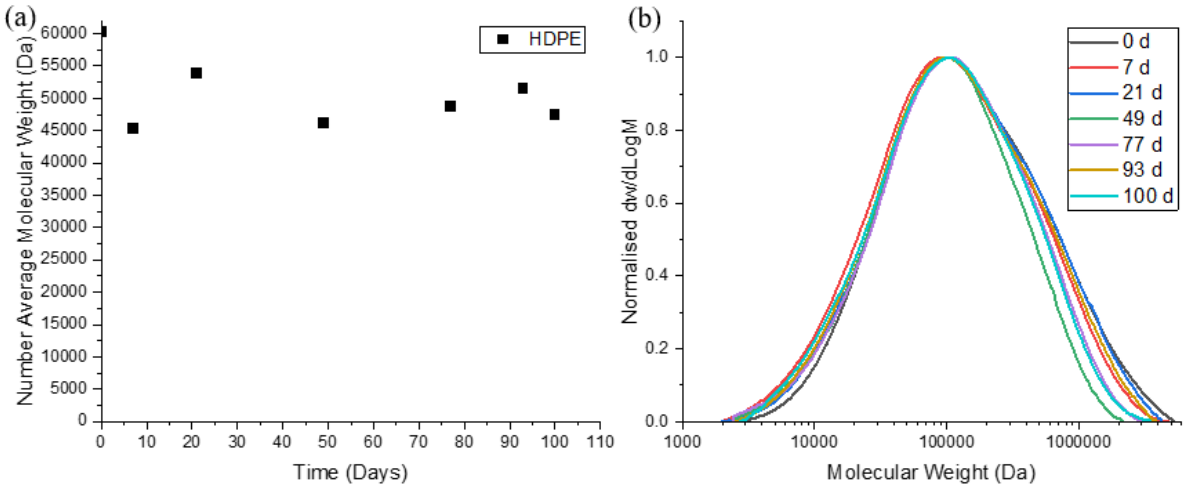

Figure 2.19 (a) Number average molecular weight as a function of time of HDPE after the reaction of $[ChCl]_2[CoCl_2{\cdot}6H_2O]_3$ and [BMIm]Cl at 90 °C. (b) Size exclusion chromatogram of the molecular weight distributions of HDPE over the course of its reaction with $[ChCl]_2[CoCl_2{\cdot}6H_2O]_3$ and [BMIm]Cl at 90 °C. Molecular weight was determined against poly(styrene) standards using $C_6H_3Cl_3$ (250 mg·L^{-1} BHT) as eluent at 160 °C

2.3.3.2 Depolymerisation of HDPE

In order to generate a DES that was able to depolymerise HDPE, the manganese-based DES $[ChCl]_2[MnCl_2{\cdot}4H_2O]$ was studied at 90 °C. Following the reaction via carbonyl group incorporation showed what looked like little progress with no indication of oxidation, however, after 49 days the CI of HDPE rose to 0.18 and continued to rise when at 100 days it reached

0.75 (Figure 2.20a). Encouraged by this result HT-GPC analysis was performed and surprisingly a prompt 83% decrease in M_n from 60,000 Da to 10,000 Da was discovered despite the lack of carbonyl group incorporation after 100 days. Unlike LDPE depolymerisations, the $Đ_M$ of HDPE only decreased over the course of the reaction which is symptomatic of the loss of VOCs from the beginning, this may explain the absence of carbonyl groups (Figure 2.20b). LDPE showed minimal change in molecular weight using the $[ChCl]_2[MnCl_2{\cdot}4H_2O]$ DES under the same reaction conditions inferring that the manganese-based DES has a higher reaction site selectivity for the secondary carbons of linear HDPE over the tertiary carbons of the branched LDPE structure.

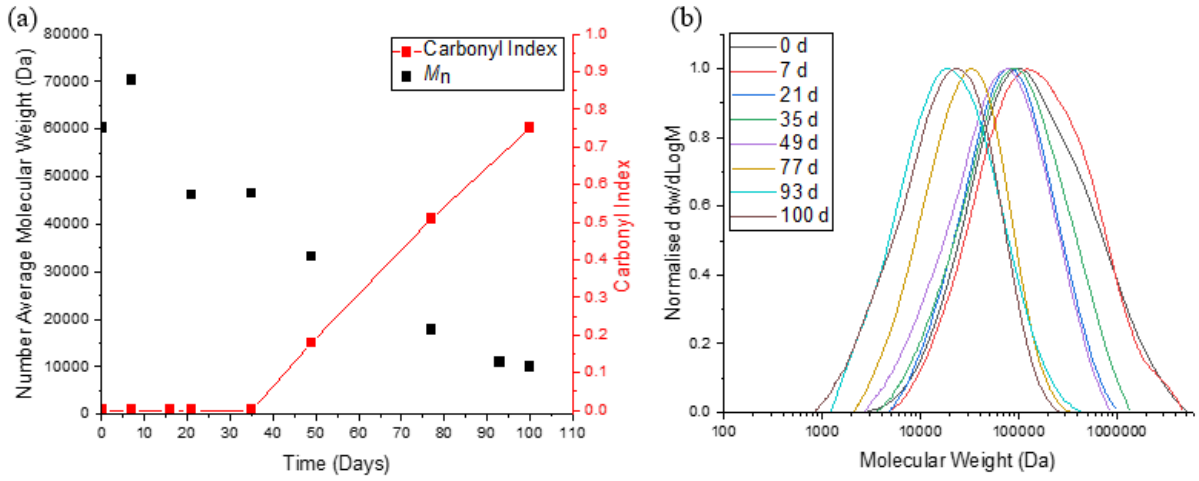

Figure 2.20 (a) Number average molecular weight and carbonyl index as a function of time of HDPE after its reaction with $[ChCl]_2[MnCl_2{\cdot}4H_2O]$ at 90 °C (b) Size exclusion chromatogram of the molecular weight distributions of HDPE over the course of its reaction with $[ChCl]_2[MnCl_2{\cdot}4H_2O]$ at 90 °C. Molecular weight was determined against poly(styrene) standards using $C_6H_3Cl_3$ (250 mg·L^{-1} BHT) as eluent at 160 °C

As with the cobalt DES, the phase transfer catalyst [BMIm]Cl (10 wt%) was added to $[ChCl]_2[MnCl_2{\cdot}4H_2O]$ to maximise surface contacts within the heterogeneous reaction and accelerate HDPE depolymerisation. Similar to before no carbonyl peaks were observed by FT-IR analysis until 77 days when the carbonyl index rose to 0.51. Of the original *M*n, 67% was

lost within the first 7 days after which the depolymerisation slowed significantly with a total M_n loss of 74% after 100 days (Figure 2.21a and 21b). Although the phase transfer catalyst initially accelerated the rate of the reaction the total M_n lost is less than the equivalent reaction with the absence of the phase transfer catalyst. Oxidation inhibition effects are evident by the stagnation of M_n loss, the radicals have reacted at all possible sites and the energy of the system is now insufficient to break any more bonds. Interestingly, when employed to LDPE the

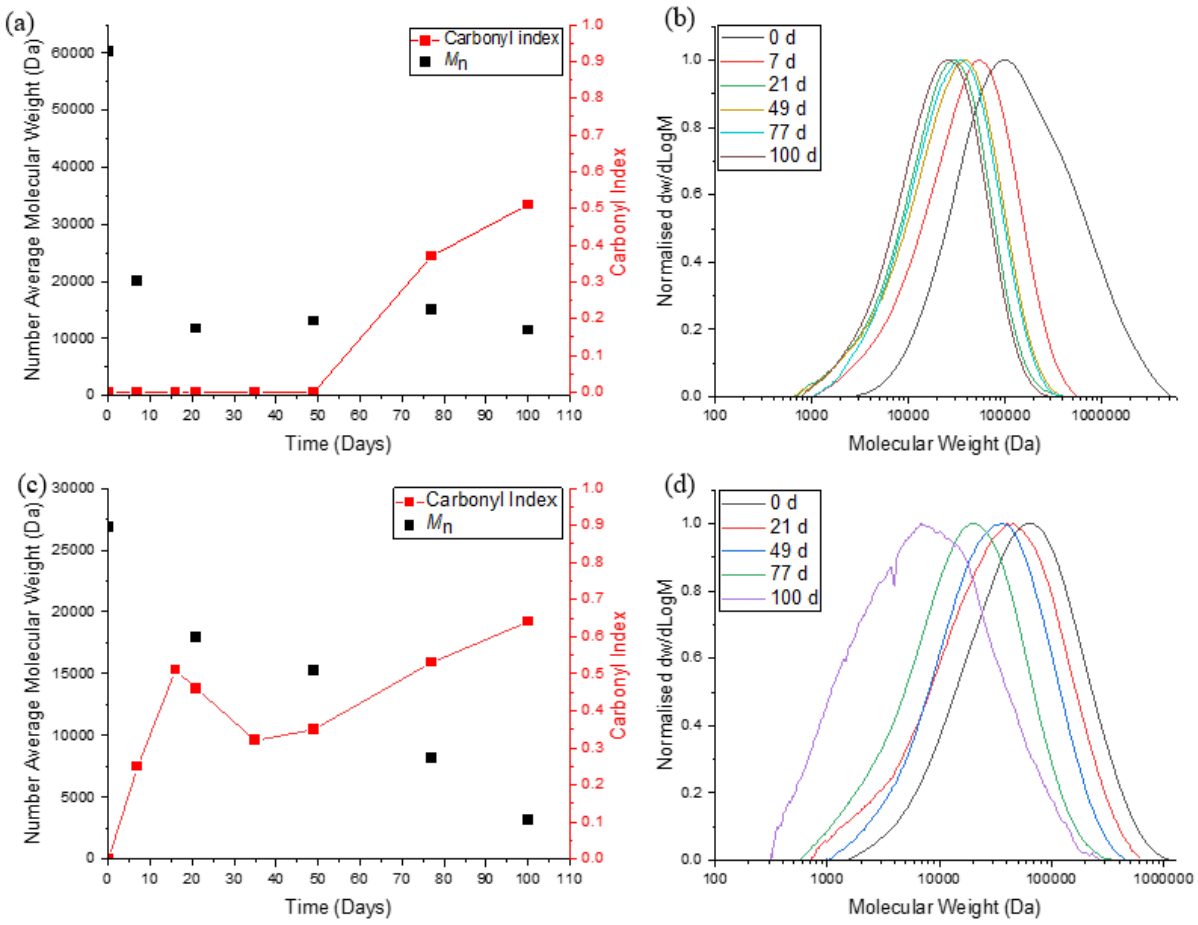

Figure 2.21 (a) Number average molecular weight and carbonyl index as a function of time of HDPE after its reaction with $[ChCl]_2[MnCl_2{\cdot}4H_2O]$ and [BMIm]Cl at 90 °C (b) Size exclusion chromatogram of the molecular weight distributions of HDPE throughout its reaction with $[ChCl]_2[MnCl_2{\cdot}4H_2O]$ and [BMIm]Cl at 90 °C. (c) Number average molecular weight and carbonyl index as a function of time of LDPE after its reaction with $[ChCl]_2[MnCl_2{\cdot}4H_2O]$ and [BMIm]Cl at 90 °C (b) Size exclusion chromatogram of the molecular weight distributions of LDPE throughout its reaction with $[ChCl]_2[MnCl_2{\cdot}4H_2O]$ and [BMIm]Cl at 90 °C.Molecular weight was determined against poly(styrene) standards using $C_6H_3Cl_3$ (250 mg·L^{-1} BHT) as eluent at 160 °C

addition of [BMIm]Cl caused depolymerisation to proceed with a linear 88% loss of M_n from 27,000 Da to 3,000 Da over 100 days (Figure 2.21c and 2.21d).

2.3.3.3 Depolymerisation of post-consumer LDPE

Depolymerising post-consumer LDPE offers up a range of different challenges compared to virgin LDPE as post-consumer plastics often contain a greater quantity of contaminants. Common contaminants such as dyes, plasticisers, stabilisers, flame retardants and antioxidants are added to enhance the physical, thermal and mechanical properties of the plastic, however, combined they can create a barrier to depolymerisation. An LDPE bag from the lab was cut into approximately 3 mm^2 pieces and tested using the optimised $[ChCl]_2[CoCl_2{\cdot}6H_2O]_3$ and [BMIm]Cl system at 90 °C.

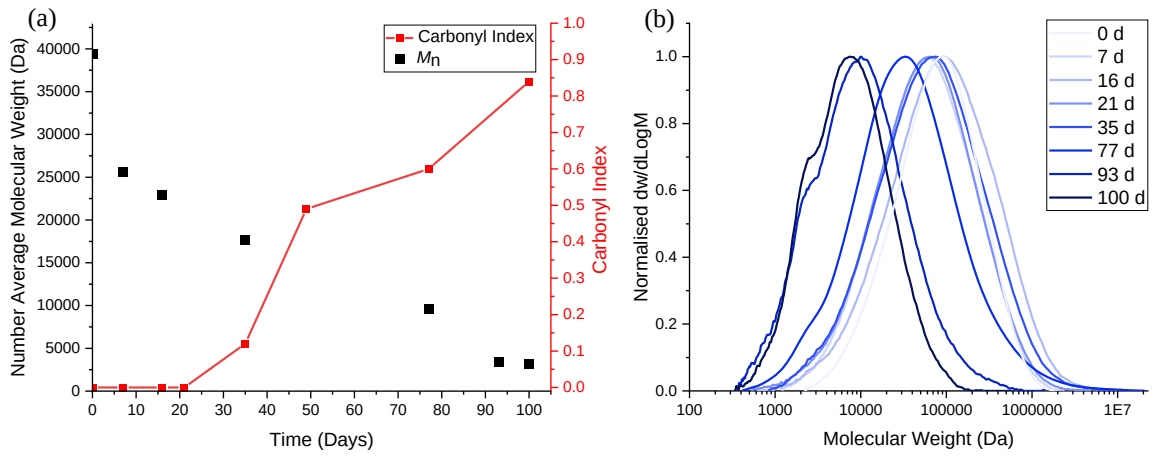

Figure 2.22 (a) Number average molecular weight and carbonyl index as a function of time of post-consumer LDPE after its reaction with $[ChCl]_2[CoCl_2{\cdot}6H_2O]_3$ and [BMIm]Cl at 90 °C (b) Size exclusion chromatogram of the molecular weight distributions of post-consumer LDPE throughout its reaction with $[ChCl]_2[CoCl_2{\cdot}6H_2O]_3$ and [BMIm]Cl at 90 °C. Molecular weight was determined against poly(styrene) standards using $C_6H_3Cl_3$ (250 $mg{\cdot}L^{-1}$ BHT) as eluent at 160 °C

Notably, following the incorporation of carbonyl groups through FT-IR spectroscopy exposed a long 21-day induction period (Figure 2.22a). The 18-day longer induction period compared to the 2 days as seen for virgin LDPE highlights the presence of antioxidants and additives.

Despite the chemical resistance enforced by the antioxidants the M_n linearly decreased by 92% of its original size (40,000 Da to 3,000 Da). The $Đ_M$ of the polymer aliquots increased from 4.5 to 8.4 before decreasing to 2.8 after 100 days (Figure 2.22b). The initial broadening of the polymers $Đ_M$ is evidence of a larger diversity of polymer chain lengths due to chain scission reactions while the subsequent narrowing of $Đ_M$ supports the loss of VOCs, similar to the mechanism for virgin LDPE samples.

2.4 Conclusion

The efficient and selective depolymerisation of LDPE into value-added materials has not been previously demonstrated because of the inherent durability and chemical inertness of the all carbon backbone of PE. Nevertheless, this chapter established the chemical recycling of LDPE and HDPE by employing earth-abundant metal-based deep eutectic solvents. In these reactions, DES acts as a dual solvent-catalyst system alleviating the need for traditional harmful organic solvents while maximising catalytic loading. The efficiency of the oxidation process is dependent on the stoichiometric ratio of the DES components, proving the synergy between the HBD:HBA, this allows for the fine-tuning of activity and selectivity. We demonstrated that acetamide and octadecanamide-based DES illustrate an overestimation of their real-life thermal stability and sustained their inappropriateness for long-duration experiments. Choline chloride proved its effectiveness as a suitable HBA with various metal salts for the successful formation of thermally more stable DES. Initial studies demonstrated aerobic oxidation of squalane using $[ChCl]_2[CoCl_2{\cdot}6H_2O]_3$ and $[ChCl]_2[MnCl_2{\cdot}4H_2O]$, yielding 37% and 32% conversion of squalane to oxidised small molecules, respectively. Applying the same $[ChCl]_2[CoCl_2{\cdot}6H_2O]_3$ DES to polyolefins, combined with phase transfer catalyst [BMIm]Cl, the systems revealed a dependence on polymer topology, selectively depolymerising LDPE to M_n = 1,500 Da after 112 days and postconsumer LDPE to M_n = 3,000 Da after 100 days. On the other hand,

$[ChCl]_2[MnCl_2{\cdot}4H_2O]$ DES showed a propensity for HDPE depolymerisation with 83% of the original M_n lost over 100 days. In contrast to previous polyolefin modifications, oxidation occurs on the PE backbone causing consecutive chain scission reactions and lowering the overall molecular weight. At the moment, there is no known method to selectively depolymerise LDPE from mixed plastic waste, therefore, these DES systems may offer the potential to bridge that gap while their tailorability also makes them applicable for all polyolefin depolymerisations.

2.5 References

1. S. Klein, I. K. Dimzon, J. Eubeler and T. P. Knepper, *Handb. Enviro. Chem.*, 2018, **58**, 231-232.
2. M. Hong and E. Y. X. Chen, *Green Chem.*, 2017, **19**, 3692-3706.
3. J. R. Jambeck, R. Geyer, C. Wilcox, T. R. Siegler, M. Perryman, A. Andrady and K. L. Law, *Science*, 2015, **347**, 1234-1242.
4. T. O. Morgen, M. Baur, I. Gottker-Schnetmann and S. Mecking, *Nat. Commun.*, 2020, **11**, 3693-3702.
5. Q. Wang, X. Yao, Y. Geng, Q. Zhou, X. Lu and S. Zhang, *Green Chem.*, 2015, **17**, 2473-2479.
6. Z. O. G. Schyns and M. P. Shaver, *Macromol. Rapid. Commun.*, 2021, **42**, 2000415-2000415.
7. G. W. Coates and Y. D. Y. L Getzler, *Nat. Rev. Mater.*, 2020, **5**, 501-516.
8. I. A. Ignatyev, W. Thielemans and B. V. Beke, *Chem. Sus. Chem*, 2014, **7**, 1579-1593.
9. S. R. Chandrasekaran, B. Kunwar, B. R. Moser, N. Rajagopalan and B. K. Sharma, *Energy Fuels*, 2015, **29**, 6068-6077.
10. J. D. Hamilton, K. H. Reinert, J. V. Hagan and W. V. Lord, *J. Air Waste Manag. Assoc.*, 1995, **45**, 247-251.
11. B. Liu, W. Fu, X. Lu, Q. Zhou and S. Zhang, *ACS Sustain. Chem. Eng.*, 2018, **7**, 3292-3300.
12. A. M. Al-Sabagh, F. Z. Yehia, G. Eshaq, A. M. Rabie and A. E. ElMetwally, *Egypt. J. Pet.*, 2016, **25**, 53-64.
13. C. Jehanno, J. Demarteau, D. Mantione, M. C. Arno, F. Ruiperez, J. L. Hedrick, A. P. Dove and H. Sardon, *Angew. Chem. Int. Ed. Engl.*, 2021, **60**, 6710-6717.
14. T. J. Fazekas, J. W. Alty, E. K. Neidhart, A. S. Miller, F. A. Leibfarth and A. E. J., *science*, 2022, **375**, 545-550.
15. C. Bae, J. F. Hartwig, N. K. B. Harris, R. O. Long, K. S. Anderson and M. A. Hillmyer, *J. Am. Chem. Soc.*, 2005, **127**, 767-776.
16. A. Bunescu, S. Lee, Q. Li and J. F. Hartwig, *ACS Cent. Sci.*, 2017, **3**, 895-903.
17. Q. Wang, X. Yao, S. Tang, X. Lu, X. Zhang and S. Zhang, *Green Chem.*, 2012, **14**, 2559-2566.

18. E. S. C. Ferreira, C. M. Pereira and A. F. Silva, *J. Electroanal. Chem.*, 2013, **707**, 52-58.
19. A. P. Abbott, J. C. Barron, G. Frisch, S. Gurman, K. S. Ryder and A. Fernando Silva, *Phys. Chem. Chem. Phys.*, 2011, **13**, 10224-10231.
20. X. Li, M. Hou, B. Han, X. Wang and L. Zou, *J. Chem. Eng.*, 2008, **53**, 548-550.
21. H. Bowen, R. Durrani, A. Delavault, E. Durand, J. Chenyu, L. Yiyang, S. Lili, S. Jian, H. Weiwei and G. Fei, *Front. Chem.*, 2022, **10**, 912411-912421.
22. Y. H. Choi, J. van Spronsen, Y. Dai, M. Verberne, F. Hollmann, I. W. Arends, G. J. Witkamp and R. Verpoorte, *Plant. Physiol.*, 2011, **156**, 1701-1705.
23. R. Wang, T. Wang, G. Yu and X. Chen, *Polym. Deg. Stab.*, 2021, **183**, 1038-1046.
24. A. E. Ünlü, A. Arıkaya and S. Takaç, *Green Process. Synth.*, 2019, **8**, 355-372.
25. H. Wang, Z. Li, Y. Liu, X. Zhang and S. Zhang, *Green Chem.*, 2009, **11**, 1568-1575.
26. K.-K. Kow and K. Sirat, *CCL*, 2015, **26**, 1311-1314.
27. Z. Naseem, R. A. Shehzad, A. Ihsan, J. Iqbal, M. Zahid, A. Pervaiz and G. Sarwari, *Chem. Phys. Lett.*, 2021, **769**.
28. V. G. Vaidyanathan and B. U. Nair, *J. Inorg. Biochem.*, 2003, **94**, 121-126.
29. R. Sanchis, A. Garcia, F. Ivars-Barcelo, S. H. Taylor, T. Garcia, A. Dejoz, M. I. Vazquez and B. Solsona, *Materials (Basel)*, 2021, **14**, 7120-7237.
30. J. Almond, P. Sugumaar, M. N. Wenzel, G. Hill and C. Wallis, *E-Polym.*, 2020, **20**, 369-381.
31. G. Konstantopoulos, P. Maroulas, D. A. Dragatogiannis, S. Koutsoumpis, A. Kyritsis and C. A. Charitidis, *Mater. Des.*, 2021, **199**, 109420-109430.

2.6 Experimental

2.6.1 Instruments

Nuclear magnetic resonance (NMR)

^{1}H and ^{13}C NMR spectra were recorded at 298 K on an Ascend Bruker 400 spectrometer equipped with a BBFO smart probe operating at 400 MHz and 100 MHz respectively. Chemical shifts of the ^{1}H NMR spectra were referenced to the solvent residual proton resonance signals: δ 7.26 ppm for *d1*–CDCl3. Spectra data was analysed using MestReNova 12.0.2 software. The resonance multiplicities for ^{1}H NMR are described as s (singlet), d (doublet), t (triplet), q (quartet) or m (multiplet).

High-temperature NMR

^{1}H and ^{13}C NMR spectra of the polyolefins were measured at 363 K on a Bruker AVANCE NEO console (2017) 400 spectrometer equipped with a 5 mm BBFO smart probe operating at 400 MHz and 100 MHz respectively. Chemical shifts of the ^{1}H NMR spectra were referenced to the solvent residual proton resonance signal: δ 6.00 ppm for *d*-TCE. 1500 scans experiments were performed for ^{1}H NMR and 21000 scans for ^{13}C NMR.

High-temperature gel permeation chromatography (HT-GPC)

HT-GPC measurements were performed in $C_6H_3Cl_3$ (+ 250 mg·L^{-1} BHT) on an Agilent 1260 Infinity high-temperature GPC (Agilent) system fitted with viscometer detectors, RI and ultraviolet (UV, λ = 309 nm) at 160 °C. Using $C_6H_3Cl_3$ (+ 250 mg·L^{-1} BHT) as the mobile phase (flow rate = 1 mL.min^{-1}) the polymers were eluted through an Agilent guard column (PLGel 5 μ, 50 × 7.5 mm) and two Agilent mixed-B columns (PLGel 5 μ, 300 × 7.5 mm). A calibration curve (M_n = 162 – 3,187.000 gmol^{-1}) was used to determine the number average molecular

weight (M_n), weight average molecular weight (M_w) and dispersity ($Đ_M = M_w/M_n$) based on polystyrene standards (Easivial PS-M/H, Agilent). A Mark-Houwink correction was applied, K = 19 for PP and K = 39 for PE and α = 0.725. All samples were run according to D6474. The samples were dissolved in $C_6H_3Cl_3$ (+ 250 mg·L^{-1} BHT) at a concentration of 1.5 mg·mL^{-1} and heated at 160 °C for 3h prior to GPC analysis being performed. Once fully dissolved the samples were injected at a flow rate of 1 mL·min^{-1} with a 100 μmL injection volume at 160 °C.

Differential scanning calorimetry (DSC)

Glass transition temperature (T_g), melting transition temperature (T_g), crystallisation temperature (T_c) and total enthalpy (ΔH_m) of melting were measured on a STARe system DSC3 equipped with an auto-sampler (Mettler Toledo, Switzerland) under a N_2 atmosphere. Samples were positioned in 40 μL aluminium pans (Mettler Toledo) and cycled between −80 to 180 °C for three heating and cooling cycles at 10 °C min^{-1}. From the second heating cycle, the glass transition temperature (T_g) was observed as the midpoint of the inflexion tangent. Normalisation and integration of the endothermic transitions enabled the total enthalpy of heating (ΔH_m) to be calculated.

Thermo-gravimetric analysis (TGA)

Dynamic and isothermal TGA data was obtained using a Q50 - Thermogravimetric Analyzer (TA instrument)**.** Thermograms were recorded under an N_2 atmosphere at a heating rate of 10 °C min^{-1}, from 10 − 600 °C, with an average sample weight of *ca*. 7 mg.

Gas Chromatography-Mass (GC-MS) Spectrometry

GC-MS analysis was used to characterise and identify oxidation products using a GCMS-QP2010 SE chromatograph mass spectrometer. Chromatographic separation was carried out on a ZB-5HT inferno achiral column (L = 30 m, ID = 0.25 mm, FT = 0.25 μm). Gas chromatography was performed with a constant helium flow of 1.0 mL min^{-1} and a 1:40 split ratio. The oven programmed temperature was set to 40 °C for 2 min then ramped at a rate of 6 °C min^{-1} up to a final temperature of 300 °C where it was held for 20 min. Total gas chromatography analysis was approximately 65 min for each sample run. The manifold, ion trap source and transfer line temperature were set at 120 °C, 220 °C and 300 °C, respectively. Mass spectra were scanned on the *m/z* 30-550 range with a rate of 1 scan s^{-1}. Product identification was achieved by comparing their mass spectra to the NIST MS library and their elution time against commercial standards.

Fourier Transform- Infrared (FT-IR) Spectroscopy

FT-IR data was obtained (neat) using a Perkin Elmer Paragon 1000 FT-IR spectrometer. 5 μL (5 mg·mL^{-1}) was deposited on top of the detectors using attenuated total reflection to measure. Wavelengths were scanned in the range of 500- 4000 cm^{-1}.

2.6.2 Materials

Squalane (99%), Cobalt chloride hexahydrate ($CoCl_2 \cdot 6H_2O$, 98-102%), Iron(II) chloride tetrahydrate ($FeCl_2 \cdot 4H_2O$, 98%), Iron(III) chloride ($FeCl_3$, 98%), Iron(III) chloride hexahydrate ($FeCl_3 \cdot 6H_2O$, 99+%), 1,1,2,2-Tetrachloroethane-*d*2 99% and chloroform (> 99.8%) were purchased from Fisher scientific. Octadecanamide (90%) was purchased from TIC Chemicals.

Manganese chloride tetrahydrate ($MnCl_2 \cdot 4H_2O$, 99%), *tert*-Butyl hydroperoxide (70% aqueous solution), hydrogen peroxide (37% aqueous solution) and Acetamide (99%), were purchased from Alfa Aesar. 1-Butyl-3-methylimidazolium chloride (98%+) was purchased from ACROS Organics. Silica gel (SiO_2 40-60 μm) and $CDCl_3$ (>99.8%) were purchased from Apollo Scientific. 1,2,4-Trichlorobenzene HPLC grade > 99% was purchased from Merck. All chemicals were used as received unless stated otherwise.

Two approaches can be employed for the synthesis of each DES, namely the direct heating method whereby starting materials are stirred at elevated temperatures until a homogeneous liquid is formed or the grinding method whereby the components are ground together using a mortar and pestle at room temperature until a homogeneous liquid is formed. Owing to the experimental simplicity of the direct heating, this method was employed for the preparation of all DES compounds. All DES were used directly without further purification.

2.6.3 Procedures

1. General procedure for the synthesis of the DES

In a 20 mL glass vial equipped with a magnetic stirrer, appropriate amounts of choline chloride were combined with a metal salt and the vial was sealed with a Teflon cap. The reaction mixture was gently stirred and heated to 90 °C for 30 min until the formation of a homogeneous liquid.

I. Synthesis of $[ChCl]_2[MnCl_2 \cdot 4H_2O]$

Using general procedure 1, reaction using choline chloride (1.4 g, 10.1 mmol, 2 equiv.) and $MnCl_2 \cdot 4H_2O$ (1.0 g, 5.05 mmol, 1 equiv.) gives the title product as a yellow viscous liquid.

II. Synthesis of [ChCl][$FeCl_2 \cdot 4H_2O$]$_2$

Using general procedure 1, reaction using choline chloride (0.35 g, 5.52 mmol, 1 equiv.) and $FeCl_2 \cdot 4H_2O$ (1.0 g, 5.03 mmol, 2 equiv.) gives the title product as a brown viscous liquid.

III. Synthesis of [ChCl][$FeCl_3 \cdot 6H_2O$]$_2$

Using general procedure 1, reaction using choline chloride (0.26 g, 1.85 mmol, 1 equiv.) and $FeCl_3 \cdot 6H_2O$ (1.0 g, 3.70 mmol, 2 equiv.) gives the title product as an orange viscous liquid.

IV. Synthesis of [ChCl][$FeCl_3$]$_2$

Using general procedure 1, reaction using choline chloride (0.43 g, 3.09 mmol, 1 equiv.) and $FeCl_3$ (1.0 g, 6.17 mmol, 2 equiv.) gives the title product as a brown viscous liquid.

V. Synthesis of [ChCl][$CoCl_2 \cdot 6H_2O$]$_3$

Using general procedure 1, reaction using choline chloride (0.36 g, 2.5 mmol, 1 equiv.) and $CoCl_2 \cdot 6H_2O$ (1.0 g, 7.70 mmol, 3 equiv.) gives the title product as a blue liquid.

2. General procedure for the thermal oxidation of squalane within a humidity chamber

DES was synthesised according to general procedure 1 and loaded into an open-top 7 mL glass vial equipped with a magnetic stirrer bar. Squalane (8.6 mL, 16.7 mmol, 1 equiv) was added into the vial, squalane formed an immiscible layer on top of the DES. The 7 mL vial was placed inside a 20 mL glass vial containing 5 mL of water and sealed with a Teflon cap, acting as a humidity chamber. The reaction vessel was heated to 90 °C for 16 days then the reactions were cooled to room temperature and GC-MS was used to identify reaction products. GC-MS samples were prepared using 1 mg of the reaction mixture in 2 mL of chloroform and filtered through a 0.22 μm syringe filter.

3. General procedure for the DES catalysed thermal depolymerisation of polyolefins within a humidity chamber.

The DES was synthesised according to procedure 1. The DES was loaded into an open-top 7 mL glass vile equipped with a magnetic stirring bar. The desired plastic (0.2 g) was then loaded into the DES and stirred well forming a heterogeneous mixture. The 7 mL vial was placed into a 20 mL glass vial containing 5 mL of water and sealed with a Teflon cap, acting as a humidity chamber. The reaction vessel was heated to a targeted temperature (90 °C) for a minimum of 30 days. Aliquots were taken at desired intervals; methanol was used to wash residual DES from the aliquots before they were dried under vacuum.

4. General procedure for phase transfer catalysed oxidation of polyolefins within a humidity chamber

The DES was synthesised according to general procedure 1 and loaded into an open-top 7 mL glass vile equipped with a magnetic stirring bar. The desired plastics (0.2 g) were then loaded into the DES and stirred well forming a heterogeneous mixture. 1-Butyl-3-methylimidazolium chloride (0.3 g, 1.7 mmol, 0.1 equiv.) was added in one portion. The 7 mL vial was placed into a 20 mL glass vial containing 5 mL of water and sealed with a Teflon cap, acting as a humidity chamber. The reaction vessel was heated to a targeted temperature (90 °C) for a minimum of 30 days. Aliquots were taken at desired intervals; methanol was used to wash residual DES from the aliquots before they were dried under vacuum.

2.7 Appendix

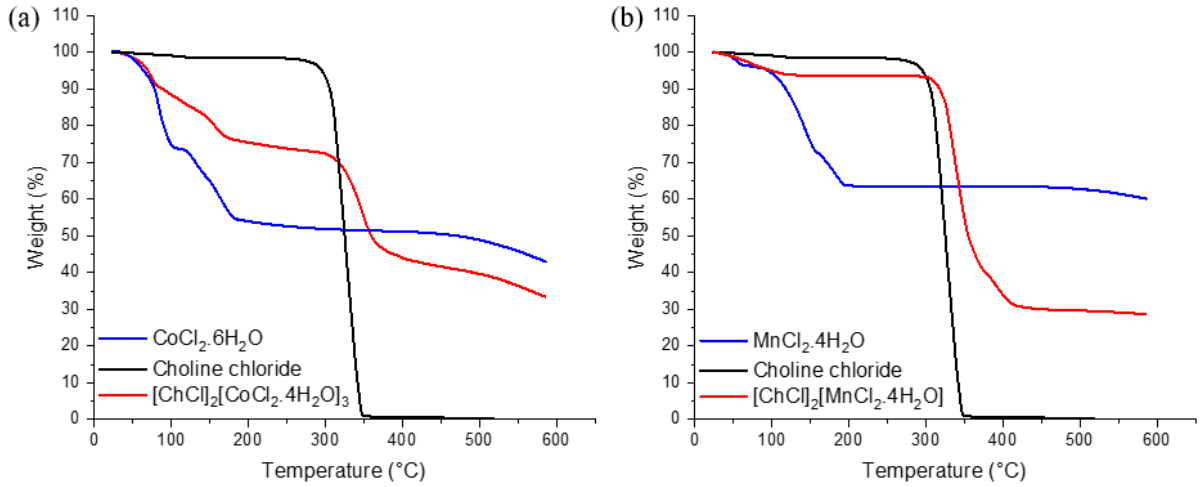

Figure 2.23 Thermogravimetric analysis of (a) $CoCl_2 \cdot 6H_2O$, choline chloride and $[ChCl]_2[CoCl_2 \cdot 6H_2O]_3$ (b) $MnCl_2 \cdot 4H_2O$, choline chloride and $[ChCl]_2[MnCl_2 \cdot 4H_2O]$ from 0 - 600 °C at a heating rate of 10 °C·min^{-1}

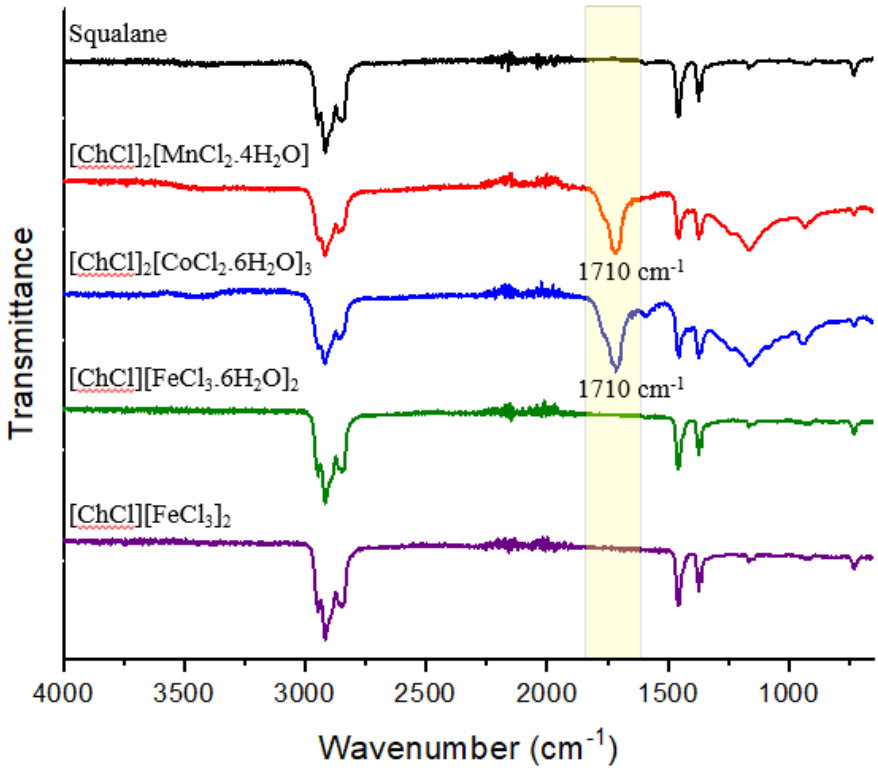

Figure 2.24 FT-IR spectra of squalane after 14-day reaction with each DES at 90 °C

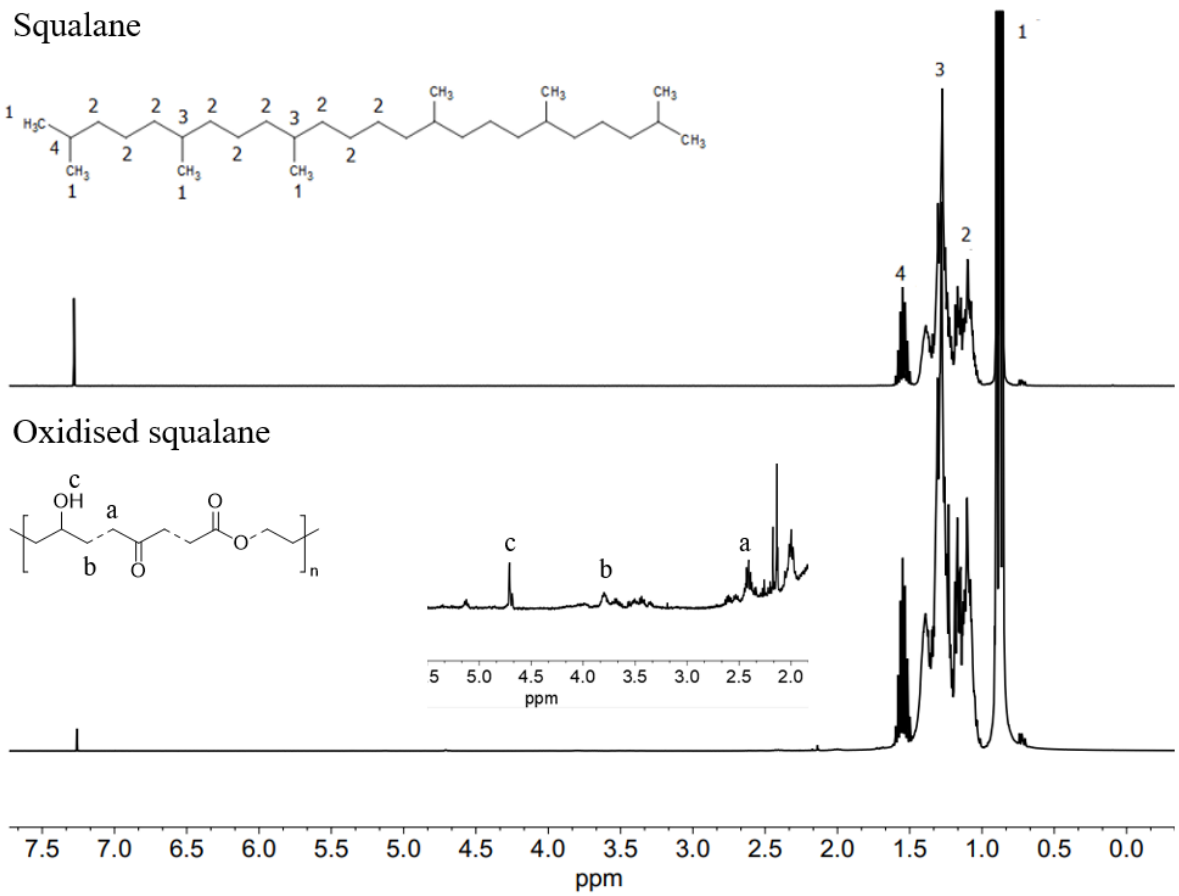

Figure 2.25 ^{1}H NMR spectrum of squalane (top) and oxidised squalane (bottom) after reacting with $[ChCl]_2[CoCl_2{\cdot}6H_2O]_3$ and [BMIm]Cl at 90 °C for 14 days (400 MHz; 298 K, $CDCl_3$)

Table 2.3 GC-MS chromatogram and its tabulated results for the oxidation product for the reaction of $[ChCl]_2[CoCl_2{\cdot}6H_2O]_3$ with squalane at 90 °C after 14 days

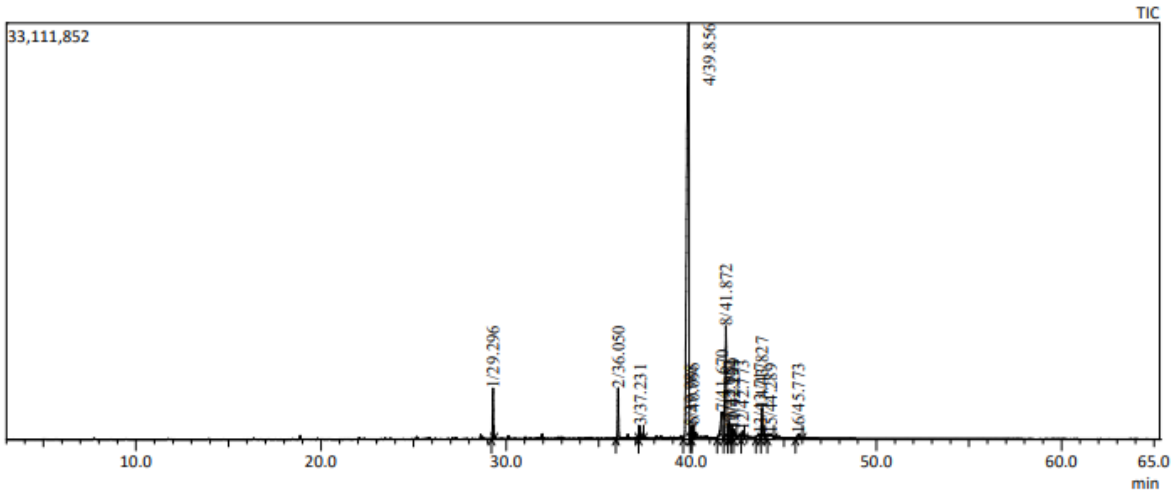

Peak Report TIC

Peak#	R.Time	I.Time	F.Time	Area	Area%	Name
1	29.296	29.210	29.360	13695460	3.07	2-Pentadecanone, 6,10,14-trimethyl-
2	36.050	35.930	37.150	18286405	4.10	2-Pentadecanone, 6,10,14-trimethyl-
3	37.231	37.150	37.430	4111277	0.92	4,8,12,16-Tetramethylheptadecan-4-olide
4	39.856	39.560	39.945	78973282	62.60	Squalane
5	39.985	39.945	40.030	3378408	0.76	Acetic acid, 3,7,11,15-tetramethyl-hexadecyl ester
6	40.096	40.030	40.170	5215477	1.17	Acetic acid, 3,7,11,15-tetramethyl-hexadecyl ester
7	41.670	41.400	41.755	24262321	5.44	2-Pentadecanone, 6,10,14-trimethyl-
8	41.872	41.755	41.975	50594937	11.35	Carbonic acid, eicosyl prop-1-en-2-yl ester
9	42.052	41.975	42.130	8146101	1.83	3,7,11,15-Tetramethylhexadecane-1,2,3-triol triacetate
10	42.191	42.130	42.225	3964951	0.89	Triacontyl heptafluorobutyrate
11	42.299	42.285	42.455	4665854	1.05	2-Methyl-cis-7,8-epoxynonadecane
12	42.773	42.700	42.870	3530614	0.79	4,8,12,16-Tetramethylheptadecan-4-olide
13	43.717	43.495	43.755	4514007	1.01	1-Octacosanol, 2,4,6,8-tetramethyl-, (all-R)-
14	43.827	43.755	43.980	13049441	2.93	3,7,11,15-Tetramethylhexadec-2-en-1-yl acetate
15	44.289	44.115	44.465	5630867	1.26	3,7,11,15-Tetramethylhexadec-2-en-1-yl acetate
16	45.773	45.635	46.005	3596100	0.81	Tetracosa-2,6,14,18,22-pentaene-10,11-diol, 2,6,10,15,19
				45615502	100.00	

Table 2.4 GC-MS chromatogram and tabulated results for the oxidation product for the reaction of [ChCl][$MnCl_2 \cdot 4H_2O$] with squalane at 90 °C after 14 days

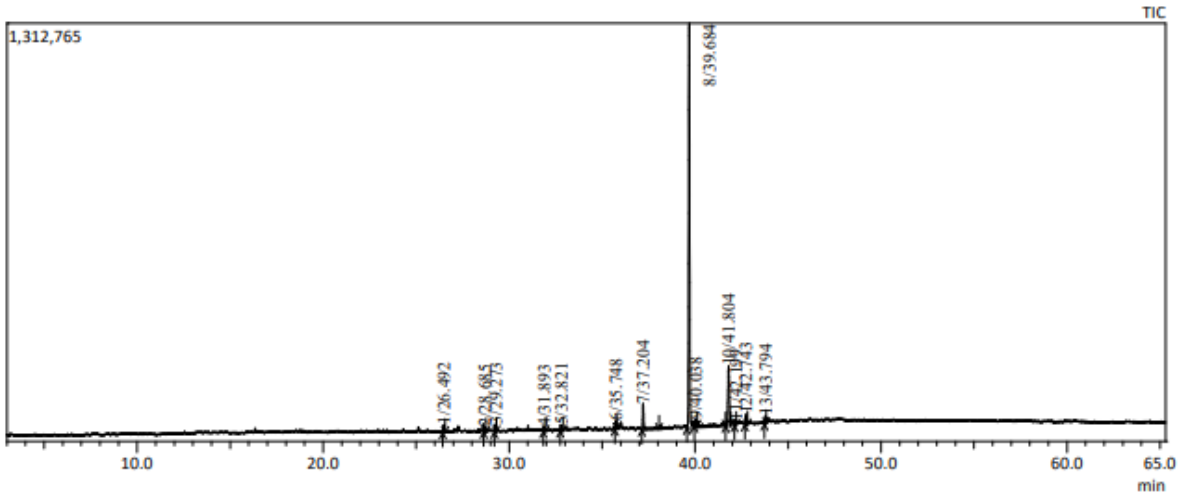

Peak Report TIC

Peak#	R.Time	I.Time	F.Time	Area	Area%	Name
1	26.492	26.425	26.560	103759	1.38	Phthalic acid, 3,5-dimethylphenyl 4-isopropylphenyl este
2	28.685	28.640	28.755	73267	0.97	Dodecyl octyl ether
3	29.273	29.205	29.325	87320	1.16	2-Pentadecanone, 6,10,14-trimethyl-
4	31.893	31.835	31.975	71850	0.95	2- Chloropropionic acid, pentadecyl ester
5	32.821	32.755	32.895	81719	1.08	n-Decanol tetrahydropyran ether
6	35.748	35.685	35.790	87635	1.16	13-Docosenamide, (Z)-
7	37.204	37.135	38.060	359789	4.77	4,8,12,16-Tetramethylheptadecan-4-olide
8	39.684	39.570	41.645	5156803	68.39	Squalane
9	40.038	39.965	40.130	100400	1.33	Acetic acid, 3,7,11,15-tetramethyl-hexadecyl ester
10	41.804	41.645	41.925	1067559	14.16	1-Hexadecanol, 3,7,11,15-tetramethyl-
11	42.199	42.110	42.210	79518	1.05	1-Tetracosene
12	42.743	42.670	42.820	157423	2.09	4,8,12,16-Tetramethylheptadecan-4-olide
13	43.794	43.730	43.830	113589	1.51	Phytol, acetate
				7540631	100.00	

Chapter 3

Radical initiator and molecular oxygen accelerated depolymerisation of polyolefins

3.1 Abstract

Polyolefins are a class of polymers derived from olefin monomeric units, such as ethylene and propylene. They are predominantly resistant to chemical recycling because of their strong unreactive carbon-carbon backbone, moreover, the current recycling techniques require elevated temperatures, the use of harsh acids and bases and high pressures. Tuneable DES formed from the complexation of choline chloride with earth-abundant metal salts, as discussed in Chapter 2, have been proposed as a catalytically active alternative to organic solvents for polyolefin depolymerisation. However, the longevity of the reactions necessitated an investigation of accelerants that are compatible under mild reaction conditions. Organic peroxides in an oxygen-rich environment are presented as radical initiators and effective co-oxidants to speed up polyolefin depolymerisation. Combined with a DES oxidant, the peroxides react with the high-energy triplet spin state of molecular oxygen (O_2), forming active hydroperoxides. The increased radical loading accelerates the molecular weight loss in both pristine and post-consumer polyolefins with an improved infinity for deleterious chain scission events. The oxygen-rich environment maximises the production of potential reactive oxygen species, promoting the loss of VOC. The potential up-cycling of the oxidised polyolefins was demonstrated through single-lap shear testing, where the increased surface functionalisation created stronger adhesives compared to unmodified polyolefins.

3.2 Introduction

Polyolefins are constituted of an inert all-carbon backbone, thus, are notoriously stable towards chemical and thermal degradation.[12, 28] Cleavage of these strong carbon-carbon bonds is crucial for the process of polyolefin depolymerisation; however, this often requires elevated temperatures and harsh reagents.[24] The first step of an oxidation reaction is the abstraction of hydrogen by free radicals. The generation of such radicals can be slow as a consequence of their high energy requirements; however, this high-energy barrier may be bypassed with the use of radical initiators.

Radicals are widely used within chemistry; they possess weak bonds with low dissociation energies that under mild conditions cleave to afford two reactive radical species. Radicals can be generated by electrolysis, redox reactions, thermally, photoinduction, and electrical discharge as well as enzymes and their reactivity and lifetime are dependent on the substituent groups.[98, 115, 116] Post-polymerisation modification using radicals is a popular technique for double-bond-containing polymers. Thiol-ene "click chemistry" is a well-adopted synthetic process whereby reaction at the pendant vinyl group can incorporate various chemical functionalities. Radical coupling involving rapid radical trapping is also an effective method for functionalisation, however, this requires radical formation on the polymer backbone.[117] Radical chain-end modification introduces functionalities on the polymer chain end, but is highly specific and limits reaction site locations.[118] The C-H alkylation of polyesters *via* photoinduced iron catalysis with radicals has also shown success but requires already existing ester functionality on the polymer backbone for targeted selectivity.[119]

Molecular oxygen, also known as dioxygen, is potentially the "greenest" oxidant as it is highly abundant in the air and environmentally friendly as its reduction product is water, moreover, it has been employed as an oxidant for olefins,[120] indoles,[121] alcohols,[122] (hetero)sulfides,[123] and

amines.[124] Dioxygen has been used to oxidise hydroquinones and catechols to their respective quinones and in turn, form a new molecule of hydrogen peroxide which can go on to initiate a new amplification cycle.[125] Olefins can also be oxidised by molecular oxygen and copper catalysts with an imidazole salt tag to form its epoxide counterpart.[120] Nevertheless, O_2 is relatively unreactive towards strong C−C and C−H bonds. Thermally induced oxidation of organic compounds is spin-forbidden as the ground state of O_2 has a high energy triple spin state which is incompatible with most organic substances' singlet state. Reactions can be induced with elevated temperatures or pressures however this goes against the green chemistry requirements. Transition metals on the other hand can facilitate oxidation as they can react with the triplet state of O_2 in the presence of an electron source forming metal-oxygen intermediates.[126] Metal-oxygen intermediates are more easily formed through the reaction of metal complexes with peroxides circumventing the unfavourable kinetics associated with direct aerobic oxidations. Hydrogen peroxide and molecular oxygen coupled with an iron complex successfully oxidise hydrocarbons into alcohols, aldehydes and ketones through the abstraction of a hydrogen atom.[127] Herein, is reported the accelerated oxidative depolymerisation of polyolefins by organic peroxides and O_2 catalysed by earth-abundant metal-based DES.

3.3 Results and discussion

3.3.1 Organic peroxides as radical initiators

The rate-determining step of an oxidation reaction is the accumulation of hydroperoxides which form *via* C-H abstraction on the polymer backbone generating free radicals that continue to chain grow into their corresponding hydroperoxides.[127] Without the influence of an external radical source, this reaction is energetically unfavourable and rarely occurs in stable hydrocarbons, thus, radical initiators are used. Organic peroxides, specifically hydrogen peroxide (H_2O_2), *tert*-butyl hydroperoxide (TBHP) and lauroyl peroxide, were chosen as the radical initiators as their low bond dissociation energy (142 kJ·mol) RO–OR bond makes them highly susceptible to homolytic cleavage to form reactive radicals (Scheme 3.1).

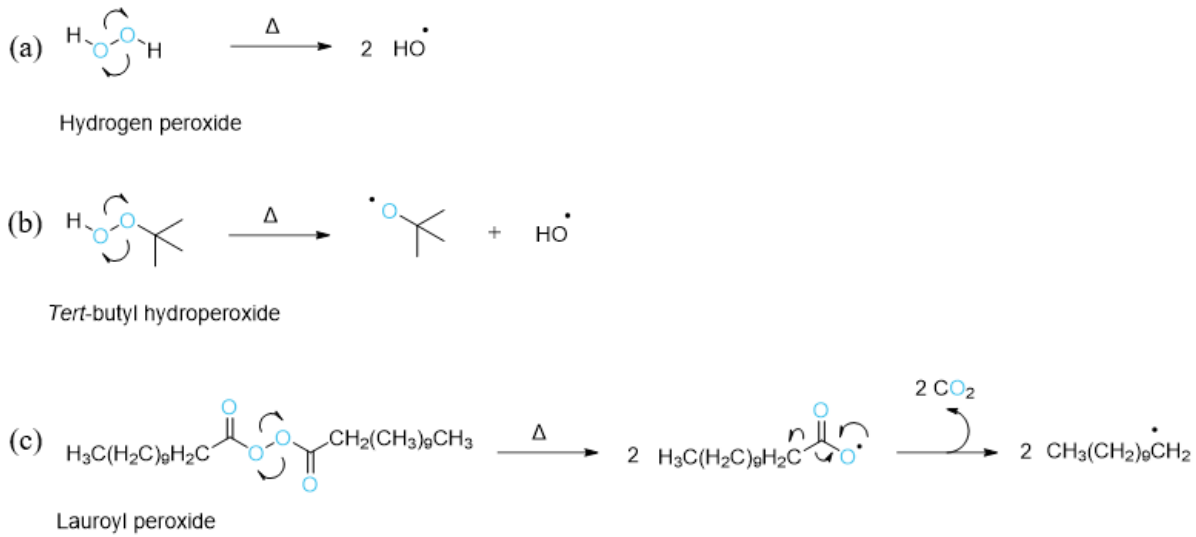

Scheme 3.1 The radical mechanism for the thermal decomposition of (a) hydrogen peroxide (b) *tert*-butyl hydroperoxide (c) lauroyl peroxide

Although the peroxide bond does not require much energy to break, metals are known to favour its dissociation, specifically metals that can undergo a one-electron redox switch, such as

manganese and cobalt. Moreover, in combination with our already oxidatively active DES, organic peroxides are thought to accelerate polyolefin oxidation.[128]

TBHP belongs to the peroxide family but is known as a hydroperoxide as it contains an RO−OH bond. It is less reactive than hydroxyl radicals (HO•) because of its alkyl substituent, however, this alkyl group is thought to increase its hydrophobicity and enhance interfacial interaction with the non-polar hydrophobic polyolefins. Furthermore, the high selectivity of peroxyl radicals for tertiary hydrogen abstraction offers the potential to apply the DES to different polyolefin topologies. For this reason, the combination of TBHP and $[ChCl]_2[CoCl_2{\cdot}6H_2O]_3$ was employed to depolymerise LDPE. Inside a humidity chamber, the DES $[ChCl]_2[CoCl_2{\cdot}6H_2O]_3$ and TBHP were stirred at 90 °C before loading in LDPE and the reaction was followed by GPC analysis. Preliminary results found a steady exponential molecular weight loss profile found an 82% loss of the original M_n after 70 days with the coarse cryo-milled LDPE becoming a fine white powder (Figure 3.1).

3.3.2 DES recyclability

To be considered as an effective catalyst the DES must be reusable over multiple cycles, so after 70 days the reaction was terminated by recovering the remaining LDPE. The remaining LDPE was filtered off and fresh LDPE was loaded into the DES, under equivalent reaction conditions, the fresh LDPE was left to react, and the cycles were compared (Figure 3.1). Resemblant exponential decay profiles were observed in both cases although the second cycle showed a faster rate of depolymerisation with a marginally lower molecular weight final polymer. The difference in rates can be related to the delay in the formation of the catalytically active species due to an induction period during the first cycle, allowing the second cycle to proceed promptly. The evaporation of water also may be a contributing factor, throughout cycle

one, because of the prolonged exposure to elevated temperatures, the DES may dehydrate, changing its hydration state and concentration. ^{1}H NMR spectroscopy of the resultant oxidised-LDPE (ox-LDPE) species revealed a complex mixture of hydrocarbons and oxygenated functional groups. Integration of the distinguishable oxygen-containing peaks found that the singlet at δ 3.65 ppm and triplet at δ 2.46 ppm possess 0.1 mol% alcohol and 6.1 mol% ketone functionality respectively (total polymer functional groups (FG) = 6.2 mol%), (Figure 3.2). The presence of ketone functionality was also confirmed by ^{13}C NMR spectroscopy, however, a lack of sensitivity, due to using a 5 mm probe, meant the corresponding downfield ketone signal is not observed (Figure 3.3). DSC analysis of the final polymer from both cycles have a crystallisation percentage of 39% thus, both cycles appear to have depolymerised the amorphous and crystalline domains at an equivalent rate (Figure 3.22).

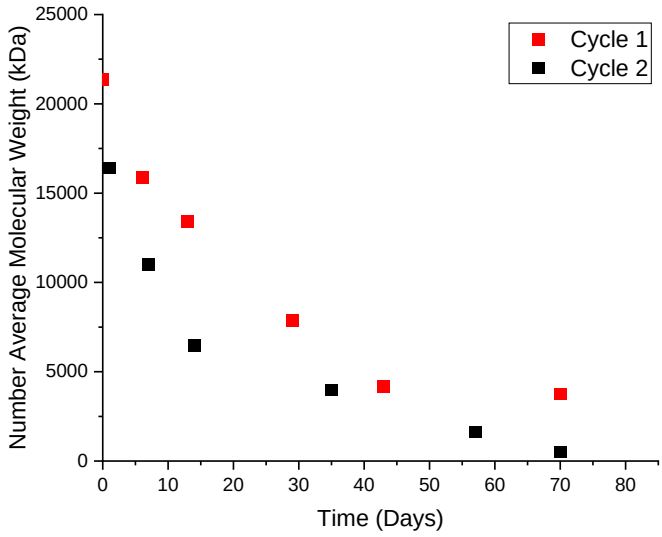

Figure 3.1 Number average molecular weight as a function of time of LDPE after its reaction with $[ChCl]_2[CoCl_2{\cdot}6H_2O]_3$ and TBHP at 90 °C over two catalytic cycles

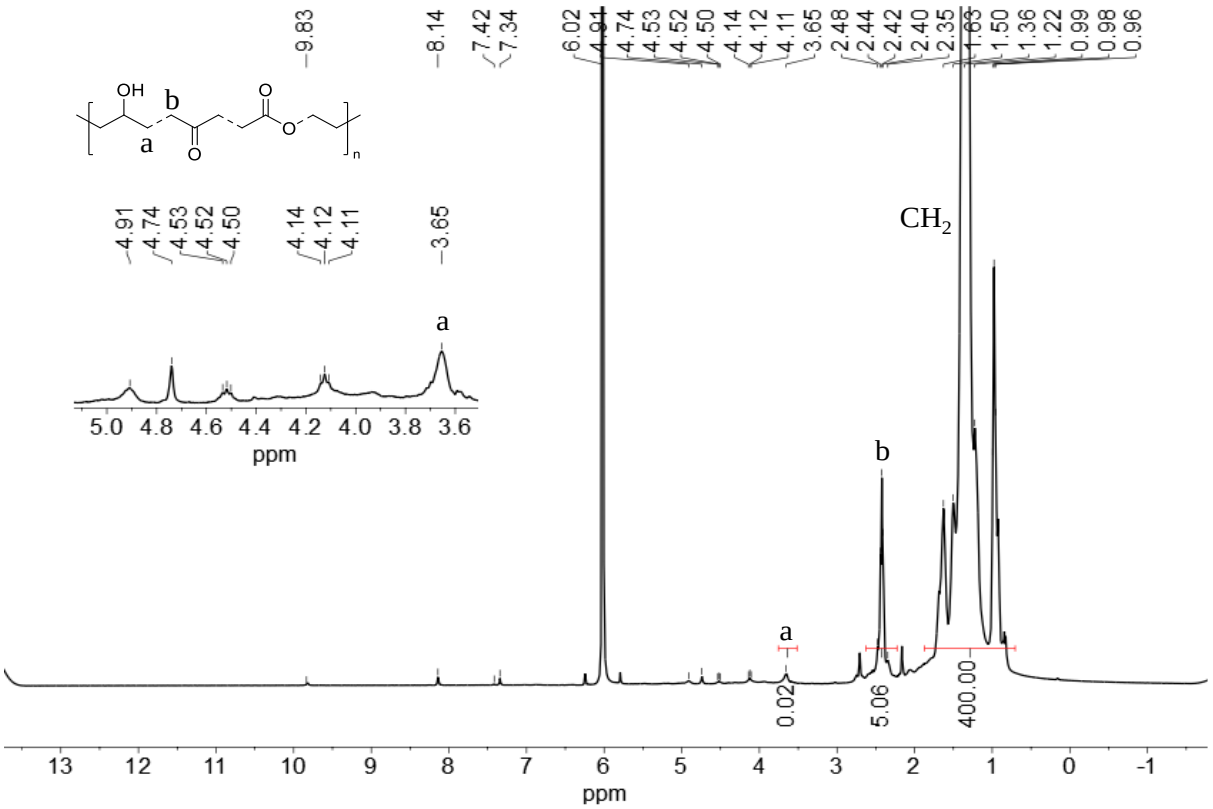

Figure 3.2 ^{1}H NMR spectrum (400 MHz, $C_2D_2Cl_4$ at 100 °C) of LDPE (FG = 6.2 mol%) after 100-day reaction with $[ChCl]_2[CoCl_2{\cdot}6H_2O]_3$ and TBHP (0.9 equiv) at 90 °C

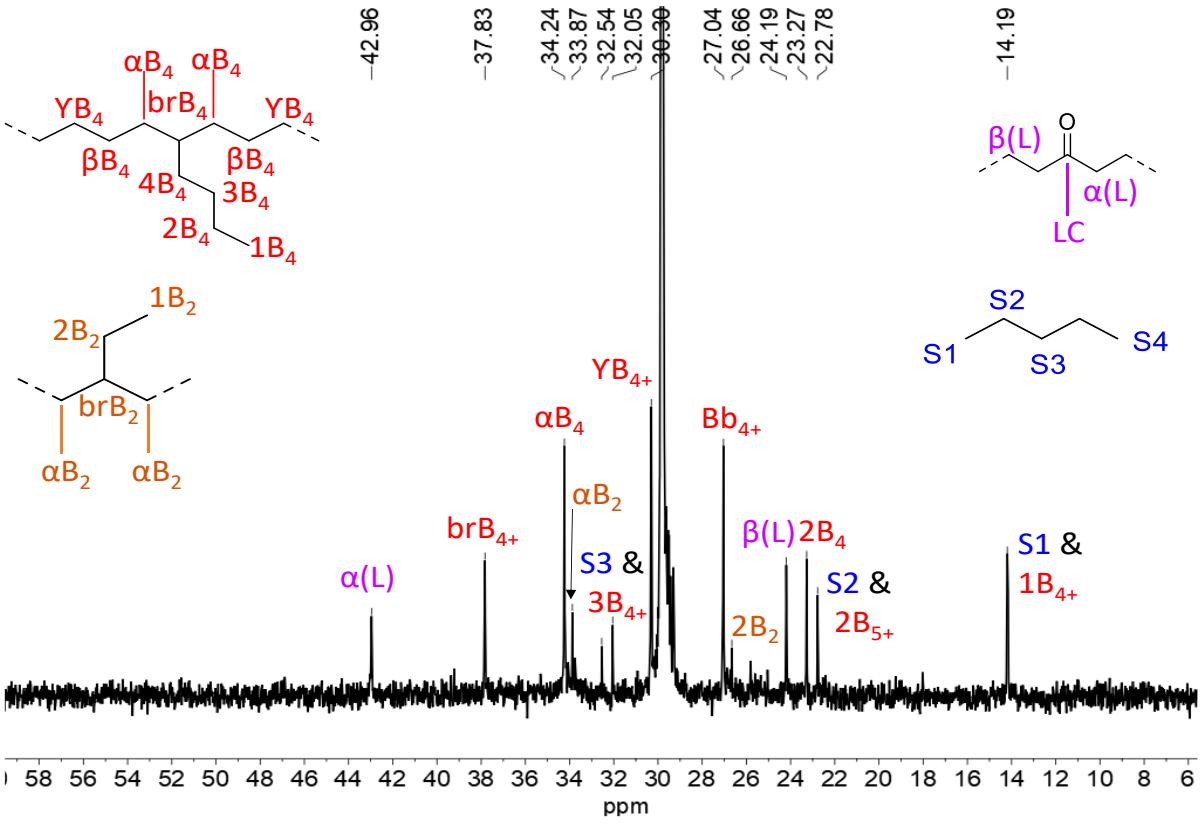

Figure 3.3 ^{13}C NMR spectrum (400 MHz, $C_2D_2Cl_4$ at 100 °C) of LDPE (FG = 6.2 mol%) after 100-day reaction with $[ChCl]_2[CoCl_2{\cdot}6H_2O]_3$ and TBHP (0.9 equiv) at 90 °C

3.3.3 Peroxides temperature dependence

Peroxide reactivity is dependent on their half-life *i.e.* the time it takes for their activity to decrease by 50%, furthermore, temperature plays a crucial role in their decomposition rate. Lowering the operating temperature was hypothesised to slow the peroxide consumption, moderating radical formation and increasing oxidation. Moreover, a parallel comparison experiment was implemented using $[ChCl]_2[CoCl_2{\cdot}6H_2O]_3$ and TBHP at 70 °C. At 90 °C an initial spike in the carbonyl index indicates rapid incorporation of ketone groups followed by a drop in carbonyl index implying the loss of ketone groups, indicative of chain scission (Figure 3.4a). This is a result of the rapid consumption of the peroxide whereas at 70 °C there is a gradual increase in the carbonyl index as the lifetime of the peroxide is extended for a more controlled radical production. The slight drop in carbonyl index after 60 days marks a loss of oxygen content suggesting the loss of VOCs. The M_n values reinforce this concept, as there is a greater and faster molecular weight loss for the reaction performed at 70 °C (Figure 3.4b). Plotting molecular weight loss as a function of time revealed an inconsistency as the M_n value increase and decrease. GPC is a quantitative analytical technique; therefore, it is possible that variations in sample concentration, temperature and calibration may be affecting the result.

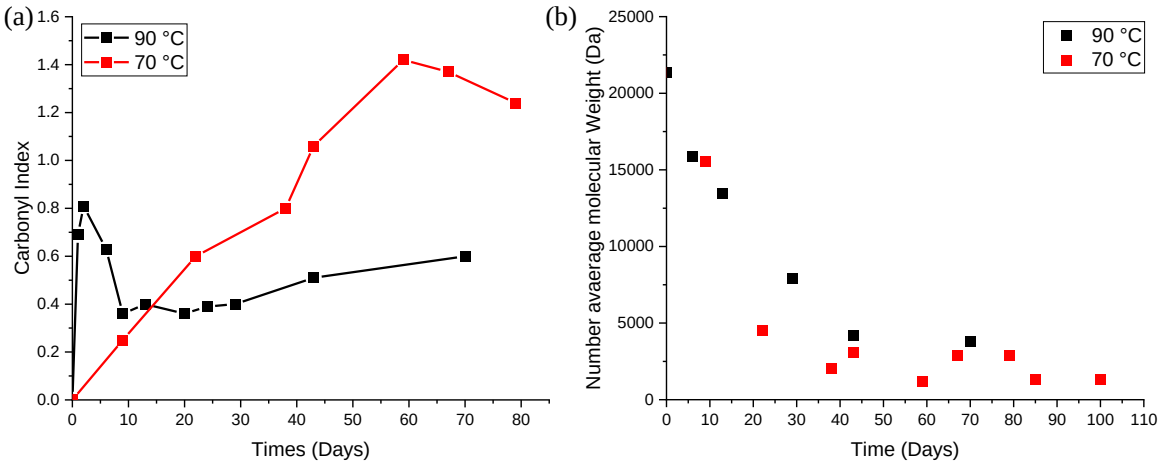

Figure 3.4 (a) Carbonyl index as a function of time for $[ChCl]_2[CoCl_2{\cdot}6H_2O]_3$ and TBHP (0.9 equiv) at 70 °C and 90 °C. (b) Number average molecular weight as a function of time for $[ChCl]_2[CoCl_2{\cdot}6H_2O]_3$ and TBHP (0.9 equiv) at 70 °C and 90 °C

Importantly, lowering the reaction temperature to 70 °C minimises the disturbance of the DES hydrogen bonding as the reaction is at a lesser risk of dehydration, subsequently, the reactions no longer need to be performed in a humidity chamber. Lowering the reaction temperature also reduces the risk of thermal decomposition of choline chloride. Peeter *et al*. found that the thermal stability of choline chloride decreases in the presence of cobalt(III) at high temperatures, leading to the formation of toxic byproducts.[129] Thus, by lowering the operating temperature the risk of choline chloride decomposition is lowered while low temperatures are industrially advantageous from an energy consumption and cost-effectiveness stance.

Encouraged by this result, the temperature was lowered to 50 °C and the depolymerisation of LDPE and HDPE was attempted under the following conditions: (i) $[ChCl]_2[CoCl_2{\cdot}6H_2O]_3$ only, (ii) $[ChCl]_2[CoCl_2{\cdot}6H_2O]_3$ and TBHP and (iii) $[ChCl]_2[MnCl_2{\cdot}4H_2O]$ only (Figure 3.18). FT-IR analysis revealed that HDPE did not undergo oxidation in the presence of the $[ChCl]_2[MnCl_2{\cdot}4H_2O]$ DES nor $[ChCl]_2[CoCl_2{\cdot}6H_2O]_3$ DES with and without the additional TBHP co-oxidant. The high activation energy required for the inert decomposition of HDPE (150−260 $kJ{\cdot}mol^{-1}$) is likely not achieved under the given conditions, while the crystallinity of HDPE may also be impeding oxidation.[130] Linear HDPE is intrinsically more densely packed than branched LDPE and is less susceptible to oxidation as its crystalline phases are inaccessible to oxygen compared to openly accessible amorphous regions. On this note, LDPE undergoes 50 °C oxidation under all three of the tested conditions. Lengthened induction periods for the DES-only reactions with LDPE are expected given that the DES acts as a pre-catalyst. At 50 °C the kinetic energy input is lowered and likely not sufficient to catalyse a one-electron redox switch in the metal centres, therefore, creating the induction period. The overall level of oxidation (carbonyl index < 1) and the rates of depolymerisation are significantly lower than at 70 °C, thus 70 °C was selected as the optimum temperature to perform further studies.

3.3.4 Post-consumer LDPE

Chapter 2 demonstrated the effective depolymerisation of post-consumer LDPE film using the $[ChCl]_2[CoCl_2{\cdot}6H_2O]_3$ DES coupled with a phase transfer catalyst. Replacing the transfer catalyst for TBHP has already been found to successfully accelerate molecular weight loss in "clean" unprocessed LDPE. However, post-consumer plastics contain a greater quantity of contaminants such as antioxidants, dyes, and stabilisers. Antioxidant-containing plastics are often the most challenging to process, as the antioxidants are used to protect the plastic from premature ageing, therefore, they heighten the polymer's resistance to chemical oxidation. A series of coloured clear, blue, and white LDPE films (the same film as in Chapter 2) were subjected to $[ChCl]_2[CoCl_2{\cdot}6H_2O]_3$ with and without TBHP at a moderate temperature (70 °C). None of the DES-only reactions produced visible oxidation evident by FT-IR spectroscopy for any of the coloured samples, while the addition of TBHP a signal at 1710 cm^{-1}, characteristic of ketone C=O stretching, can be seen in all cases (Figure 3.5a). Notably, the carbonyl index profiles are unique and divergent for the individual colours with their level of oxidation as follows; white > clear > blue.

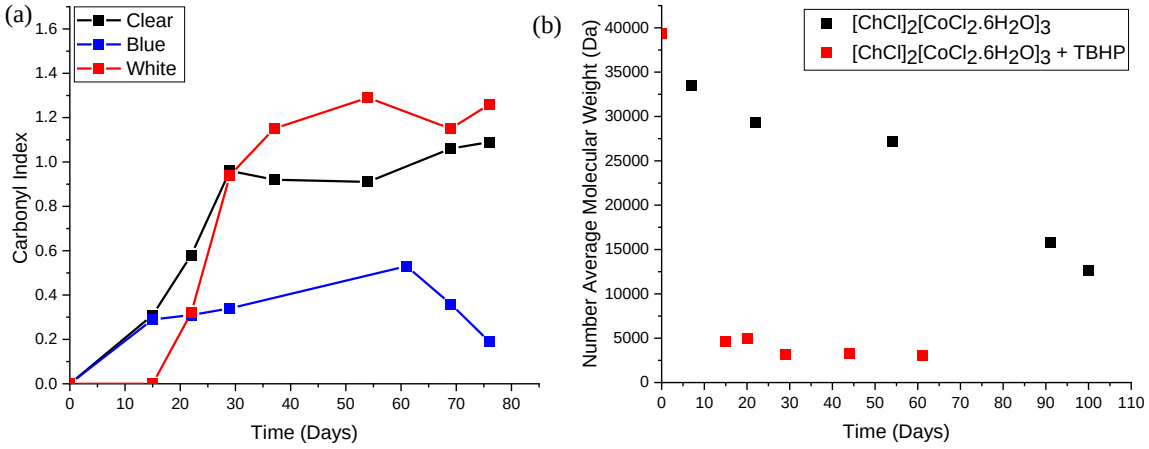

Figure 3.5 (a) Carbonyl index as a function of time of clear, blue and white post-consumer LDPE film throughout the reaction with $[ChCl]_2[CoCl_2{\cdot}6H_2O]_3$ and TBHP at 70 °C (b) Number average molecular weight as a function of time for the reaction of clear post-consumer LDPE with $[ChCl]_2[CoCl_2{\cdot}6H_2O]_3$ DES with and without TBHP (0.9 equiv) at 70 °C

It is interesting to note the roles the dyes are playing in the film's susceptibility to oxidation, in this case, the blue dye is impeding oxidation while the white caused an induction period before a steep oxygen incorporation. After seven days, a fine white powder can be seen in the place of both the clear and white films while the blue film remains as a film. As the dyes affected the solubility of the sample, only the GPC chromatograms of the clear LDPE were analysed. Curiously, not only did the TBHP accelerate the depolymerisation and show a reduction in molecular weight so too did the DES-only reaction, despite showing no signals of oxidation. This unique discovery implies that the LDPE film is breaking down *via* non-oxidative pathways and presumably forming mixed hydrocarbon products (Figure 3.5b).

3.3.5 Hydrogen peroxide catalysed oxidation

Hydrogen peroxide (H_2O_2) is an ideal oxidant as its only by-products are water and oxygen. Although its use was not considered initially, because of the high polarity of its radicals, their

high reactivity offers the potential to target chemically stable polyolefin bonds. $[ChCl]_2[MnCl_2{\cdot}4H_2O]$ and $[ChCl]_2[CoCl_2{\cdot}6H_2O]_3$ DES were loaded individually with 0.45 equivalents of H_2O_2, powdered LDPE and heated to 70 °C. For both catalytic systems, the polyolefin oxidation and subsequent depolymerisation were observed (Figure 3.6a and 3.6b). The lower temperature, although effective for moderating the decomposition of the peroxide, caused a 21-day induction period for the manganese-based DES and an overall slow loss of molecular weight.

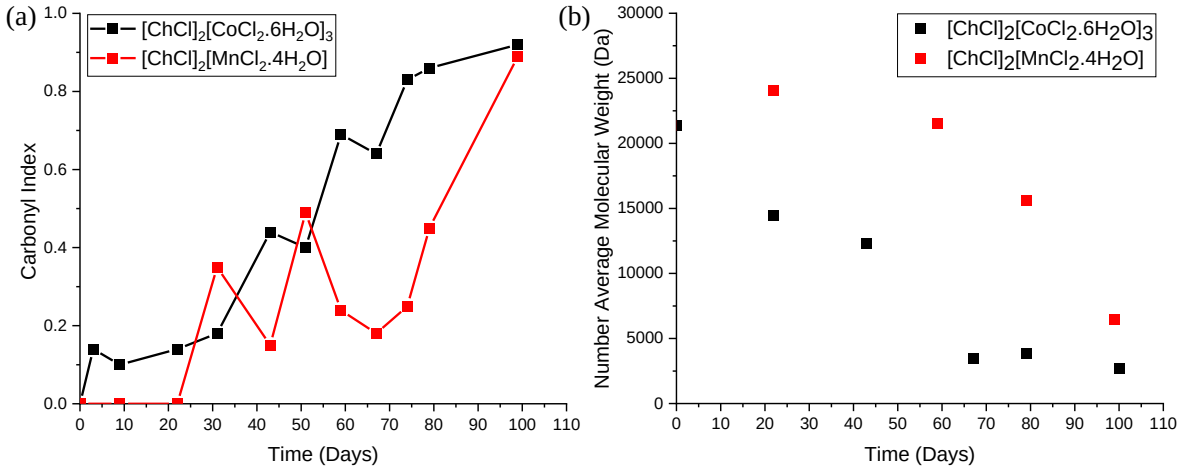

Figure 3.6 (a) Carbonyl index as a function of time for reaction of LDPE with $[ChCl]_2[CoCl_2{\cdot}6H_2O]_3$ and $[ChCl]_2[MnCl_2{\cdot}4H_2O]$ DES and H_2O_2 (0.45 equiv) at 70 °C (b) Number average molecular weight as a function of time for the reaction of LDPE with $[ChCl]_2[CoCl_2{\cdot}6H_2O]_3$ and $[ChCl]_2[MnCl_2{\cdot}4H_2O]$ DES and H_2O_2 (0.45 equiv) at 70 °C

3.3.6 Molecular oxygen reactions

3.3.6.1 TAM IV experiments

All depolymerisations up to this point have been performed under aerobic conditions. Notably, the O_2 content in air is only 20% while the remaining 80% is predominantly comprised of inert nitrogen (N_2), thus limiting potential oxidation events. By substituting atmospheric conditions for an O_2 atmosphere, the presence of potential reactive oxygen species can be maximised. It

was reported that the activation energy for PE decomposition can be lowered from 150 − 260 kJ·mol under inert conditions to 80 −143 kJ·mol in the presence of O_2.[131] Inspired by these results, depolymerisation experiments of LDPE were performed using $[ChCl]_2[CoCl_2{\cdot}6H_2O]_3$ DES in air and oxygen atmospheres at 70 °C and the resultant exotherms were measured by TAM IV analysis (Figure 3.7). For the depolymerisation performed under air, an exotherm of magnitude 46.91 J was released. In systems in which the depolymerisation was performed under an oxygen atmosphere, an exotherm of 224.66 J was released, a 5-fold increase, indicating that a greater number of oxidation events is occurring. The heat flow for the reactions under oxygen also exceeded that of the reactions performed in air (142.95 μW and 42.39 μW respectively). Interestingly, in both systems, induction periods are observed, similar to the ones seen by FT-IR spectroscopy, with an onset after 4.5 days in air and 3.5 days in oxygen. A reduction in the exotherm released after approximately 30 and 38 days in air and oxygen respectively, indicating the slowing/end of their reactions. Overall the TAM IV experiments proved that a greater number of oxidation events are achieved on the polyolefins under an oxygen atmosphere compared to air.

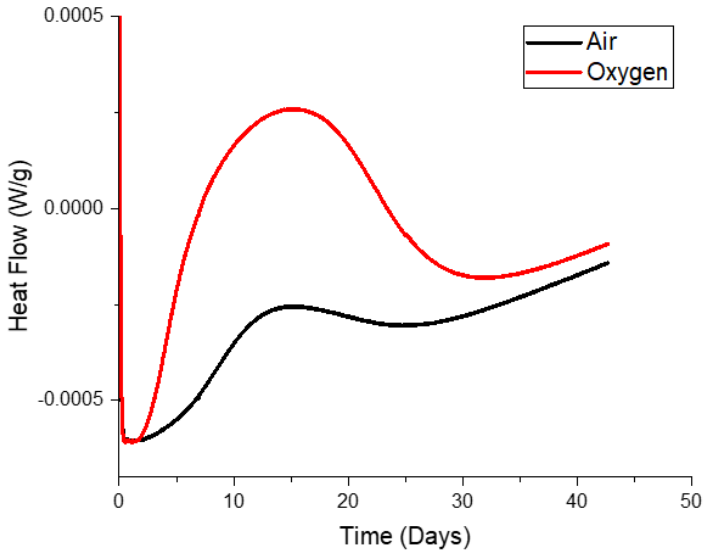

Figure 3.7 TAM IV thermogram for the reaction of $[ChCl]_2[CoCl_2{\cdot}6H_2O]_3$ with LDPE under air and oxygen atmosphere at 70 °C

3.3.6.2 Tert-butyl hydroperoxide

Individually, TBHP and an oxygen atmosphere, in the presence of a DES, have demonstrated the effective depolymerisation of LDPE, therefore, it was hypothesised that the reaction of the organic peroxide under an oxygen-rich atmosphere will further accelerate the depolymerisation of LDPE. An oxygen atmosphere was applied to the optimised $[ChCl]_2[CoCl_2{\cdot}6H_2O]_3$ DES and TBHP system at 70 °C. As expected, the uptake of oxygen by LDPE increased considerably in the oxygen-rich atmosphere while the oxygen ingress was steadier under air. The mechanism by which O_2 accelerates the decomposition is thought to be *via* its reaction with the alkyl radicals formed after TBHP decomposition to afford alkyl hydroperoxides which decompose into their corresponding ketones. To this end, the depolymerisation of LDPE under an oxygen atmosphere was significantly faster with 73% of its original M_n lost within the first 4 days (96% loss in total after 100 days) compared to the in-air experiment where it only lost 27% after 9 days (94% in total) (Figure 3.8a). A plateau in molecular weight loss between 1,000 – 3,000 Da is shown under both conditions, as a first hypothesis it was thought that the depolymerisation of easily accessible amorphous regions happens first, with only the densely packed inaccessible crystalline regions remaining. However, when calculating the percentage of crystallinity of the polymers obtained in air and oxygen after the 100-day reaction, a minimal change was observed (41% and 39% respectively) when compared to the pristine LDPE (40%) (Figure 3.23). For the crystallinity to remain constant both the amorphous and crystalline regions should depolymerise at the same rate, thus eliminating the influence of crystallinity. Low molecular weight shoulders are observed in the GPC chromatogram for LDPE under oxygen creating a trimodal profile, the same is not observed under air. These shoulders show the evolution of chain cleavage reactions creating a short chain majority and thus the $Đ_M$ of the samples increase over time.

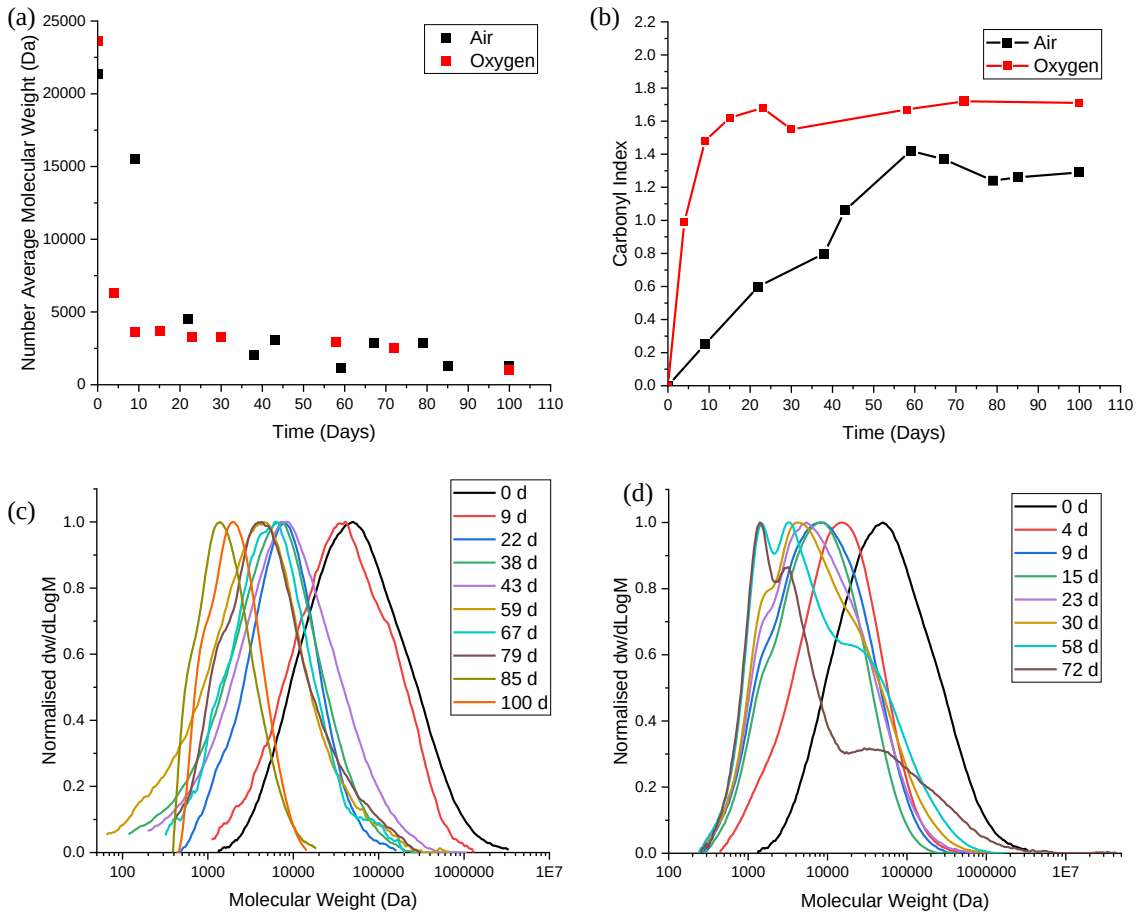

Figure 3.8 (a) Number average molecular weight as a function of time for LDPE after $[ChCl]_2[CoCl_2{\cdot}6H_2O]_3$ and TBHP (0.9 equiv) reaction at 70 °C under air and oxygen atmospheres. (b) Carbonyl index as a function of time of LDPE after $[ChCl]_2[CoCl_2{\cdot}6H_2O]_3$ and TBHP (0.9 equiv) reaction at 70 °C under air and oxygen atmospheres. Size exclusion chromatogram of the molecular weight distributions of LDPE during its reaction with $[ChCl]_2[CoCl_2{\cdot}6H_2O]_3$ and TBHP (0.9 equiv) at 70 °C under (c) air (d) oxygen. Molecular weight was determined against poly(styrene) standards using $C_6H_3Cl_3$ (250 mg·L^{-1} BHT) as eluent at 160 °C

After exploring LDPE, the depolymerisation of HDPE was investigated under an O_2 atmosphere. Applying the same $[ChCl]_2[CoCl_2{\cdot}6H_2O]_3$ and TBHP system to HDPE revealed the same elevation in oxygen ingress into the polymer chain under O_2, as observed through FT-IR spectroscopy (Figure 3.9b). The loss in M_n is evident in both cases, nevertheless, the in-air reaction follows a steady linear decrease while the O_2 reaction gives a rapid 62% loss within the first 14 days followed by a moderate decline. The reactions were terminated after 100 days where both resulted in a 3,000 Da polymer.

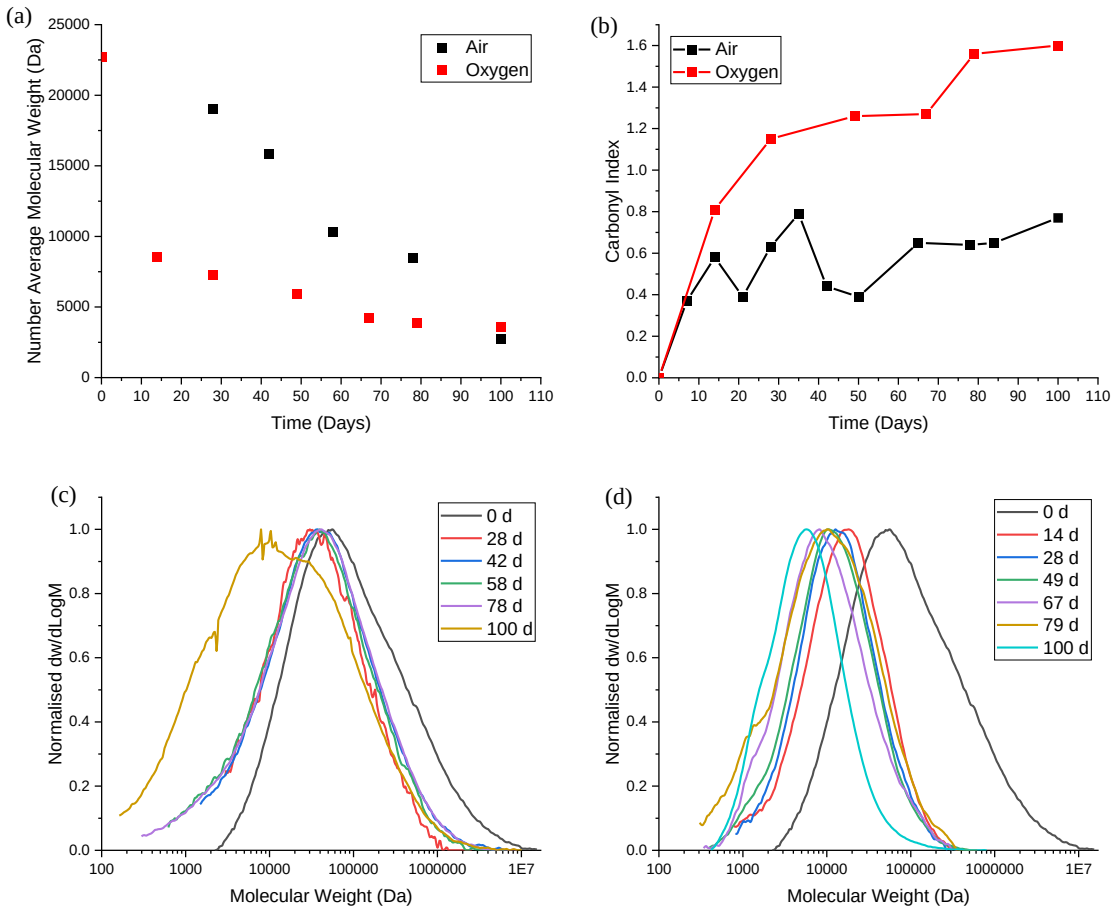

Figure 3.9 (a) Number average molecular weight as a function of time for HDPE after $[ChCl]_2[CoCl_2{\cdot}6H_2O]_3$ and TBHP (0.9 equiv) reaction at 70 °C under air and oxygen atmospheres. (b) Carbonyl index as a function of time of HDPE after $[ChCl]_2[CoCl_2{\cdot}6H_2O]_3$ and TBHP (0.9 equiv) reaction at 70 °C under air and oxygen atmospheres. Size exclusion chromatogram of the molecular weight distributions of HDPE during its reaction with $[ChCl]_2[CoCl_2{\cdot}6H_2O]_3$ and TBHP (0.9 equiv) at 70 °C under (c) air (d) oxygen. Molecular weight was determined against poly(styrene) standards using $C_6H_3Cl_3$ (250 mg·L^{-1} BHT) as eluent at 160 °C

3.3.6.3 Lauroyl peroxide

Lauroyl peroxide is a diacyl peroxide with two long C11 alkyl chains on either side of its peroxide group and upon homolytic cleavage of the O-O bond forms peroxyl radicals. The non-polar alkyl groups are expected to improve the hydrophobicity of the radical leading to a better interaction with LDPE, therefore, it was tested for LDPE depolymerisation accordingly using $[ChCl]_2[CoCl_2{\cdot}6H_2O]_3$ under air and oxygen atmospheres at 70 °C (Scheme 3.2). Under air, the reactions progressed slowly with 24% of the original M_n lost after 14 days. Intriguingly, the polymers $Đ_M$ progressively narrowed with time, unlike DES-only reactions, where a broadening in the GPC traces is first observed as indicative of consecutive chain scission events followed by a signal narrowing. The prompt narrowing implies the immediate loss of VOC. A slower reaction compared to its hydroperoxide counterpart, TBHP, may result from their respective $t_{1/2}$. Lauroyl peroxide has an average $t_{1/2}$ of 10 hours in the range of 20 – 75 °C while TBHP lies within the range of 133 – 172 °C, moreover, at 70 °C lauroyl peroxide activity will be lower than TBHP at an equivalent stage in the reaction. It is notable that it is dependent on the reaction conditions and the solvent used and thus will differ in every system and the values stated above are averages across varying conditions.

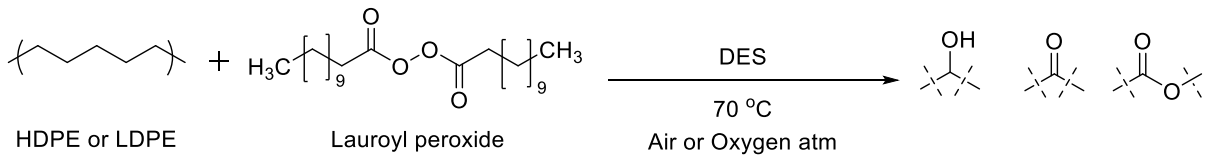

Scheme 3.2 General representation of the HDPE or LDPE oxidation using a DES and lauroyl peroxide radical initiator

DSC analysis indicated a rise in the crystallisation rate with a T_c shift from 99 to 103 °C (Figure 3.11e). An increase in chain mobility and a decrease in molecular size suggest LDPE can no longer form its regular crystal structure. Not surprisingly, the molecular weight of LDPE

subjected to an oxygen-rich atmosphere showed a sharp loss of M_n with 82% loss within the first 14 days, 70% faster than in air (Figure 3.11a). An immediate narrowing of $Đ_M$ is likewise present and although the narrowing is accelerated under the O_2 atmosphere as it is present under both conditions, this observation relates to the actions of lauroyl peroxide. The development of a bimodal GPC chromatogram after 49 days suggests that the bulk of the polymer is breaking down and short chains are forming. Different to the experiment performed under air, the T_c of the resultant polymer (T_c = 98 °C) under oxygen resembles more closely to unreacted LDPE (T_c = 95 °C), with no distinct regions associated with ox-LDPE species, implying a more uniform degradation with the loss of VOCs. ^{13}C NMR spectroscopy of the resultant ox-LDPE after the 100-day reaction under air gives predominantly alkyl branching signals with only a minor indication of oxygenated species (Figure 3.10). ^{1}H NMR spectroscopy supports this observation with a 2.7 mol% ketone and 0.2 mol% alcohol group incorporation (total FG = 2.9 mol%) (Figure 3.19). The lack of functionality in the NMR spectra reinforms the loss of oxidised VOCs. NMR spectra of LDPE after reacting under oxygen were not obtained due to instrument downtime, however, it was hypothesised that less oxygenated species will be present in the NMR spectra due to increased loss of VOCs.

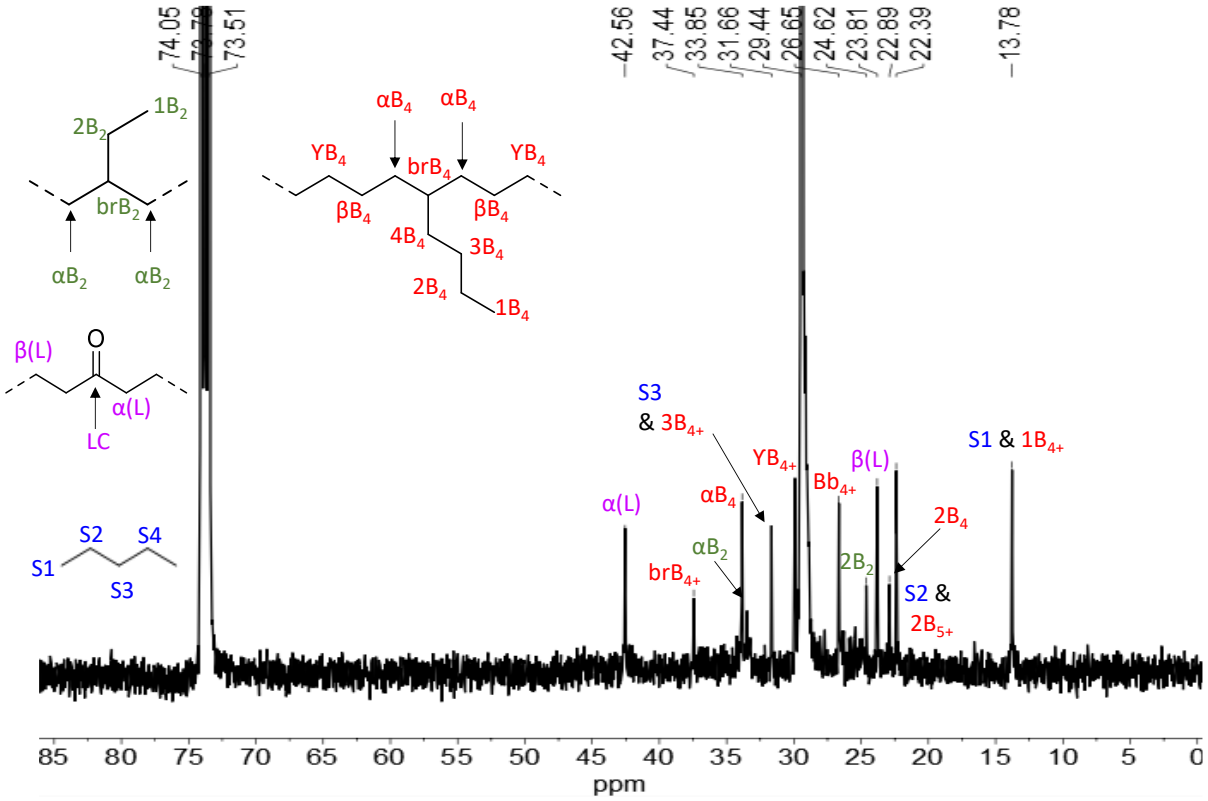

Figure 3.10 ^{13}C NMR spectrum (400 MHz, $C_2D_2Cl_4$ at 100 °C) of LDPE (FG = 2.9 mol %) after 100-day reaction with $[ChCl]_2[CoCl_2{\cdot}6H_2O]_3$ and lauroyl peroxide (0.15 equiv) at 70 °C in air

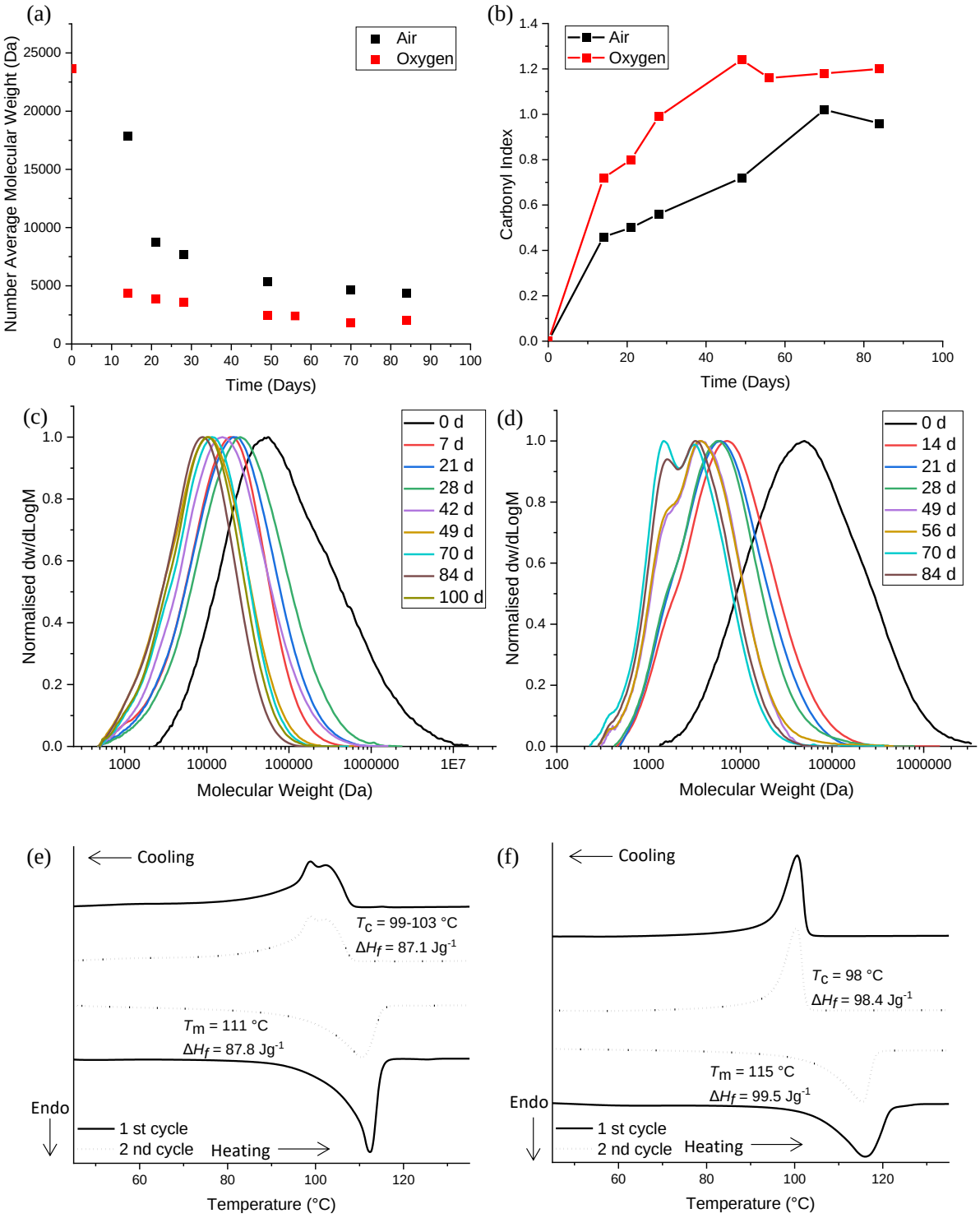

Figure 3.11 (a) Number average molecular weight as a function of time for LDPE after $[ChCl]_2[CoCl_2{\cdot}6H_2O]_3$ and lauroyl peroxide (0.15 equiv) reaction at 70 °C under air and oxygen atmospheres. (b) Carbonyl index as a function of time of LDPE after $[ChCl]_2[CoCl_2{\cdot}6H_2O]_3$ and lauroyl peroxide (0.15 equiv) reaction at 70 °C under air and oxygen atmospheres. Size exclusion chromatogram of the molecular weight distributions of LDPE during its reaction with $[ChCl]_2[CoCl_2{\cdot}6H_2O]_3$ and lauroyl peroxide (0.15 equiv) at 70 °C under (c) air (d) oxygen. DSC thermograms for the first (top) and second (bottom) heating cycles for LDPE after a 100-day reaction with $[ChCl]_2[CoCl_2{\cdot}6H_2O]_3$ and lauroyl peroxide (0.15 equiv) at 70 °C at a heating rate of 10 °C·min^{-1} under (e) air (f) oxygen. Molecular weight was determined against poly(styrene) standards using $C_6H_3Cl_3$ (250 mg·L^{-1} BHT) as eluent at 160 °C

Despite the lack of proposed primary and secondary hydrogen abstraction preference by peroxyl radicals the reaction using $[ChCl]_2[CoCl_2{\cdot}6H_2O]_3$ and lauroyl peroxide (0.15 equiv) was performed on HDPE at 70 °C. ^{13}C NMR spectroscopy performed on the 100-day oxidised HDPE shows the same visible environments as that found in the oxidised LDPE spectra suggesting a similar product distribution. Integration of the ox-HDPE ^{1}H NMR spectrum revealed 2.7 mol% ketone groups and 1.3 mol% alcohol groups, bringing the combined total functional group content to 4.0 mol% (Figure 3.20). Notably, even under air, lauroyl peroxide rapidly accelerates HDPE decomposition with a 76% M_n loss after 14 days and a total M_n loss of 84% after 100 days. Nevertheless, the oxygen atmosphere reaction outperforms this with 87% M_n loss after 14 days, reaching 90% after 100 days (Figure 3.13a).

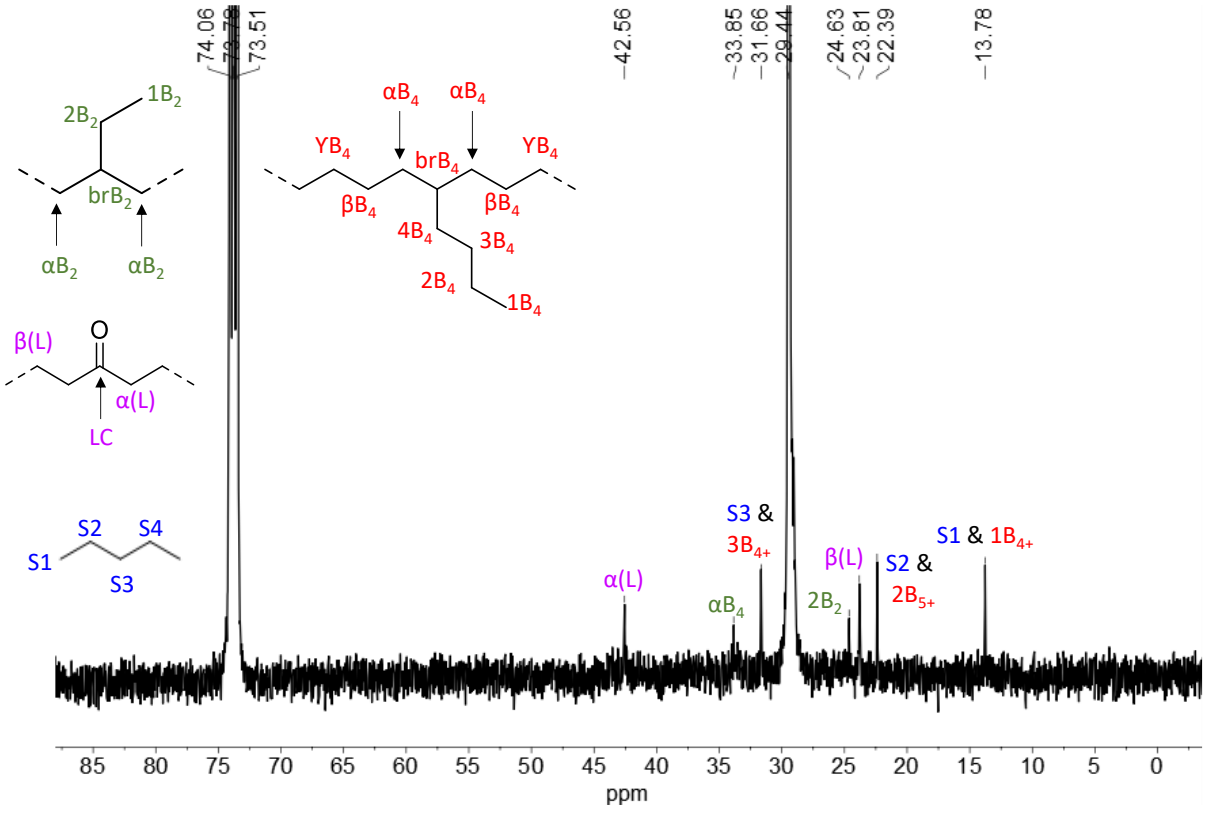

Figure 3.12 ^{13}C NMR spectrum (400 MHz, $C_2D_2Cl_4$ at 100 °C) of HDPE (FG = 4.0 mol%) after 100-day reaction with $[ChCl]_2[CoCl_2{\cdot}6H_2O]_3$ and lauroyl peroxide (0.15 equiv) at 70 °C in air

Contrary to the observations made for LDPE, temperature-induced crystallisation of the ox-HDPE species shifts progressively towards lower temperatures with increased levels of oxidation. Unmodified semi-crystalline HDPE readily crystallises at approximately 131 °C whereas its oxidised form, as a consequence of its lower molecular weight and less linear structures, cannot orientate into the same regular crystalline domains and therefore its crystallisation is compromised (Figure 3.24). The behaviour of the ox-HDPE species during a melt transition can give further insight into the unique crystallisation phases of the newly formed ox-HDPE species, as the T_m of HDPE crystallites decreases with increasing levels of oxidation (T_m = 128 and 125 °C for air and oxygen respectively). Lower energy is required to induce a melt transition of oxidised HDPE species as they possess crystal defects such as oxygenated groups, branching sites and double bonds. This is reinforced by calculating the percentage of crystallinity present in both samples relative to their starting HDPE polymer. Pristine HDPE has a crystallinity of 54% and after reacting under air its crystallinity increased to 58%. Increasing crystallinity alludes to the amorphous regions having been primarily targeted leaving behind crystalline domains. The reverse was observed under an oxygen atmosphere with a lower 40% crystallinity remaining, implying that chain rupture occurred in both amorphous and crystalline phases. Densely packed crystalline domains make oxygen permutation challenging however this can be overcome under the O_2 atmosphere.

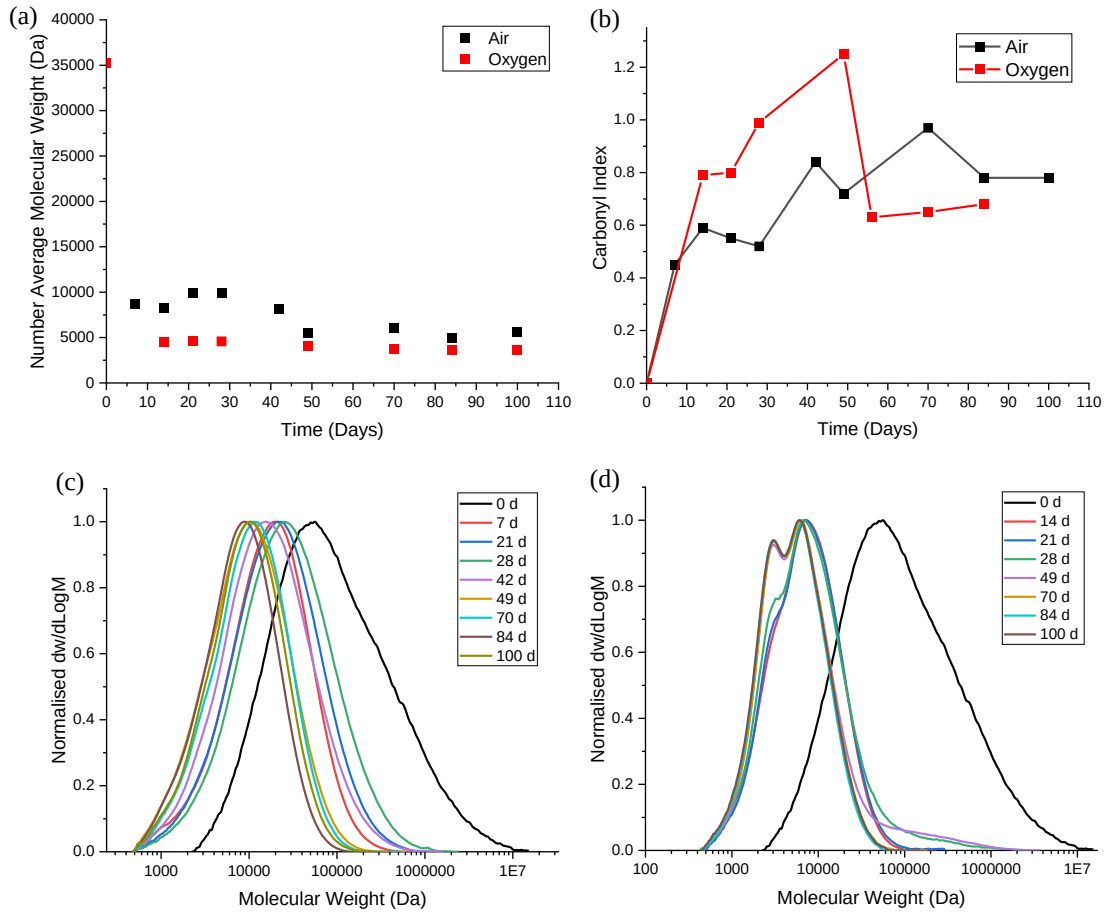

Figure 3.13 Number average molecular weight as a function of time for HDPE after $[ChCl]_2[CoCl_2{\cdot}6H_2O]_3$ and lauroyl peroxide (0.15 equiv) reaction at 70 °C under air and oxygen atmospheres. (b) Carbonyl index as a function of time of HDPE after $[ChCl]_2[CoCl_2{\cdot}6H_2O]_3$ and lauroyl peroxide (0.15 equiv) reaction at 70 °C under air and oxygen atmospheres. Size exclusion chromatogram of the molecular weight distributions of HDPE during its reaction with $[ChCl]_2[CoCl_2{\cdot}6H_2O]_3$ and lauroyl peroxide (0.15 equiv) at 70 °C under (c) air (d) oxygen. Molecular weight was determined against poly(styrene) standards using $C_6H_3Cl_3$ (250 mg·L^{-1} BHT) as eluent at 160 °C

When combining the manganese-based DES, $[ChCl]_2[MnCl_2{\cdot}4H_2O]$, and lauroyl peroxide with LDPE at 70 °C, much of the same influence as TBHP under air and oxygen is observed. Following the incorporation of carbonyl functionality as a function of time gives a smooth incorporation profile with only a plateau after 84 days in both instances (Figure 3.14b). Under air, 75% of the original M_n of LDPE is lost after 100 days while a significant 98% is lost under an oxygen atmosphere. When plotting M_n loss as a function of time, not all of the aliquots follow the expected downward trend, this is possibly a result of the non-uniform GPC trace profiles

caused by the formation of low molecular weight shoulders (Figure 3.14a). The terminal M_n under oxygen was recorded at 360 Da, however, as this value is outside the lower calibration limit on the GPC, it is plausible that the polymer is of insufficient size to be recorded causing the M_n value to stagnate, as seen in this case. Scrutinising LDPEs molecular weight distributions in both cases shows a clear divergence in GPC chromatograms, (Figure 3.14c and d). Performing the reaction under oxygen shows the development of low molecular weight shoulders after 49 days which becomes progressively dominant. The formation of the shoulders broadens the $Đ_M$ alluding to chain scission reactions. DSC analysis shows that the ox-LDPE species under both atmospheres have a lower percentage of crystallinity (30% and 33% for air and oxygen respectively) and increased T_c compared to unmodified LDPE (Figure 3.25a and 3.25b). A double crystallisation peak is observed under air which is indicative of both high and low molecular weight species. Increased crystal defects created by oxygenated groups result in smaller crystals and easier crystallisation, hence the increased T_c.

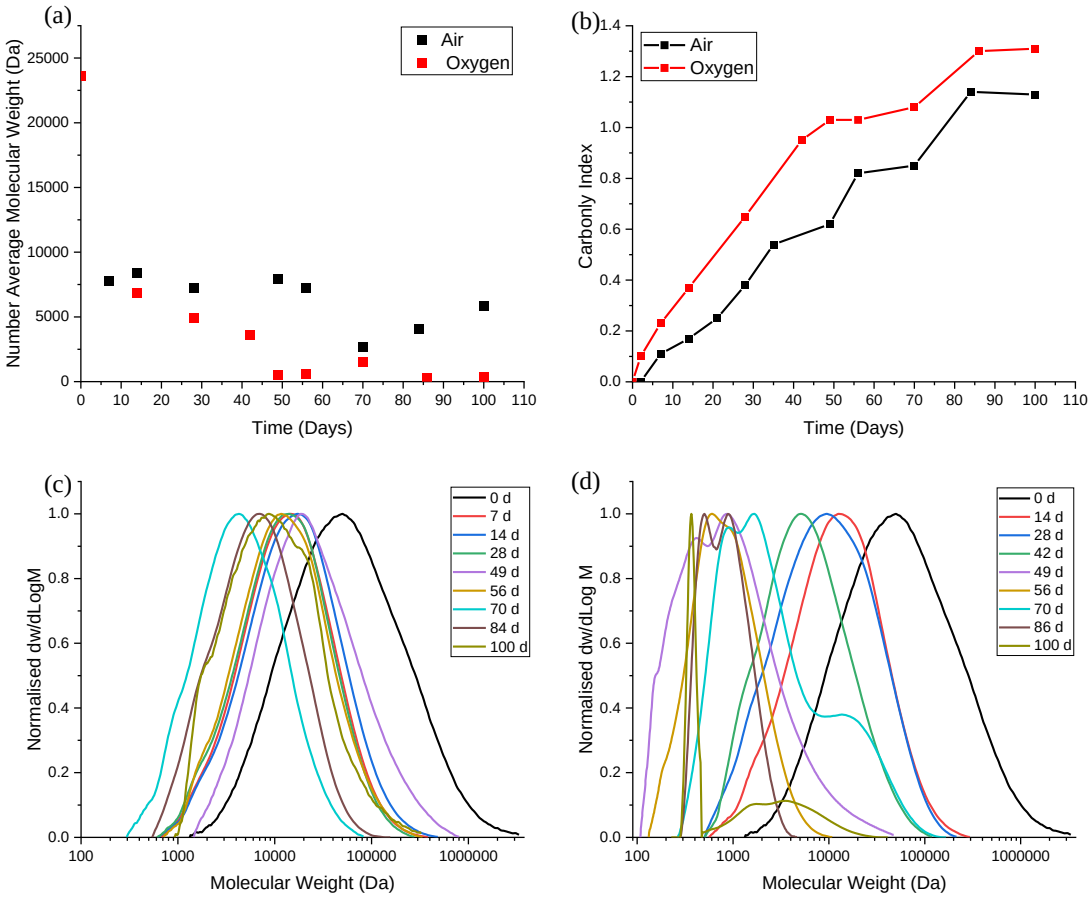

Figure 3.14 Number average molecular weight as a function of time for LDPE after $[ChCl]_2[MnCl_2{\cdot}4H_2O]$ and lauroyl peroxide (0.15 equiv) reaction at 70 °C under air and oxygen atmospheres. (b) Carbonyl index as a function of time of LDPE after $[ChCl]_2[MnCl_2{\cdot}4H_2O]$ and lauroyl peroxide (0.15 equiv) reaction at 70 °C under air and oxygen atmospheres. Size exclusion chromatogram of the molecular weight distributions of LDPE during its reaction with $[ChCl]_2[MnCl_2{\cdot}4H_2O]$ and lauroyl peroxide (0.15 equiv) at 70 °C under (c) air (d) oxygen. Molecular weight was determined against poly(styrene) standards using $C_6H_3Cl_3$ (250 mg·L^{-1} BHT) as eluent at 160 °C

As demonstrated previously, $[ChCl]_2[MnCl_2{\cdot}4H_2O]$ shows a greater proclivity for the oxidation of linear HDPE versus branched LDPE, and the same trend can be observed with the addition of lauroyl peroxide. Lauroyl peroxide accelerates the depolymerisation of HDPEunder both scenarios with a considerable 91% and 99% M_n lost after 100 days under air and oxygen atmosphere, respectively. Again, it is likely that the terminal 480 Da polymer (oxygen) is at the lowest limit of the GPC calibration curve, and it could have smaller oligomers generated (Figure 3.15a). Observations of shoulders on the GPC trace are evident after 4 days of reaction under

oxygen, while they are only present after 100 days in air. Semi-crystalline HDPE has both easily accessible amorphous and impermeable to oxygen crystalline phases and the profile of the shouldering supports the concept of preferential depolymerisation of the amorphous regions. The lack of shoulders observed in reactions performed in an air atmosphere is coupled with a high resultant crystallinity of the remaining ox-HDPE (69%). On the other hand, the predominantly bimodal GPC profile of the in-oxygen ox-HDPE samples have a crystallinity lower (41%) than virgin HDPE (54%). It is important to note that FT-IR spectroscopy of all ox-

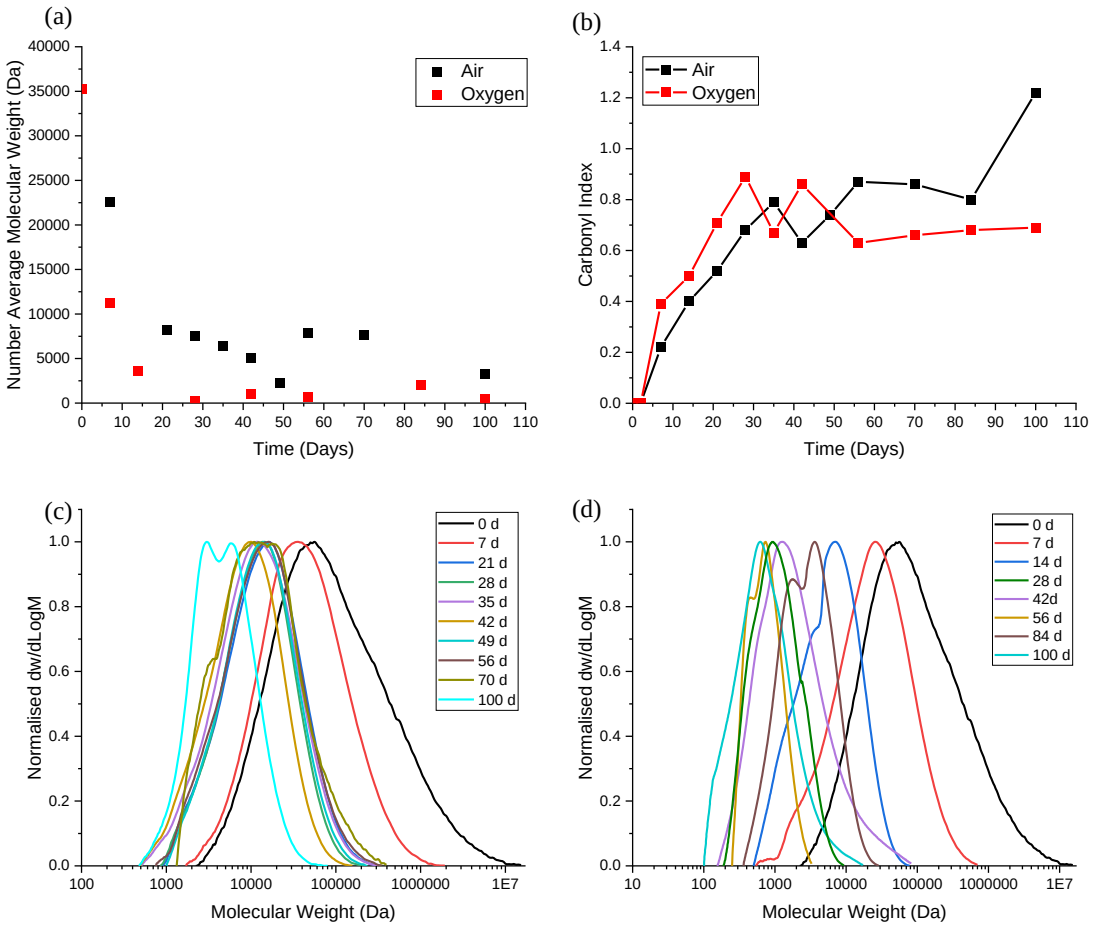

Figure 3.15 (a) Number average molecular weight as a function of time for HDPE after $[ChCl]_2[MnCl_2{\cdot}4H_2O]$ and lauroyl peroxide (0.15 equiv) reaction at 70 °C under air and oxygen atmospheres. (b) Carbonyl index as a function of time of HDPE after $[ChCl]_2[MnCl_2{\cdot}4H_2O]$ and lauroyl peroxide (0.15 equiv) reaction at 70 °C under air and oxygen atmospheres. Size exclusion chromatogram of the molecular weight distributions of HDPE during its reaction with $[ChCl]_2[MnCl_2{\cdot}4H_2O]$ and lauroyl peroxide (0.15 equiv) at 70 °C under (c) air (d) oxygen. Molecular weight was determined against poly(styrene) standards using $C_6H_3Cl_3$ (250 mg·L^{-1} BHT) as eluent at 160 °C

LDPE and ox-HDPE samples, until this point, have only identified the C=O stretching bandof a ketone group (wavenumber 1710 cm^{-1}) and no ester functionality was observed (1740 cm^{-1}).

3.3.6.4 Post-consumer LDPE

Lauroyl peroxide coupled with molecular oxygen has already proven to be the most effective catalyst system at accelerating LDPE depolymerisation, however, it has yet to tackle the challenge of depolymerising post-consumer plastics. Clear post-consumer LDPE film was subject to $[ChCl]_2[CoCl_2 \cdot 6H_2O]_3$ and lauroyl peroxide in an oxygen atmosphere at a moderate 70 °C temperature (Figure 3.16). The carbonyl index profile follows a steady increase over the course of the reaction reaching a peak of 2.2. Most of the molecular weight loss was accomplished within 7 days with a loss of 95% of the original M_n, while ~100% was lost after 56 days (M_n = 117 Da). Near complete depolymerisation into small molecular chains is noticeable early in the GPC chromatagrams with the evolution of low molecular weight shoulders. These shoulders dominate the chromatogram with the broader higher molecular weight shoulders diminishing as a function of time. The study was terminated after 56 days as there was no evidence of the film remaining, thus implying complete conversion into VOCs. The majority of the molecular weight loss was accomplished before the first aliquot was taken on day 7, therefore, to better understand the trend in weight loss, aliquots would be required daily during the first 7 days. Repeating this experiment with headspace analysis would allow for the identification of the VOC released during the reaction giving insights into the mechanism. Further investigation is required in the depolymerisation of HDPE.

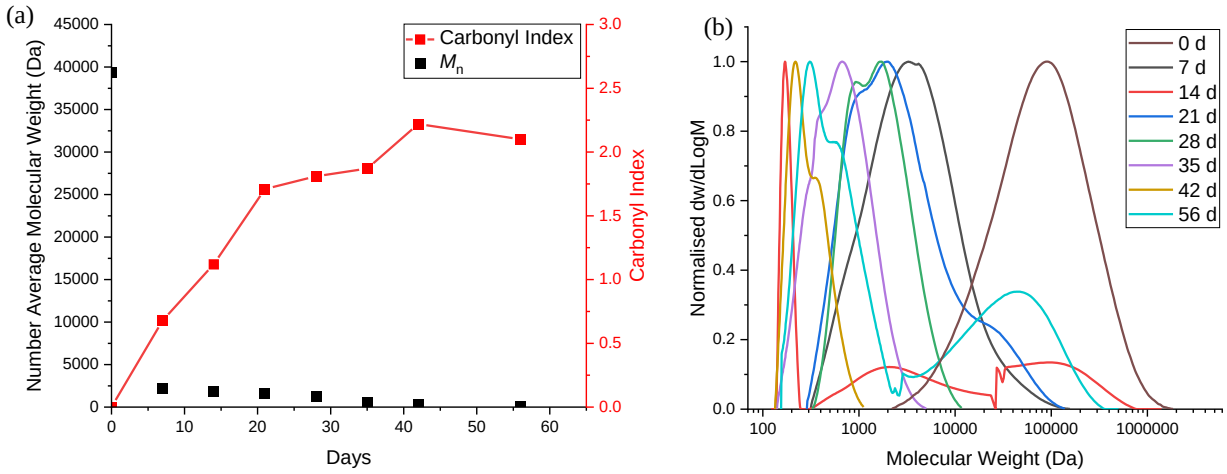

Figure 3.16 (a) Number average molecular weight and carbonyl index as a function of time of post-consumer LDPE after its reaction with $[ChCl]_2[CoCl_2{\cdot}6H_2O]_3$ and lauroyl peroxide at 70 °C under O_2 (b) Size exclusion chromatogram of the molecular weight distributions of post-consumer LDPE throughout its reaction with $[ChCl]_2[CoCl_2{\cdot}6H_2O]_3$ and lauroyl peroxide at 70 °C under O_2. Molecular weight was determined against poly(styrene) standards using $C_6H_3Cl_3$ (250 mg·L^{-1} BHT) as eluent at 160 °C

3.3.7 Adhesion tests

It is challenging to achieve full PE conversion; following the promising results obtained in depolymerising both LDPE and HDPE, the potential upcycling prospects of the oxidised species were investigated. LDPE and HDPE were oxidised using $[ChCl]_2[CoCl_2{\cdot}6H_2O]_3$ and lauroyl peroxide as a co-oxidant for 7 days at 70 °C. The resulting oxidation and consequent adhesion promotion have been characterised by single-lap shear testing using HDPE substrates. It is important to note that FT-IR analysis of the HDPE substrate showed a small number of ketone groups. Notoriously, polyethylene has weak interactions, therefore, not surprisingly LDPE barely adhered to the HDPE interface with a low strain at break (ε_b = 19.4 ± 5.5%) and stress at break (σ_b = 0.2 ± 0 MPa), ox-LDPE on the other hand, with a carbonyl index of 1.5 doubled the strain and stress at break (ε_b = 39.0 ± 3.4% and σ_b = 0.5 ± 0.1 MPa respectively)

(Figure 3.17a). Incorporating a small amount of carbonyl functional groups into the polymer chain resulted in a 2-fold increase in adhesion strength despite the lower molecular weight.

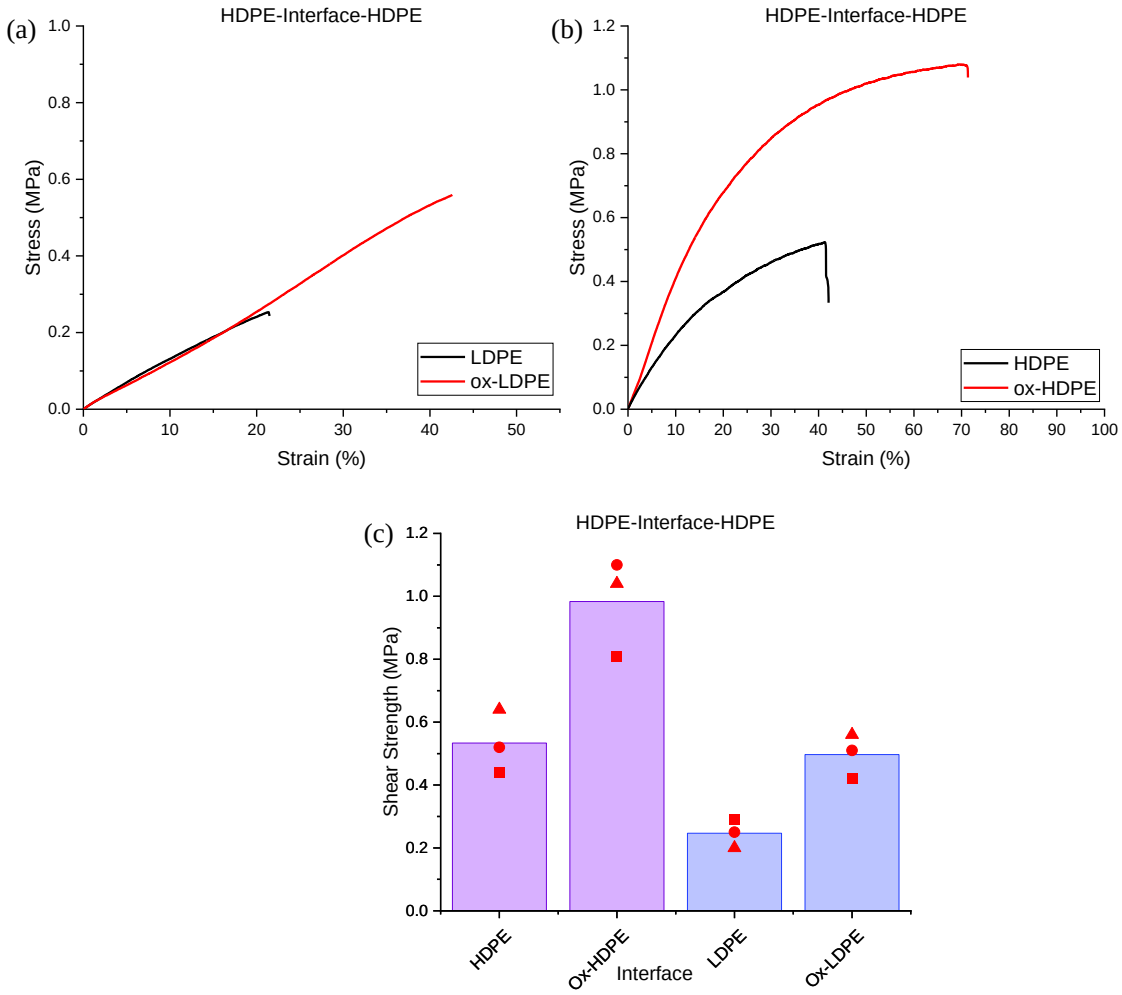

Figure 3.17 Single lap-shear tests of HDPE-Interface-HDPE at a 1.5 mm·min^{-1} strain rate with the interface being: (a) LDPE and ox-LDPE (b) HDPE and ox-HDPE (c) Shear strength of HDPE-interface-HDPE samples where the interface is HDPE, ox-HDPE, LDPE and ox-LDPE with n = 3

An analogous result was achieved in ox-HDPE samples with an enlarged stress and strain at break (ε_b = 47.4 ± 23.3% and σ_b = 1.0 ± 0.2 MPa respectively) compared to unmodified HDPE (ε_b = 40.4 ± 16.0% and σ_b = 0.5 ± 0.1 MPa) (Figure 3.17b). We attributed this improved adhesion strength to strong interactions between the functionalised polyethylenes with the functional groups on the interface surface of HDPE. Importantly, despite both oxidised PE samples being

of lower molecular weight (ox-LDPE M_n = 14 kDa and ox-HDPE M_n = 18 kDa) than their unmodified polymers (LDPE M_n = 22 kDa and HDPE M_n = 47 kDa) they still reach a greater shear strength (Figure 3.26). Without the use of a peroxide co-oxidant *i.e.* $[ChCl]_2[CoCl_2{\cdot}6H_2O]_3$ and [BMIm]Cl, the molecular weight loss of LDPE is lower but has a comparable carbonyl index, thus providing scope to routes for stronger PE adhesion.

3.4 Conclusion

The chemical and thermal resistance shown by polyolefins owning to their stable all-carbon backbones limits their chemical recyclability. This chapter investigates the accelerated depolymerisation of low- and high-density PE using novel DES following two approaches.

Firstly, organic peroxides were used as radical initiators. Subsequential radical generation produced a high density of reactive oxygen species capable of forming oxygenated functional groups on the polymer backbone. Increased radical loading accelerated the molecular weight loss of both polyolefin topologies with an improved affinity for deleterious chain scission events. Despite giving rise to extremely reactive hydroxy radicals, H_2O_2 accelerated the depolymerisation the least of all the peroxides tests, therefore, the use of a low polarity alkyl substituent group on the radical species was required for better compatibility with the non-polar polyolefins owing to their heterogeneous reaction. The recoverability of the DES revealed little change in its catalytic activity after two depolymerisation cycles.

Secondly, oxygen-rich environments were utilised to maximise the generation of potential reactive oxygen species. Subsequent reactions showed that with or without a radical initiator the added oxygen greatly increased the rate of depolymerisation of LDPE and HDPE with evidence of increased chain scission events and loss of VOCs. Oxygen atmosphere reactions showed less dependence on the polymer crystallinity than in-air reactions with the resultant low

molecular weight polymers having near to the same crystallinity percentage as the starting polymer. The contaminants in post-consumer LDPE did not impede its successful depolymerisation into small molecules, however, the influence of dyes on the DES is still unclear and would require further investigation.

The potential value-added up-cycling of the now oxidised LDPE and HDPE into stronger adhesives revealed improved shear strength in both cases, however, greater control is required to target specific functional group content and therefore potential adhesion strength. The work described in this chapter provides a good starting point for the development of a simple solvent-free and low-temperature polyolefin depolymerisation, however, further work is needed to identify the reaction products and thus to build a better understanding of the reaction mechanism.

3.5 References

1. J. Gu, H. Kim and H. Lim, *Energy Convers. Manag.*, 2022, **270**, 116256-116260.
2. I. A. Ignatyev, W. Thielemans and B. V. Beke, *Chem. Sus. Chem*, 2014, **7**, 1579-1593.
3. R. Miandad, M. Rehan, M. A. Barakat, A. S. Aburiazaiza, H. Khan, I. M. I. Ismail, J. Dhavamani, J. Gardy, A. Hassanpour and A.-S. Nizami, *Front. Energy Res.*, 2019, **7**, 1-17.
4. H. Xiang, J. He, W. Qian, M. Qiu, H. Xu, W. Duan, Y. Ouyang, Y. Wang and C. Zhu, *Molecules*, 2023, **28**, 857.
5. G. Lyngsie, L. Krumina, A. Tunlid and P. Persson, *Sci. Rep.*, 2018, **8**, 10834-10843.
6. Z. Ma, K. T. Mahmudov, V. A. Aliyeva, A. V. Gurbanov, M. F. C. Guedes da Silva and A. J. L. Pombeiro, *Coord. Chem. Rev.*, 2021, **437**, 213859-213887.
7. S. Coiai, E. Passaglia and F. Cicogna, *Polym. Int.*, 2018, **68**, 27-63.
8. N. Li, S. Yang, Z. Huang and X. Pan, *Macromolecules*, 2021, **54**, 6000-6005.
9. Z. Zhang, X. Li, D. Zhou, S. Ding, M. Wang and R. Zeng, *J. Am. Chem. Soc.*, 2023, **145**, 7612-7620.
10. G. Yang, H. Du, J. Liu, Z. Zhou, X. Hu and Z. Zhang, *Green Chem.*, 2017, **19**, 675-681.
11. H. Xu, S. Yamaguchi, T. Mitsudome and T. Mizugaki, *EurJOC*, 2022, **2022**, 1-5.
12. T. Mallat and A. Baiker, *Chem. Rev.*, 2004, **104**, 3037−3058.
13. K.-J. Liu, J.-H. Deng, J. Yang, S.-F. Gong, Y.-W. Lin, J.-Y. He, Z. Cao and W.-M. He, *Green Chem.*, 2020, **22**, 433-438.
14. K. Suzuki, T. Watanabe and S. Murahashi, *J. Org. Chem.*, 2013, **78**, 2301-2310.
15. E. Sella and D. Shabat, *Org. Biomol. Chem.*, 2013, **11**, 5074-5078.
16. S. Fukuzumi, Y. Lee, J. Jung and W. Nam, *Green Chem.*, 2018, **20**, 948-963.
17. Q. Zhang, J. D. Gorden and C. R. Goldsmith, *Inorg. Chem.*, 2013, **52**, 13546-13554.
18. F. Posada, P. Malfreytb and J.-L. Gardette, *Comput. Theor. Polym.*, 2001, **11**, 95-104.
19. I. Oluwoye, M. Altarawneh, J. Gore and B. Z. Dlugogorski, *Combust. Flame*, 2015, **162**, 3681-3690.
20. N. Gascoin, G. Fau, P. Gillard and A. Mangeot, *JAAP*, 2013, **101**, 45-52.

3.6 Experimental

3.6.1 Instruments

Nuclear magnetic resonance (NMR)

^{1}H and ^{13}C NMR spectra were recorded at 298 K on an Ascend Bruker 400 spectrometer equipped with a BBFO smart probe operating at 400 MHz and 100 MHz respectively. Chemical shifts of ^{1}H NMR spectra were referenced to the solvent residual proton resonance signals: δ 7.26 ppm for *d1*–$CDCl_3$. Spectra data was analysed using MestReNova 12.0.2 software. The resonance multiplicities for ^{1}H NMR spectra are described as s (singlet), d (doublet), t (triplet), q (quartet) or m (multiplet).

High-temperature NMR

^{1}H and ^{13}C NMR spectra of the polyolefins were measured at 363 K on a Bruker AVANCE NEO console (2017) 400 spectrometer equipped with a 5 mm BBFO smart probe operating at 400 MHz and 100 MHz respectively. Chemical shifts of ^{1}H NMR spectra were referenced to the solvent residual proton resonance signal: δ 6.00 ppm for *d*-TCE. 1500 scans experiments were performed for ^{1}H NMR and 21000 scans for ^{13} C NMR.

High-temperature gel permeation chromatography (HT-GPC)

HT-GPC measurements were performed in $C_6H_3Cl_3$ (+ 250 mg·L^{-1} BHT) on an Agilent 1260 Infinity high-temperature GPC (Agilent) system fitted with viscometer detectors, RI and ultraviolet (UV, λ = 309 nm) at 160 °C. Using $C_6H_3Cl_3$ (+ 250 mg·L^{-1} BHT) as the mobile phase (flow rate = 1 mL.min^{-1}) the polymers were eluted through an Agilent guard column (PLGel 5 μ, 50 × 7.5 mm) and two Agilent mixed-B columns (PLGel 5 μ, 300 × 7.5 mm). A calibration curve (M_n = 162 – 3,187.000 $gmol^{-1}$) was used to determine the number average molecular

weight (M_n), weight average molecular weight (M_w) and dispersity ($Đ_M = M_w/M_n$) based on polystyrene standards (Easivial PS-M/H, Agilent). A Mark-Houwink correction was applied, K = 19 for PP and K = 39 for PE and α = 0.725. All samples were run according to D6474. The samples were dissolved in $C_6H_3Cl_3$ (+ 250 mg·L^{-1} BHT) at a concentration of 1.5 mg·mL^{-1} and heated at 160 °C for 3h prior to GPC analysis being performed. Once fully dissolved the samples were injected at a flow rate of 1 mL·min^{-1} with a 100 μmL injection volume at 160 °C.

Differential scanning calorimetry (DSC)

Glass transition temperature (T_g), melting transition temperature (T_m), crystallisation temperature (T_c) and total enthalpy (ΔH_m) of melting were measured on a STARe system DSC3 equipped with an auto-sampler (Mettler Toledo, Switzerland) under a N_2 atmosphere. Samples were positioned in 40 μL aluminium pans (Mettler Toledo) and cycled between −80 to 180 °C for three heating and cooling cycles at 10 °C min^{-1}. From the second heating cycle, the glass transition temperature (T_g) was observed as the midpoint of the inflextion tangent. Normalisation and integration of the endothermic transitions enabled the total enthalpy of heating (ΔH_m) to be calculated.

Thermo-gravimetric analysis (TGA)

Dynamic and isothermal TGA data was obtained using a Q50 - Thermogravimetric Analyzer (TA instrument)**.** Thermograms were recorded under an N_2 atmosphere at a heating rate of 10 °C·min^{-1}, from 10 − 600 °C, with an average sample weight of *ca*. 7 mg.

Gas chromatography-mass (GC-MS) spectrometry

GC-MS analysis was used to characterise and identify oxidation products using a GCMS-QP2010 SE chromatograph mass spectrometer. Chromatographic separation was carried out on a ZB-5HT inferno achiral column (L = 30 m, ID = 0.25 mm, FT = 0.25 μm). Gas chromatography was performed with a constant helium flow of 1.0 mL min^{-1} and a 1:40 split ratio. The oven programmed temperature was set to 40 °C for 2 min then ramped at a rate of 6 °C min^{-1} up to a final temperature of 300 °C where it was held for 20 min. Total gas chromatography analysis was approximately 65 min for each sample run. The manifold, ion trap source and transfer line temperature were set at 120 °C, 220 °C and 300 °C, respectively. Mass spectra were scanned on the *m/z* 30-550 range with a rate of 1 scan s^{-1}. Product identification was achieved by comparing their mass spectra to the NIST MS library and their elution time against commercial standards.

Fourier transform- infrared (FT-IR) spectroscopy

FT-IR data was obtained (neat) using a Perkin Elmer Paragon 1000 FT-IR spectrometer. 5 μL (5 mg·mL^{-1}) was deposited on top of the detectors using attenuated total reflection to measure. Wavelengths were scanned in the range of 500- 4000 cm^{-1}.

Lap shear testing

Adhesion testing was performed according to ASTM D1200-10[14] using a Testomic M350-5CT universal mechanical testing instrument fitting with a 100 kN load cell. Polymer films of LDPE, HDPE, ox-LDPE and ox-HDPE were prepared by compression moulding at 140 °C for 15 mins. Specifically, the polymer samples were placed in a 50 × 40 × 0.5 mm stainless steel mould

between two sheets of Teflon film and were pressed with a clamping force of 2000 kg before being allowed to cool to room temperature while still under force. Once cooled 10 × 10 mm squares were cut from the film and placed on the end of a HDPE adherend (top and bottom, in an antiparallel arrangement) and a clamp or vinyl masking tape was used to secure it in place (e.g. HDPE–LDPE–HDPE). The samples were placed in a preheated oven at 115 °C for 30 mins before being removed and allowed to cool to room temperature. Shims were applied to the lap joint ends for the correct alignment of the samples in the tensiometer. All samples were tested at a 1.5 mm·min^{-1} strain rate until failure with a minimum of 3 reproducible results reported.

3.6.2 Materials

Manganese chloride tetrahydrate ($MnCl_2 \cdot 4H_2O$, 99%) was purchased from Alfa Aesar. Tert-butyl hydroperoxide (70% aqueous solution), lauroyl peroxide, 99%, hydrogen peroxide (35 wt% solution in water), choline chloride, > 98%, Cobalt chloride hexahydrate ($CoCl_2 \cdot 6H_2O$, 98-102%) and 1,1,2,2-Tetrachloroethane-*d*2 99% were purchased from Fisher Scientific UK Limited. 1,2,4-Trichlorobenzene HPLC grade > 99% was purchased from Merck. All chemicals were used as received unless stated otherwise.

3.6.3 Procedures

Two approaches can be employed for the synthesis of each DES, namely the direct heating method whereby starting materials are stirred at elevated temperatures until a homogeneous liquid is formed or the grinding method whereby the components are ground together using a mortar and pestle at room temperature until a homogeneous liquid is formed. Owing to the experimental simplicity of direct heating, this method was employed for the preparation of all DES compounds. All DES were used without further purification.

1. General procedure for the synthesis of the DES

In a 20 mL glass vial equipped with a magnetic stirrer, the appropriate amount of choline chloride was combined with a metal salt. The reaction mixture was gently heated to 70 °C for 30 min until the formation of a homogeneous liquid.

VI. Synthesis of $[ChCl]_2[MnCl_2{\cdot}4H_2O]$

Using general procedure 1, the reaction using choline chloride (1.4 g, 10.1 mmol, 2 equiv.) and $MnCl_2{\cdot}4H_2O$ (1.0 g, 5.05 mmol, 1 equiv.) gives the title product as a yellow viscous liquid.

VII. Synthesis of $[ChCl]_2[CoCl_2{\cdot}6H_2O]_3$

Using general procedure 1, the reaction using choline chloride (0.77 g, 5.60 mmol, 2 equiv.) and $CoCl_2{\cdot}6H_2O$ (2.0 g, 8.30 mmol, 3 equiv.) gives the title product as a blue liquid.

2. General procedure for the DES catalysed thermal oxidation of polyolefins without a humidity chamber.

For reactions performed at 70 °C, the use of a humidity chamber is no longer necessary and therefore the reaction procedure is as follows: DES were synthesised according to procedure 1 and the DES was loaded into a 20 mL glass vial equipped with a magnetic stirring bar. The desired plastic (0.2g) was then loaded into the same vial and sealed with a Teflon cap. The reaction mixture was then stirred at 70 °C for 100 days. Aliquots were taken at the desired intervals; methanol was used to wash any residual DES from the polyolefin before the sample was dried under vacuum.

3. General procedure for the hydrogen peroxide oxidation of polyolefins.

DES $[ChCl]_2[CoCl_2{\cdot}6H_2O]_3$ was synthesised according to the procedure above and was loaded into a 20 mL glass vial equipped with a magnetic stirring bar and heated to 70 °C. The desired plastic (0.2 g) was loaded into the same vial and stirred until fully incorporated before hydrogen peroxide (0.04 mL, 1.3 mmol, 0.45 equiv) was added in one portion. The vial was sealed with a Teflon cap and left to stir at 70 °C for 100 days. Aliquots were taken at desired intervals; methanol was used to wash any residual DES from the aliquots before they were dried under vacuum.

4. General procedure for the Lauroyl peroxide oxidation of polyolefins.

DES $[ChCl]_2[CoCl_2{\cdot}6H_2O]_3$ was synthesised according to the procedure above and was loaded into a 20 mL glass vial equipped with a magnetic stirring bar and heated to 70 °C. The desired plastic (0.2 g) was loaded into the same vial and stirred until fully incorporated before Lauroyl peroxide (0.17 mg, 4.2 mmol, 0.15 equiv) was added in one portion. The vial was sealed with a Teflon cap and left to stir at 70 °C for 100 days. Aliquots were taken at desired intervals; methanol was used to wash residual any DES from the aliquots before they were dried under vacuum.

5. General procedure for the *tert*-butyl hydroperoxide oxidation of polyolefins.

DES $[ChCl]_2[CoCl_2{\cdot}6H_2O]_3$ was synthesised according to the procedure above and was loaded into a 20 mL glass vial equipped with a magnetic stirring bar and heated to 70 °C. The desired plastic (0.2 g) was loaded into the same vial and stirred until fully incorporated before *tert*-butyl hydroperoxide (0.24 mL, 2.5 mmol, 0.9 equiv) was added in one portion. The vial was sealed with a Teflon cap and left to stir at 70 °C for 100 days. Aliquots were taken at desired intervals;

methanol was used to wash residual any DES from the aliquots before they were dried under vacuum.

6. General procedure for the oxidation of polyolefins under dioxygen atmospheres

DES $[ChCl]_2[CoCl_2{\cdot}6H_2O]_3$ was synthesised according to the general procedure 1 and loaded into an open-top 20 mL glass vile equipped with a magnetic stirring bar and heated to 70 °C. The desired plastic (0.2 g) was loaded into the same vial and stirred until fully incorporated before *tert*-butyl hydroperoxide (0.24 mL, 2.5 mmol, 0.9 equiv) was added in one portion. A septa was added, and an oxygen balloon was used to flush air from the headspace of the vial, this process was repeated three times. Once all the air had been removed from the vial the sealed reaction was left to stir at 70 °C for 100 days. Aliquots were taken at desired intervals by first removing the rubber septa, taking the aliquot, placing the septa back onto the vial and flushing the headspace with an oxygen balloon three times. The aliquots were washed using methanol to remove any residual DES before they were dried under vacuum.

3.7 Appendix

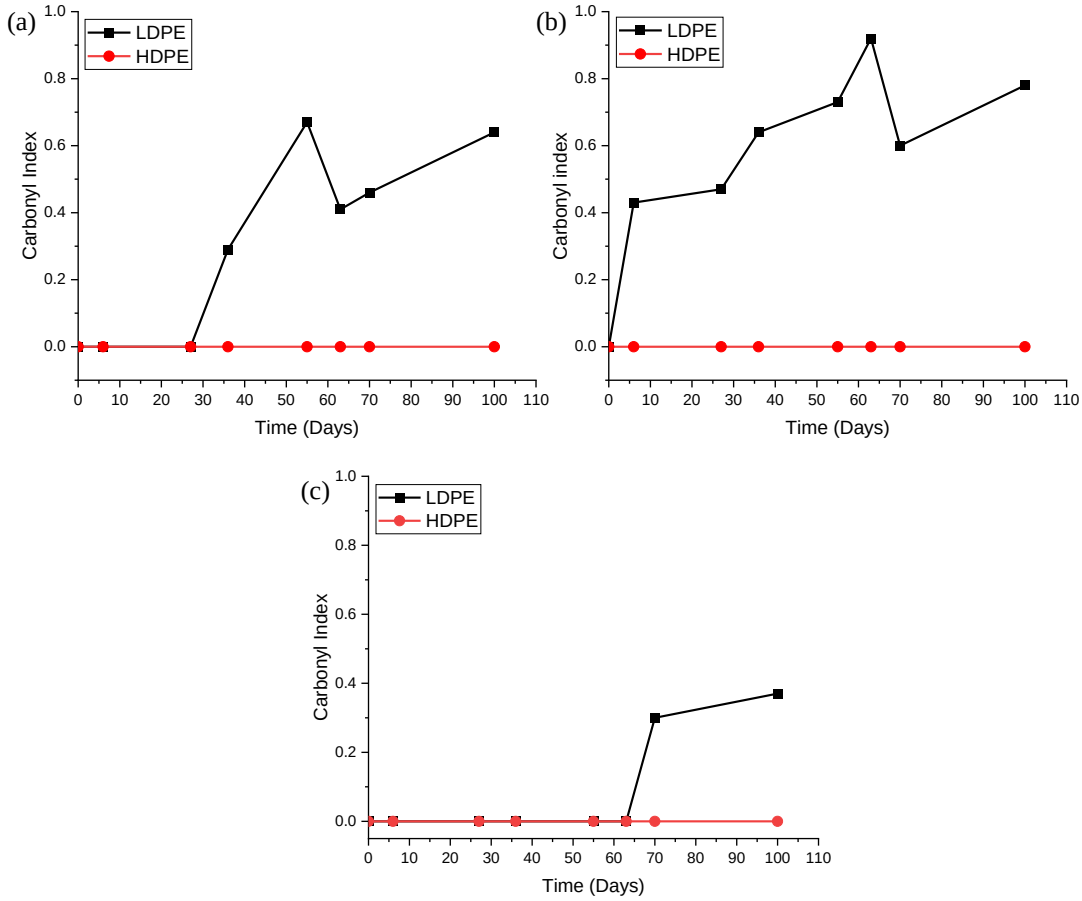

Figure 3.18 Carbonyl index as a function of time of LDPE and HDPE at 50 °C by reaction of (a) $[ChCl]_2[CoCl_2{\cdot}6H_2O]_3$ only (b) $[ChCl]_2[CoCl_2{\cdot}6H_2O]_3$ and TBHP (0.9 equiv) (c) $[ChCl]_2[MnCl_2{\cdot}4H_2O]$ only

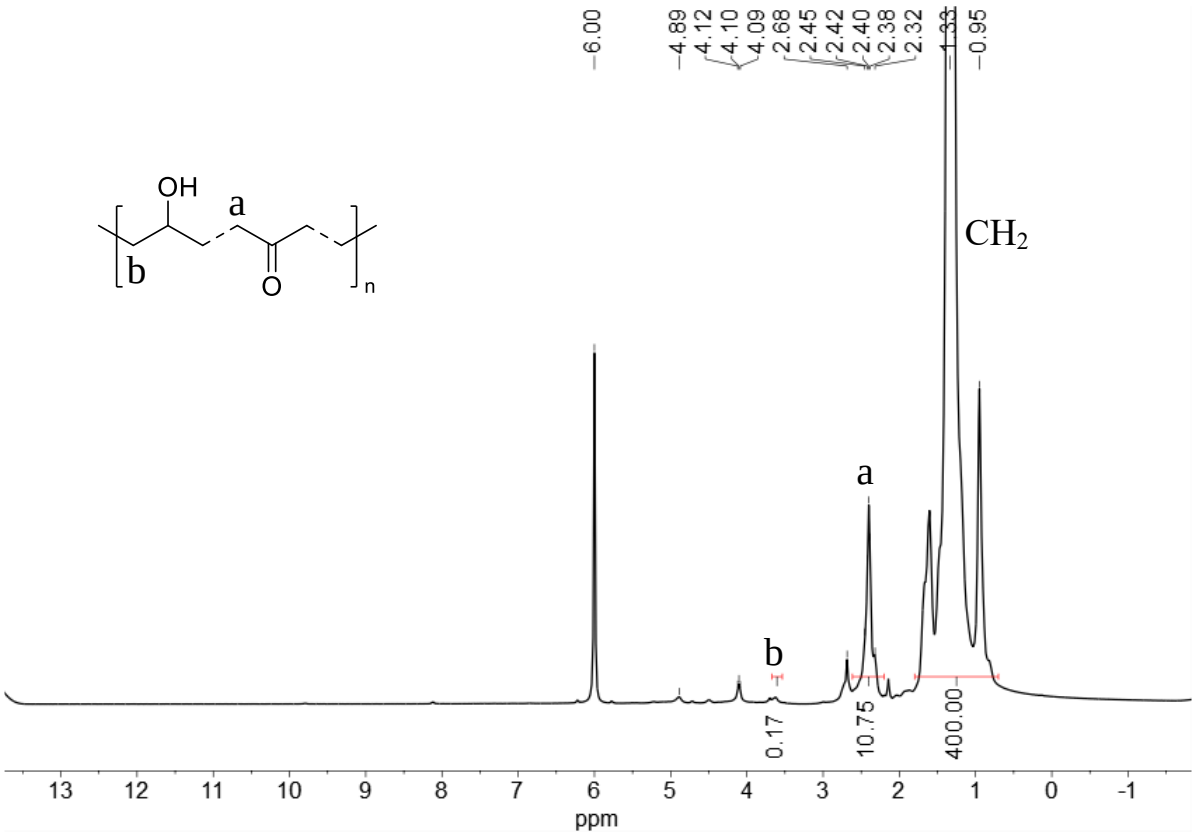

Figure 3.19 ^{1}H NMR spectraum (101 MHz, $C_2D_2Cl_4$ at 100 °C) of LDPE (FG = 2.9 mol %) after 100-day reaction with $[ChCl]_2[CoCl_2{\cdot}6H_2O]_3$ and lauroyl peroxide (0.15 equiv) at 70 °C

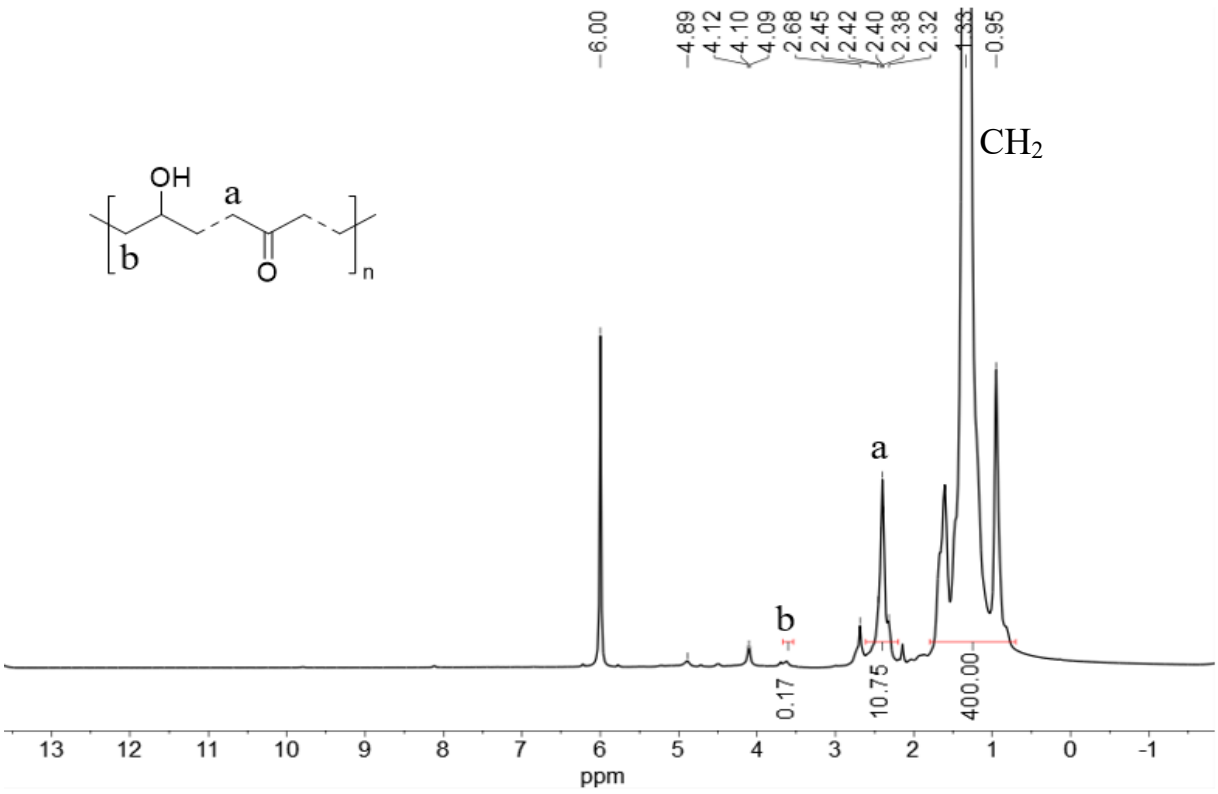

Figure 3.20 ^{1}H NMR spectrum (101 MHz, $C_2D_2Cl_4$ at 100 °C) of HDPE (FG = 4.0 mol %) after 100-day reaction with $[ChCl]_2[CoCl_2{\cdot}6H_2O]_3$ and lauroyl peroxide (0.15 equiv) at 70 °C

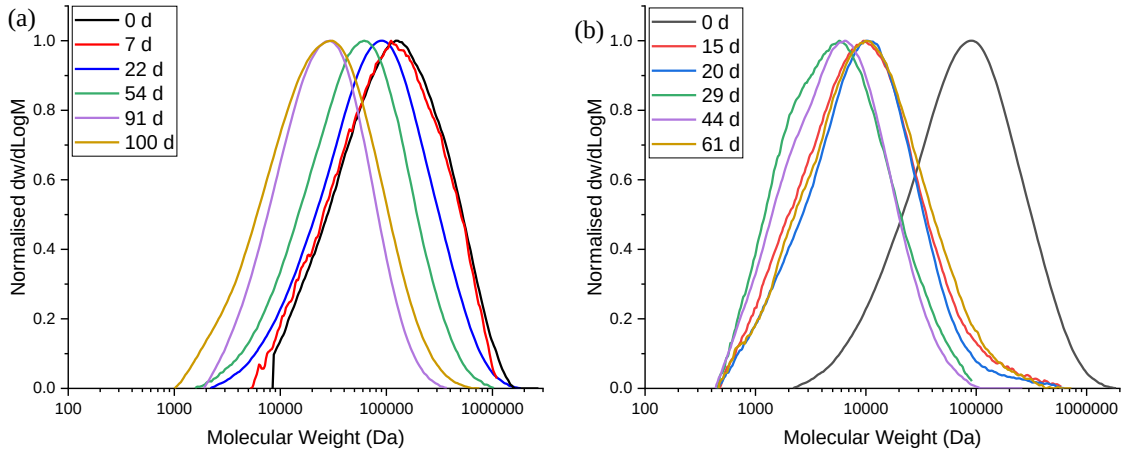

Figure 3.21 (a) Size exclusion chromatogram of the molecular weight distributions of clear post-consumer LDPE throughout its reaction with $[ChCl]_2[CoCl_2{\cdot}6H_2O]_3$ at 70 °C (b) Size exclusion chromatogram of the molecular weight distributions of clear post-consumer LDPE throughout its reaction with $[ChCl]_2[CoCl_2{\cdot}6H_2O]_3$ and TBHP at 70 °C. Molecular weight was determined against poly(styrene) standards using $C_6H_3Cl_3$ (250 mg·L^{-1} BHT) as eluent at 160 °C

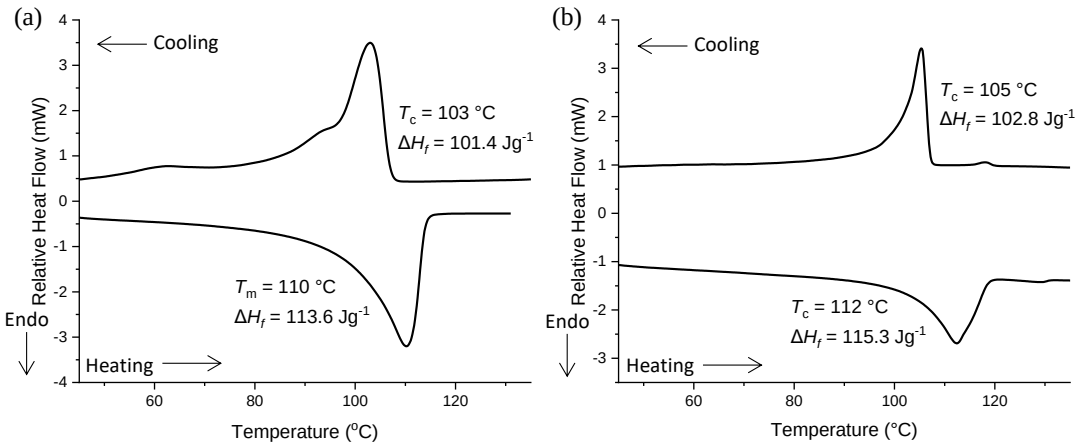

Figure 3.22 DSC thermogram of the second heating cycle and cooling cycle of LDPE after repetitive reaction cycles of $[ChCl]_2[CoCl_2{\cdot}6H_2O]_3$ and TBHP after 70 days at 90 °C (a) First cycle (b) Second cycle

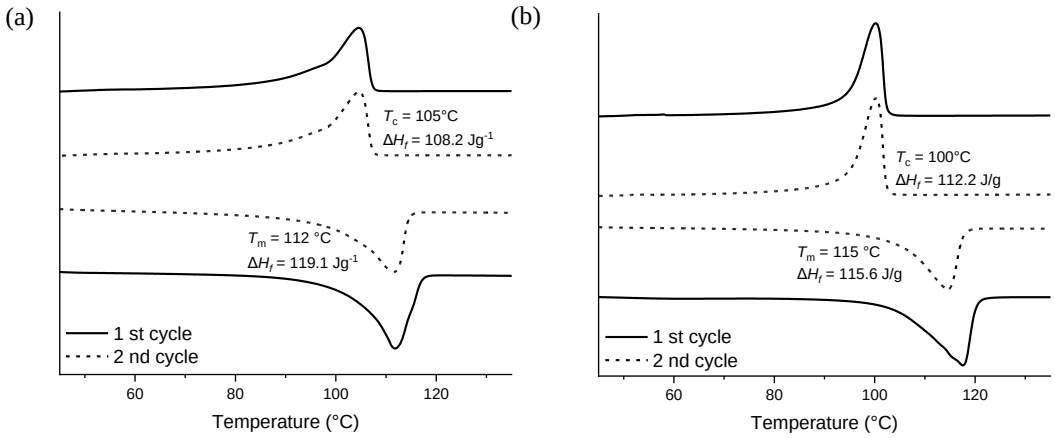

Figure 3.23 DSC thermograms for the first (solid line) and second (dashed line) heating cycles for LDPE after a 100-day reaction with $[ChCl]_2[CoCl_2{\cdot}6H_2O]_3$ and TBHP (0.9 equiv) at 70 °C at a heating rate of 10 °C·min under (a) air (b) oxygen

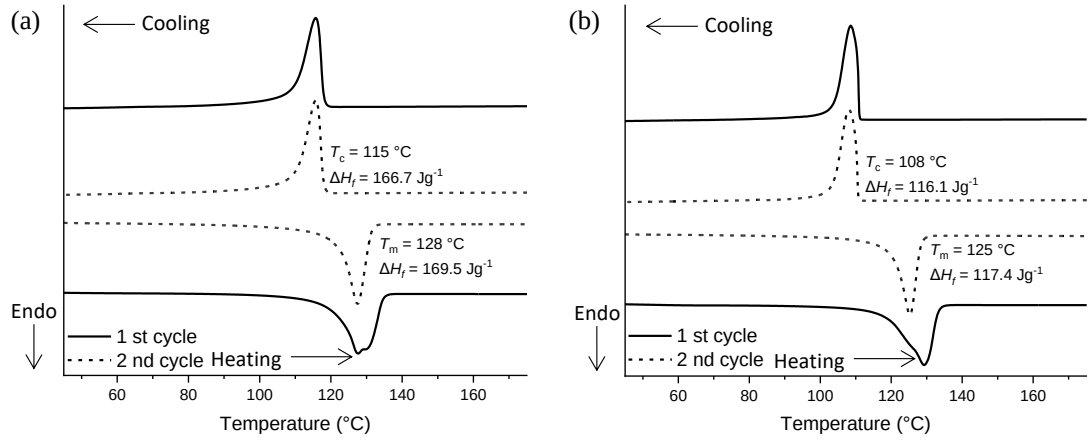

Figure 3.24 DSC thermograms for the first (solid line) and second (dashed line) heating cycles for HDPE after a 100-day reaction with $[ChCl]_2[CoCl_2{\cdot}6H_2O]_3$ and lauroyl peroxide (0.9 equiv) at 70 °C at a heating rate of 10 °C·min^{-1} under (a) air (b) oxygen

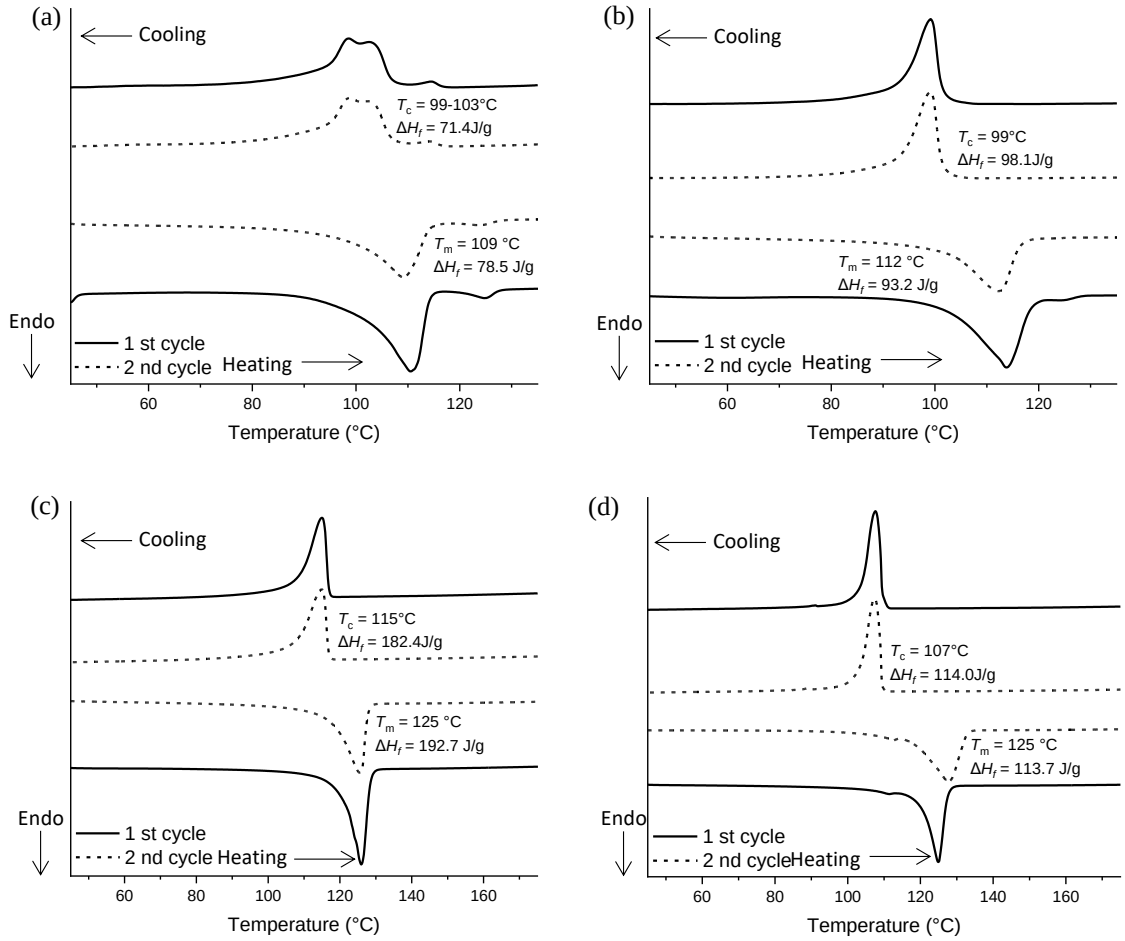

Figure 3.25 DSC thermograms for the first (solid line) and second (dashed line) heating cycles for LDPE after a 100-day reaction with $[ChCl]_2[MnCl_2{\cdot}4H_2O]$ and lauroyl peroxide (0.15 equiv) at 70 °C at a heating rate of 10 °C·min^{-1} under (a) air (b) oxygen. DSC thermograms for the first (top) and second (bottom) heating cycles for HDPE after a 100-day reaction with $[ChCl]_2[MnCl_2{\cdot}4H_2O]$ and lauroyl peroxide (0.15 equiv) at 70 °C at a heating rate of 10 °C·min^{-1} under (c) air (d) oxygen

Table 3.1 Summary of the single lap adhesion strength of HDPE-Interface-HDPE polymers at a strain rate of 1.5 mm·min^{-1}

HDPE-Interface-HDPE	ε_b[a] (%)	σ_b[b] (MPa)	M_w[c] (kDa)	M_n[d] (kDa)	$Đ_M$[e]
HDPE	40.4 ± 16.0	0.5 ± 0.1	314	47	6.7
Ox-HDPE	47.4 ± 23.3	1.0 ± 0.2	51	18	2.9
LDPE	19.4 ± 5.4	0.2 ± 0.0	75	22	3.5
Ox-LDPE	39.0 ± 3.4	0.5 ± 0.1	45	14	3.2

(a) Strain at break (b) Stress at break (c) Weight average molecular weight (d) Number average molecular weight (e) Dispersity. All uncertainties are presented as a standard deviation of n = 3 samples

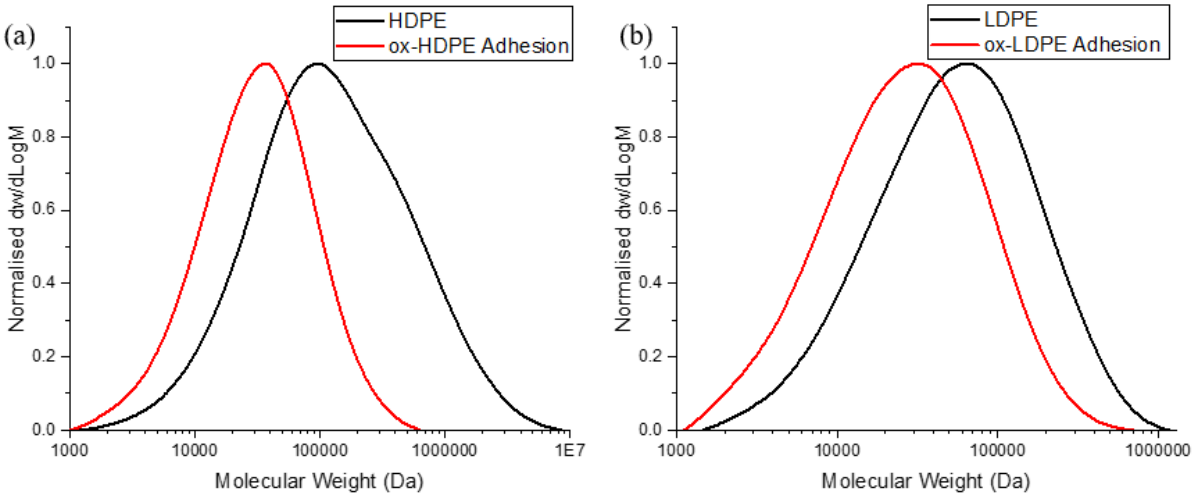

Figure 3.26 Normalised average molecular weight of polyethylenes used for single lap-shear adhesion testing (a) HDPE and ox-HDPE (b) LDPE and ox-LDPE. Molecular weight was determined against poly(styrene) standards using $C_6H_3Cl_3$ (250 mg·L^{-1} BHT) as eluent at 160 °C

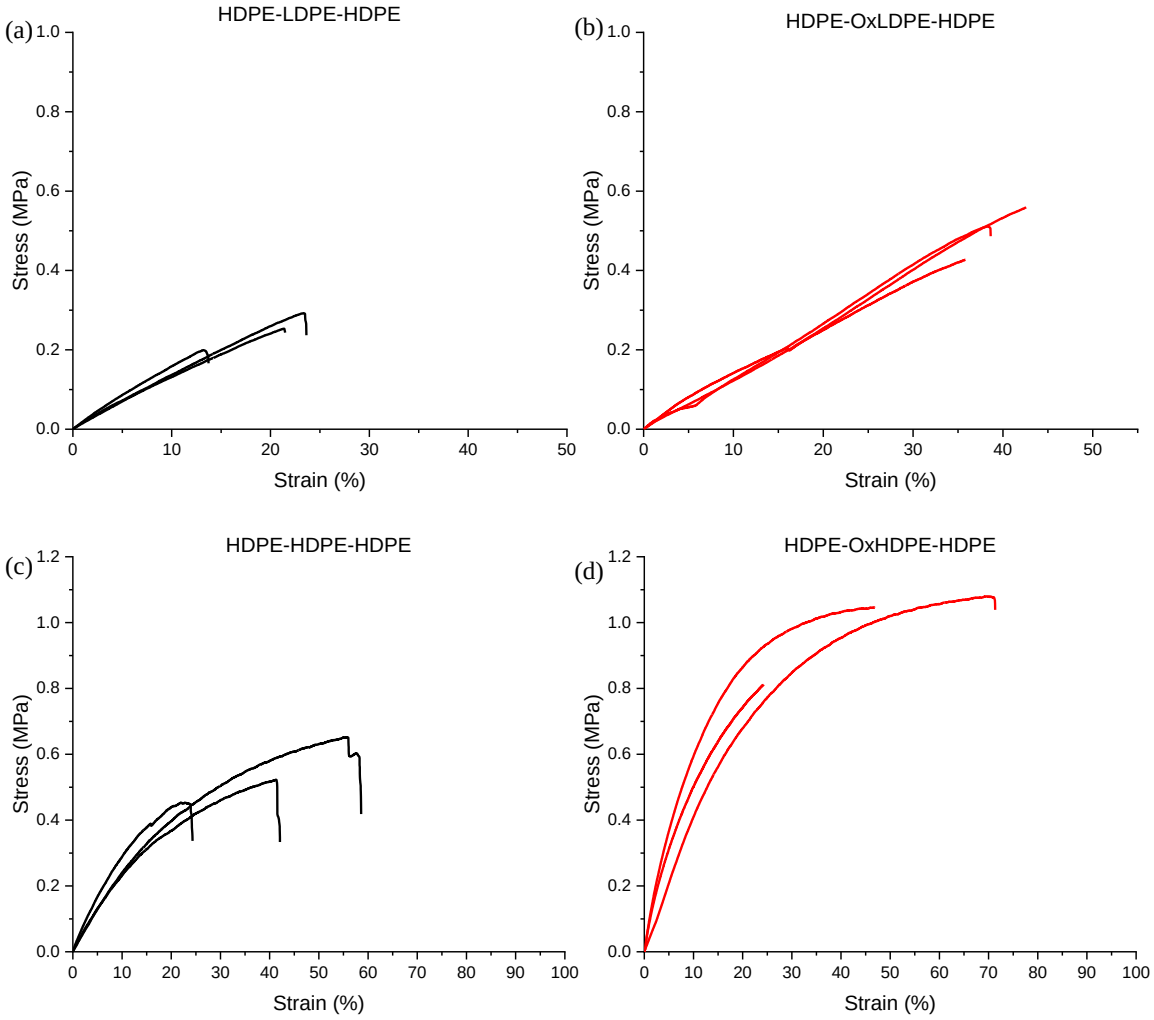

Figure 3.27 Stress *vs* strain curve for HDPE-Interface-HDPE single shear lap tests for (a) LDPE (b) Ox-LDPE (c) HDPE and (d) Ox-HDPE. All tests were performed at a strain rate of 1.5 mm·min^{-1} for n = 3 samples

Chapter 4

Sustainable blend and copolymer elastomers derived from isohexides for tuneable mechanical and degradation performance

4.1 Manuscript details and overview

Title: Sustainable blend and copolymer elastomers derived from isohexides for tuneable mechanical and degradation performance.

Authors: E. J. Catterson[1], C. J. Stubbs[1], J. C. Worch[1], A. P. Dove[1]

Affiliations:

[1] School of Chemistry, The University of Birmingham, Edgbaston, Birmingham, B152TT, United Kingdom

Overview:

Developing degradable plastics derived from renewable feedstocks would relieve the strain that commonly employed non-degradable plastics place on finite resources and the environment. Therefore, the objective of this chapter was to investigate the effect of stereochemistry on the thermal, mechanical and hydrolytic degradation properties of a series of physical blends and copolymers of renewable isohexide-based polyurethane elastomers.

By adopting step-growth polymerisation, stereoisomers isosorbide and isomannide were incorporated into high molecular weight polyurethanes. Both homopolymers are amorphous and present similar physical and mechanical behaviour to traditional elastomers. The tough elastomers experience a strain-hardening effect with comparable stress vs strain profiles.

To investigate the impact of stereochemistry, physical blends and copolymers of isosorbide and isomannide polyurethanes, at varying ratios, were synthesised. The copolymers and blended samples maintain the elastic character with improved mechanical performance compared to their homopolymers. Ageing of the sample revealed that IMPU showed improved mechanical strength while ISPU behaved more plastic-like.

Lastly, accelerated hydrolytic degradation studies exposed that blends and copolymers with a high percentage of IMPU content degraded faster than both IMPU and ISPU homopolymers revealing independent control of their degradation rate. As a result, it was concluded that by simply altering the ratio and the stereochemistry of the Isohexide unit the mechanical properties of the resultant polymer remain similar, but their hydrolytic degradation pathway can be shortened.

4.2 Abstract

The synthesis of degradable elastomers with strong mechanical properties and tailorable degradation pathways sourced from simple renewable feedstocks has been a grand challenge of polymer chemistry. Degradable elastomers are sought-after because of their potential to reduce the accumulation of plastic waste in the environment and lessen our reliance on finite fossil fuels, however, typically synthetic elastomers require covalently cross-linked networks which hamper their reprocessability. Herein, we report the synthesis and characterisation of high-performance linear alternating strong thermoplastics using renewable isohexides (isomannide (IM) and isosorbide (IS)). The chemical similarity of the isohexides, due to stereoisomerism, enabled both copolymerisation and easy facile physical blending to afford polymers with similar or better mechanical properties compared to the homopolymers. Hydrolytic degradation experiments of the copolymers and physical blends reveal that their mechanical behaviour could be decoupled from the degradation rate, allowing for independent control over degradability and mechanical properties.

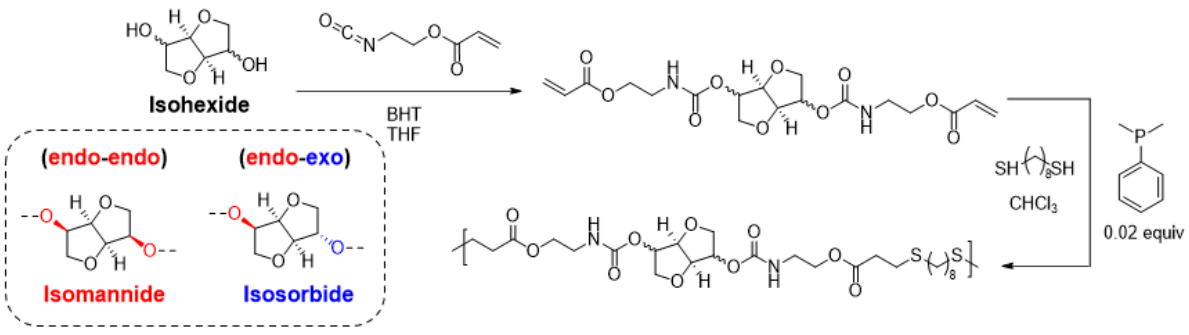

Scheme 4.1 Synthesis of renewably sourced isohexide-containing polyurethanes via step-growth polymerisation

4.3 Introduction

Commonly thought of as an alternative to conventual volcanized rubber, thermoplastic elastomers (TPE) are biphasic materials that possess both “hard” semi-crystalline or glassy thermoplastics and “soft” elastomer segments physically cross-linked through covalent bonding.[132] TPE derive their elastic behaviour from the ratios and composition of the hard and soft blocks, increased hard block content improves the material strength but limits their extendibility.[133] TPE can be thermally reprocessed by melt extrusion, unlike their chemically crosslinked analogues making it a more sustainable alternative, however, TPE synthesis heavily relies on finite petrochemicals necessitating the substitution to a more renewable feedstock.[134]

No polymeric material is designed to last forever, however, for plastics such as polyolefins, the homogeneity of their all-carbon backbone leaves them chemically resistant to degradation and leads them to persist in the environment for long after their end of use.[135] Polymer's susceptibility to degrade, *i.e.*, their degradation kinetics, is akin to factors such as the content of functional groups in their polymer backbone, molecular weight (M_w), density and their diffusion coefficient of water. Generally, it is desirable to introduce targetable functional groups onto the polymer backbone. For example, esters facilitate degradation by dissociative chain-cleavage mechanisms. Modification of the monomeric unit before polymerisation using polymerisation-tolerant functional groups can give rise to a library of degradable polymer backbones. However, some functionalities may be incompatible with the polymerisation process or may be susceptible to damage by harsh conditions and therefore can be introduced by the direct modification of the backbone via functional group interconversion after the polymerisation event.[136] To date, most approaches to modifying the polymer in such a way have resulted in issues surrounding incomplete reactions and a lack of selectivity.[137] To limit our

dependence on finite resources, while also addressing the issue of sustainability, bio-based monomers derived from renewable sources have piqued interest in the last few decades.[138]

Use of the glucose-derived isosorbide cyclic unit is widespread within polymers, gaining considerable interest as a promising bio-based monomer exhibiting attractive chirality, rigidity, and biodegradability as well as its compatibility in forming polyesters with improved material properties.[139-141] By discretely alternating the chirality of the two hydroxyl groups on the *cis*-fused tetrahydrofuran rings, stereoisomers isomannide, isosorbide and isoiodide (II) are formed. Collectively known as isohexides, their reactivity varies since their hydroxyl groups become more or less accessible depending on the steric requirement.[142, 143] Polymerisation of the isohexide monomers generates regioirregular polymers, with the exception of some ring-opening polymerisations, embracing the inherent geometric isomerism to lever control of the thermomechanical properties of the materials.[144]

Herein, we report the synthesis and characterisation of a family of isohexide-based polyurethanes whose properties can be rationally manipulated by tailoring the influence of the isohexide's stereochemistry. The incorporation of the isohexide stereoisomers into high molar mass polymers was achieved by thiol-ene click polymerisation of an isohexide-containing diacrylate with 1,8-octanedithiol. We demonstrated that changes in mechanical properties can solely be attributed to stereoisomerism and the presence of significant hydrogen bonding networks rather than major microstructure changes to the polymer architecture. The chemical similarity and compatibility of the IS and IM monomers allowed for easy physical blending and copolymerisation accessing a larger family of unique polyurethanes. Blends and copolymers reveal that their mechanical behaviour can be decoupled from their hydrolytic degradation rates allowing for independent control.

4.4 Results and discussion

4.4.1 Preparation of IMPU and ISPU

The incorporation of IS and IM stereoisomers into polyurethanes was achieved by the phosphine-catalysed thiol-ene click polymerisation of the isohexide-containing diacrylate with 1,8-octanedithiol (Scheme 4.1).[133, 145, 146] Internal urethane units are reasoned to enhance thermomechanical properties by promoting a strong hydrogen-bonding network while also providing hydrolysable ester linkage for later degradation.[147] This efficient synthesis, utilising the commercially available isohexides, yields non-cross-linked and linear high molecular weight isosorbide polyurethane (ISPU, M_w = 158 kDa, $Đ_M$ = 31.1) and isomannide polyurethane (IMPU, M_w = 125 kDa, $Đ_M$ = 12.3). As a consequence of the uncontrollable characteristics of step-growth polymerisation, oligomers form irreversibly resulting in a broad distribution of molecular weights with batch-to-batch variation.[148] DSC analysis showed both resulting polymers to be amorphous *i.e.,* their molecular structure is randomly oriented, and ISPU and IMPU both exhibit a T_g below 23 °C.

4.4.2 Material properties of IMPU and ISPU

With the renewable sugar-based isohexide backbone the polymers display high thermal stability with onset decomposition temperatures (T_d) upwards of 286 °C. This allowed for the use of heat compression moulding, forming flexible thin films suitable for mechanical analysis. Thermally processed polymers were annealed for 7 days at ambient temperature (22 °C) before mechanical testing to ensure thermal equilibrium had been achieved. ISPU and IMPU were uniaxially strained by tensile testing at a strain rate of 10 mm·min^{-1} until failure. Both perform as tough elastomers with a strain hardening effect, where the polymer chains orient in the direction of the uniaxial deformation causing the stress to increase significantly relative to the rate of strain,

resulting in a high ultimate tensile strength.[149] Rheological frequency sweeps were conducted on both homopolymers at various temperatures. These sweeps demonstrated the frequency-dependent behaviour of the homopolymer's storage and loss moduli, providing insight into their elastic and viscous properties. Deformation at lower frequencies is dominated by the loss moduli while deformation at higher frequencies is dominated by the storage moduli. IMPU shows deformation at higher frequencies than ISPU and thus exhibits greater elastic character (Figures 4.61 and 4.62). To assess the significance of hydrogen bonding, ISPU and IMPU were also tensile tested at 2 mm·min^{-1} and 100 mm·min^{-1}. Altering the strain rate of both the samples proved that on time scales shorter than the association time of reversible bonds the materials exhibited a greater Youngs modulus. (Figure 4.1 and 4.56). The hydrogen bonds act as dynamic crosslinks creating a network, as they have insufficient time to rearrange, allowing the elastic character to dominate. Alternatively, at slower rates of sample deformation, the dynamic hydrogen bonds have sufficient time to rearrange, favouring the sample's viscous character showing a greater strain at break. The difference in stereochemistry was notable as ISPU exhibits a high toughness (208.9 MJ·m^3) with an average strain at break (ε_b = 1024.0%) and stress at break (σ_b = 51 MPa) whereas IMPU exhibits a smaller ultimate toughness (165.6 MJ·m^3), strain at break (ε_b = 966.0%) and stress at break (σ_b = 45 MPa) despite their chemical similarity. ISPU also appears stiffer with a higher Youngs modulus (6.09 MPa) than IMPU (3.80 MPa).

4.4.3 Ageing

Ageing of one, three, six and twelve weeks of the homopolymers at 22 °C revealed that after 6 weeks IMPU continues to behave as an elastomer but with a higher ultimate tensile toughness (287.0 MJ·m^3), and greater strain at break (ε_b = 1058.0%) and stress at break (σ_b = 78 MPa) compared to tests after annealing for one week. ISPU however, begins to exhibit "plastic-like"

behaviour with a yield strength of 10.9 MPa, corresponding to the stress at the end of the elastic region. However, after which the plastic region is entered, and deformation is no longer recoverable; it is permanent. Such plastic-like behaviour is usually only accessible via the semi-crystalline isohexide stereoisomer isoidide polyurethane (IIPU), however, isoidide is more challenging to synthesise and is not as readily available as isosorbide. DSC analysis showed that aged ISPU remains amorphous, yet its T_g has increased from 16 °C after one week to 20 °C after week six (Figure 4.63b). The increase in T_g supports ISPU's harder and more brittle behaviour. Wide-angle X-ray scattering (WAXS) studies also confirmed that both IMPU and ISPU remain amorphous with a broad signal with a low scattering angle ($2\theta < 30$) and the absence of any Bragg peaks (Figure 4.63a).

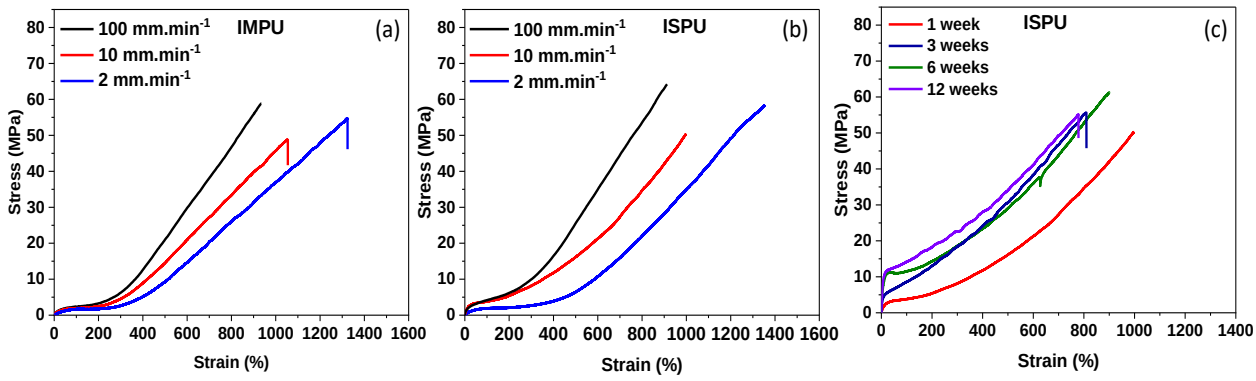

Figure 4.1 (**a**) Stress vs. strain curve for IMPU at 2, 10 and 100 mm·min^{-1} (22 °C, n = 3, annealed at 25 °C for 7 days). (**b**) Stress vs. strain curve for ISPU at 2, 10 and 100 mm·min^{-1} (22 °C, n = 3, annealed at 25 °C for 7 days). (**c**) Stress vs. strain curve for aged ISPU Stress vs. strain curve for aged ISPU after 1, 3, 6 and 12 weeks at 10 mm·min^{-1} (22 °C, n = 3, annealed at 22 °C for 1, 3, 6 and 12 weeks respectively)

4.4.4 Physical blends

To further investigate the effects of stereochemistry, the influence of physically blending IMPU and ISPU was examined. Physical blending offers a quick and simple method for accessing a range of polymeric systems with diverse material properties from distinctly unique polymers.

The blend composition can drastically alter the degradative behaviour and mechanical performance of the polymer leading to fine manipulation of targeted properties.[150] Nevertheless, an important shortcoming means that blending polymers can often form immiscible layers, macroscopic phase separation and defects. This creates badly phase dispersed morphologies resulting in poor material properties, a result of incompatible compositions, which can hamper mechanical recycling efforts and reduce the overall quality of the end-recycled products.[151] In the presented work such limitations are sought to be negated by the chemical similarity and isomeric nature of ISPU and IMPU leading to a convenient, low cost and composition-controlled method for tailoring chemical and mechanical properties. Physical blends from 10 – 90% IMPU (90 – 10% ISPU) were made by dissolving the appropriate ratios of each isohexide polyurethane in chloroform until a homogeneous fluid was achieved. ^{1}H NMR spectroscopy confirmed the desired composition for each blend was retained in the final polymer while DSC analysis established that all blends were amorphous with a single T_g values below 23 °C. All blends showed similar or greater ultimate toughness than their homopolymers, however, there is no obvious trend (Figure 4.2). Blends *b*-$IM_{70}IS_{30}$, *b*-$IM_{50}IS_{50}$, *b*-$IM_{40}IS_{60}$ and *b*-$IM_{20}IS_{80}$ all undergo discontinuous failure while tensile testing exhibits an abrupt unloading event. It has been reported in the literature that physically blending polymers results in larger less dispersed domains while copolymerisation results in a greater number of finely dispersed domains, therefore offering the opportunity to explore the influence of copolymerisation.[146, 152]

4.4.5 Copolymers

Composition-controlled copolymers were obtained by altering the ratio of each monomer feedstock and copolymerising with 1,8-octanedithiol. DSC analysis confirmed that all polymers were amorphous with a single T_g value less than 23 °C. All copolymers presented a similar, if

not better, tensile profile to the elastomeric ISPU and IMPU samples with an increase in toughness and strength as a consequence of strain hardening (Figure 4.2). These observations suggest that discrete manipulation *via* copolymerisation creates polyurethanes with enhanced mechanical performance arising from stereochemically distinct hydrogen bonding networks between stoichiometrically identical materials.

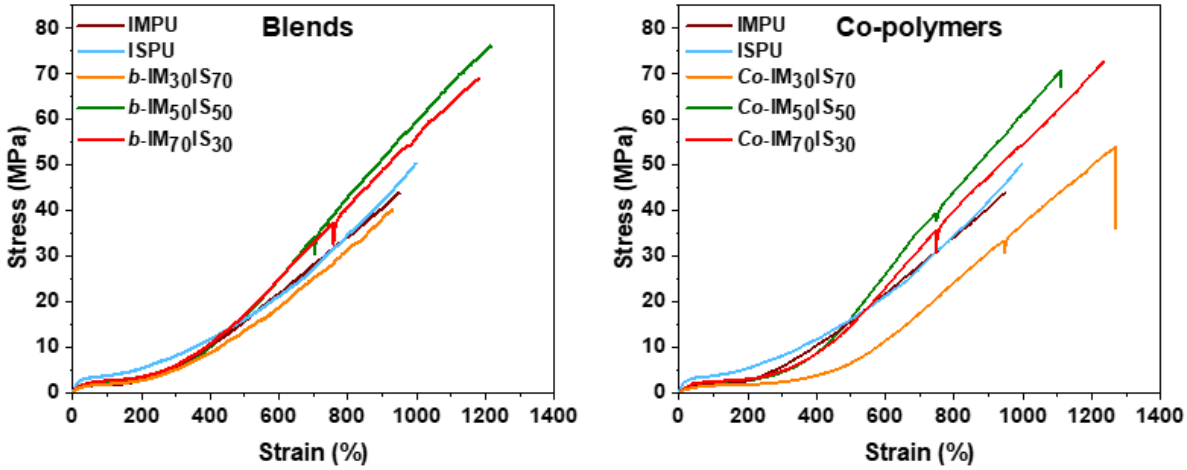

Figure 4.2 Representative stress vs. strain curve for physical blends and copolymers of IMPU and ISPU at 10 mm·min^{-1} (22 °C, n = 3, annealed at 25 °C for 7 days)

4.4.6 Hydrolytic degradation

Petroleum-derived polymers are known for their resistance to degradation in the environment, a consequence of the hydrophobicity imparted on them due to their non-functional group containing carbon-carbon backbone. ISPU and IMPU however, contain chemical functionality that offers the potential for hydrolytic degradation (oxygen and nitrogen). Accelerated degradation studies were performed by placing an 8 mm × 0.5 mm disk of each polymer film in a 1 M NaOH solution in triplicate at a controlled temperature of 25 °C while shaken. Rates of degradation are often related to crystallinity, the more crystalline the sample the less penetrable the bulk of the material is to water leading to higher levels of surface degradation

and a slower overall degradation rate. As both IMPU and ISPU are amorphous, it was hypothesised that their rate of degradation would be similar. However, after 91 days IMPU had lost 100% of its original mass while ISPU had lost only 51%, and 100% mass loss was achieved after 112 days. This observation suggests that their mechanical properties are decoupled from their hydrolytic degradation rates; however, both are solely attributed to stereoisomerism rather than significant microstructure changes to the polymer architecture.

Physical blends of IMPU and ISPU revealed that blends with higher IMPU content, between 70-90%, degraded far more rapidly (49 days faster) than stereopure IMPU, even with comparable thermomechanical properties (Figure 4.3). All remaining blends degraded at an intermediate rate between IMPU and ISPU. Despite both blends and copolymers containg the same percentage of each isohexide block, they exhibit significantly different hydrolytic degradation rates. Copolymers containing 40-90% IM have a steep rate of degradation with 100% mass loss after 42 days, while copolymers with 10-30% IM content degrade within 70 to 84 days (Figure 4.3). As both copolymers and blends are amorphous with all T_g's within the range of 13-23 °C, the diverse degradation profiles suggest that crystallinity is not influencing the rate of degradation.

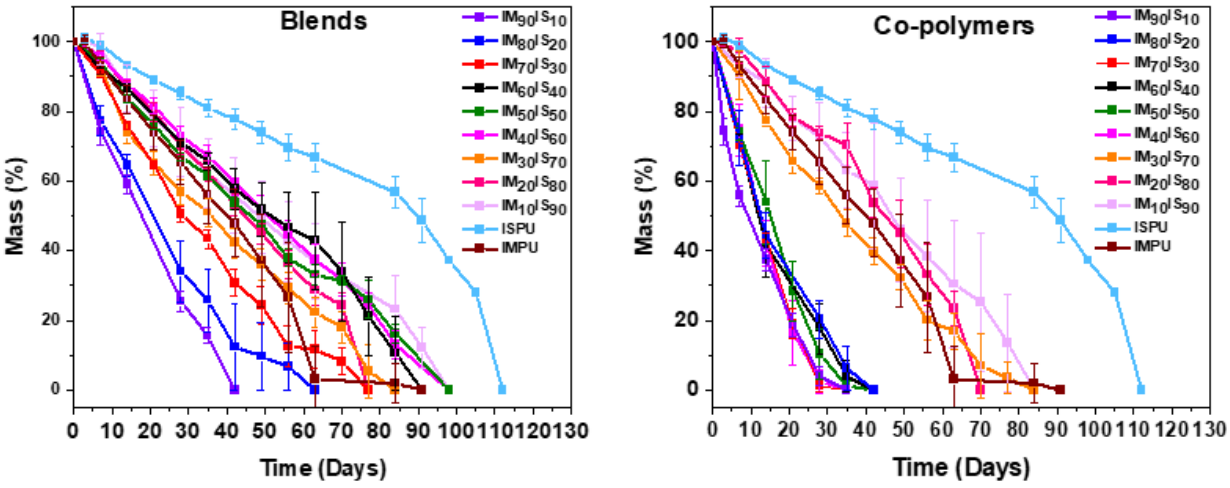

Figure 4.3 Normalised weight loss of IMPU, ISPU, their blends and copolymers during accelerated hydrolytic degradation (1 M NaOH at 25 °C, n =3)

4.5 Conclusion

With minor changes of the stereochemistry along the polymer backbone, amorphous elastomers ISPU and IMPU were synthesised by step-growth polymerisation displaying comparable mechanical properties. Typically, such control requires significant changes in microstructures, however, by utilising the isomeric nature of the renewably sourced isohexide building blocks these properties can be simply accessed. Upon ageing, both homopolymers remained amorphous, however, IMPU showed improved mechanical strength while ISPU behaved more plastic-like resembling its semi-crystalline stereoisomer isoidide. The chemical similarity of IS and IM allowed for easy facile blending and copolymerisation, generating a library of mechanically stronger elastomers. Accelerated degradation studies exposed that the blends and copolymers with a high percentage of IMPU degraded faster than both homopolymers revealing that their mechanical behaviour can be decoupled from their hydrolytic degradation rates allowing for independent control.

4.6 References

1. R. Geyer, J. R. Jambeck and K. L. Law, *Sci. Adv.*, 2017, **3**, 1700782-1700787.
2. M. Jefferson, *Energy Res. Soc. Sci.*, 2019, **56**, 101229-101237.
3. M. W. Ryberg, M. Z. Hauschild, F. Wang, S. Averous-Monnery and A. Laurent, *Resour. Conserv. Recycl.*, 2019, **151**, 104459-104469.
4. H. Sardon and A. P. Dove, *Science*, 2018, **17**, 380-381.
5. J. R. Jambeck, R. Geyer, C. Wilcox, T. R. Siegler, M. Perryman, A. Andrady and K. L. Law, *Science*, 2015, **347**, 1234-1242.
6. A. Chamas, H. Moon, J. Zheng, Y. Qiu, T. Tabassum, J. H. Jang, M. Abu-Omar, S. L. Scott and S. Suh, *ACS Sustain. Chem. Eng.*, 2020, **8**, 3494-3511.
7. L. Jeffry, M. Y. Ong, S. Nomanbhay, M. Mofijur, M. Mubashir and P. L. Show, *Fuel*, 2021, **301**, 121017.
8. H. V. Ford, N. H. Jones, A. J. Davies, B. J. Godley, J. R. Jambeck, I. E. Napper, C. C. Suckling, G. J. Williams, L. C. Woodall and H. J. Koldewey, *Sci. Total. Environ.*, 2022, **806**, 150392-150403.
9. M. Shen, W. Huang, M. Chen, B. Song, G. Zeng and Y. Zhang, *J. Clean. Prod.*, 2020, **254**, 120138-120151.
10. H. Bouwmeester, P. C. Hollman and R. J. Peters, *Environ. Sci. Technol.*, 2015, **49**, 8932-8947.
11. J. D. Hamilton, K. H. Reinert, J. V. Hagan and W. V. Lord, *J. Air Waste Manag. Assoc.*, 1995, **45**, 247-251.
12. I. A. Ignatyev, W. Thielemans and B. V. Beke, *Chem. Sus. Chem*, 2014, **7**, 1579-1593.
13. J. Morris, *J. Hazard. Mater.*, 1996, **47**, 277-293.
14. T. F. M. Ojeda, E. Dalmolin, M. M. C. Forte, R. J. S. Jacques, F. M. Bento and F. A. O. Camargo, *Polym. Degrad. Stab.*, 2009, **94**, 965-970.
15. X. Liu, C. Gao, P. Sangwan, L. Yu and Z. Tong, *J. Appl. Polym. Sci.*, 2014, **131**, 40750-40765.
16. J. C. Salcedo Reyes, O. A. Castañeda Uribe, L. D. Gomez Méndez, A. M. Pedroza Rodríguez and R. A. Poutou Piñales, *Univ. Sci.*, 2023, **28**, 65-139.
17. A. J. Sipinen and R. d. R, *J. Environ. Polym. Degrad.*, 1993, **1**, 193-202.
18. D. K. Mandal, H. Bhunia, P. K. Bajpai, A. Kumar, G. Madhu and G. B. Nando, *J. Polym. Environ.*, 2017, **26**, 1061-1071.
19. P. K. Roy, P. Surekha, R. Raman and C. Rajagopal, *Polym. Degrad. Stab.*, 2009, **94**, 1033-1039.
20. S. Selke, R. Auras, T. A. Nguyen, E. Castro Aguirre, R. Cheruvathur and Y. Liu, *Environ. Sci. Technol.*, 2015, **49**, 3769-3777.
21. C. G. Schirmeister and R. Mulhaupt, *Macromol. Rapid. Commun.*, 2022, **43**, 2200247-2200288.
22. A. S. Burange, M. B. Gawande, F. L. Y. Lam, R. V. Jayaram and R. Luque, *Green. Chem.*, 2015, **17**, 146-156.
23. S. R. Chandrasekaran, B. Kunwar, B. R. Moser, N. Rajagopalan and B. K. Sharma, *Energy Fuels*, 2015, **29**, 6068-6077.
24. R. Miandad, M. Rehan, M. A. Barakat, A. S. Aburiazaiza, H. Khan, I. M. I. Ismail, J. Dhavamani, J. Gardy, A. Hassanpour and A.-S. Nizami, *Front. Energy Res.*, 2019, **7**, 1-17.
25. A. M. Al-Sabagh, F. Z. Yehia, G. Eshaq, A. M. Rabie and A. E. ElMetwally, *Egypt. J. Pet.*, 2016, **25**, 53-64.
26. A. Pifer and A. Sen, *J. Commum.*, 1998, **37**, 3306-3308.
27. X. Zhong, Y. Zhao, Y. Qian and Y. Zou, *Mater. Sci. Mater. Rev.*, 2017, **1**, 1-11.
28. J. Gu, H. Kim and H. Lim, *Energy Convers. Manag.*, 2022, **270**, 116256-116260.
29. Y. Miao, Y. Zhao, G. I. N. Waterhouse, R. Shi, L. Z. Wu and T. Zhang, *Nat. Commun.*, 2023, **14**, 4242-4250.
30. H. A. Maddah, *Am. J. Polym. Sci.*, 2016, **6**, 1-11.
31. G. W. Coates and Y. D. Y. L Getzler, *Nat. Rev. Mater.*, 2020, **5**, 501-516.

32. X. Jia, C. Qin, T. Friedberger, Z. Guan and Z. Huang, *J. Mater. Sci.*, 2016, **2**, 1-7.
33. J. Saleem, Z. K. B. Moghal, R. A. Shakoor, A. S. Luyt and G. McKay, *Polym.*, 2023, **15**, 3072-3085.
34. A. Rahimi and J. M. García, *Nat. Rev. Chem.*, 2017, **1**, 1-11.
35. A. Németh, M. Blazsó, P. Baranyai and T. Vidóczy, *JAAP*, 2008, **81**, 237-242.
36. N. Gascoin, A. Navarro-Rodriguez, P. Gillard and A. Mangeot, *Polym. Degrad. Stab.*, 2012, **97**, 1466-1474.
37. A. Ray, K. Zhu, Y. V. Kissin, A. E. Cherian, G. W. Coates and A. S. Goldman, *ChemComm*, 2005, 3388-3390.
38. F. Zhang, M. Zeng, R. D. Yapert, J. Sun, Y. Lee and A. LaPointe, *Science*, 2020, **23**, 437-441.
39. A. S. Goldman, A. H. Roy, Z. Huang, R. Ahuja, W. Schinski and M. Brookhart, *Science*, 2006, **312**, 257-261.
40. Z. Huang, E. Rolfe, E. C. Carson, M. Brookhart, A. S. Goldman, H. S. El-Khalafy and R. H. MacArthur, *Adv. Synth. Catal.*, 2010, **352**, 125-135.
41. L. C. Lerici, M. S. Renzini and L. B. Pierella, *Procedia Materials Science*, 2015, **8**, 297-303.
42. C. J. Adams, M. J. Earle and K. R. Seddon, *Green Chem.*, 2000, **2**, 21-24.
43. E. J. Borsig, *Pure Appl. Chem.*, 1999, **A36**, 1699-1704.
44. K. E. Russell, *Prog. Polym. Sci.*, 2002, **27**, 1007-1011.
45. K. Koo, P. F. Fu and M. T. J., *Macromolecules*, 1999, **32**, 981-993.
46. G. Xu and T. C. Chung, *J. Am. Chem. Soc.*, 1999, **121**, 6763-6766.
47. H. W. Bonne, P. S. Athey, M. J. Mullins, D. Philipp, M. R. and W. A. Goddard, *J. Am. Chem. Soc.*, 2002, **124**, 8790-8799.
48. J. B. Williamson, W. I. Czaplyski, E. J. Alexanian and F. A. Leibfarth, *Angew. Chem. Int. Ed.*, 2018, **57**, 6261-6265.
49. X. Shao, C. Xu, L. Lu and Q. Shen, *J. Org. Chem.*, 2015, **80**, 3012-3021.
50. T. J. Fazekas, J. W. Alty, E. K. Neidhart, A. S. Miller, F. A. Leibfarth and E. J. Alexanian, *Science*, 2022, **375**, 545-550.
51. L. Chen, K. G. Malollari, A. Uliana, D. Sanchez, P. B. Messersmith and J. F. Hartwig, *Chem*, 2021, **7**, 137-145.
52. C. Bae, J. F. Hartwig, N. K. B. Harris, R. O. Long, K. S. Anderson and M. A. Hillmyer, *J. Am. Chem. Soc.*, 2005, **127**, 767-776.
53. A. Bunescu, S. Lee, Q. Li and J. F. Hartwig, *ACS Cent. Sci.*, 2017, **3**, 895-903.
54. E. Bäckström, K. Odelius and M. Hakkarainen, *Ind. Eng. Chem. Res.*, 2017, **56**, 14814-14821.
55. M. M. Díaz-Requejo, P. Wehrmann, M. D. Leatherman, S. Trofimenko, S. Mecking, M. Brookhart and P. J. Pérez, *Macromolecules*, 2005, 4966-4969.
56. J. B. Eastwood, L. A. Hammarback, T. J. Burden, I. P. Clark, M. Towrie, A. Robinson, I. J. S. Fairlamb and J. M. Lynam, *Organometallics*, 2023, **42**, 1766-1773.
57. N. B. Boaen and M. A. Hillmyer, *Macromolecules*, 2003, **30**, 7027-7034.
58. J. Zawadiak, B. Orlińska and A. A. Marek, *J. Appl. Polym. Sci.*, 2013, **127**, 976-981.
59. Q. Wang, X. Yao, Y. Geng, Q. Zhou, X. Lu and S. Zhang, *Green Chem.*, 2015, **17**, 2473-2479.
60. E. L. Smith, A. P. Abbott and K. S. Ryder, *Chem. Rev.*, 2014, **114**, 11060-11082.
61. D. E. Crawford, L. A. Wright, S. L. James and A. P. Abbott, *Chem. Commun.*, 2016, **52**, 4215-4218.
62. C. Florindo, F. S. Oliveira, L. P. N. Rebelo, A. M. Fernandes and I. M. Marrucho, *ACS Sustain. Chem. Eng.*, 2014, **2**, 2416-2425.
63. M. A. R. Martins, S. P. Pinho and J. A. P. Coutinho, *J. Solution. Chem.*, 2018, **48**, 962-982.
64. R. Amoroso, F. Hollmann and C. Maccallini, *Molecules*, 2021, **26**, 6286-6301.
65. G. García, M. Atilhan and S. Aparicio, *Chem. Phys. Lett.*, 2015, **634**, 151-155.
66. P. Kalhor and K. Ghandi, *Molecules*, 2019, **24**, 4012-4049.
67. C. Seyler, C. Capello, S. Hellweg, C. Bruder, D. Bayne, A. Huwiler and K. Hungerbu1hler, *Ind. Eng. Chem. Res.*, 2006, **45**, 7700-7709.

68. Q. Wang, X. Yao, S. Tang, X. Lu, X. Zhang and S. Zhang, *Green Chem.*, 2012, **14**, 2559-2566.
69. Q. Zhang, K. De Oliveira Vigier, S. Royer and F. Jerome, *Chem. Soc. Rev.*, 2012, **41**, 7108-7146.
70. C. Ma, A. Laaksonen, C. Liu, X. Lu and X. Ji, *Chem. Soc. Rev.*, 2018, **47**, 8685-8720.
71. I. Bashir, A. H. Dar, K. K. Dash, V. K. Pandey, U. Fayaz, R. Shams, S. Srivastava and R. Singh, *Sustain. Chem. Pharm.*, 2023, **33**, 101102-101118.
72. T. Khezeli, A. Daneshfar and R. Sahraei, *J. Chromatogr. A.*, 2015, **1425**, 25-33.
73. E. S. C. Ferreira, C. M. Pereira and A. F. Silva, *J. Electroanal. Chem.*, 2013, **707**, 52-58.
74. A. P. Abbott, J. C. Barron, G. Frisch, S. Gurman, K. S. Ryder and A. Fernando Silva, *Phys. Chem. Chem. Phys.*, 2011, **13**, 10224-10231.
75. X. Li, M. Hou, B. Han, X. Wang and L. Zou, *J. Chem. Eng.*, 2008, **53**, 548-550.
76. H. Bowen, R. Durrani, A. Delavault, E. Durand, J. Chenyu, L. Yiyang, S. Lili, S. Jian, H. Weiwei and G. Fei, *Front. Chem.*, 2022, **10**, 912411-912421.
77. J. Cao, B. Qi, J. Liu, Y. Shang, H. Liu, W. Wang, J. Lv, Z. Chen, H. Zhang and X. Zhou, *RSC Advances*, 2016, **6**, 21612-21616.
78. Y. H. Choi, J. van Spronsen, Y. Dai, M. Verberne, F. Hollmann, I. W. Arends, G. J. Witkamp and R. Verpoorte, *Plant. Physiol.*, 2011, **156**, 1701-1705.
79. M. Hayyan, A. Abo-Hamad, M. A. AlSaadi and M. A. Hashim, *Nanoscale. Res. Lett.*, 2015, **10**, 1004-1015.
80. M. Zhou, O. A. Fakayode, A. E. Ahmed Yagoub, Q. Ji and C. Zhou, *Renew. Sust. Energ. Rev.*, 2022, **156**, 111986-112010.
81. R. Wang, T. Wang, G. Yu and X. Chen, *Polym. Deg. Stab.*, 2021, **183**, 1038-1046.
82. A. E. Ünlü, A. Arıkaya and S. Takaç, *Green Process. Synth.*, 2019, **8**, 355-372.
83. H. Wang, Z. Li, Y. Liu, X. Zhang and S. Zhang, *Green Chem.*, 2009, **11**, 1568-1575.
84. B. Liu, W. Fu, X. Lu, Q. Zhou and S. Zhang, *ACS Sustain. Chem. Eng.*, 2018, **7**, 3292-3300.
85. A. N. Paparella, S. Perrone, A. Salomone, F. Messa, L. Cicco, V. Capriati, F. M. Perna and P. Vitale, *Catalysts*, 2023, **13**, 1035-1054.
86. L. Liu, H. Yao, Q. Zhou, X. Yao, D. Yan, J. Xu and X. Lu, *J. Environ. Chem. Eng.*, 2022, **10**, 107512-107524.
87. X. Song, W. Hu, W. Huang, H. Wang, S. Yan, S. Yu and F. Liu, *J. Chem. Eng.*, 2020, **388**, 124324-124333.
88. K. Loos, R. Zhang, I. Pereira, B. Agostinho, H. Hu, D. Maniar, N. Sbirrazzuoli, A. J. D. Silvestre, N. Guigo and A. F. Sousa, *Front. Chem.*, 2020, **8**, 585-592.
89. C. Tang, X. Qiu, Z. Cheng and N. Jiao, *Chem. Soc. Rev.*, 2021, **50**, 8067-8101.
90. A. N. CAMPBELL and S. S. STAHL, *Acc. Chem. Res.*, 2011, **45**, 851-863.
91. A. A. Andia, M. R. Miner and K. A. Woerpel, *Org. Lett.*, 2015, **17**, 2704-2707.
92. Y. Yan, P. Feng, Q. Z. Zheng, Y. F. Liang, J. F. Lu, Y. Cui and N. Jiao, *Angew. Chem. Int. Ed. Engl.*, 2013, **52**, 5827-5831.
93. H. Liu, J. T. Yu and C. Pan, *Chem. Commun. (Camb)*, 2021, **57**, 6707-6724.
94. D. Barnard, K. R. Hargrave and G. M. C. Higgins, *J. Chem. Soc.*, 1956, 2845.
95. R. L. Luck and N. K. Newberry, *J. Phys. Org. Chem.*, 2022, **35**, 4326-4340.
96. A. Ushakova, V. Zatsepin, M. Varfolomeev and D. Emelyanov, *J. Combust.*, 2017, **2017**, 2526596.
97. S. E. Balaghi, E. Safaei, L. Chiang, E. W. Wong, D. Savard, R. M. Clarke and T. Storr, *Dalton. Trans.*, 2013, **42**, 6829-6839.
98. Z. Ma, K. T. Mahmudov, V. A. Aliyeva, A. V. Gurbanov, M. F. C. Guedes da Silva and A. J. L. Pombeiro, *Coord. Chem. Rev.*, 2021, **437**, 213859-213887.
99. W. G. Barb, J. H. Baxendale, P. George and K. R. Hargrave, *Trans. Faraday Soc.*, 1951, **47**, 462-500.
100. A. Martinsson, M. Hasani, A. Potthast and H. Theliander, *Cellulose*, 2020, **27**, 7191-7202.
101. A. Martinsson, M. Hasani and H. Theliander, *Holzforschung*, 2023, **77**, 318-325.

102. S. M. Mitroka, T. D. Smiley, J. M. Tanko and A. M. Dietrich, *Polym. Degrad. Stab.*, 2013, **98**, 1369-1377.
103. S. Klein, I. K. Dimzon, J. Eubeler and T. P. Knepper, *Handb. Enviro. Chem.*, 2018, **58**, 231-232.
104. M. Hong and E. Y. X. Chen, *Green Chem.*, 2017, **19**, 3692-3706.
105. T. O. Morgen, M. Baur, I. Gottker-Schnetmann and S. Mecking, *Nat. Commun.*, 2020, **11**, 3693-3702.
106. Z. O. G. Schyns and M. P. Shaver, *Macromol. Rapid. Commun.*, 2021, **42**, 2000415-2000415.
107. C. Jehanno, J. Demarteau, D. Mantione, M. C. Arno, F. Ruiperez, J. L. Hedrick, A. P. Dove and H. Sardon, *Angew. Chem. Int. Ed. Engl.*, 2021, **60**, 6710-6717.
108. T. J. Fazekas, J. W. Alty, E. K. Neidhart, A. S. Miller, F. A. Leibfarth and A. E. J., *science*, 2022, **375**, 545-550.
109. K.-K. Kow and K. Sirat, *CCL*, 2015, **26**, 1311-1314.
110. Z. Naseem, R. A. Shehzad, A. Ihsan, J. Iqbal, M. Zahid, A. Pervaiz and G. Sarwari, *Chem. Phys. Lett.*, 2021, **769**.
111. V. G. Vaidyanathan and B. U. Nair, *J. Inorg. Biochem.*, 2003, **94**, 121-126.
112. R. Sanchis, A. Garcia, F. Ivars-Barcelo, S. H. Taylor, T. Garcia, A. Dejoz, M. I. Vazquez and B. Solsona, *Materials (Basel)*, 2021, **14**, 7120-7237.
113. J. Almond, P. Sugumaar, M. N. Wenzel, G. Hill and C. Wallis, *E-Polym.*, 2020, **20**, 369-381.
114. G. Konstantopoulos, P. Maroulas, D. A. Dragatogiannis, S. Koutsoumpis, A. Kyritsis and C. A. Charitidis, *Mater. Des.*, 2021, **199**, 109420-109430.
115. H. Xiang, J. He, W. Qian, M. Qiu, H. Xu, W. Duan, Y. Ouyang, Y. Wang and C. Zhu, *Molecules*, 2023, **28**, 857.
116. G. Lyngsie, L. Krumina, A. Tunlid and P. Persson, *Sci. Rep.*, 2018, **8**, 10834-10843.
117. S. Coiai, E. Passaglia and F. Cicogna, *Polym. Int.*, 2018, **68**, 27-63.
118. N. Li, S. Yang, Z. Huang and X. Pan, *Macromolecules*, 2021, **54**, 6000-6005.
119. Z. Zhang, X. Li, D. Zhou, S. Ding, M. Wang and R. Zeng, *J. Am. Chem. Soc.*, 2023, **145**, 7612-7620.
120. G. Yang, H. Du, J. Liu, Z. Zhou, X. Hu and Z. Zhang, *Green Chem.*, 2017, **19**, 675-681.
121. H. Xu, S. Yamaguchi, T. Mitsudome and T. Mizugaki, *EurJOC*, 2022, **2022**, 1-5.
122. T. Mallat and A. Baiker, *Chem. Rev.*, 2004, **104**, 3037−3058.
123. K.-J. Liu, J.-H. Deng, J. Yang, S.-F. Gong, Y.-W. Lin, J.-Y. He, Z. Cao and W.-M. He, *Green Chem.*, 2020, **22**, 433-438.
124. K. Suzuki, T. Watanabe and S. Murahashi, *J. Org. Chem.*, 2013, **78**, 2301-2310.
125. E. Sella and D. Shabat, *Org. Biomol. Chem.*, 2013, **11**, 5074-5078.
126. S. Fukuzumi, Y. Lee, J. Jung and W. Nam, *Green Chem.*, 2018, **20**, 948-963.
127. Q. Zhang, J. D. Gorden and C. R. Goldsmith, *Inorg. Chem.*, 2013, **52**, 13546-13554.
128. F. Posada, P. Malfreytb and J.-L. Gardette, *Comput. Theor. Polym.*, 2001, **11**, 95-104.
129. N. Peeters, K. Janssens, D. de Vos, K. Binnemans and S. Riano, *Green Chem.*, 2022, **24**, 6685-6695.
130. I. Oluwoye, M. Altarawneh, J. Gore and B. Z. Dlugogorski, *Combust. Flame*, 2015, **162**, 3681-3690.
131. N. Gascoin, G. Fau, P. Gillard and A. Mangeot, *JAAP*, 2013, **101**, 45-52.
132. R. J. Spontak and N. P. Patel, *Curr. Opin. Colloid Interface Sci.*, 2000, **5**, 334-341.
133. S. R. Petersen, H. Prydderch, J. C. Worch, C. J. Stubbs, Z. Wang, J. Yu, M. C. Arno, A. V. Dobrynin, M. L. Becker and A. P. Dove, *Angew. Chem. Int. Ed.*, 2022, **61**, 1-8.
134. Y. Miwa, J. Kurachi, Y. Kohbara and S. Kutsumizu, *Commun. Chem.*, 2018, **1**, 5-10.
135. A. Chamas, H. Moon, J. Zheng, Y. Qiu, T. Tabassum, J. H. Jang, M. Abu-Omar, S. L. Scott and S. Suh, *ACS Sustainable Chem. Eng.*, 2020, **8**, 3494-3511.
136. A. Creamer, C. S. Wood, P. D. Howes, A. Casey, S. Cong, A. V. Marsh, R. Godin, J. Panidi, T. D. Anthopoulos, C. H. Burgess, T. Wu, Z. Fei, I. Hamilton, M. A. McLachlan, M. M. Stevens and M. Heeney, *Nat. Commun.*, 2018, **9**, 3237-3246.

137. Q. Carboue, S. Fadlallah, M. Lopez and F. Allais, *Macromol. Rapid. Commun.*, 2022, **43**, e2200254.
138. Y. Zhu, C. Romain and C. K. Williams, *Nature*, 2016, **540**, 354-362.
139. Y. Xu, G. Hua, M. Hakkarainen and K. Odelius, *Biomacromolecules*, 2018, **19**, 3077-3085.
140. J. Chen, J. Wu, J. Qi and H. Wang, *ACS Sustain. Chem. Eng.*, 2018, **7**, 1061-1071.
141. J. Wang, S. Mahmud, X. Zhang, J. Zhu, Z. Shen and X. Liu, *ACS Sustain. Chem. Eng.*, 2019, **7**, 6401-6411.
142. D. Braun and M. Bergmann, *J. Prakt. Chem.*, 1992, **334**, 298-310.
143. F. Fenouillot, A. Rousseau, G. Colomines, R. Saint-Loup and J. P. Pascault, *Prog. Polym. Sci.*, 2010, **35**, 578-622.
144. D. J. Saxon, M. Nasiri, M. Mandal, S. Maduskar, P. J. Dauenhauer, C. J. Cramer, A. M. LaPointe and T. M. Reineke, *J. Am. Chem. Soc.*, 2019, **141**, 5107-5111.
145. C. J. Stubbs, J. C. Worch, H. Prydderch, M. L. Becker and A. P. Dove, *Macromolecules*, 2019, **53**, 174-181.
146. C. J. Stubbs, J. C. Worch, H. Prydderch, Z. Wang, R. T. Mathers, A. V. Dobrynin, M. L. Becker and A. P. Dove, *J. Am. Chem. Soc.*, 2022, **144**, 1243-1250.
147. J. Lai, H. Huang, M. Lin, Y. Xu, X. Li and B. Sun, *Front. Microbiol.*, 2022, **13**, 1-26.
148. Y. Wu, M. Ding, J. Wang, B. Zhao, Z. Wu, P. Zhao, D. Tian, Y. Ding and A. Hu, *CCS Chem.*, 2020, **2**, 64-70.
149. R. S. Hoy and M. O. Robbins, *J. Polym. Sci., Part B: Polym. Phys.*, 2006, **44**, 3487-3500.
150. F. P. La Mantia, M. Morreale, L. Botta, M. C. Mistretta, M. Ceraulo and R. Scaffaro, *Polym. Degrad. and Stab.*, 2017, **145**, 79-92.
151. L. A. Utracki, *CJCE*, 2002, **80**, 1008-1016.
152. A.-C. Albertsson and Y. Liu, *J. Macromol. Sci. A*, 2006, **34**, 1457-1482.

4.7 Experimental

4.7.1 Instruments

Nuclear magnetic resonance (NMR) Spectroscopy

NMR spectroscopy experiments were performed in deuterated $CDCl_3$ (99.8% D) with ^1H spectra referenced to the residual protic solvent peak ($CHCl_3$ at δ = 7.26 ppm) and ^{13}C NMR spectra referenced to the residual solvent signal ($CDCl_3$ at δ = 77.16 ppm). NMR spectroscopy experiments were performed at 298 K on a Bruker 400 MHz spectrometer for ^1H and 100.57 MHz for ^{13}C. Spectra data was analysed using MestReNova 12.0.2 software. The resonance multiplicities for ^1H NMR are described as s (singlet), d (doublet), t (triplet), q (quartet) or m (multiplet).

Size exclusion chromatography (SEC)

SEC of the polymers were performed in $CHCl_3$ on an Agilent 1260 Infinity II Multi-detector GPC/SEC system with RI, UV (λ = 309 nm), and viscometer detectors. Using $CHCl_3$ (buffered with NEt_3) as the mobile phase (flow rate = 1 mL.min^{-1}, 40 °C) the polymers were eluted through an Agilent guard column (PLGel 5 μM, 50 × 7.5 mm) and two Agilent mixed-C columns (PLGel 5 μM, 300 × 7.5 mm). Number average molecular weight (M_n), weight average molecular weight (M_w) and dispersity ($Đ_M = M_w/M_n$) were determined using Agilent GPC/SEC software (vA.02.01) against a 15-point calibration curve (M_p = 162 – 3,187,000 g·mol^{-1}) based on polystyrene standards (Easivial PS-M/H, Agilent).

Thermal gravimetric analysis (TGA)

Thermal decomposition temperatures of the polymers were measured on a Q550 Auto Thermogravimetric analyser. TGA thermograms were recorded at a heating rate of 10 °C·min^{-1} from 25 °C to 600 °C under an inert N_2 atmosphere.

Differential scanning calorimetry (DSC)

The thermal characteristics of the polymers were determined using a STARe system DSC3 (Mettler Toledo Switzerland). DSC calorigrams were recorded under an inert N_2 atmosphere at a heating rate of 10 °C·min^{-1} from -50 °C to 200 °C for two cycles. Each sample was loaded into 40 μL aluminium pans at weights ranging between 5-10 mg. From the second heating cycle, the glass transition temperature (T_g) was observed as the midpoint of the inflexion tangent.

Wide angle X-ray scattering (WAXS)

WAXS was performed on a Panalytical Empyrean utilising Cu radiation ($K_{\alpha1}$ and $K_{\alpha2}$ radiation (l = 1.5406 Å and 1.5444 Å respectively)) and equipped with a Pixel Medipix 3D detector. Polymer film samples were prepared onto low background Si-wafer sample holders and standard "powder" 2θ–θ diffraction scans were carried out in the angular range from 4° to 60° 2θ at room temperature.

Mechanical testing

Tensile testing

Mechanical characteristics were investigated using a testometric M350-5CT universal mechanical testing instrument fitting with a 10 kN load cell. Samples were first prepared into thin films. Approximately 1.5 g of polymer was added into a 40 × 50 × 0.50 mm stainless steel mould and placed in a pre-heated press at 160 °C where it was left to heat for 10 minutes (with no force) between two Teflon sheets. Then, 2000 kg of pressure was applied to the sample for 5 minutes before 4 × (500 kg pressure/release) cycles were performed. The sample was heated for a further 5 minutes at 2000 kg pressure before being cooled down to 25 °C while still under pressure. Films were annealed for 7 days at 22 °C. Finally, uniform dog bones were hand-pressed from the film using an ASTM Die D-638 Type V cutter. Each dog bone was clamped in hydrolytic clamps and subjected to uniaxial elongation at a rate of 10 $mm.min^{-1}$ until failure. A minimum of 3 tensile tests were averaged to find the ultimate tensile strain and stress for each polymer sample.

Rheology

Rheology experiments were performed using an Anton Paar MCR 302 on polymer film discs (8 × 0.5 mm) cut from the same samples used for tensile testing as discussed above. Temperature was controlled with a P-PTD 200/AIR Peltier and a P-PTD 200 hood. Frequency sweeps were performed at 1% strain from 0.1 to 100 rad·s-1 at 5 °C intervals between the temperatures of 140 °C to 170 °C for ISPU and 100 °C to 130 °C for IMPU.

4.7.2 Materials

1,4:3,6-Dianhydro-D-mannitol (isomannide), 95% was purchased from Merck Life Science. 2-Isocyanatoethyl acrylate (stabilised with BHT) was purchased from Tokyo Chemical Industry UK Ltd. Isosorbide, 98% was purchased from Fisher Scientific UK Limited. 1,8-Octanedithiol > 97% was distilled before use and stored in an ampoule under an inert atmosphere. Dimethylphenyl phosphine, 99% was bought under an inert atmosphere and transferred via a cannula into an ampoule and stored under an inert atmosphere.

4.7.3 Procedures

Synthesis of isomannide urethane monomer

Into a 250 mL round bottom flask isomannide (68.2 mmol, 10.0 g, 1 equiv), 2-isocyanatoethyl acrylate (164.2 mmol, 20.5 mL, 2.4 equiv), butylated hydroxytoluene (50 mg), 70 mL THF and 10 mL DMF were loaded and stirred at room temperature. Once fully combined dibutyltin dilaurate (0.14 mmol, 80.8 µL, 0.002 equiv) was added in one portion causing a mild exotherm. The reaction was left to stir overnight at 22 °C (*ca.* 16h). TLC performed in 100% ethyl acetate confirmed the consumption of isomannide. Diethyl ether (150 mL) was added to the reaction mixture causing the precipitate to form instantly, the reaction mixture was left in the fridge for 4 h (4 °C). The precipitate was filtered and washed with diethyl ether (2 × 100 mL) and the crude product was dried in *vacuo.* The crude product was recrystallised in a mixture of ethyl acetate/hexane (a large excess of ethyl acetate) to yield a white solid (21.3 g, 73 %). ^{1}H NMR (400 MHz, Chloroform-*d*) δ 6.41 (dd, J = 17.3, 1.4 Hz, 2H), 6.10 (dd, J = 17.3, 10.4 Hz, 2H), 5.85 (dd, J = 10.5, 1.4 Hz, 2H), 5.33 – 5.21 (m, 2H), 5.08 (td, J = 7.0, 3.6 Hz, 2H), 4.73 – 4.59 (m, 2H), 4.23 (t, J = 5.3 Hz, 4H), 4.04 (dd, J = 9.1, 6.5 Hz, 2H), 3.81 – 3.68 (m, 2H), 3.49 (p, J

= 5.6 Hz, 4H). ^{13}C NMR (101 MHz, Chloroform-*d*) δ 166.10, 155.57, 131.61, 128.02, 80.91, 74.35, 70.59, 63.50, 40.36.

Synthesis of isosorbide urethane monomer

Into a 250 mL round bottom flask isosorbide (68.2 mmol, 10.0 g, 1 equiv), 2-isocyanatoethyl acrylate (164.2 mmol, 20.5 mL, 2.4 equiv), butylated hydroxytoluene (50 mg), 70 mL THF and 10 mL DMF was loaded and stirred at room temperature. Once fully combined dibutyltin dilaurate (0.14 mmol, 80.8 µL, 0.002 equiv) was added in one portion causing a mild exotherm. The reaction was left to stir overnight at 22 °C (*ca.* 16h). TLC performed in 100% ethyl acetate confirmed the consumption of isosorbide. Diethyl ether (150 mL) was added to the reaction mixture causing the precipitate to form instantly, the reaction mixture was left in the fridge for 4 h (4 °C). The precipitate was filtered and washed with diethyl ether (2 × 100 mL) and the crude product was dried in *vacuo.* The crude product was recrystallised in a mixture of ethyl acetate/hexane (a large excess of ethyl acetate) to yield a white solid (23.4 g, 80 %). ^{1}H NMR (400 MHz, Chloroform-*d*) δ 6.42 (dt, J = 17.3, 1.3 Hz, 2H), 6.11 (ddd, J = 17.3, 10.4, 1.5 Hz, 2H), 5.86 (dt, J = 10.4, 1.5 Hz, 2H), 5.21 (d, J = 6.0 Hz, 1H), 5.11 (dq, J = 11.8, 5.6 Hz, 3H), 4.75 (t, J = 4.8 Hz, 1H), 4.49 (d, J = 4.4 Hz, 1H), 4.23 (t, J = 5.3 Hz, 4H), 4.04 – 3.89 (m, 3H), 3.70 (dd, J = 9.5, 6.3 Hz, 1H), 3.49 (dq, J = 8.9, 5.3 Hz, 4H). ^{13}C NMR (101 MHz, Chloroform-*d*) δ 166.14, 166.10, 155.61, 155.27, 131.67, 131.63, 128.02, 85.93, 81.11, 78.72, 74.55, 73.87, 70.09, 63.52, 63.48, 40.34.

General preparation of Isohexide polyurethane via step-growth polymerisation

A 20 mL scintillation vial was charged 1,8-octanedithiol (3.5691 g, 20.0 mmol, 1.0 equiv) and a separate 100 mL round bottom flask was charged with the isohexide urethane (8.5723 g,

20.0 mmol, 1.0 equiv). The thiol was quantitively transferred to the isohexide urethane-containing round bottom flask using $CHCl_3$ (50 mL). The reaction mixture was left to stir for 15 minutes (22 °C) before being cooled to 0 °C in an ice bath and dimethylphenylphosphine (DMPP) (57.0 μL, 0.4 mmol, 0.02 equiv) added in one portion causing a mild exotherm. The reaction was removed from the ice and left to stir overnight at 22 °C (*ca.* 16h). The viscous reaction mixture was diluted with chloroform (400 mL) and precipitated dropwise into diethyl ether (1000 mL). The polymer was dried in *vacuo* at ambient temperature for 12 h and again at 120 °C overnight (*ca.* 16 h) to yield a white solid.

Physical blending method: b-IM/IS

IMPU and ISPU were combined in their appropriate ratios for a total polymer weight of 2 g (1.8 g IMPU + 0.2 g ISPU (90/10): 1.6 g IMPU + 0.4 g ISPU (80/20): 1.4 g IMPU + 0.6 g ISPU (70/30): 1.2 g IMPU + 0.8 g ISPU (60/40): 1.0 g IMPU + 1.0 g ISPU (50/50): 0.8 g IMPU + 1.2 g ISPU (40/60): 0.6 g IMPU + 1.4 g ISPU (30/70): 0.4 g IMPU + 1.6 g ISPU (20/80): 0.2 g IMPU + 1.8 g ISPU (10/90) in a 20 mL scintillation vial. Each polymer blend was dissolved in 15 mL of $CHCl_3$. Once solubilised, the polymer solution was decanted into a Teflon sheet and left to air dry for several hours before being dried in *vacuo* at 120 °C overnight (*ca.* 16 h) affording a blended homopolymer sample.

IMPU

Yield = 73% SEC analysis ($CHCl_3$ + 0.5% NEt_3) M_w = 125.5 kDa, M_n = 10.2 kDa, M_p = 95.8 kDa, $Đ_M$ = 12.3.

^{1}H NMR (400 MHz, Chloroform-*d*) δ 5.34 (s, 2H), 5.08 (q, J = 6.1 Hz, 2H), 4.66 (d, J = 4.2 Hz, 2H), 4.30 – 4.10 (m, 4H), 4.11 – 3.92 (m, 2H), 3.88 – 3.63 (m, 2H), 3.46 (p, J = 5.3 Hz,

4H), 2.77 (t, *J* = 7.1 Hz, 4H), 2.61 (t, *J* = 7.2 Hz, 4H), 2.57 – 2.44 (m, 4H), 1.57 (qd, *J* = 8.3, 7.7, 6.2 Hz, 4H), 1.47 – 1.19 (m, 8H). ^{13}C NMR (101 MHz, Chloroform-*d*) δ 172.00, 155.64, 80.90, 74.41, 70.57, 63.62, 40.31, 34.81, 32.25, 29.60, 29.18, 28.87, 27.06.

ISPU

Yield = 80% SEC analysis ($CHCl_3$ + 0.5% NEt_3) M_w = 158.1 kDa, M_n = 5.0 kDa, M_p = 119.8 kDa, $Đ_M$ = 31.1.

^{1}H NMR (400 MHz, Chloroform-*d*) δ 5.28 (d, *J* = 26.6 Hz, 2H), 5.10 (dd, *J* = 11.9, 6.3 Hz, 2H), 4.76 (t, *J* = 4.8 Hz, 1H), 4.49 (d, *J* = 4.5 Hz, 1H), 4.30 – 4.08 (m, *J* = 5.5, 5.1 Hz, 4H), 4.08 – 3.86 (m, 3H), 3.85 – 3.62 (m, 1H), 3.59 – 3.27 (m, 4H), 2.77 (t, *J* = 7.2 Hz, 4H), 2.62 (t, *J* = 7.2 Hz, 4H), 2.52 (t, *J* = 7.4 Hz, 4H), 1.62 – 1.51 (m, 4H), 1.47 – 1.20 (m, 8H). ^{13}C NMR (101 MHz, Chloroform-*d*) δ 171.97, 155.67, 155.34, 86.01, 81.13, 78.75, 77.48, 77.36, 77.16, 76.84, 74.55, 73.86, 70.17, 63.65, 63.60, 40.28, 34.80, 32.25, 29.59, 29.18, 28.87, 27.12, 27.10.

Blends:

***b*-IM$_{50}$IS$_{50}$**

SEC analysis ($CHCl_3$ + 0.5% NEt_3) M_w = 114.1 kDa, M_n = 10.5 kDa, M_p = 90.3 kDa, $Đ_M$ = 10.9

^{1}H NMR (400 MHz, Chloroform-*d*) δ 5.41 – 5.17 (m, 2H), 5.09 (dd, *J* = 12.5, 6.8 Hz, 2H), 4.66 (d, *J* = 4.2 Hz, 1H), 4.49 (d, *J* = 4.4 Hz, 1H), 4.18 (h, *J* = 6.3 Hz, 4H), 4.05 (dd, *J* = 9.1, 6.6 Hz, 1H), 4.01 – 3.87 (m, 2H), 3.84 – 3.63 (m, *J* = 7.1, 6.1 Hz, 1H), 3.45 (q, *J* = 5.4 Hz, 4H), 2.77 (t, *J* = 7.2 Hz, 4H), 2.69 – 2.56 (m, 4H), 2.51 (t, *J* = 7.4 Hz, 4H), 1.65 – 1.47 (m, 4H), 1.47 – 1.19 (m, 8H). ^{13}C NMR (101 MHz, Chloroform-*d*) δ 171.98, 171.95, 155.64, 155.33, 85.99, 81.12, 80.89, 78.73, 77.48, 77.16, 76.84, 74.54, 74.40, 73.85, 70.56, 70.15, 63.61, 40.28, 34.80, 34.79, 32.24, 32.23, 29.58, 29.17, 28.85, 27.11, 27.08, 27.05.

***b*-IM$_{90}$IS$_{10}$**

SEC analysis ($CHCl_3$ + 0.5% NEt_3) M_w = 125.7 kDa, M_n = 5.6 kDa, M_p = 96.7 kDa, $Đ_M$ = 22.5.

***b*-IM$_{80}$IS$_{20}$**

SEC analysis ($CHCl_3$ + 0.5% NEt_3) M_w = 127.6 kDa, M_n = 6.1 kDa, M_p = 99.6 kDa, $Đ_M$ = 20.9.

***b*-IM$_{70}$IS$_{30}$**

SEC analysis ($CHCl_3$ + 0.5% NEt_3) M_w = 88.9 kDa, M_n = 6.2 kDa, M_p = 77.3 kDa, $Đ_M$ = 14.4.

***b*-IM$_{60}$IS$_{40}$**

SEC analysis ($CHCl_3$ + 0.5% NEt_3) M_w = 115.0 kDa, M_n = 5.7 kDa, M_p = 81.2 kDa, $Đ_M$ = 20.1.

***b*-IM$_{40}$IS$_{60}$**

SEC analysis ($CHCl_3$ + 0.5% NEt_3) M_w = 103.6 kDa, M_n = 8.3 kDa, M_p = 82.8 kDa, $Đ_M$ = 12.5.

***b*-IM$_{30}$IS$_{70}$**

SEC analysis ($CHCl_3$ + 0.5% NEt_3) M_w =120.0 kDa, M_n = 6.0 kDa, M_p = 85.2 kDa, $Đ_M$ = 20.0.

***b*-IM$_{20}$IS$_{80}$**

SEC analysis ($CHCl_3$ + 0.5% NEt_3) M_w = 180.0 kDa, M_n = 18.0 kDa, M_p = 141.4 kDa, $Đ_M$ = 10.0.

***b*-IM$_{10}$IS$_{90}$**

SEC analysis ($CHCl_3$ + 0.5% NEt_3) M_w = 177.5 kDa, M_n = 5.9 kDa, M_p = 141.4 kDa, $Đ_M$ = 30.2.

<u>Co-polymers:</u>

***co*-IM$_{50}$IS$_{50}$**

SEC analysis ($CHCl_3$ + 0.5% NEt_3) M_w = 87.2 kDa, M_n = 6.1 kDa, M_p = 82.8 kDa, $Đ_M$ = 14.2

^{1}H NMR (400 MHz, Chloroform-*d*) δ 5.34 (d, J = 10.7 Hz, 1H), 5.17 – 4.98 (m, 2H), 4.74 (t, J = 4.8 Hz, 1H), 4.64 (d, J = 4.2 Hz, 1H), 4.47 (d, J = 4.4 Hz, 1H), 4.25 – 4.08 (m, 4H), 4.08 – 3.97 (m, 1H), 3.98 – 3.81 (m, 2H), 3.71 (dt, J = 15.2, 8.7 Hz, 1H), 3.44 (p, J = 5.8, 5.3 Hz, 4H), 2.75 (t, J = 7.2 Hz, 4H), 2.59 (t, J = 7.3 Hz, 4H), 2.50 (t, J = 7.4 Hz, 4H), 1.63 – 1.44 (m, 4H), 1.43 – 1.17 (m, 8H). ^{13}C NMR (101 MHz, Chloroform-*d*) δ 171.93, 171.91, 155.59, 155.28, 85.94, 81.06, 80.84, 78.67, 77.48, 77.16, 76.84, 74.48, 74.33, 73.79, 70.51, 70.11, 63.55, 40.22, 34.75, 34.73, 32.18, 29.53, 29.36, 29.11, 28.80, 27.05, 27.03, 26.99.

***co* -IM$_{90}$IS$_{10}$**

SEC analysis ($CHCl_3$ + 0.5% NEt_3) M_w = 136.4 kDa, M_n = 12.1 kDa, M_p = 121.0 kDa, $Đ_M$ = 11.3.

***co* -IM$_{80}$IS$_{20}$**

SEC analysis ($CHCl_3$ + 0.5% NEt_3) M_w = 179.9 kDa, M_n = 10.7 kDa, M_p = 160.5 kDa, $Đ_M$ = 16.8.

***co* -IM$_{70}$IS$_{30}$**

SEC analysis ($CHCl_3$ + 0.5% NEt_3) M_w = 98.4 kDa, M_n = 9.6 kDa, M_p = 80.4 kDa, $Đ_M$ = 10.3.

***co* -IM$_{60}$IS$_{40}$**

SEC analysis ($CHCl_3$ + 0.5% NEt_3) M_w = 96.9 kDa, M_n = 7.8 kDa, M_p = 75.8 kDa, $Đ_M$ = 12.3.

***co* -IM$_{40}$IS$_{60}$**

SEC analysis ($CHCl_3$ + 0.5% NEt_3) M_w = 88.5 kDa, M_n = 7.3 kDa, M_p = 74.4 kDa, $Đ_M$ = 12.2.

***co* -IM$_{30}$IS$_{70}$**

SEC analysis ($CHCl_3$ + 0.5% NEt_3) M_w = 104.4 kDa, M_n = 13.4 kDa, M_p = 93.0 kDa, $Đ_M$ = 7.7

***co* -IM$_{20}$IS$_{80}$**

SEC analysis ($CHCl_3$ + 0.5% NEt_3) M_w = 103.6 kDa, M_n = 8.3 kDa, M_p = 82.8 kDa, $Đ_M$ = 12.5

***co*-IM$_{10}$IS$_{90}$**

SEC analysis ($CHCl_3$ + 0.5% NEt_3) M_w = 115.0 kDa, M_n = 5.7 kDa, M_p = 81.2 kDa, $Đ_M$ = 20.1

4.8 Appendix

NMR Spectra:

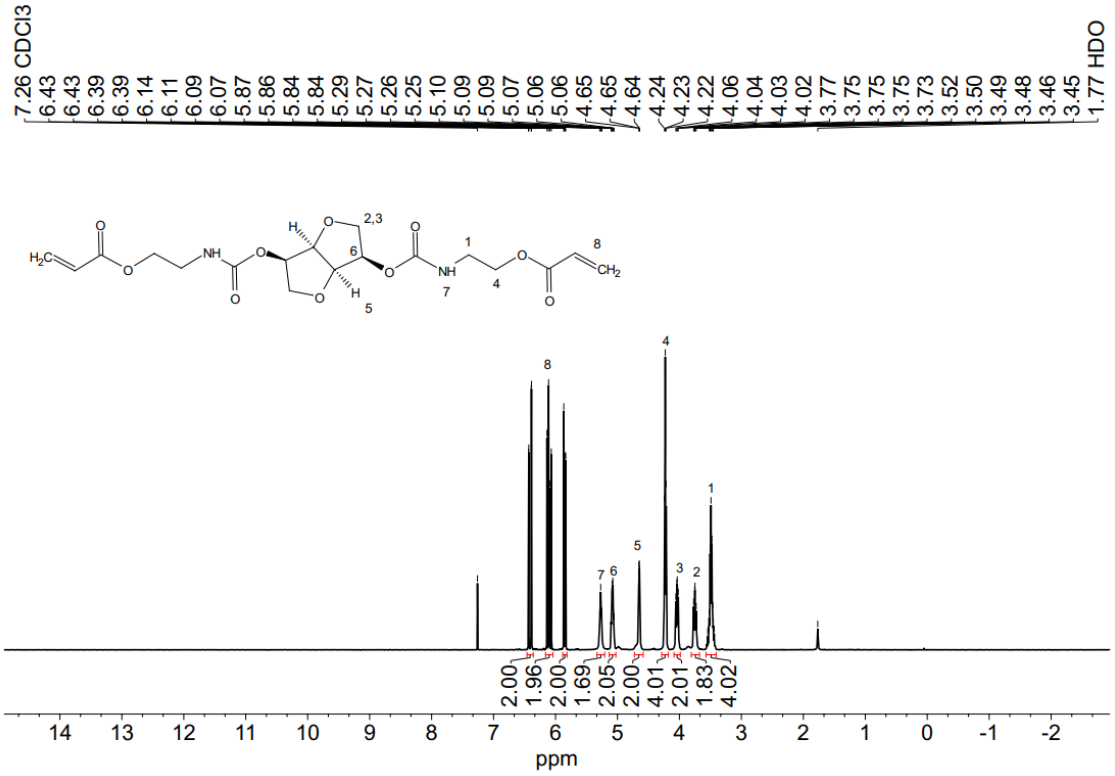

Figure 4.4 ^{1}H NMR spectrum of isomannide urethane (400 MHz, 298 K, $CDCl_3$)

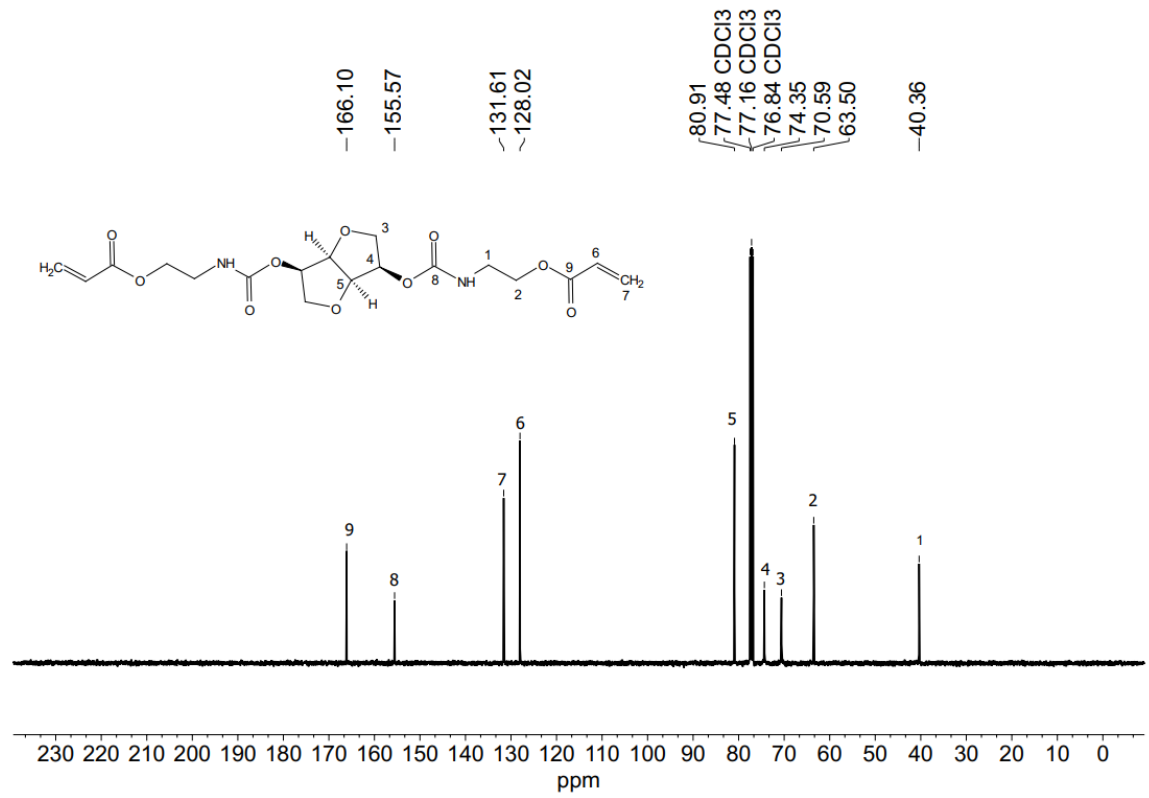

Figure 4.5 ^{13}C NMR spectrum of isomannide urethane (100.57 MHz, 298 K, $CDCl_3$)

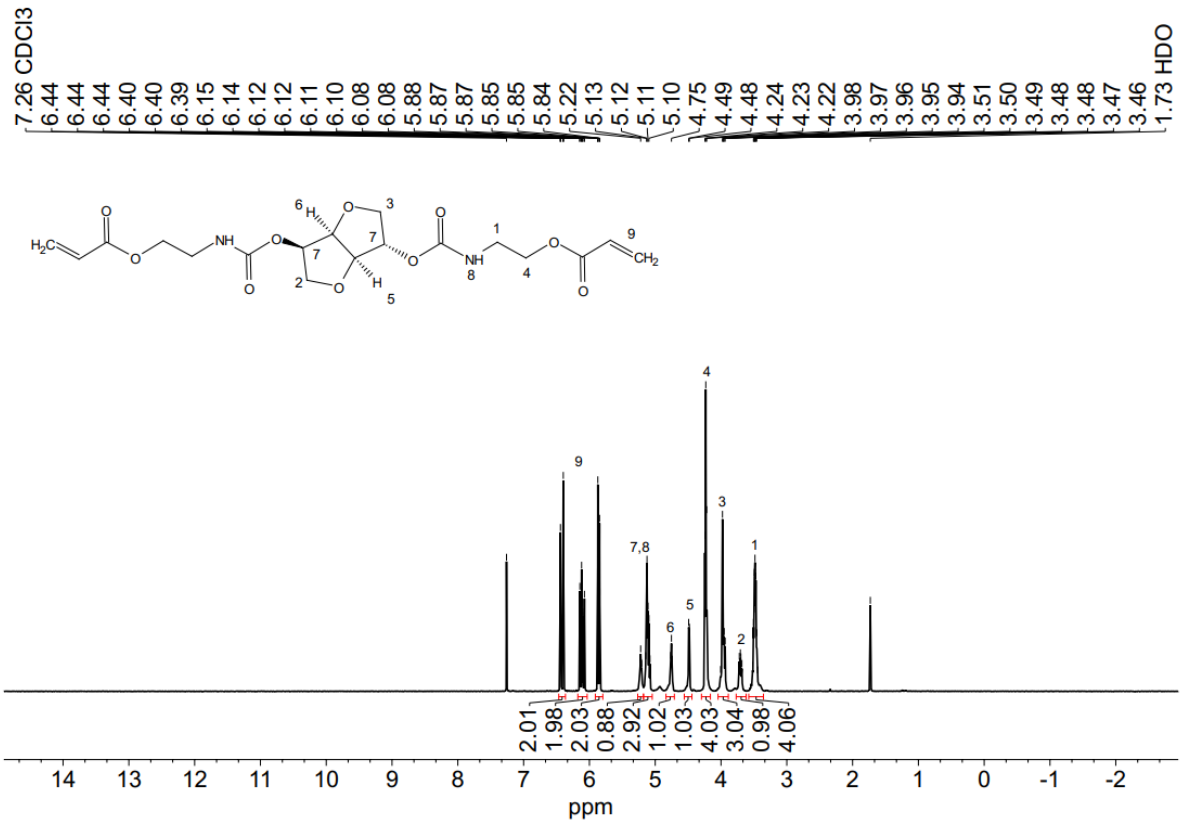

Figure 4.6 ^{1}H NMR spectrum of isosorbide urethane (400 MHz, 298 K, $CDCl_3$)

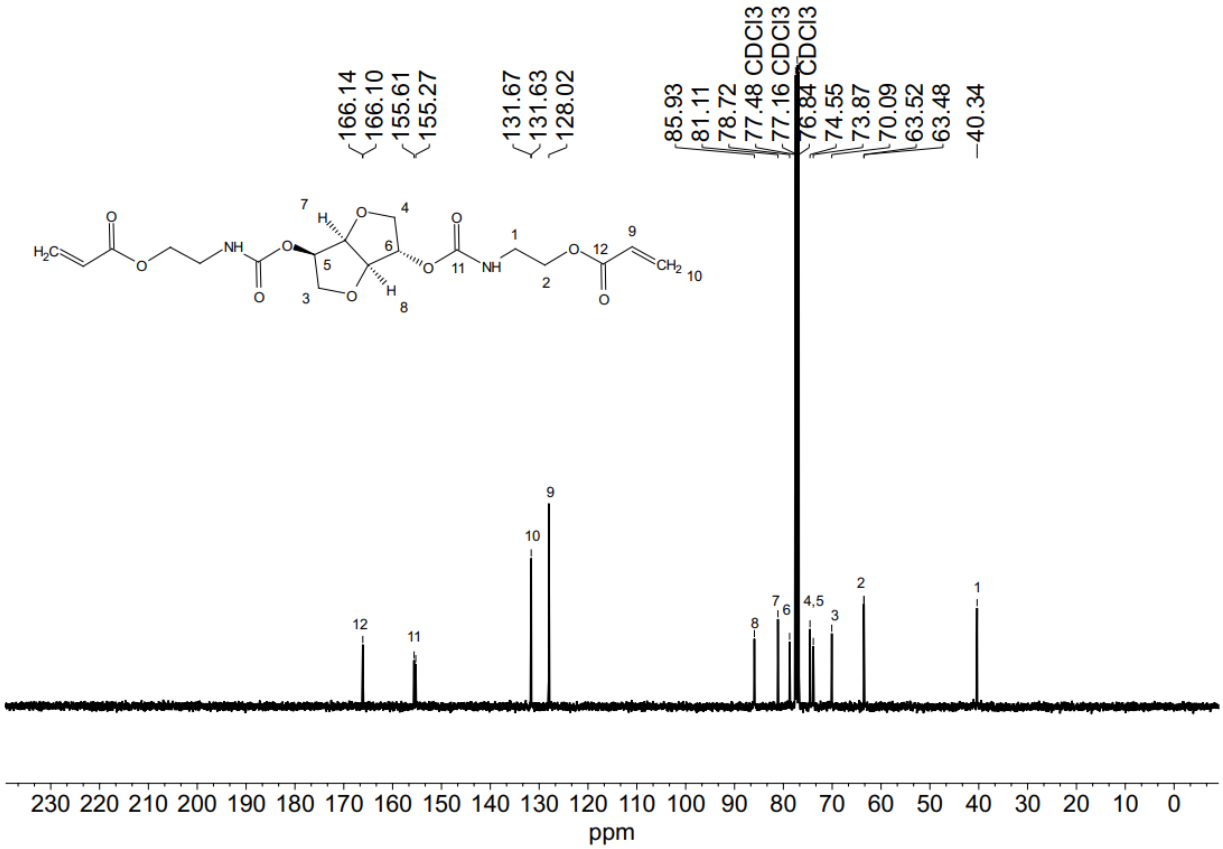

Figure 4.7 ^{13}C NMR spectrum of isosorbide urethane (100.57 MHz, 298 K, $CDCl_3$)

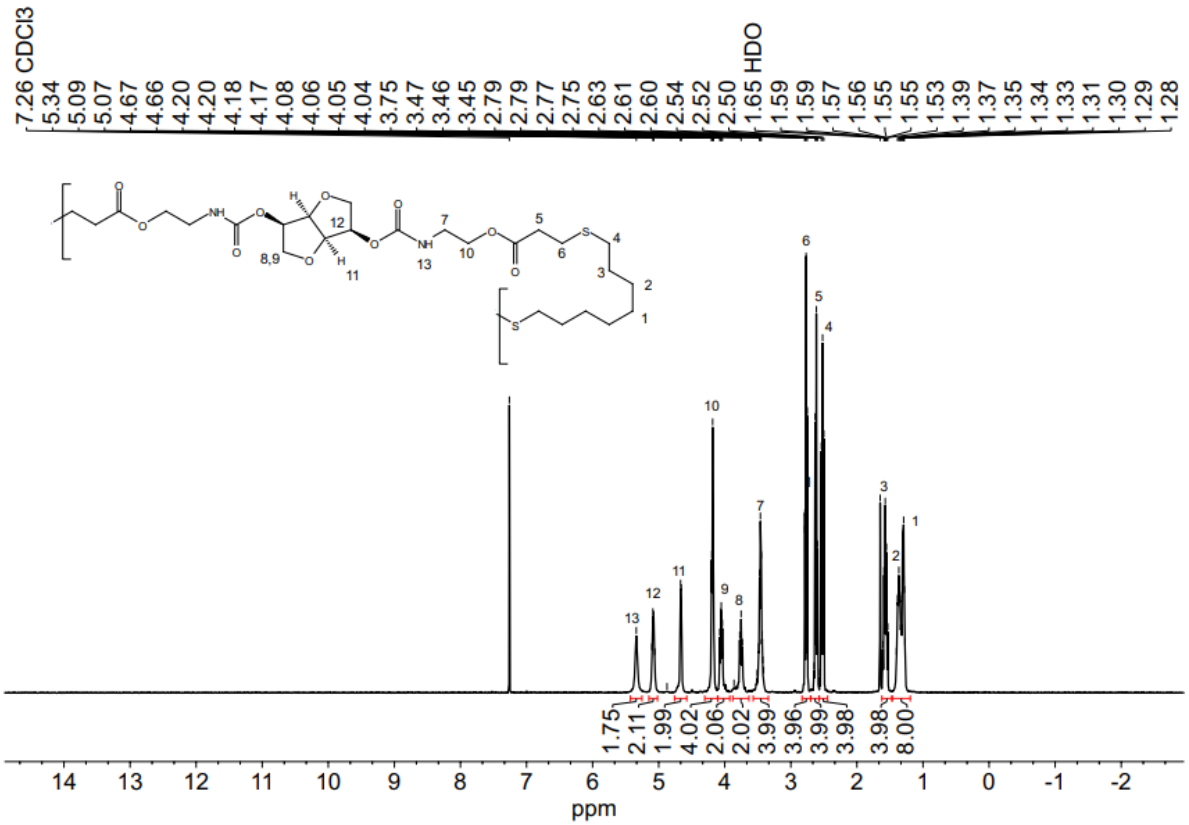

Figure 4.8 ^{1}H NMR spectrum of isomannide polyurethane (400 MHz, 298 K, $CDCl_3$)

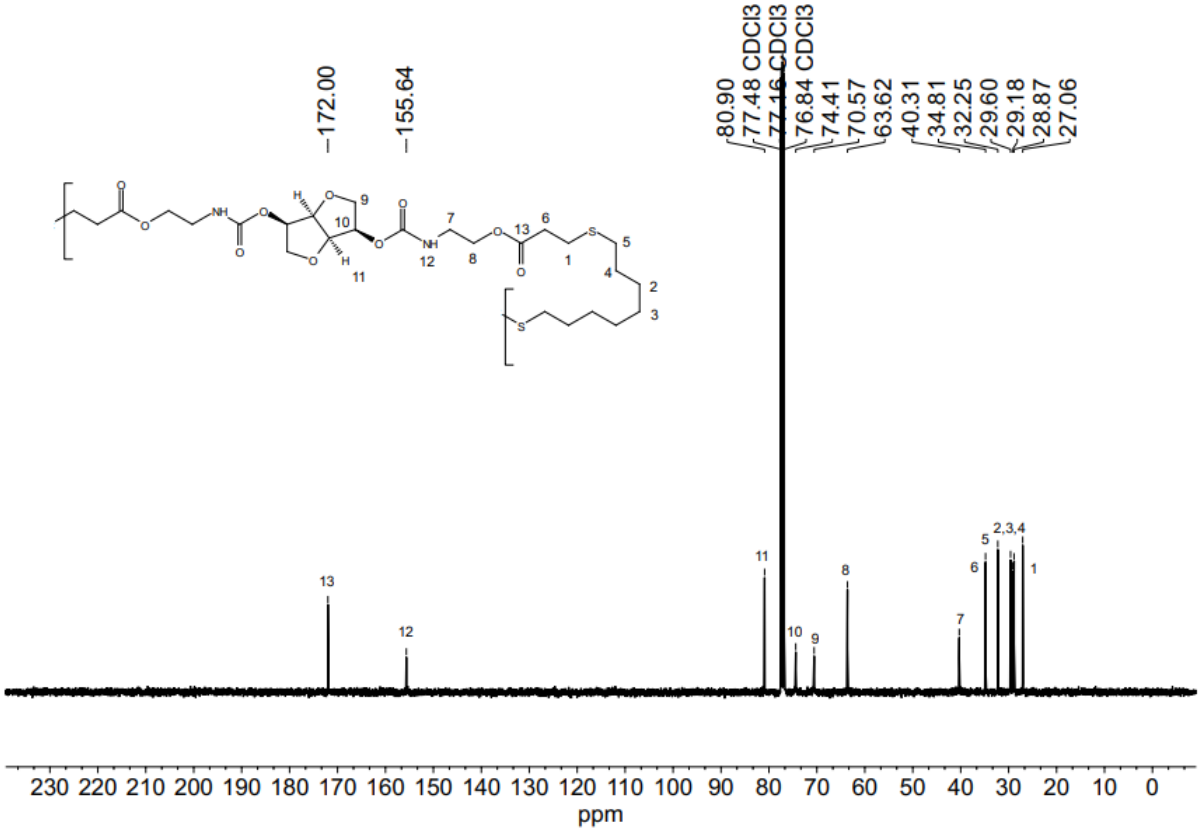

Figure 4.9 ^{13}C NMR spectrum of isomannide polyurethane (100.57 MHz, 298 K, $CDCl_3$)

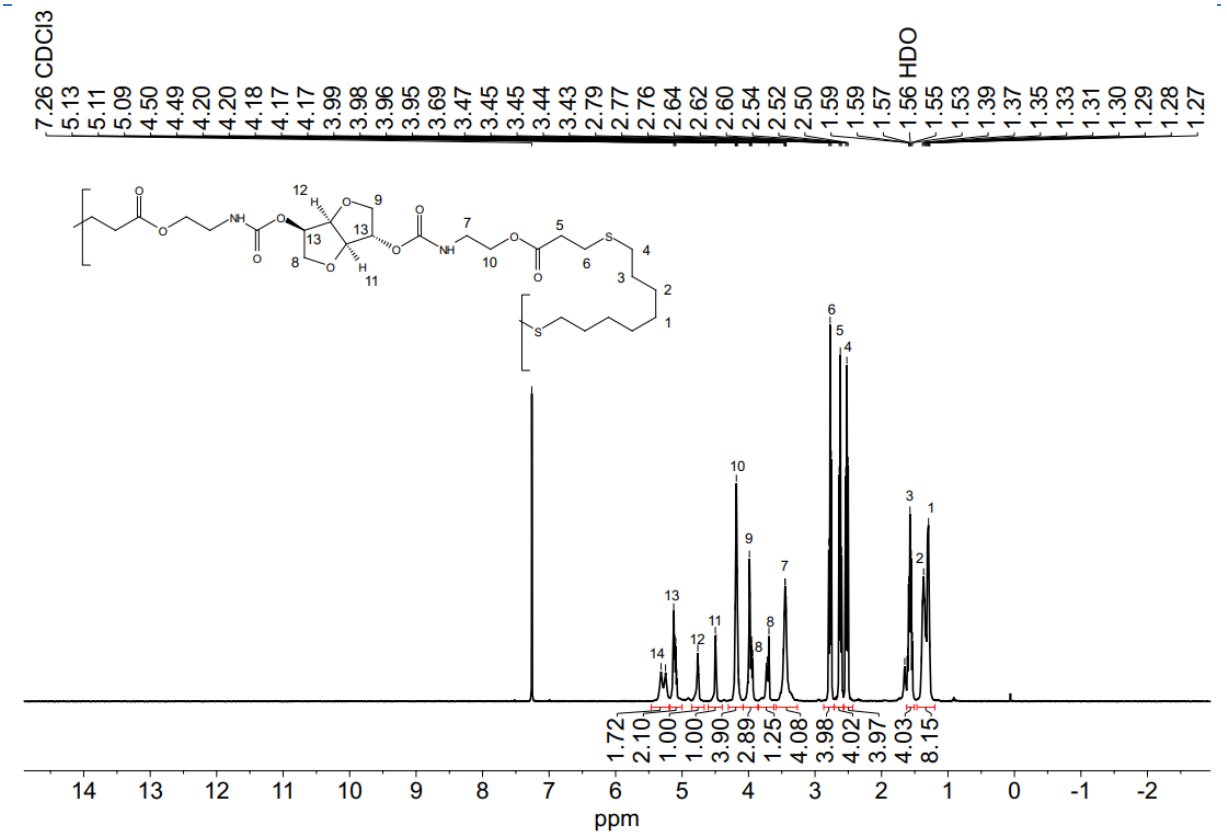

Figure 4.10 ^{1}H NMR spectrum of isosorbide polyurethane (400 MHz, 298 K, $CDCl_3$)

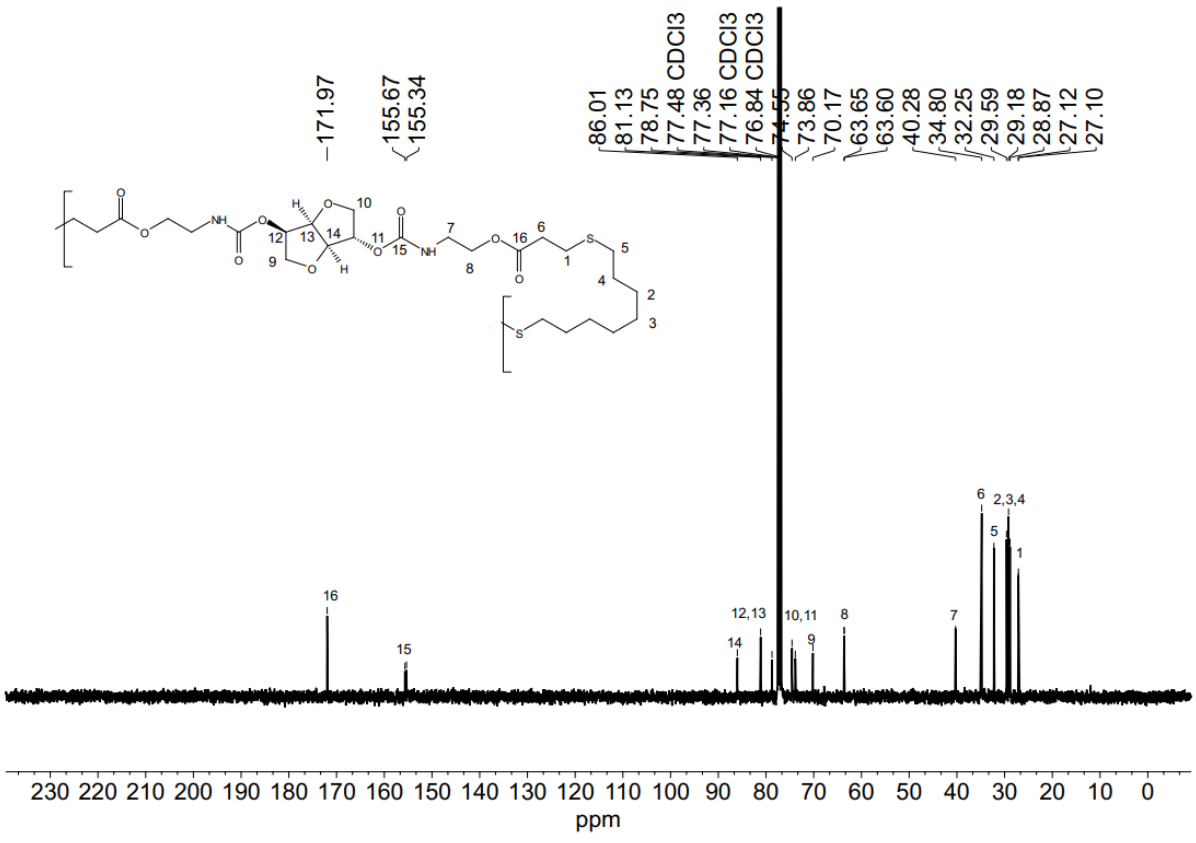

Figure 4.11 ^{13}C NMR spectrum of isosorbide polyurethane (100.57 MHz, 298 K, $CDCl_3$)

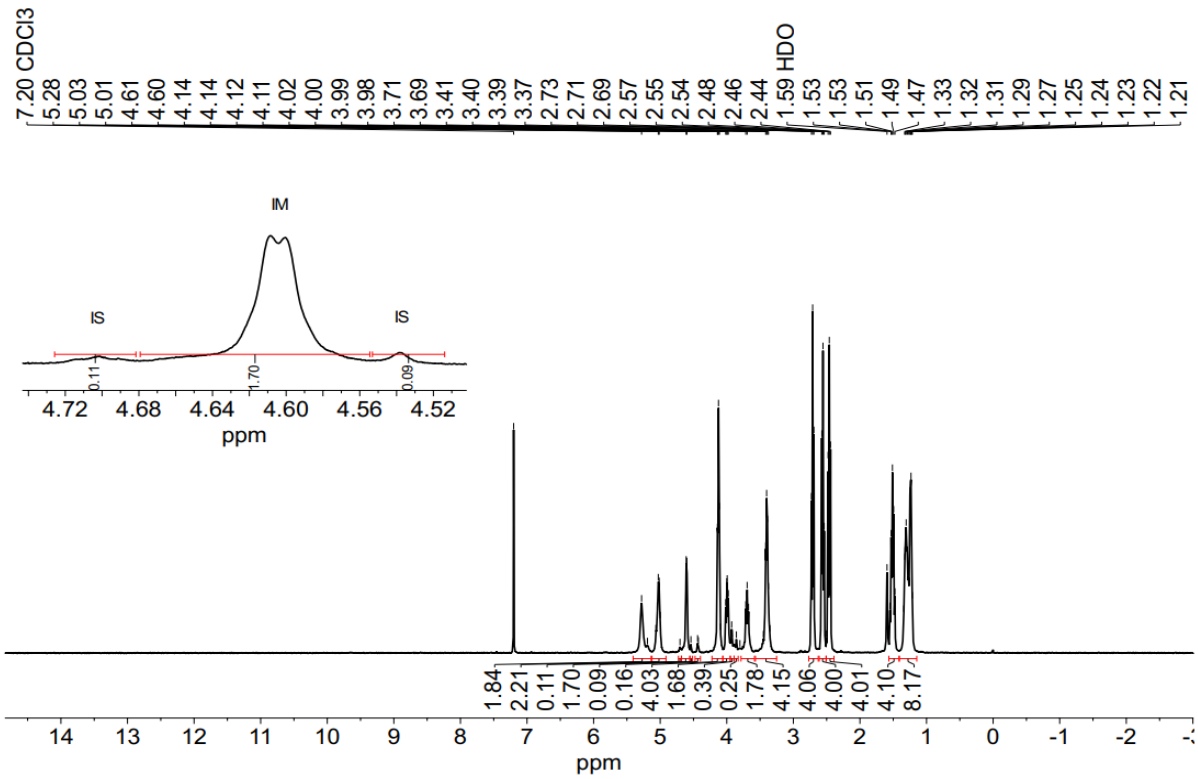

Figure 4.12 ^{1}H NMR spectrum of b-IM$_{90}$IS$_{10}$ (400 MHz, 298 K, $CDCl_3$)

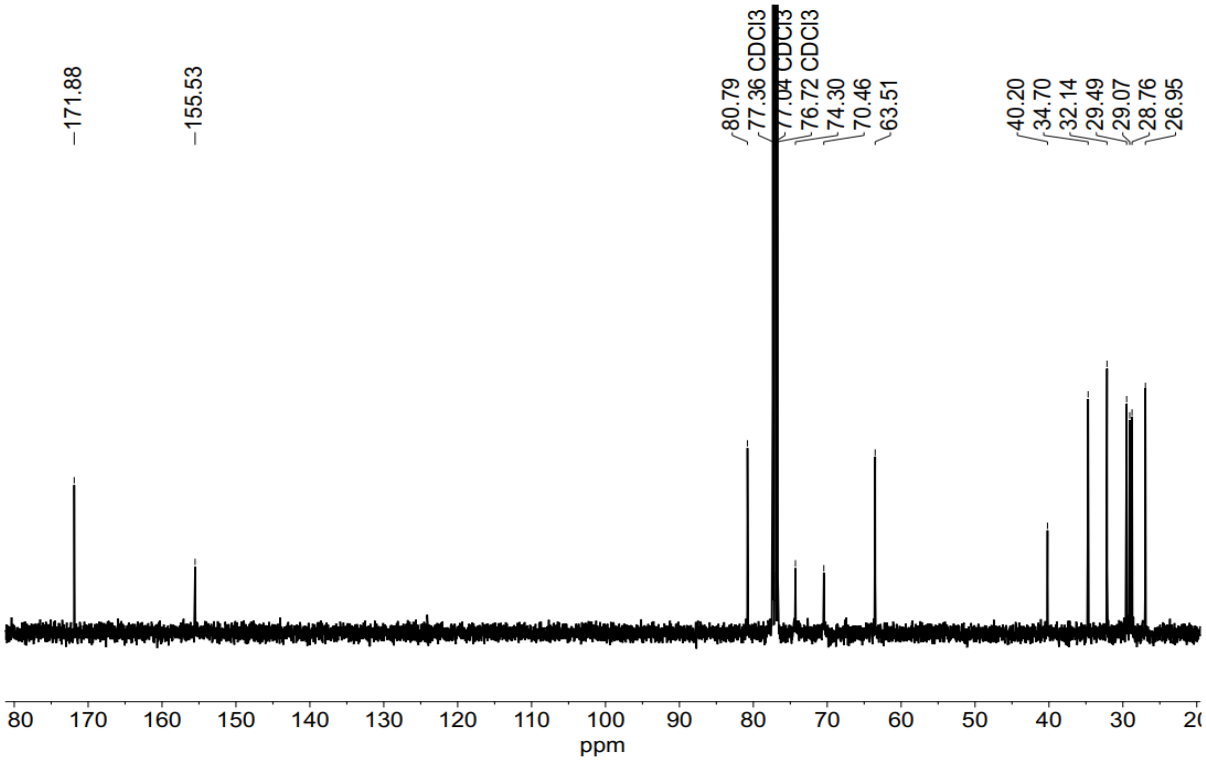

Figure 4.13 ^{13}C NMR spectrum of b-IM$_{90}$IS$_{10}$ (100.57 MHz, 298 K, $CDCl_3$)

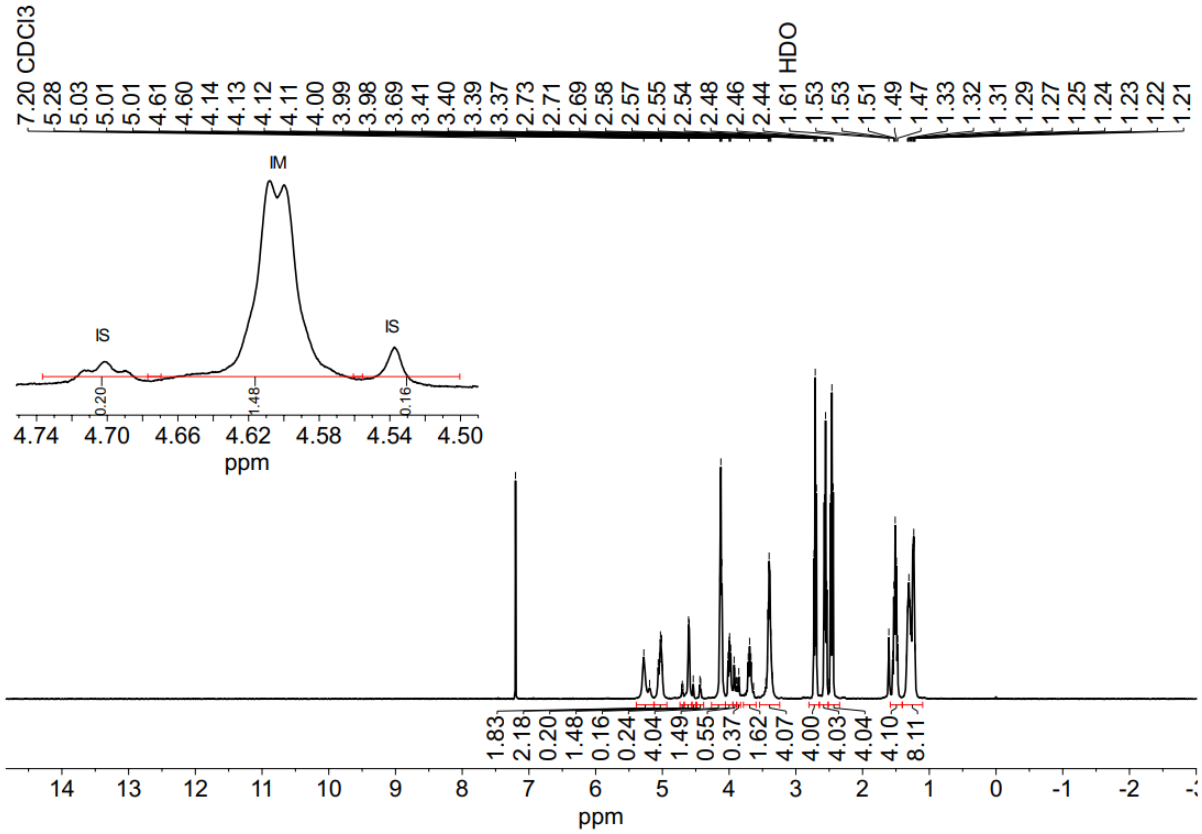

Figure 4.14 ^{1}H NMR spectrum of b-$IM_{80}IS_{20}$ (400 MHz, 298 K, $CDCl_3$)

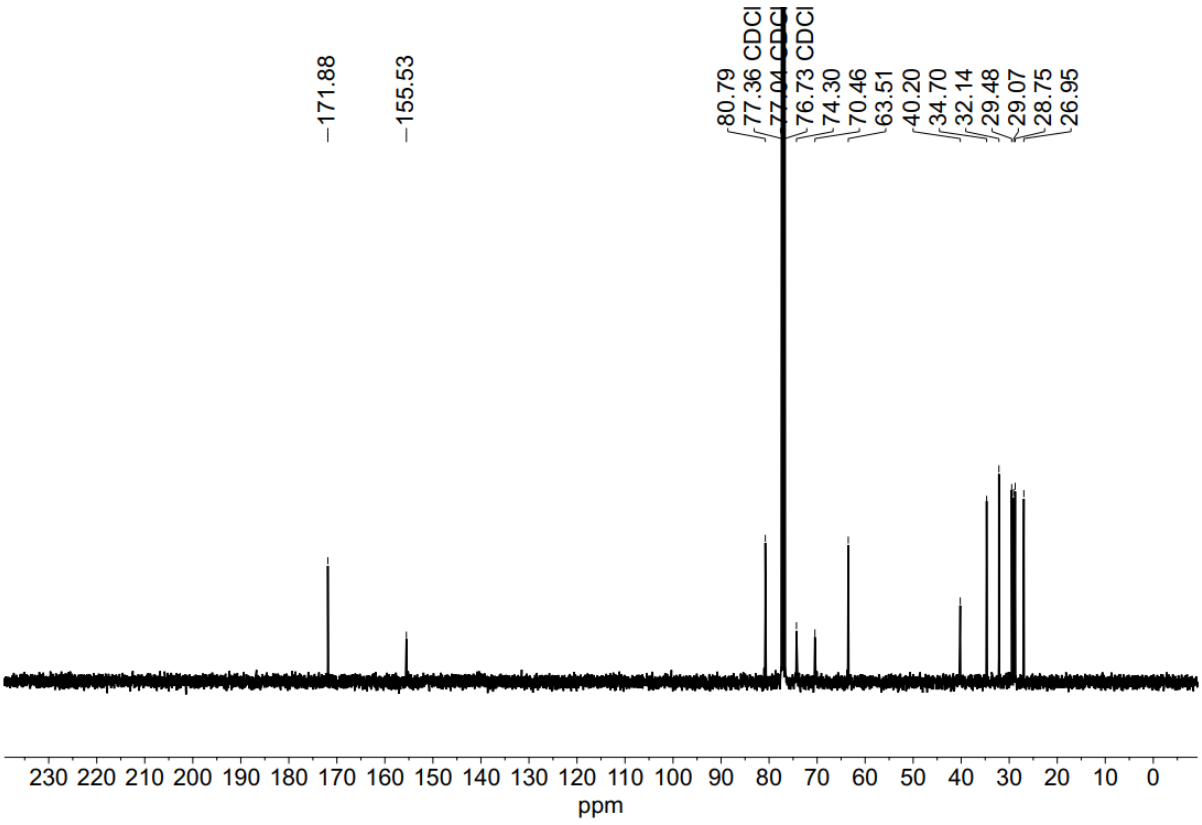

Figure 4.15 ^{13}C NMR spectrum of b-$IM_{80}IS_{20}$ (100.57 MHz, 298 K, $CDCl_3$)

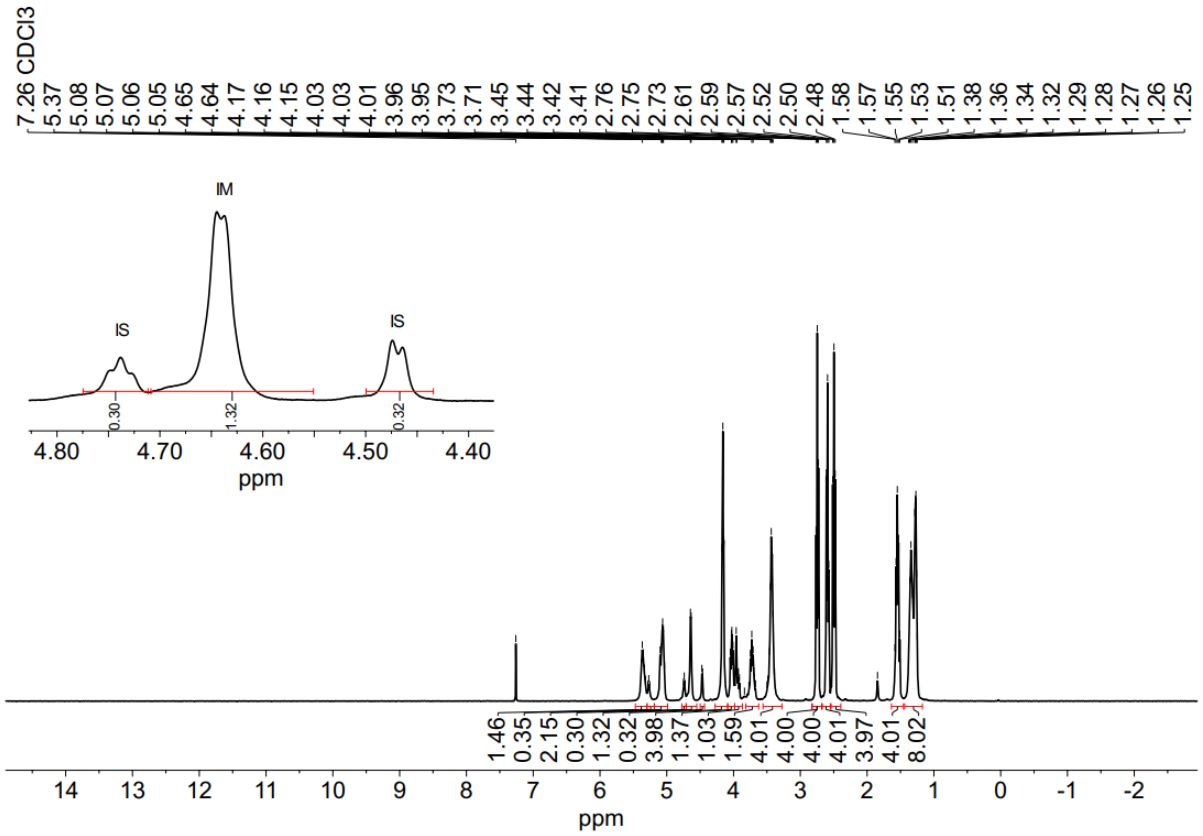

Figure 4.16 ^{1}H NMR spectrum of b-IM$_{70}$IS$_{30}$ (400 MHz, 298 K, $CDCl_3$)

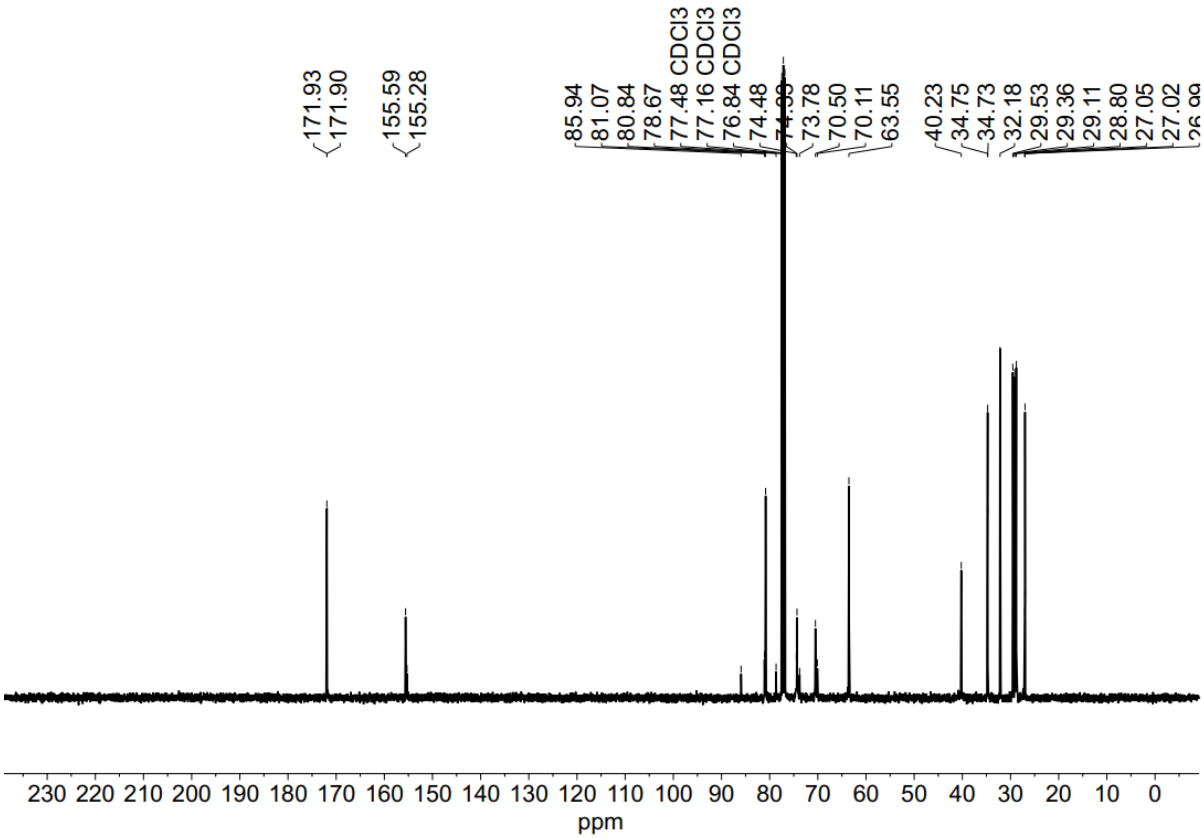

Figure 4.17 ^{13}C NMR spectrum of b-IM$_{70}$IS$_{30}$ (100.57 MHz, 298 K, $CDCl_3$)

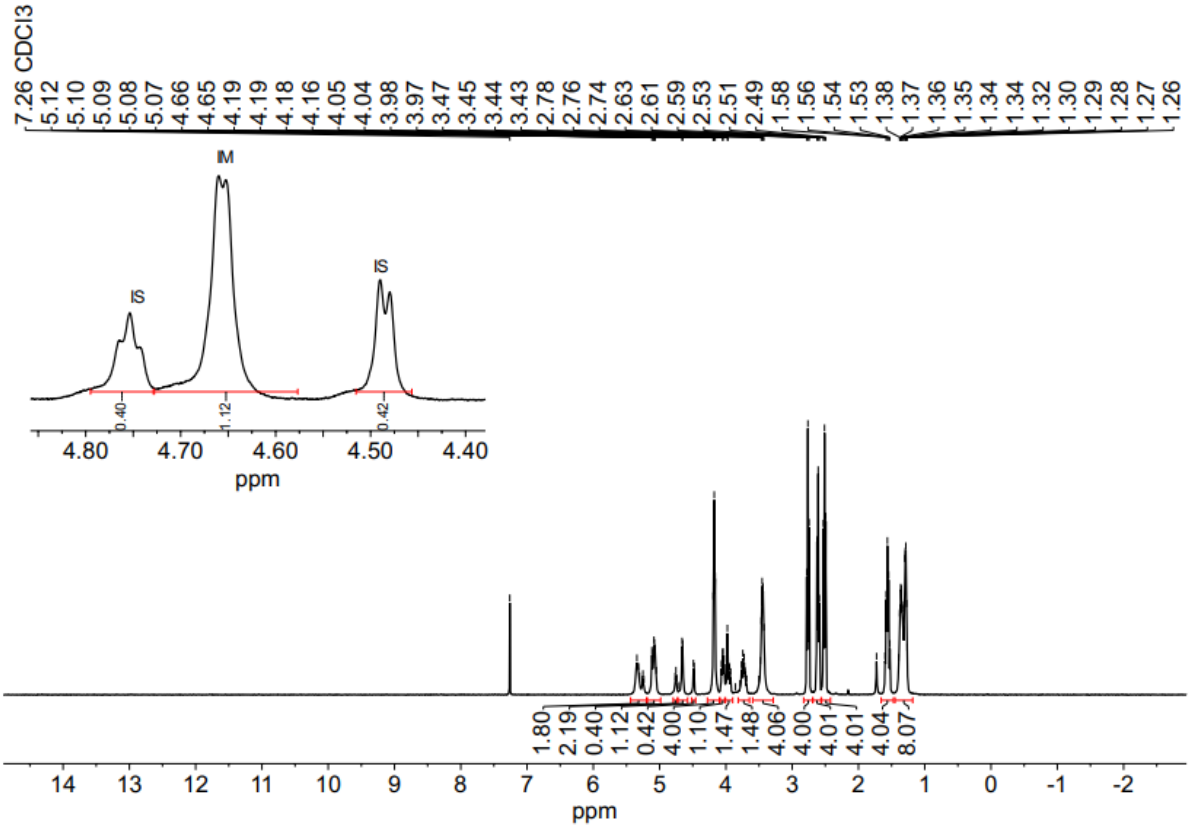

Figure 4.18 ^{1}H NMR spectrum of b-$IM_{60}IS_{40}$ (400 MHz, 298 K, $CDCl_3$)

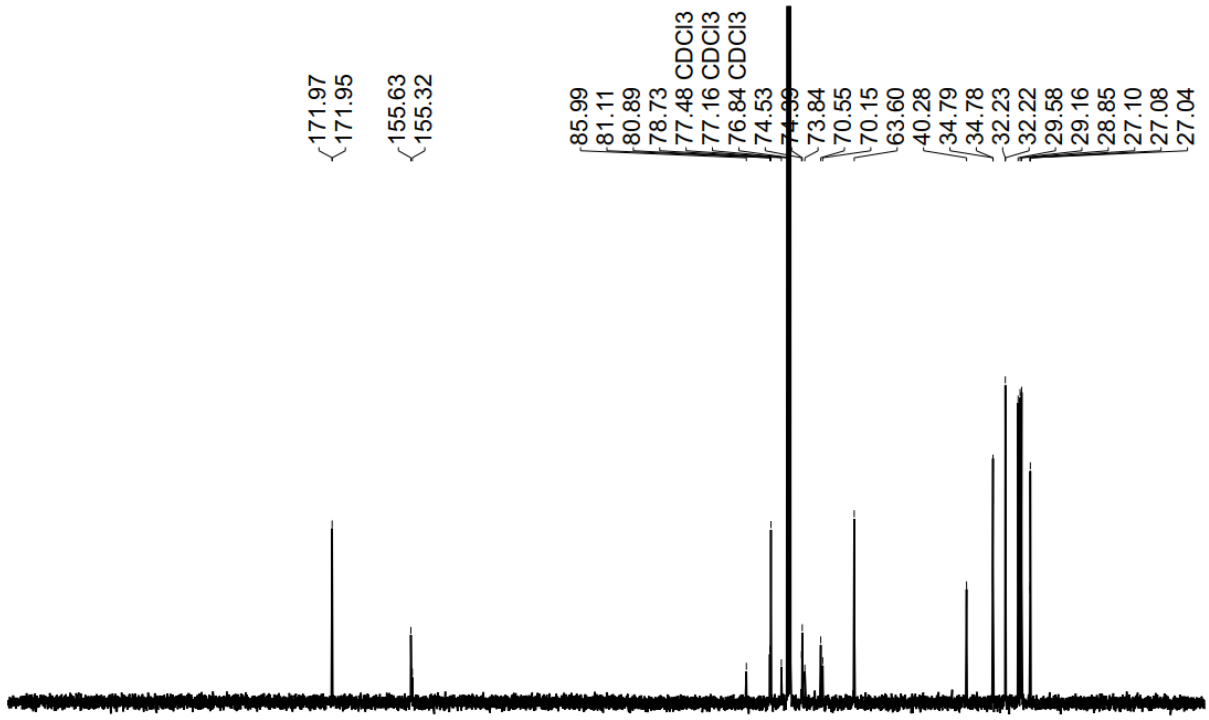

Figure 4.19 ^{13}C NMR spectrum of b-$IM_{60}IS_{40}$ (100.57 MHz, 298 K, $CDCl_3$)

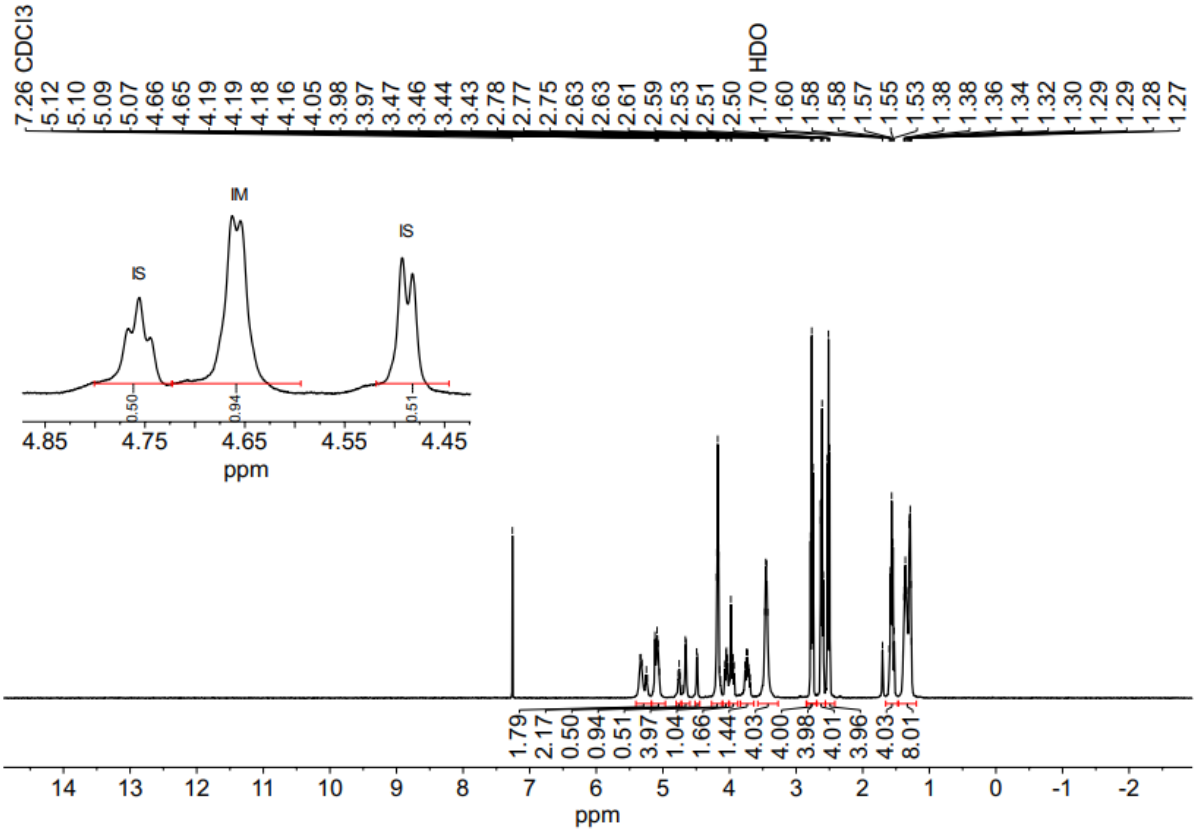

Figure 4.20 ^{1}H NMR spectrum of b-IM$_{50}$IS$_{50}$ (400 MHz, 298 K, $CDCl_3$)

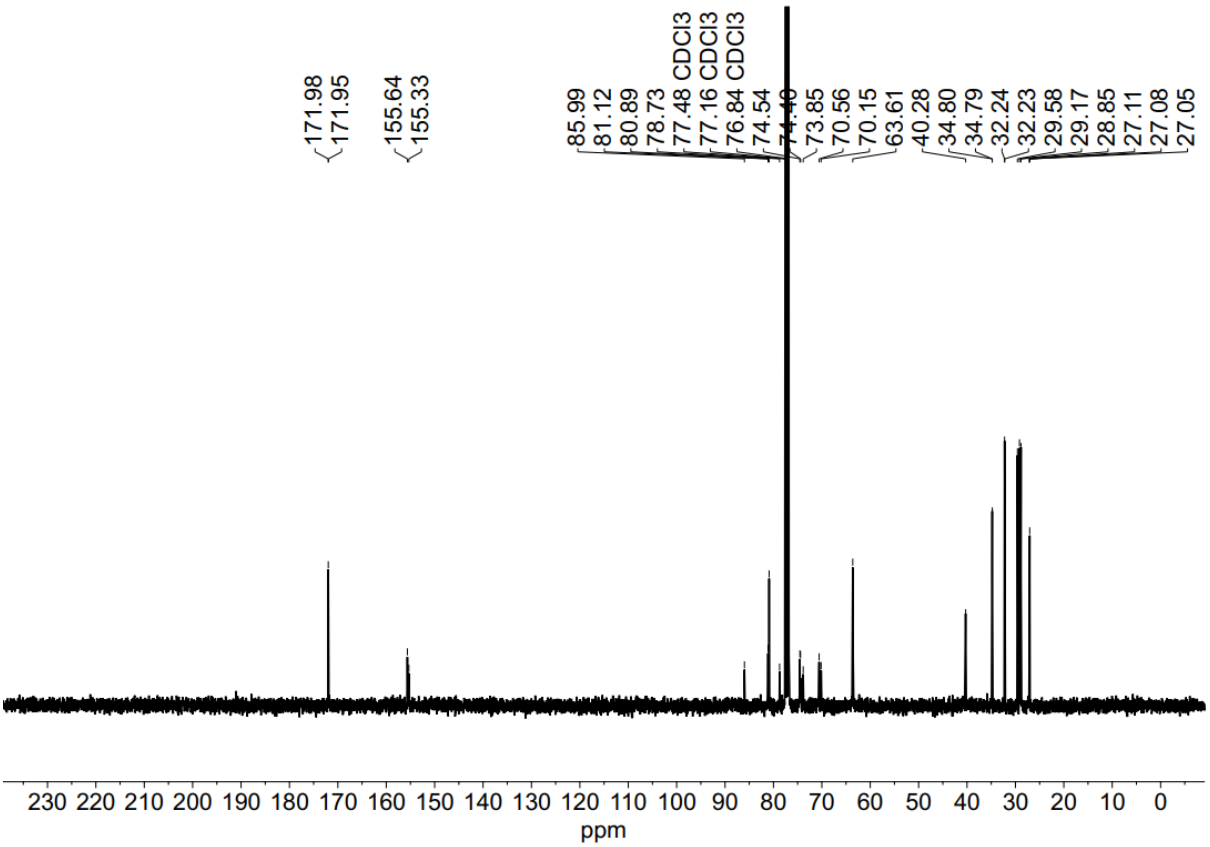

Figure 4.21 ^{13}C NMR spectrum of b-IM$_{50}$IS$_{50}$ (100.57 MHz, 298 K, $CDCl_3$)

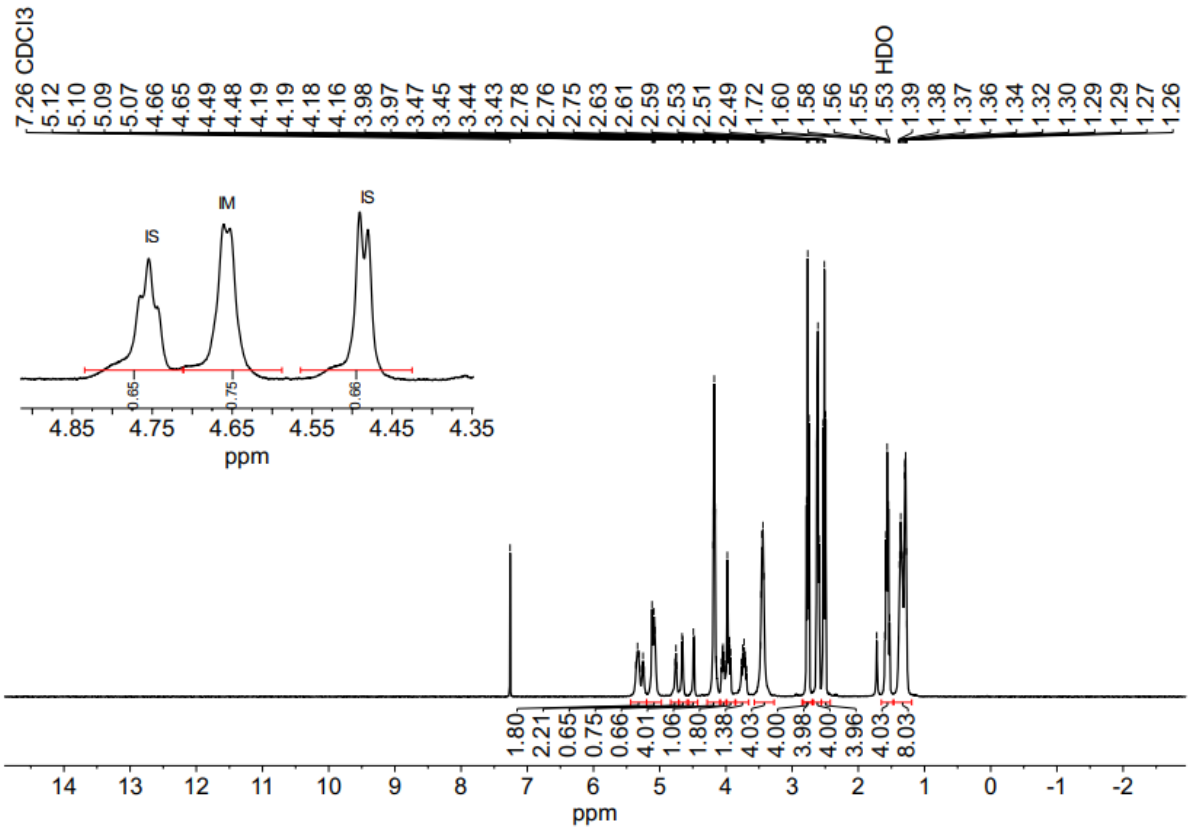

Figure 4.22 ^{1}H NMR spectrum of b-IM$_{40}$IS$_{60}$ (400 MHz, 298 K, $CDCl_3$)

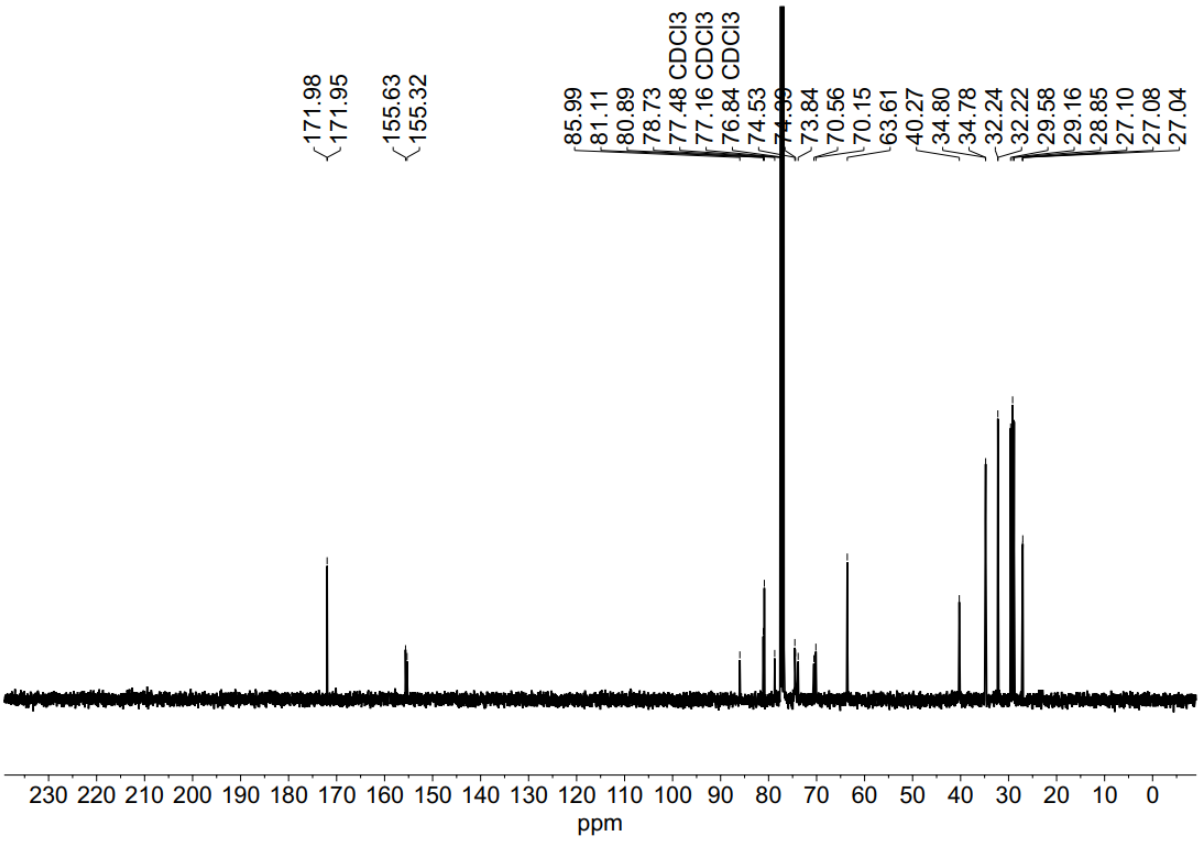

Figure 4.23 ^{13}C NMR spectrum of b-IM$_{40}$IS$_{60}$ (100.57 MHz, 298 K, $CDCl_3$)

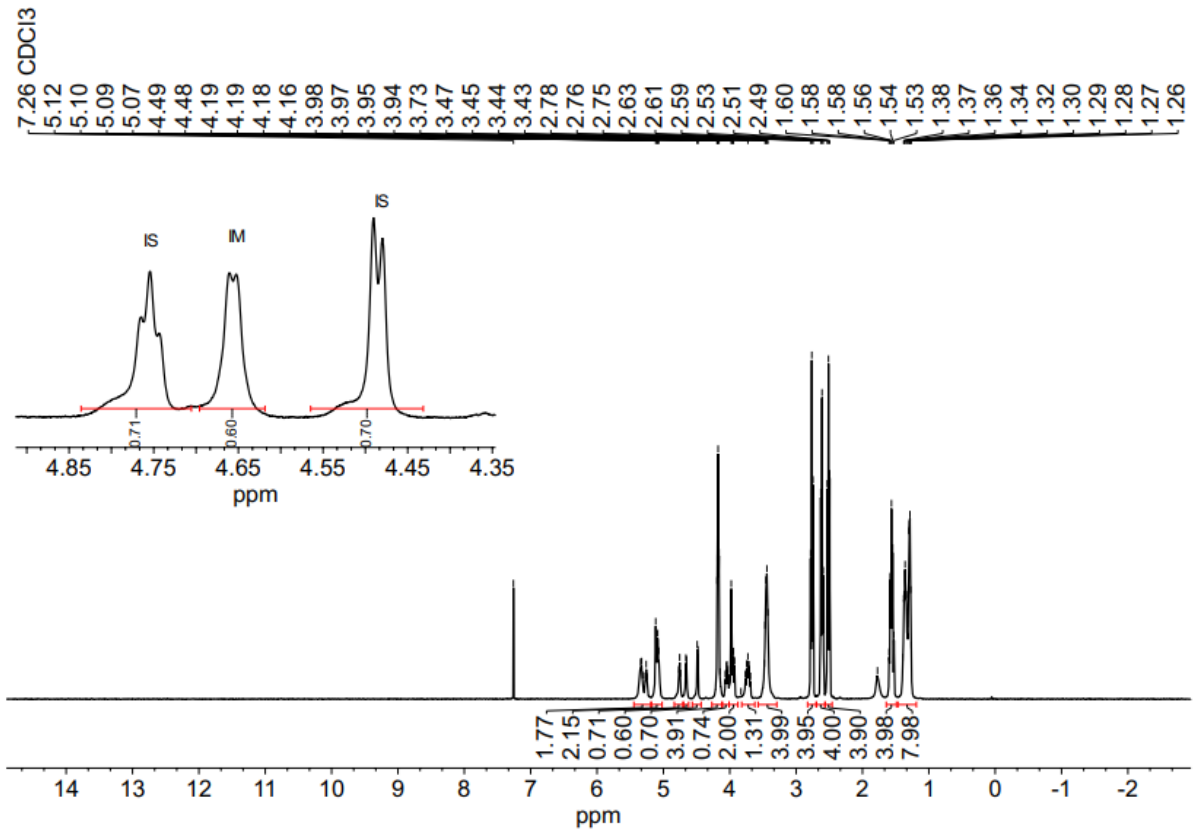

Figure 4.24 ^{1}H NMR spectrum of b-IM$_{30}$IS$_{70}$ (400 MHz, 298 K, $CDCl_3$)

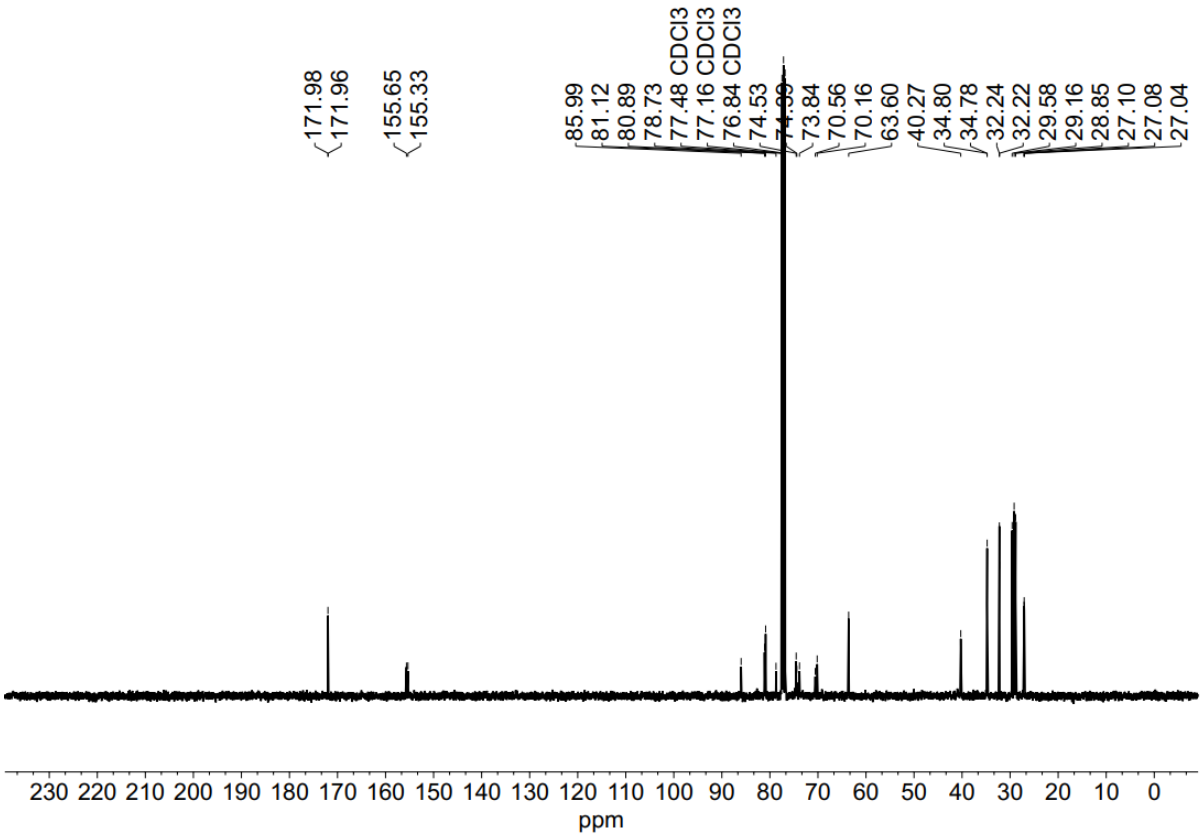

Figure 4.25 ^{13}C NMR spectrum of b-IM$_{30}$IS$_{70}$ (100.57 MHz, 298 K, $CDCl_3$)

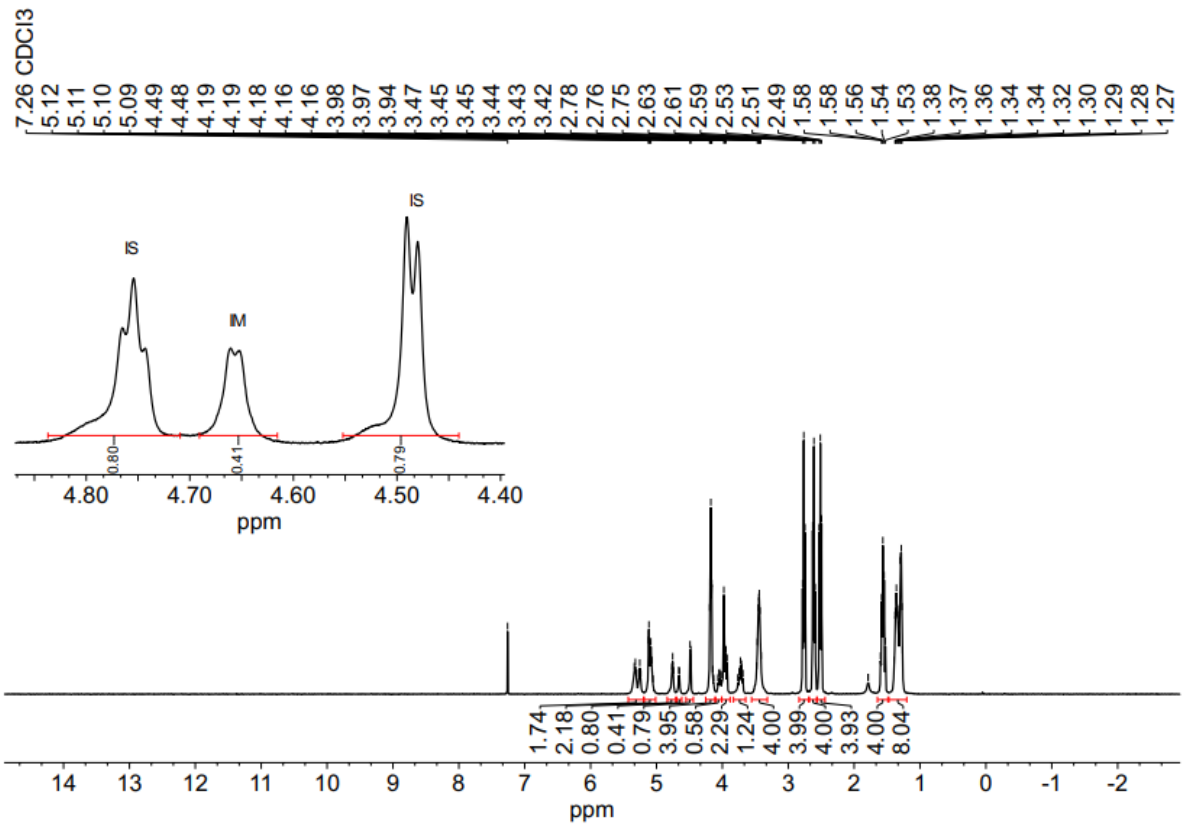

Figure 4.26 ^{1}H NMR spectrum of b-$IM_{20}IS_{80}$ (400 MHz, 298 K, $CDCl_3$)

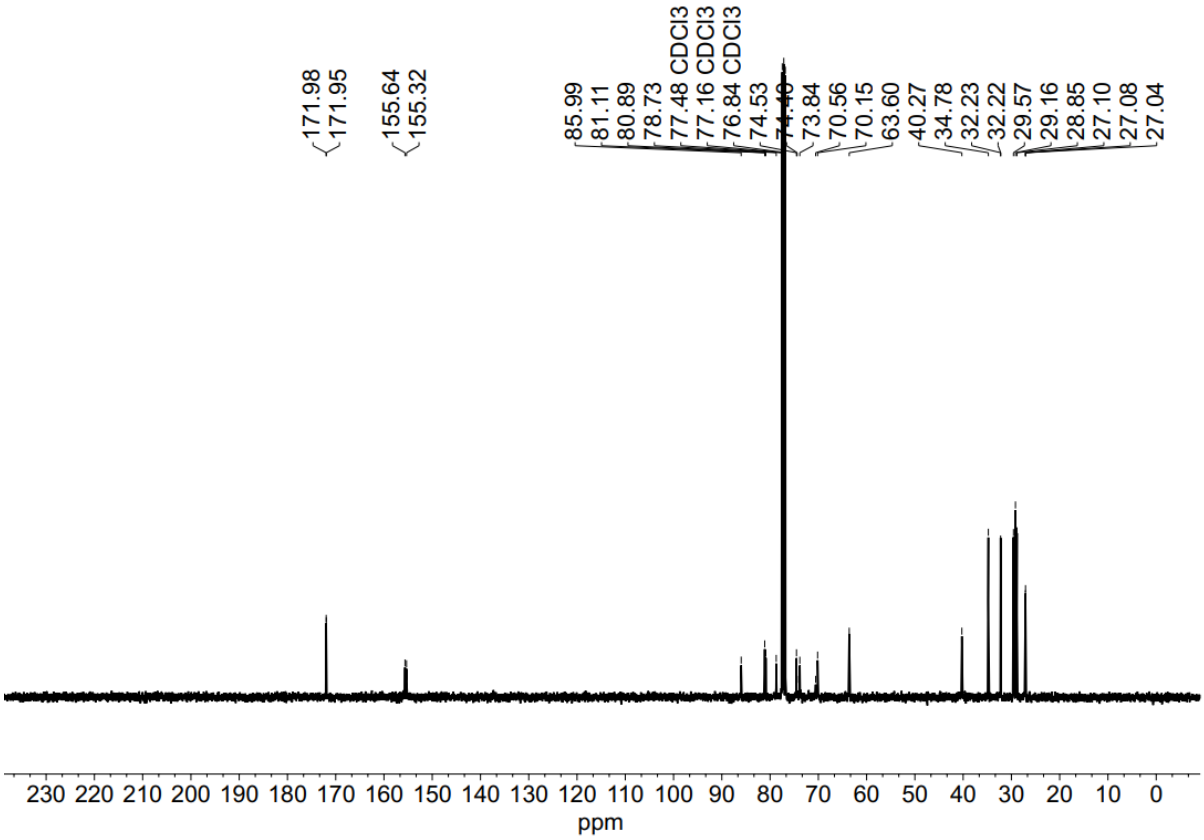

Figure 4.27 ^{13}C NMR spectrum of b-$IM_{20}IS_{80}$ (100.57 MHz, 298 K, $CDCl_3$)

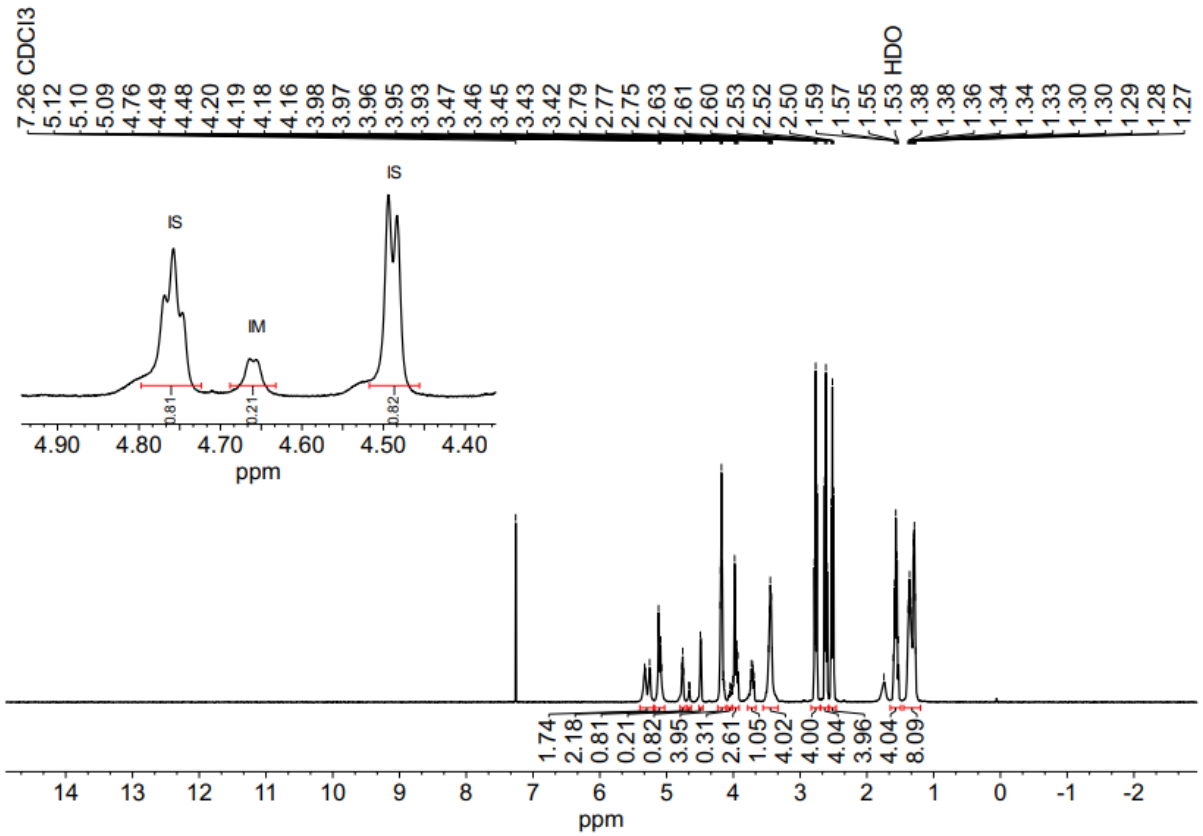

Figure 4.28 ^{1}H NMR spectrum of b-$IM_{10}IS_{90}$ (400 MHz, 298 K, $CDCl_3$)

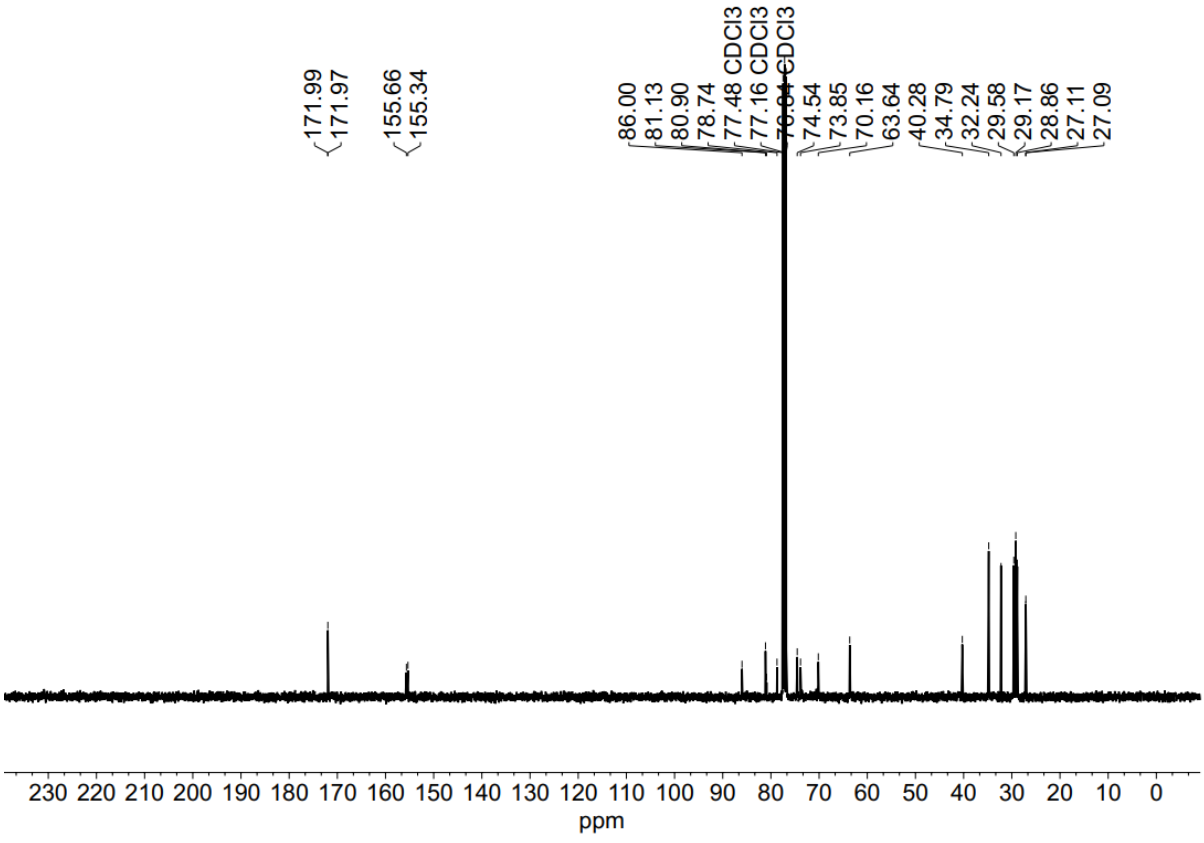

Figure 4.29 ^{13}C NMR spectrum of b-$IM_{10}IS_{90}$ (100.57 MHz, 298 K, $CDCl_3$)

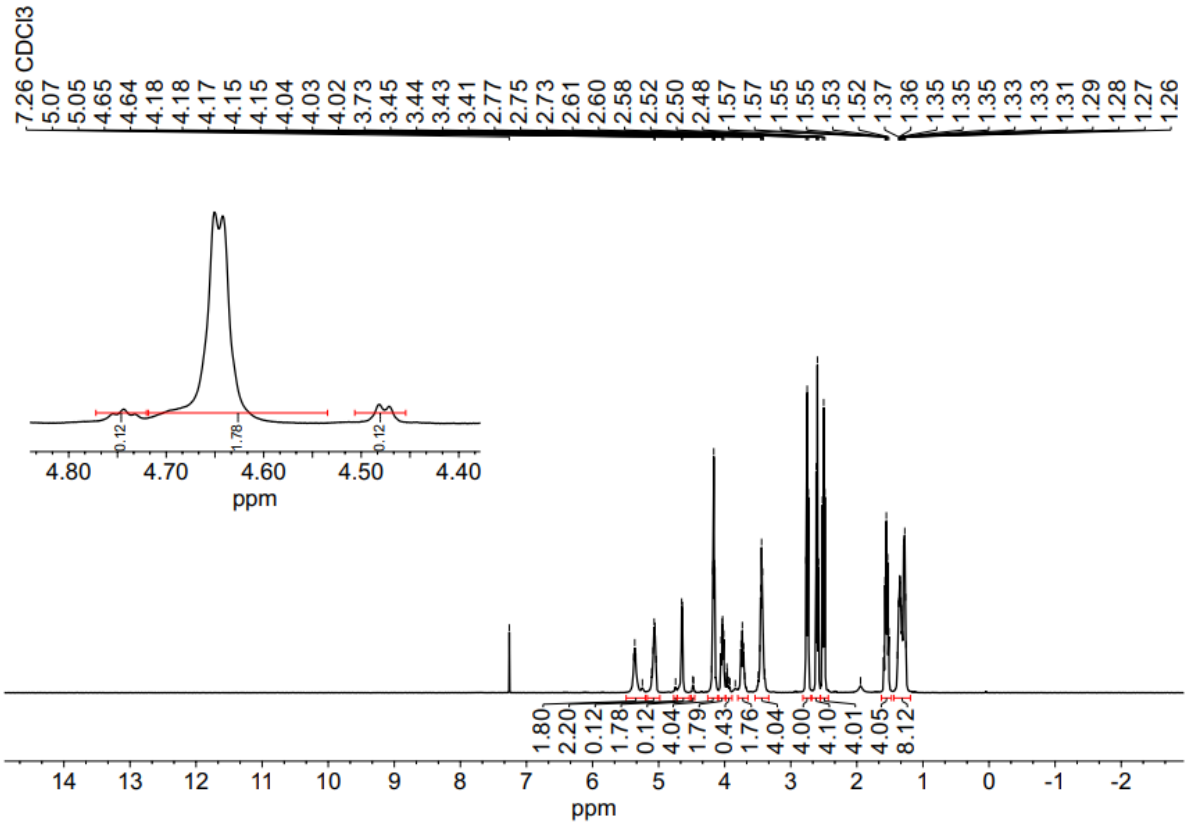

Figure 4.30 ^{1}H NMR spectrum of co-IM$_{90}$IS$_{10}$ (400 MHz, 298 K, $CDCl_3$)

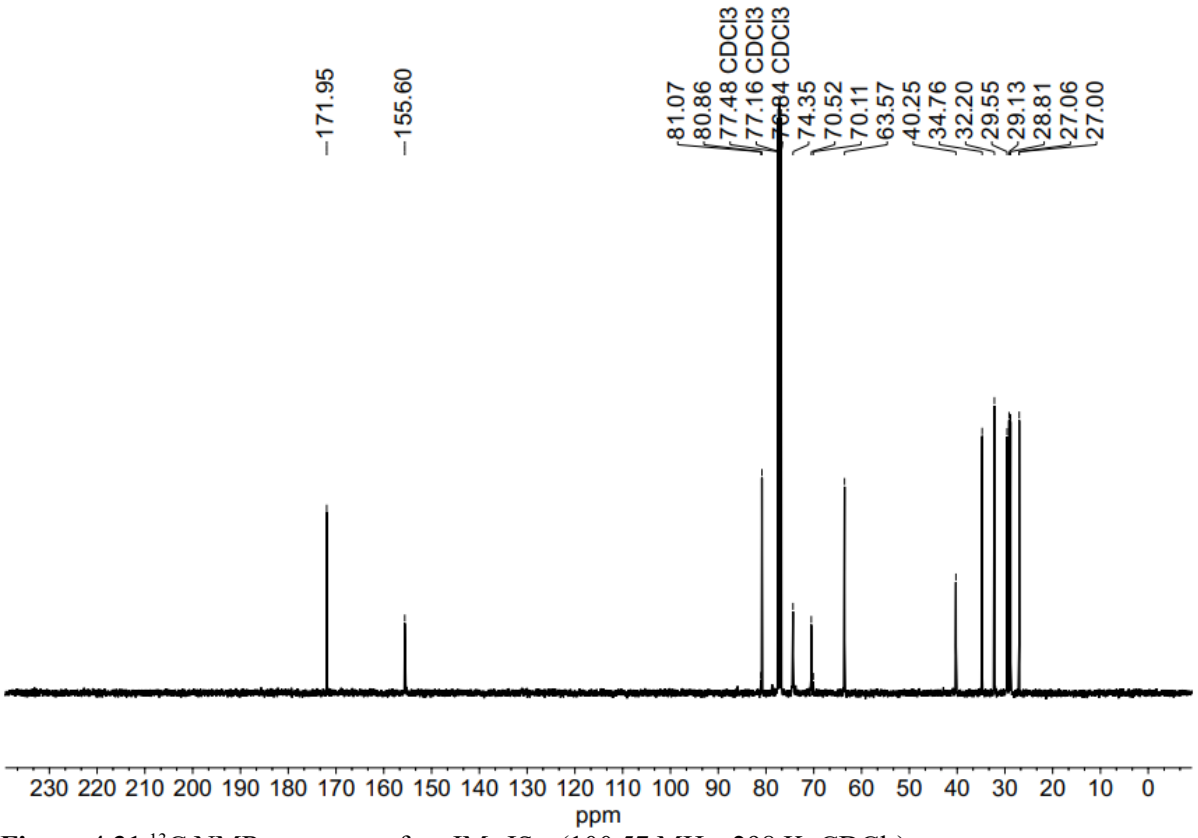

Figure 4.31 ^{13}C NMR spectrum of co-IM$_{90}$IS$_{10}$ (100.57 MHz, 298 K, $CDCl_3$)

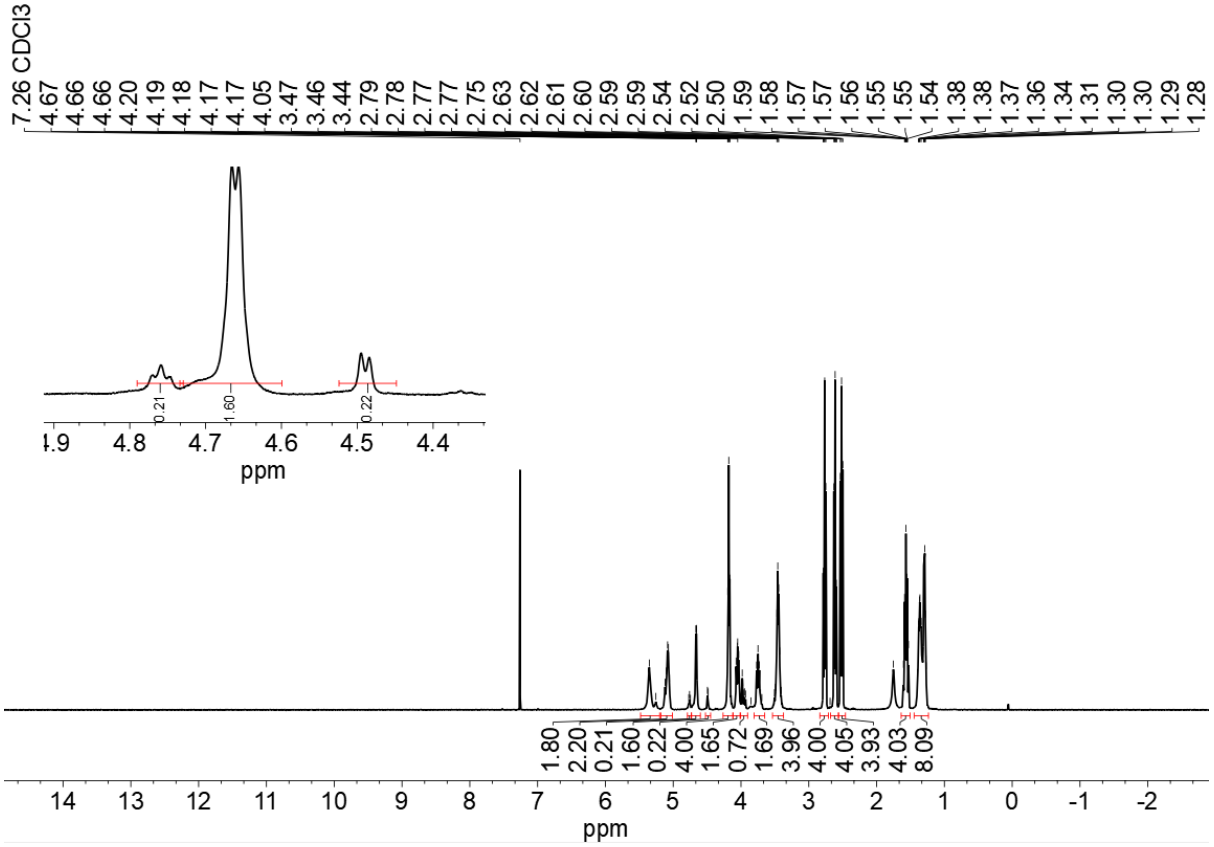

Figure 4.32 ^{1}H NMR spectrum of co-$IM_{80}IS_{20}$ (400 MHz, 298 K, $CDCl_3$)

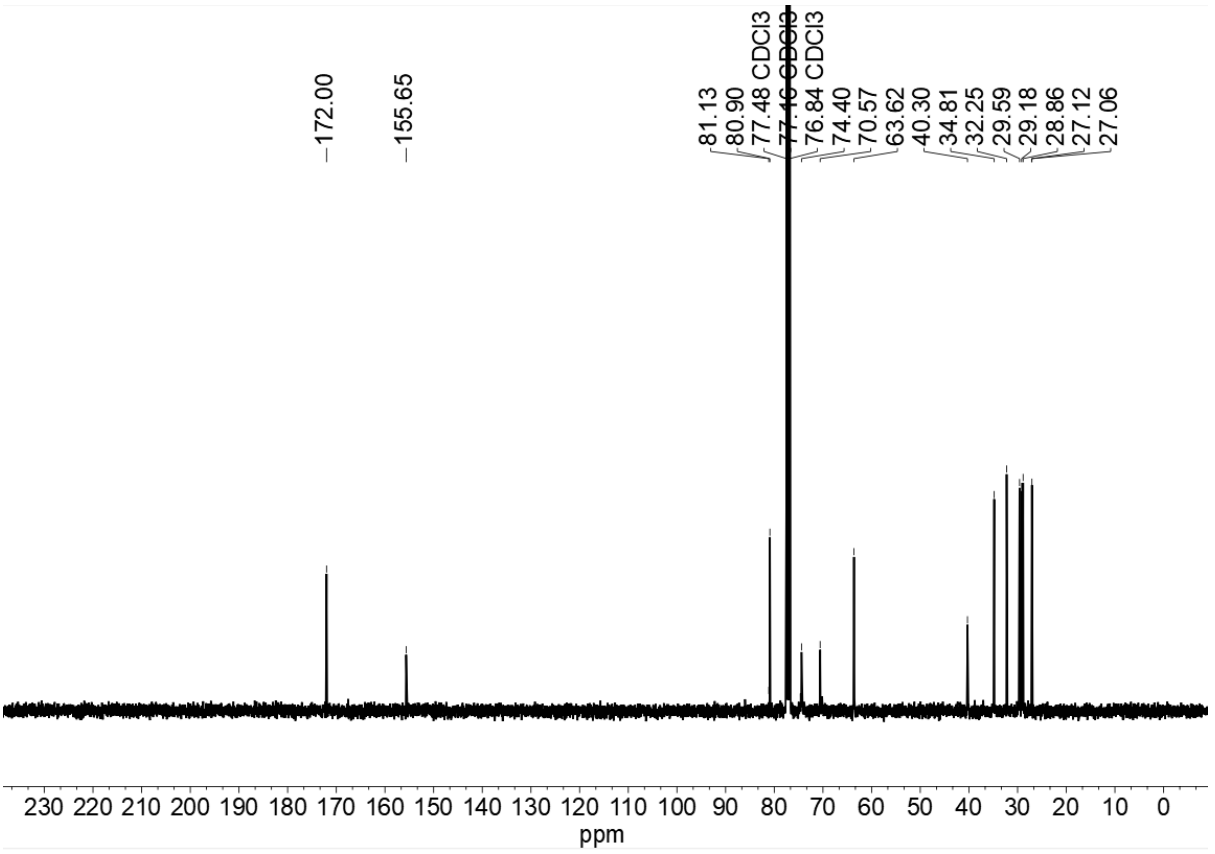

Figure 4.33 ^{13}C NMR spectrum of co-$IM_{80}IS_{20}$ (100.57 MHz, 298 K, $CDCl_3$)

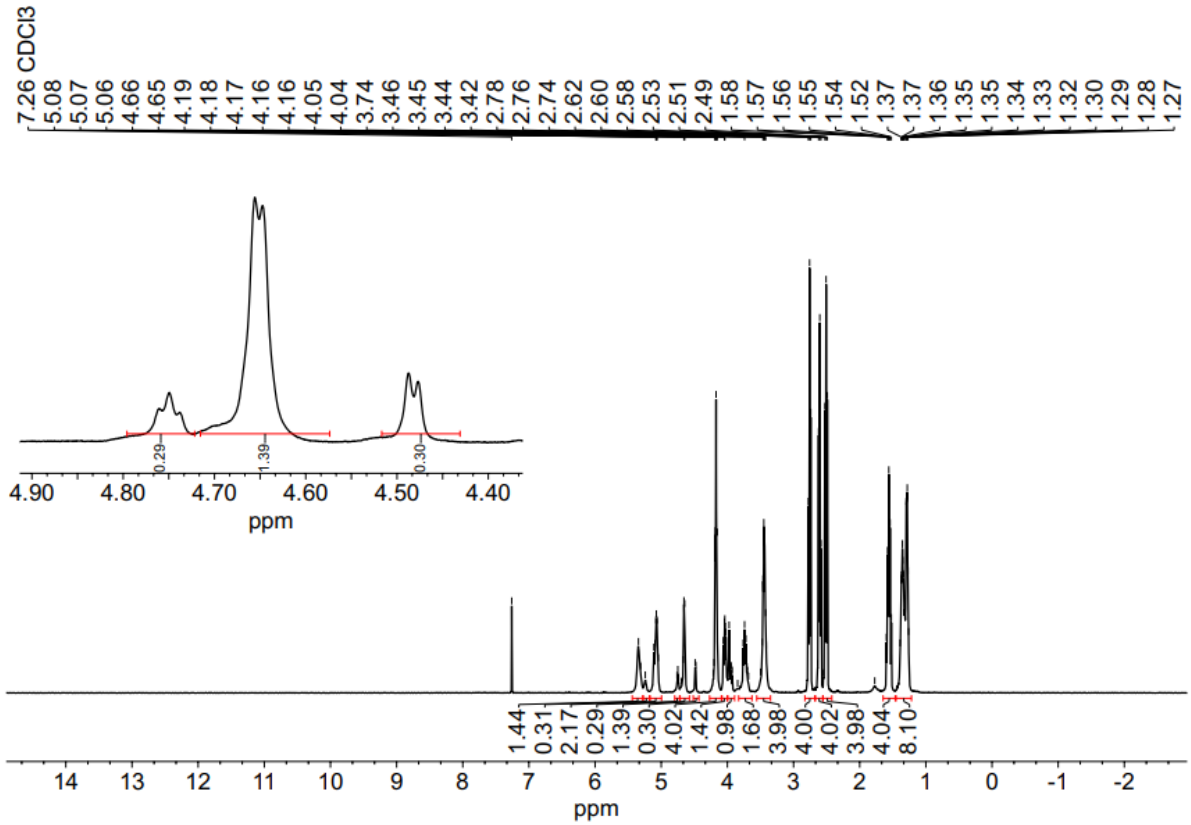

Figure 4.34 ^{1}H NMR spectrum of co-$IM_{70}IS_{30}$ (400 MHz, 298 K, $CDCl_3$)

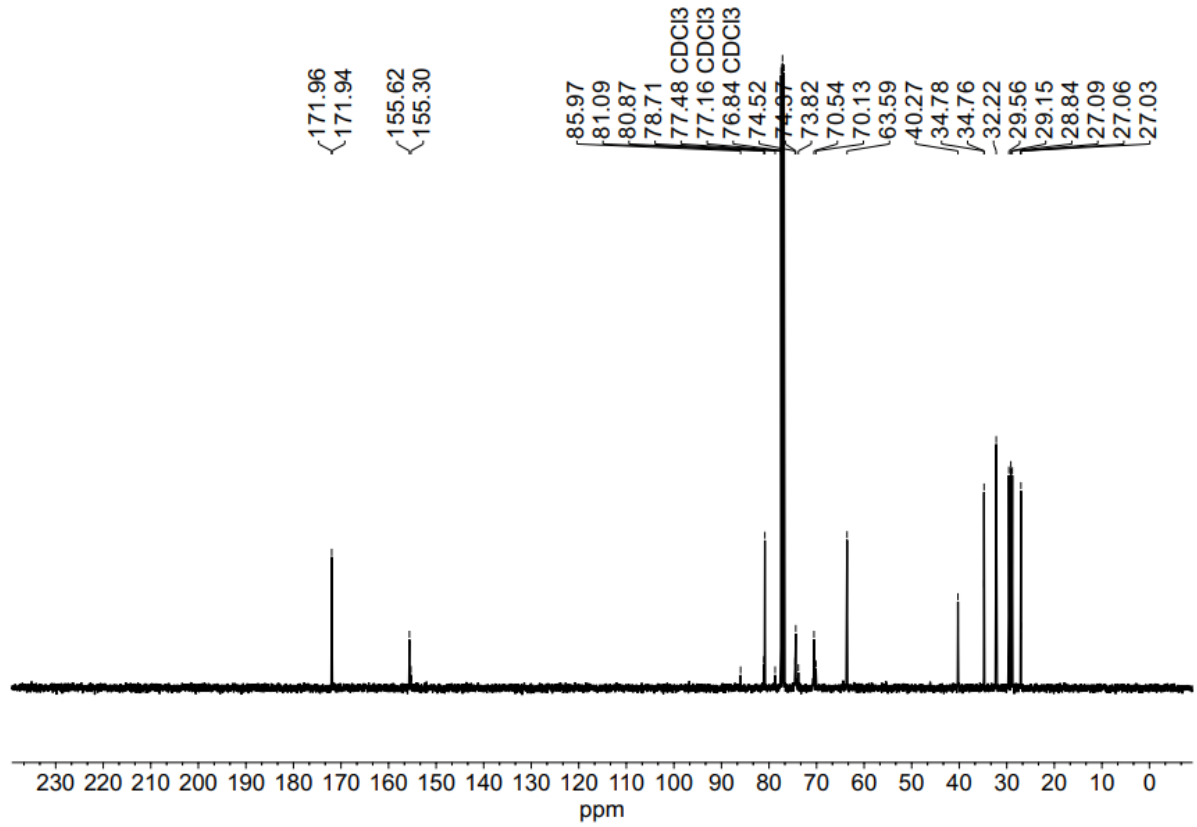

Figure 4.35 ^{13}C NMR spectrum of co-$IM_{70}IS_{30}$ (100.57 MHz, 298 K, $CDCl_3$)

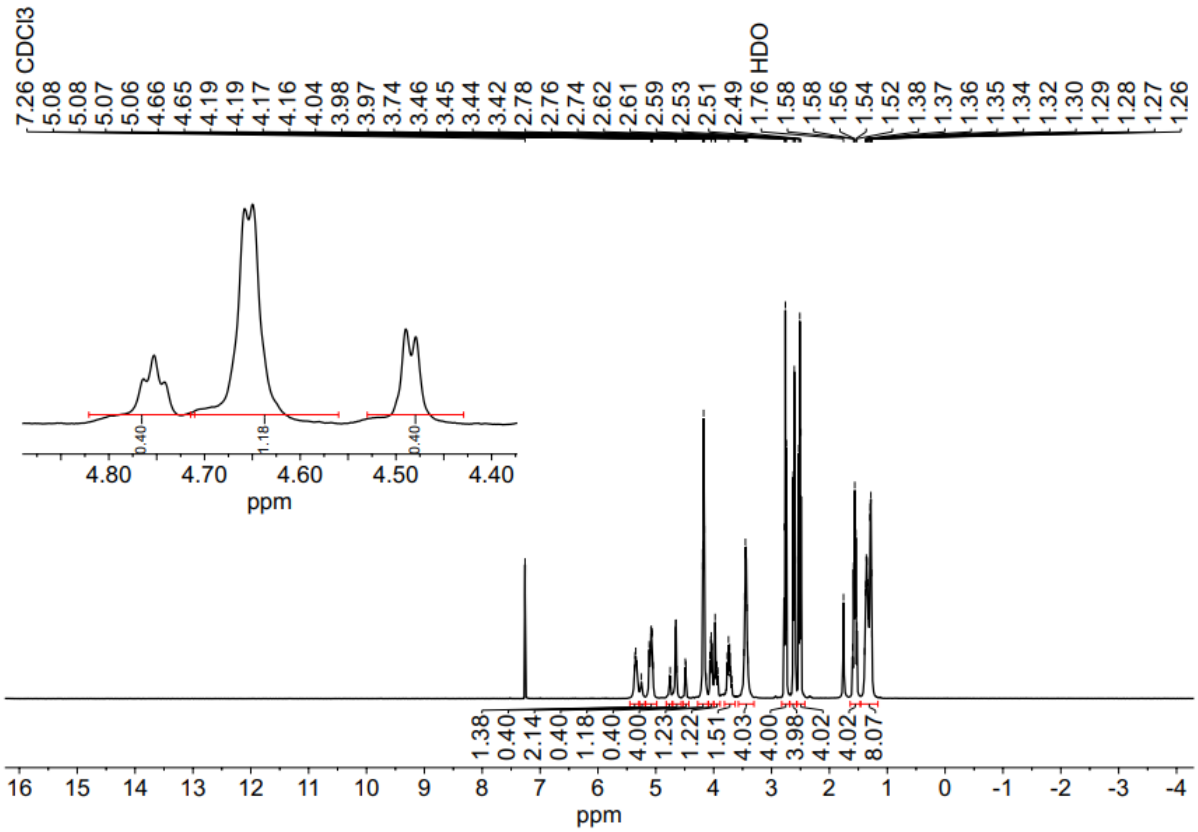

Figure 4.36 ^{1}H NMR spectrum of co-$IM_{60}IS_{40}$ (400 MHz, 298 K, $CDCl_3$)

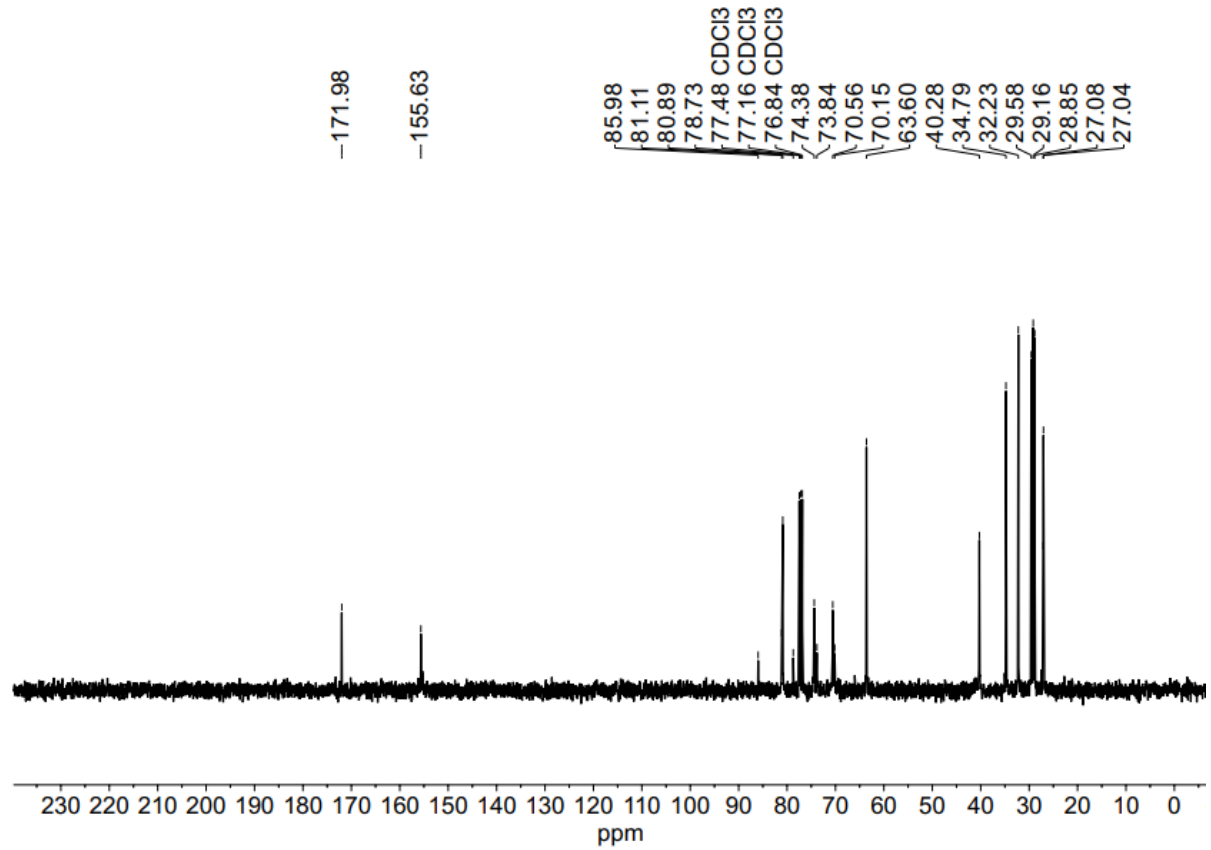

Figure 4.37 ^{13}C NMR spectrum of co-$IM_{60}IS_{40}$ (100.57 MHz, 298 K, $CDCl_3$)

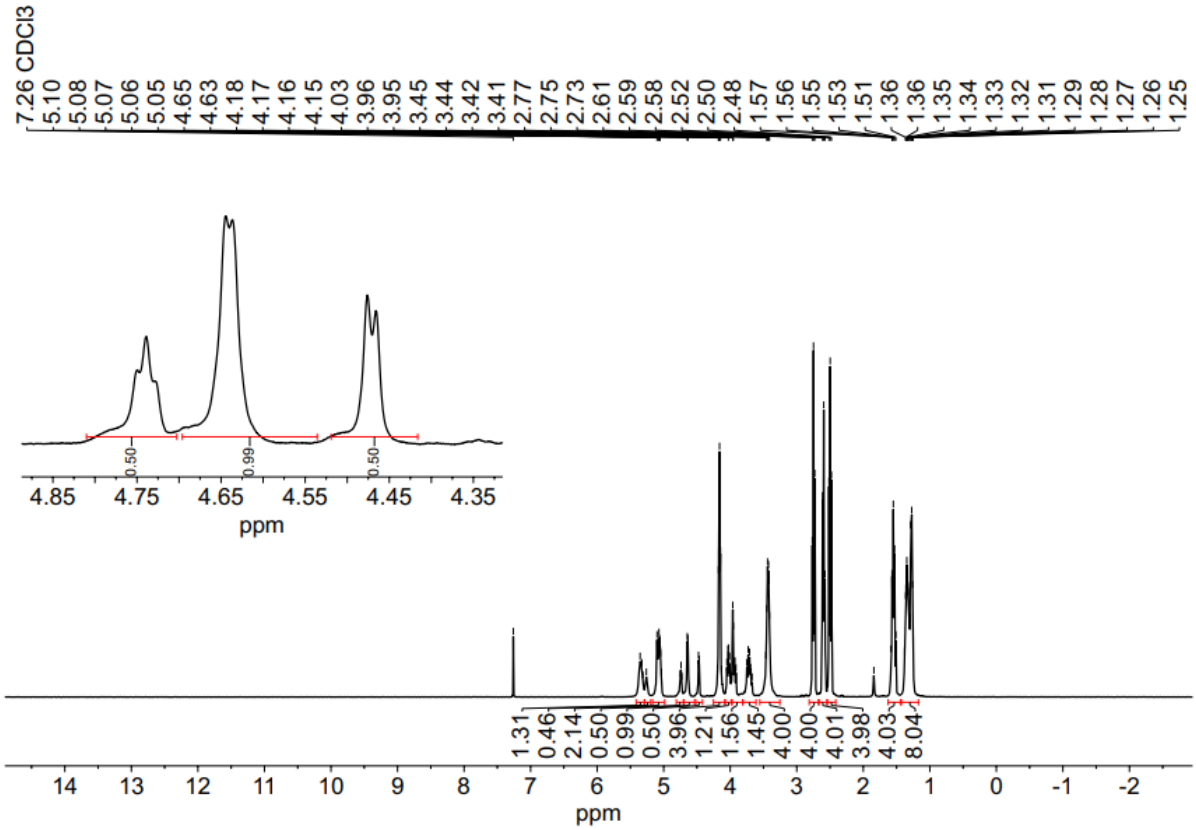

Figure 4.38 ^{1}H NMR spectrum of co-$IM_{50}IS_{50}$ (400 MHz, 298 K, $CDCl_3$)

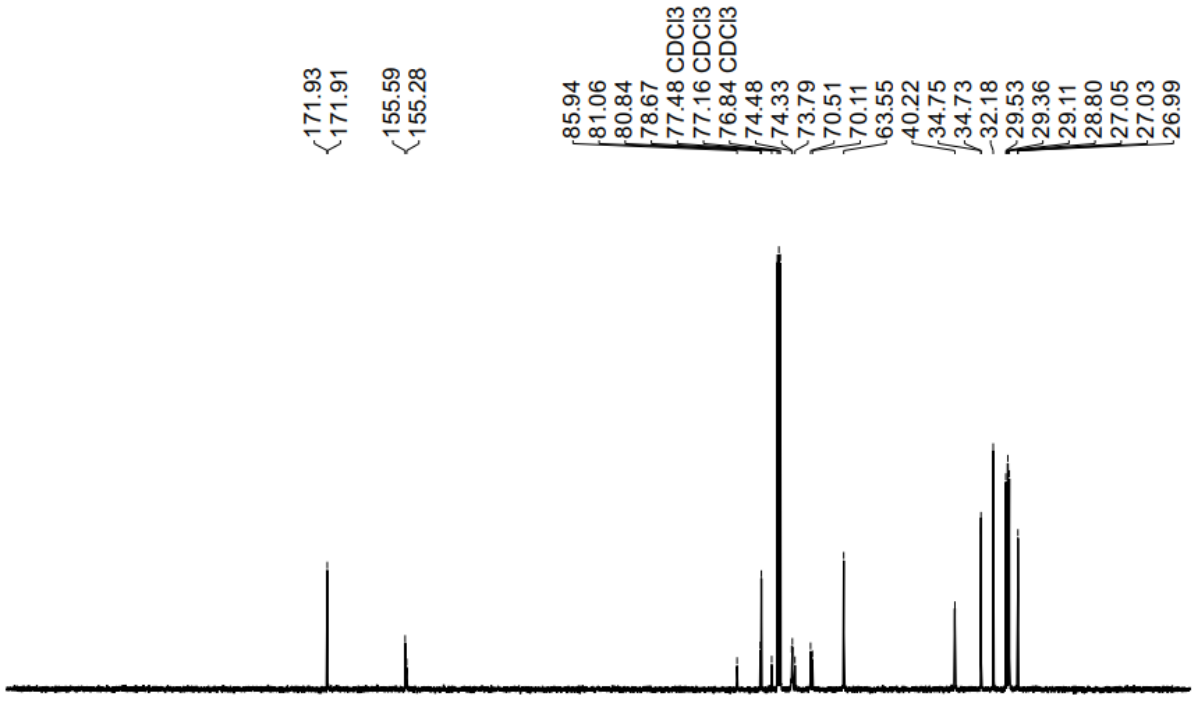

Figure 4.39 ^{13}C NMR spectrum of co-$IM_{50}IS_{50}$ (100.57 MHz, 298 K, $CDCl_3$)

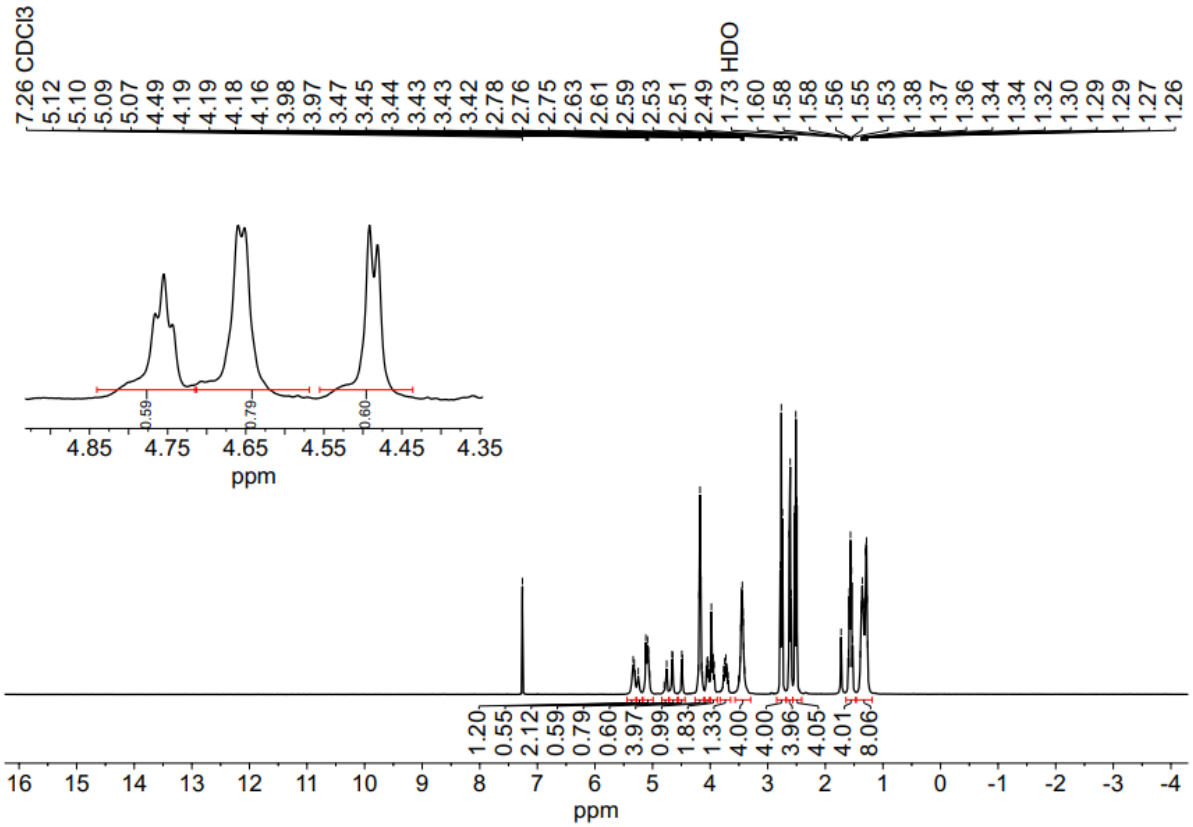

Figure 4.40 ^{1}H NMR spectrum of co-$IM_{40}IS_{60}$ (400 MHz, 298 K, $CDCl_3$)

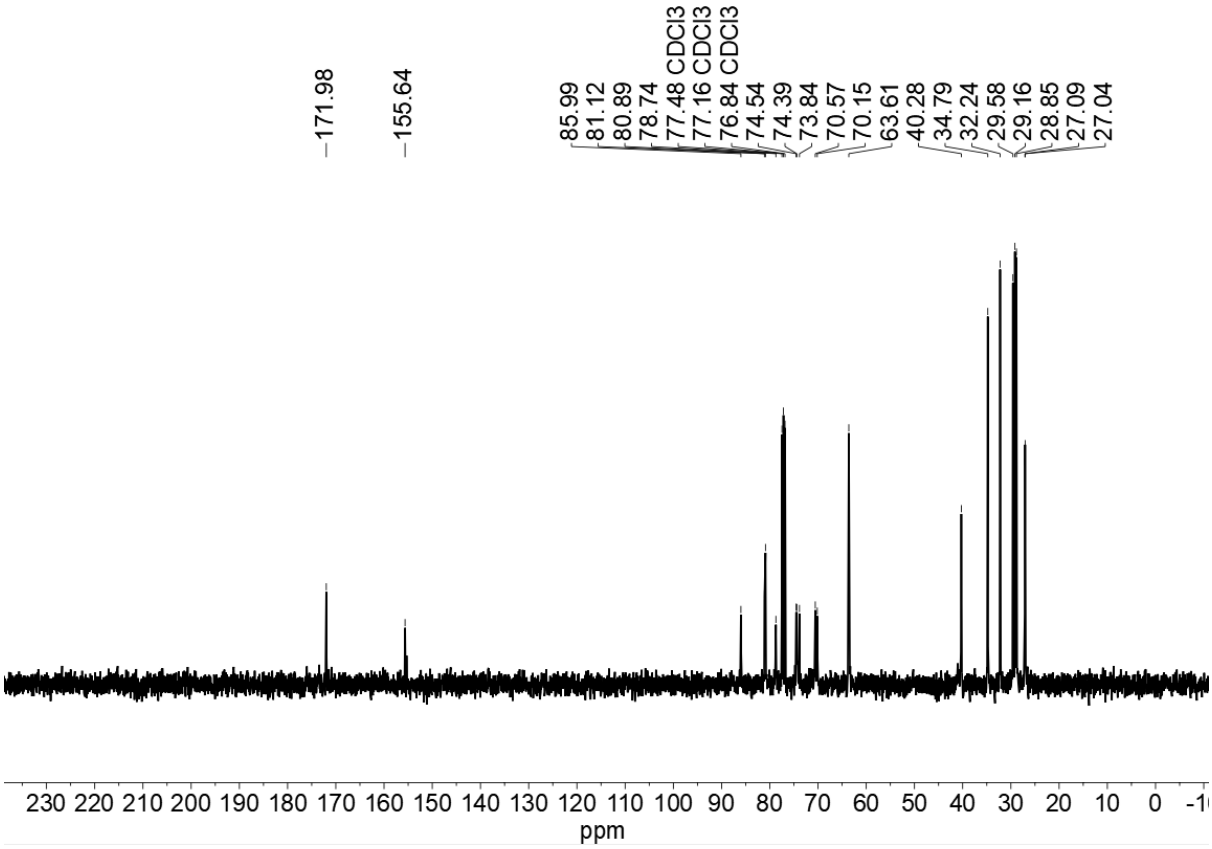

Figure 4.41 ^{13}C NMR spectrum of co-$IM_{40}IS_{60}$ (100.57 MHz, 298 K, $CDCl_3$)

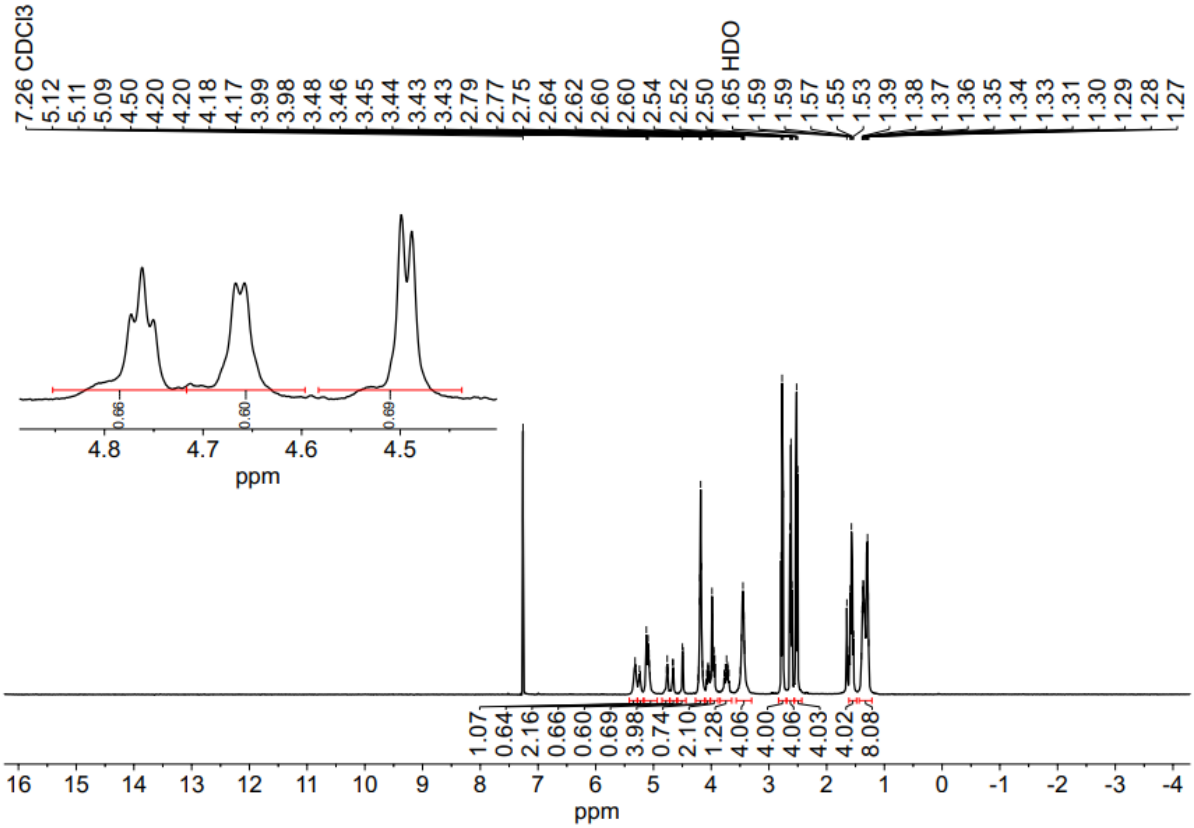

Figure 4.42 ^{1}H NMR spectrum of co-$IM_{30}IS_{70}$ (400 MHz, 298 K, $CDCl_3$)

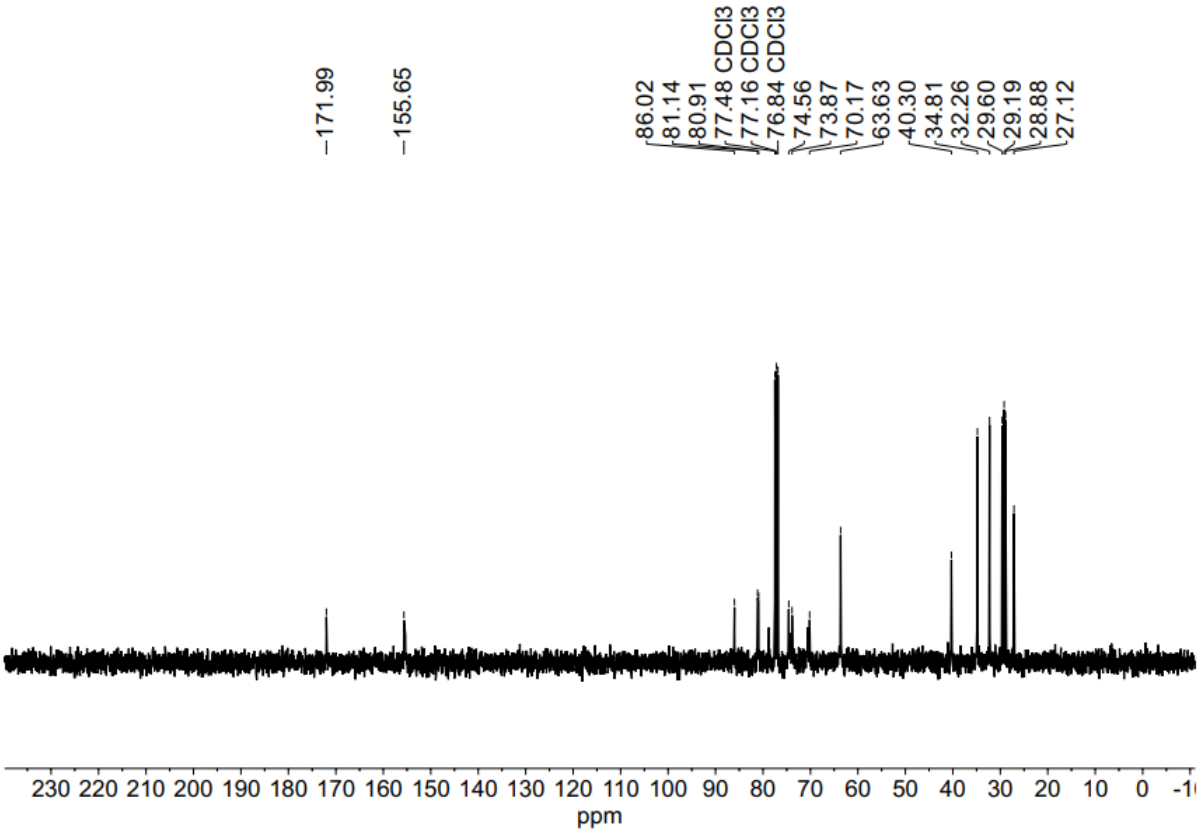

Figure 4.43 ^{13}C NMR spectrum of co-$IM_{30}IS_{70}$ (100.57 MHz, 298 K, $CDCl_3$)

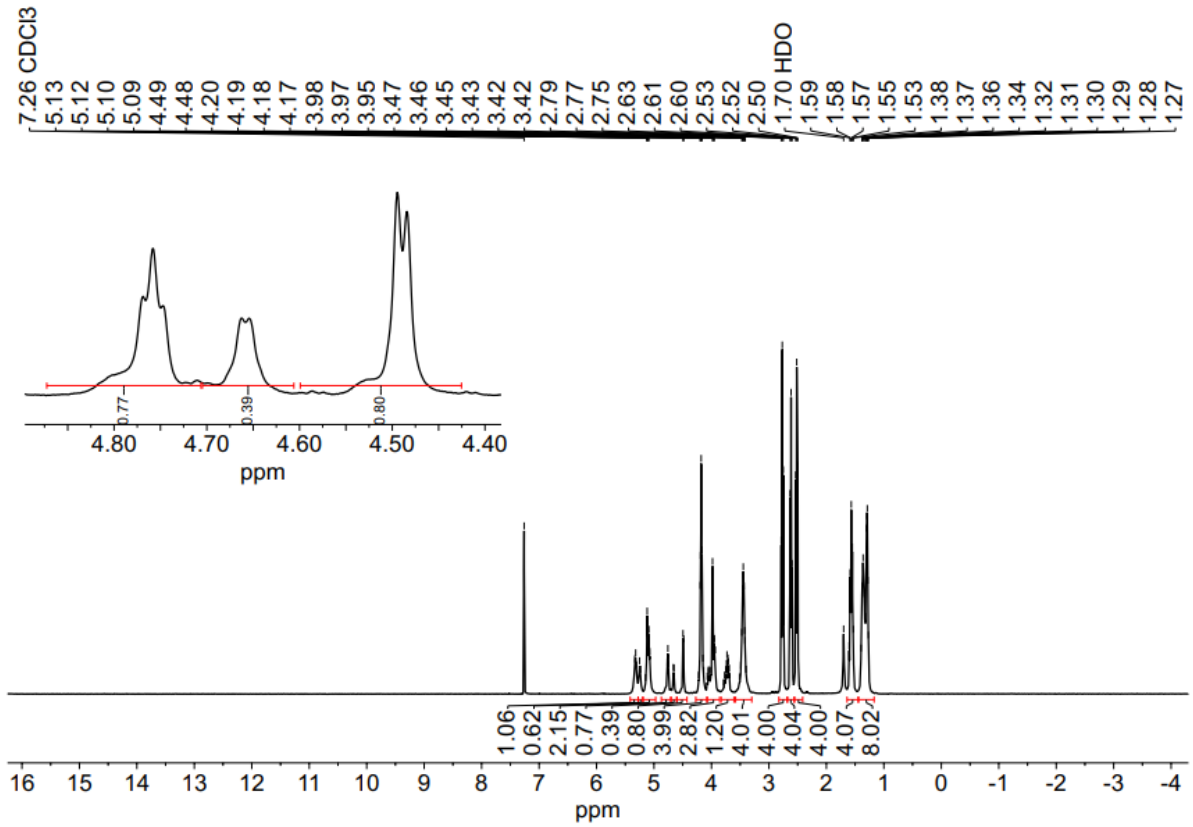

Figure 4.44 ^{1}H NMR spectrum of co-$IM_{20}IS_{80}$ (400 MHz, 298 K, $CDCl_3$)

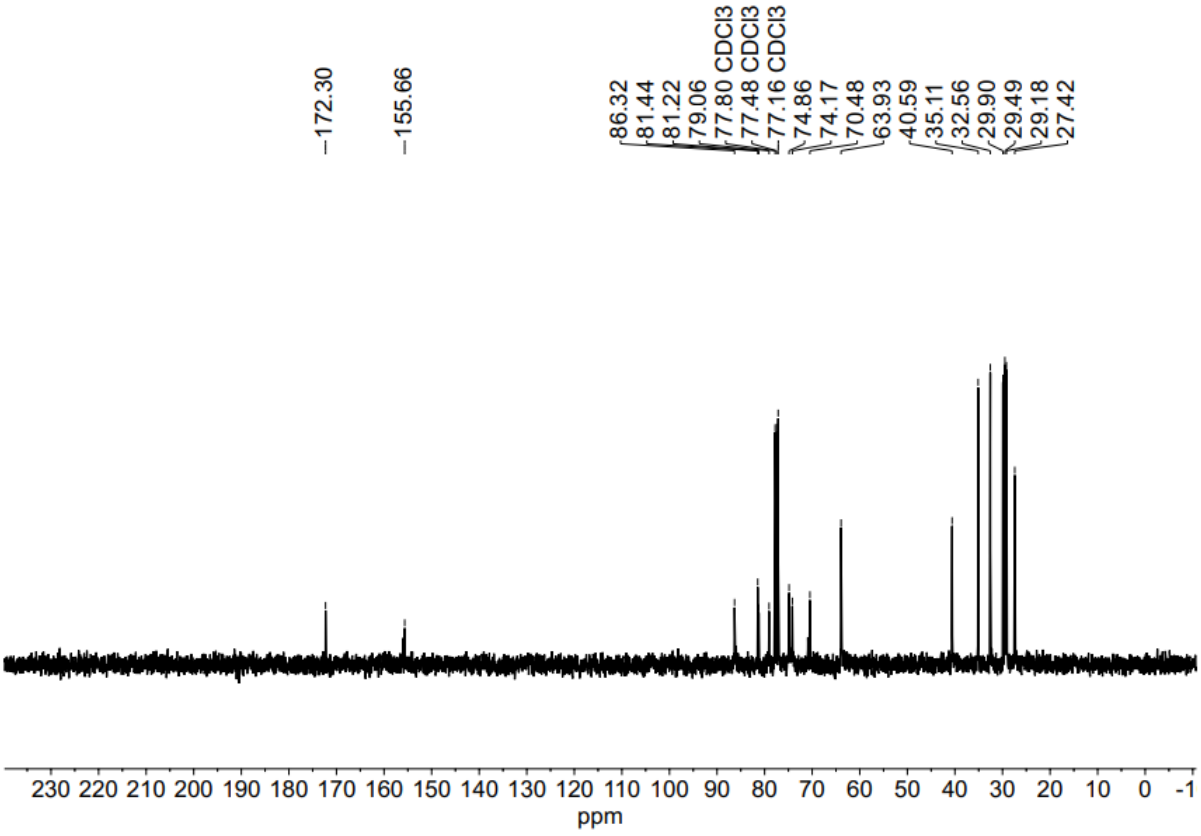

Figure 4.45 ^{13}C NMR spectrum of co-$IM_{20}IS_{80}$ (100.57 MHz, 298 K, $CDCl_3$)

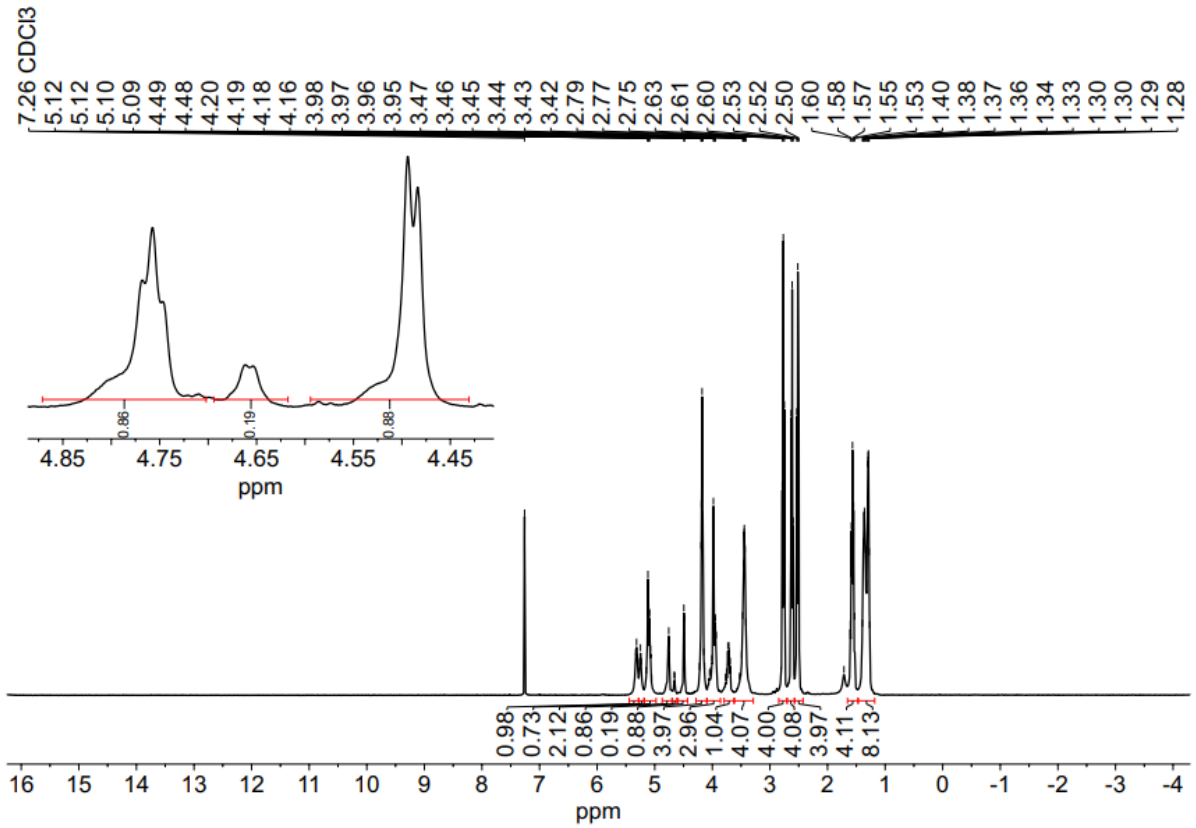

Figure 4.46 ^{1}H NMR spectrum of co-$IM_{10}IS_{90}$ (400 MHz, 298 K, $CDCl_3$)

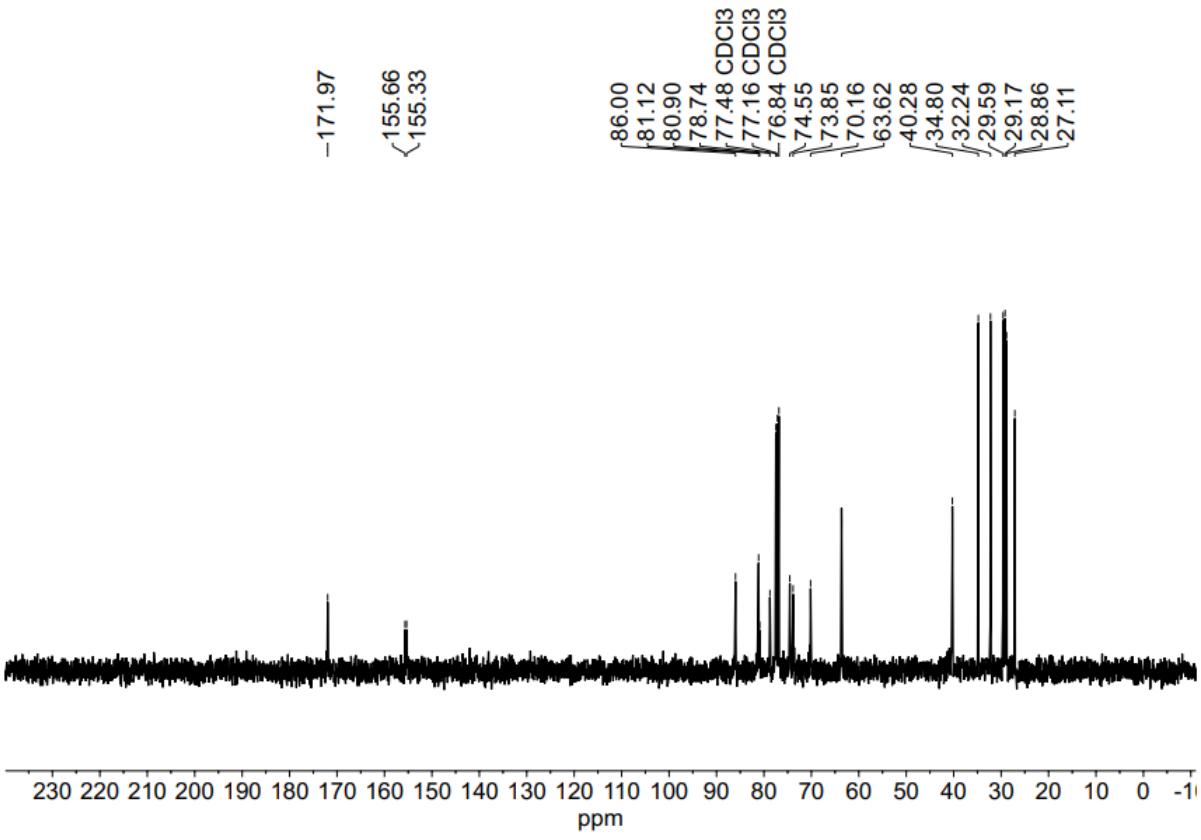

Figure 4.47 ^{13}C NMR spectrum of co-$IM_{10}IS_{90}$ (100.57 MHz, 298 K, $CDCl_3$)

DSC thermograms of homopolymers

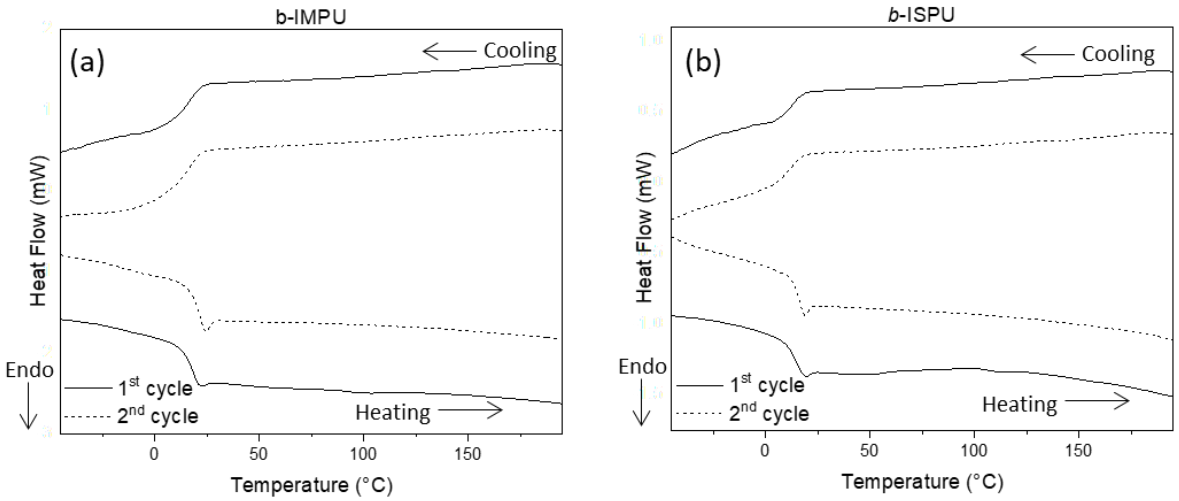

Figure 4.48 Differential scanning calorimetry thermograms of the first and second heating cycle of the homopolymers at a heating rate of 10 °C·min^{-1} (a) IMPU (b) ISPU

DSC thermograms of blends

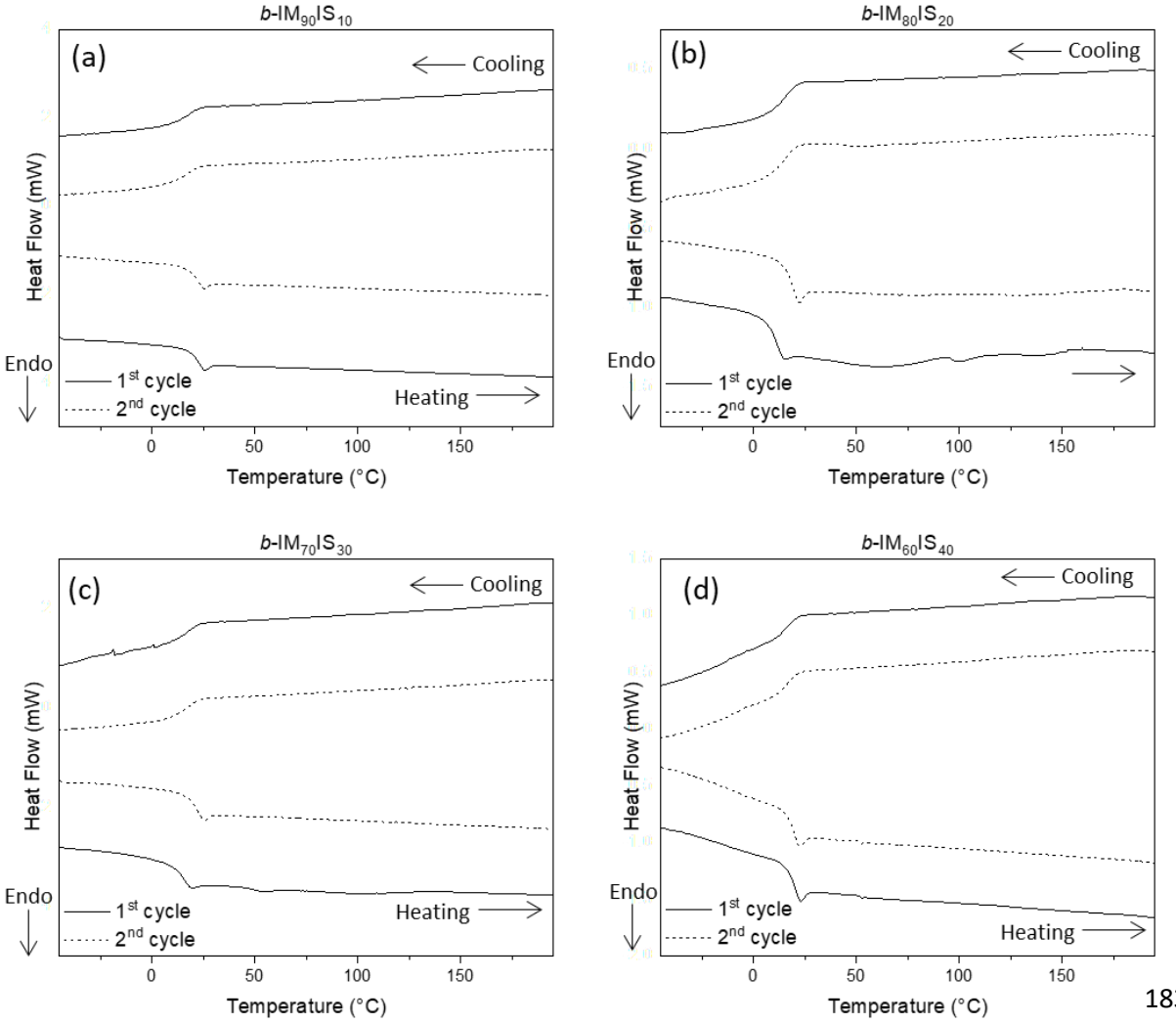

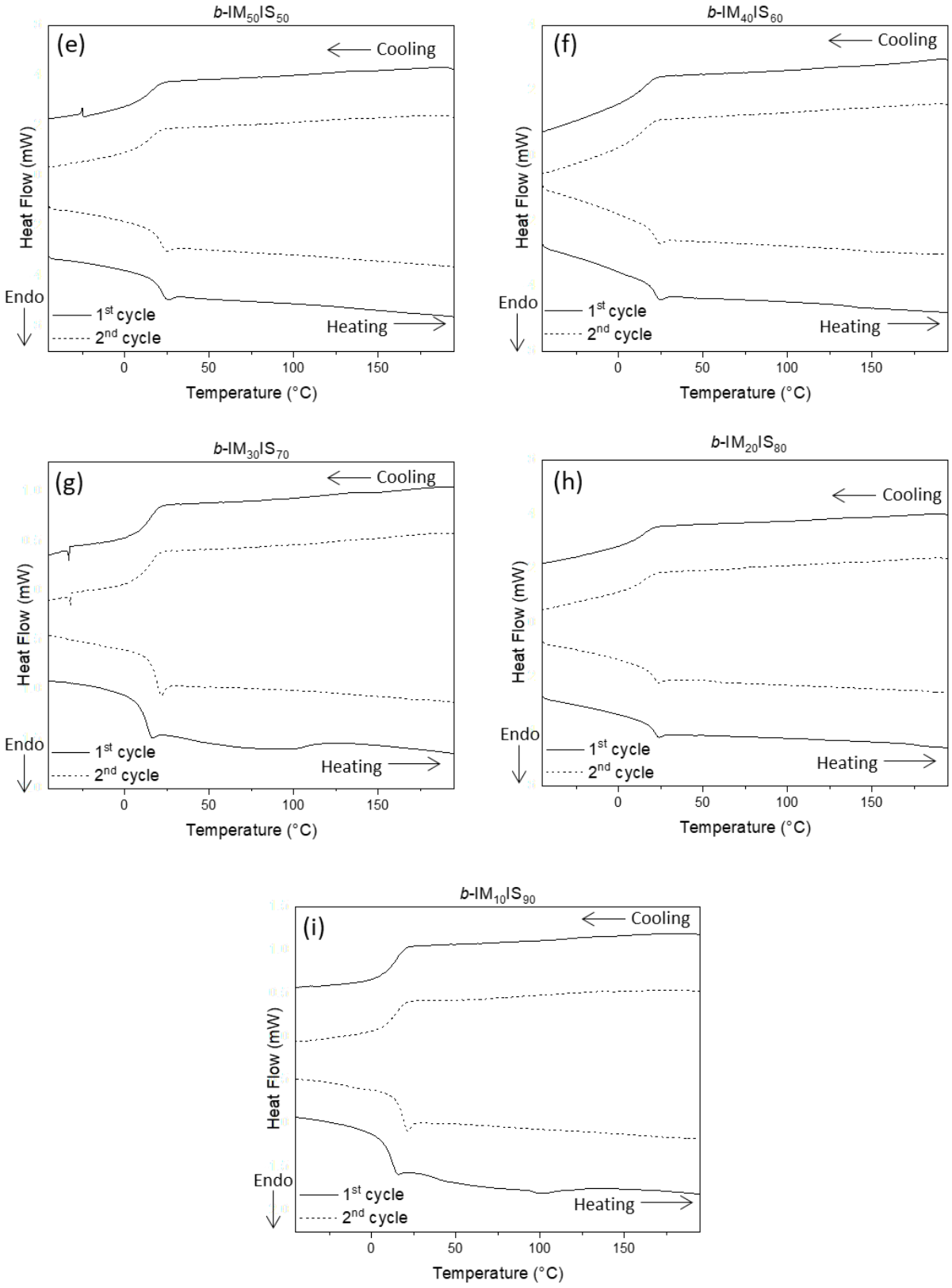

Figure 4.49 Differential scanning calorimetry thermograms of the first and second heating and cooling cycle of the blends at a heating rate of 10 °C·min^{-1} (a) b-IM$_{90}$IS$_{10}$ (b) b-IM$_{80}$IS$_{20}$ (c) b-IM$_{70}$IS$_{30}$ (d) b-IM$_{60}$IS$_{40}$ (e) b-IM$_{50}$IS$_{50}$ (f) b-IM$_{40}$IS$_{60}$ (g) b-IM$_{30}$IS$_{70}$ (h) b-IM$_{20}$IS$_{80}$ (i) b-IM$_{10}$IS$_{90}$

DSC thermograms of the co-polymers

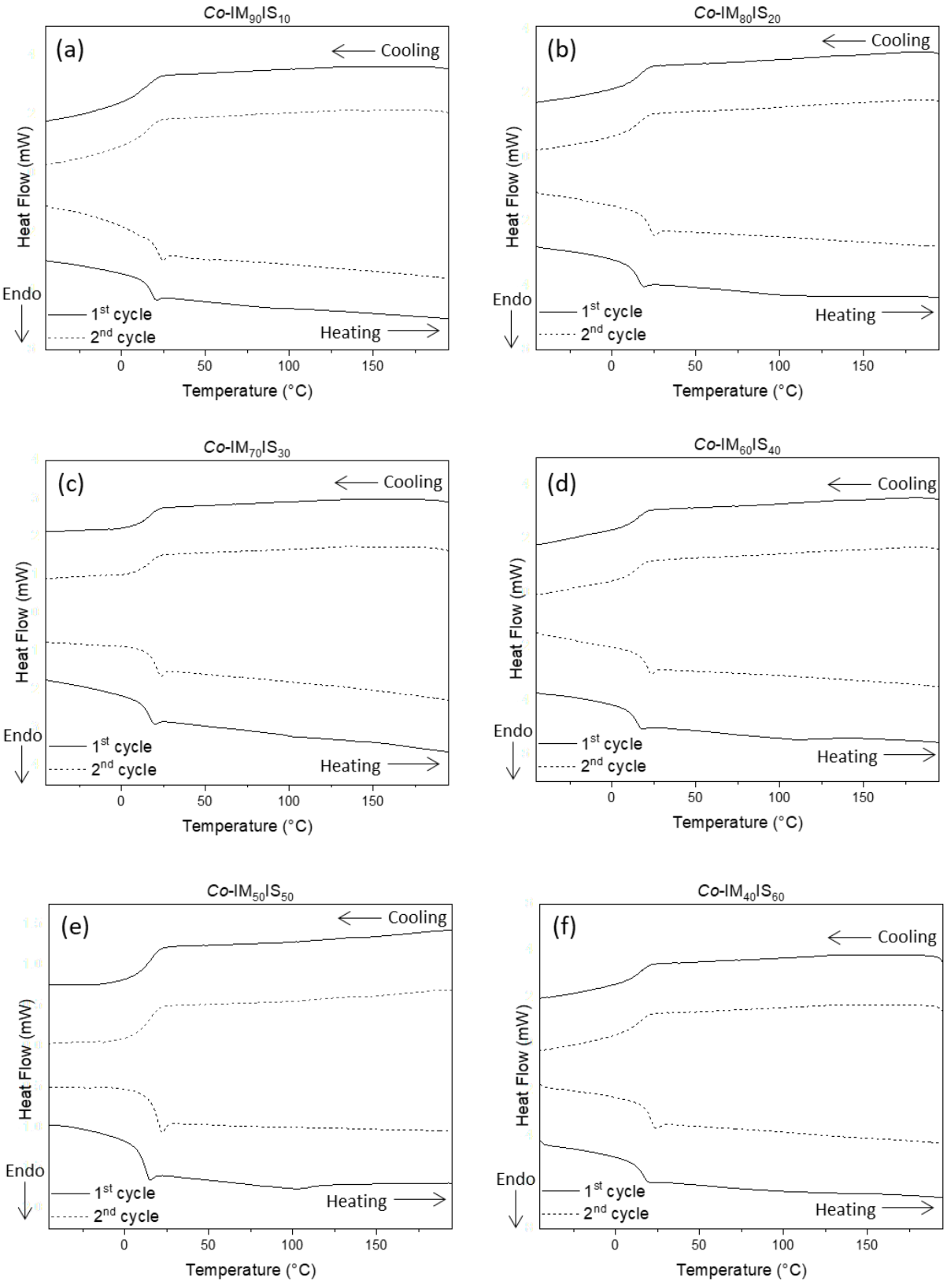

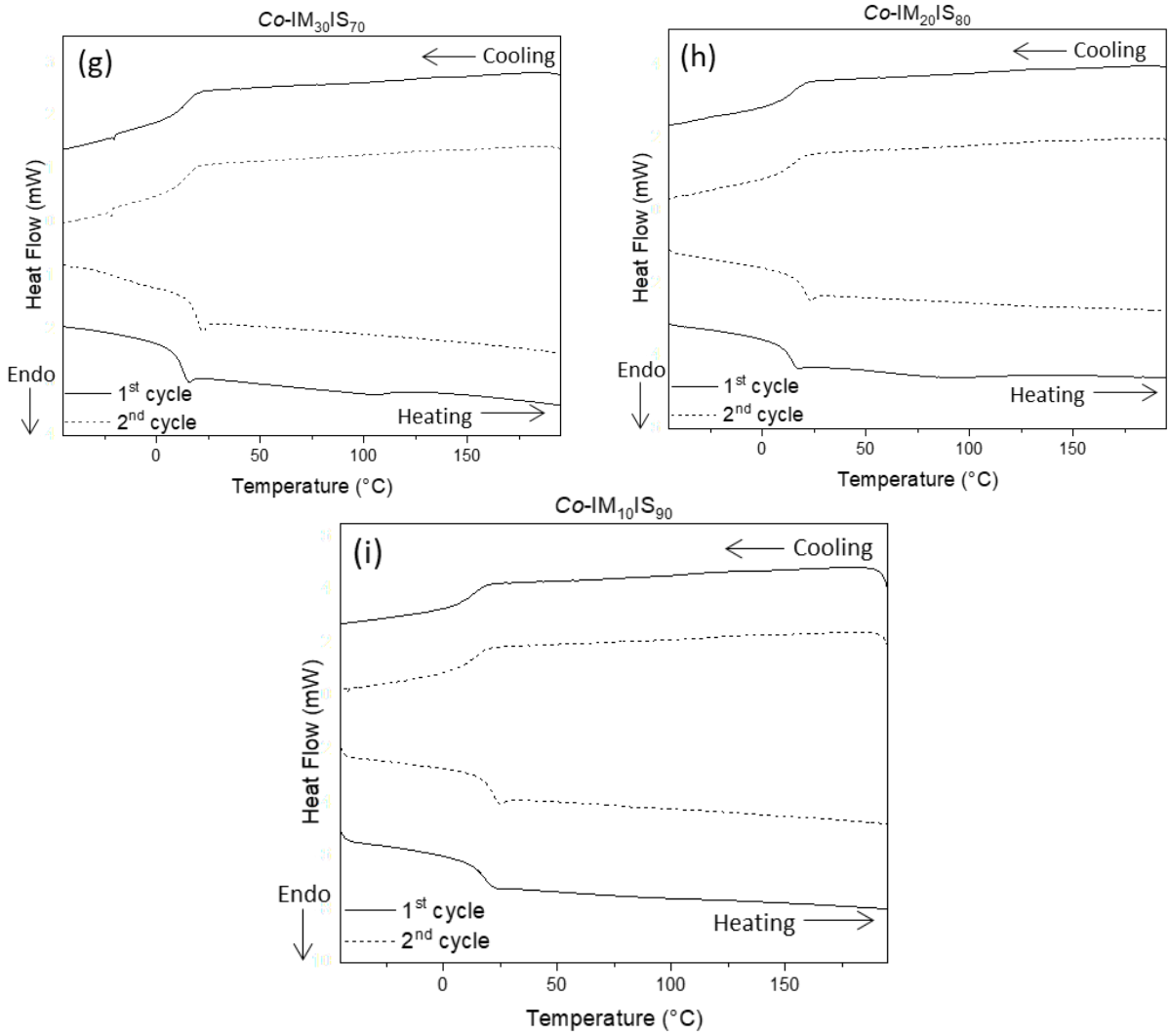

Figure 4.50 Differential scanning calorimetry thermograms of the first and second heating and cooling cycle of the co-polymers at a heating rate of 10 °C·min^{-1} (a) co-IM$_{90}$IS$_{10}$ (b) co-IM$_{80}$IS$_{20}$ (c) co-IM$_{70}$IS$_{30}$ (d) co-IM$_{60}$IS$_{40}$ (e) co-IM$_{50}$IS$_{50}$ (f) co-IM$_{40}$IS$_{60}$ (g) co-IM$_{30}$IS$_{70}$ (h) co-IM$_{20}$IS$_{80}$ (i) co-IM$_{10}$IS$_{90}$

GPC data for the blends

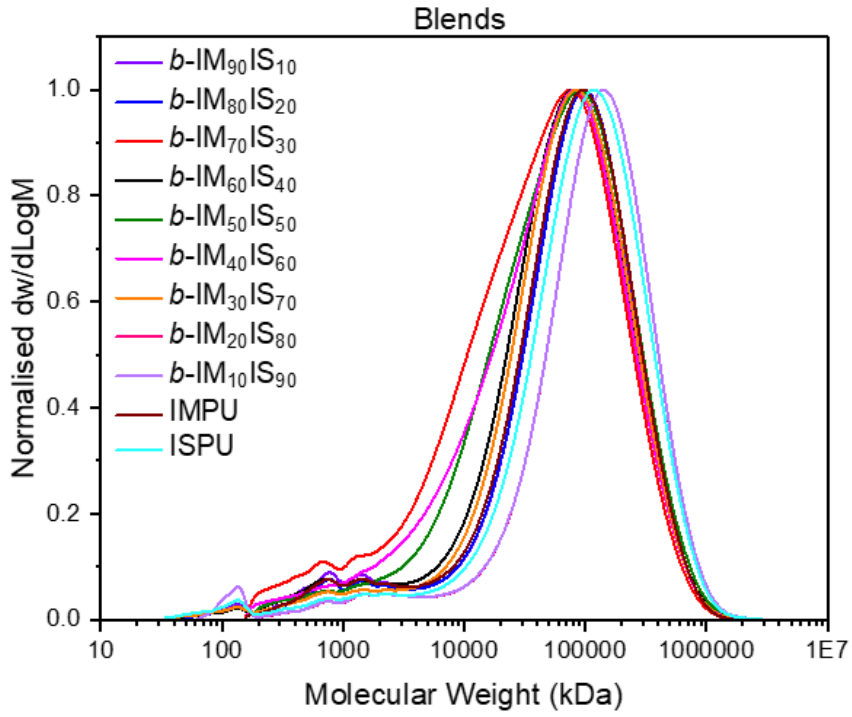

Figure 4.51 Normalised size exclusion chromatography of the homopolymers are their blends, ($CHCl_3$ + 0.5% NEt_3) analysed against poly(styrene) (PS) standards

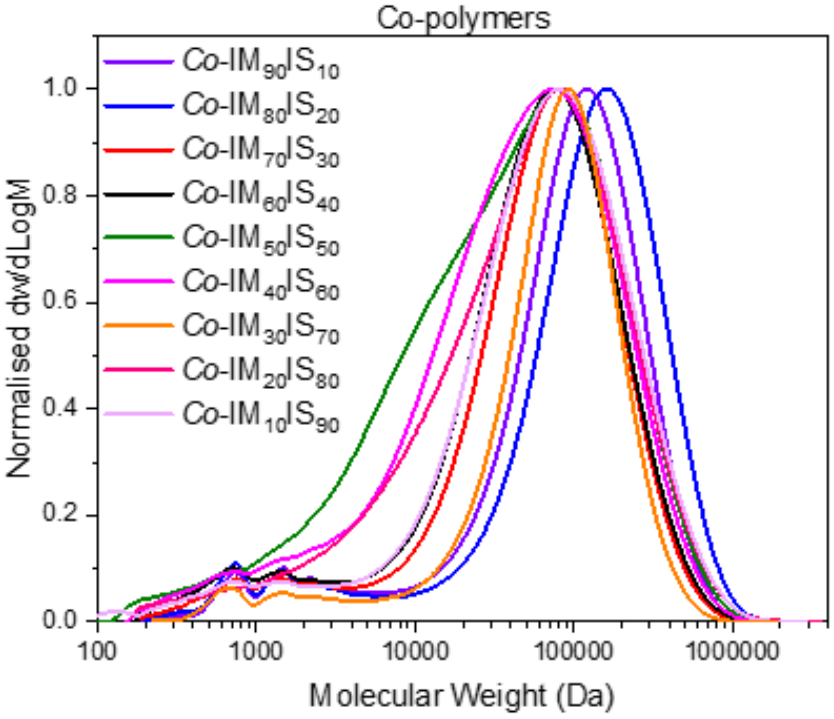

Figure 4.52 Normalised size exclusion chromatography of the co-polymers, ($CHCl_3$ + 0.5% NEt_3) analysed against poly(styrene) (PS) standards

Stress vs strain curves for homopolymers

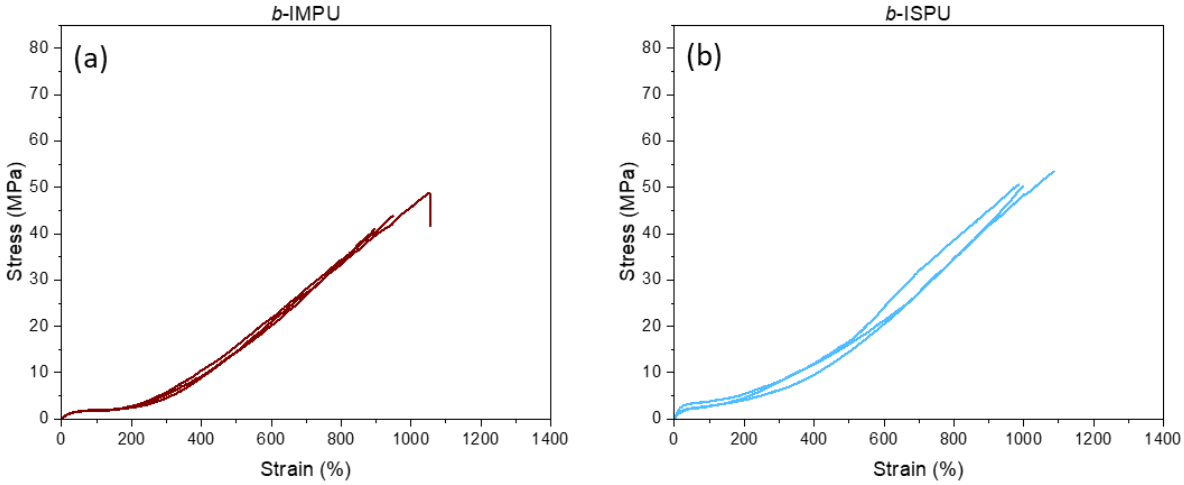

Figure 4.53 Stress vs strain curve of the homopolymers at a strain rate of 10 mm·min^{-1} (a) IMPU (b) ISPU

Stress vs strain curves of the blends

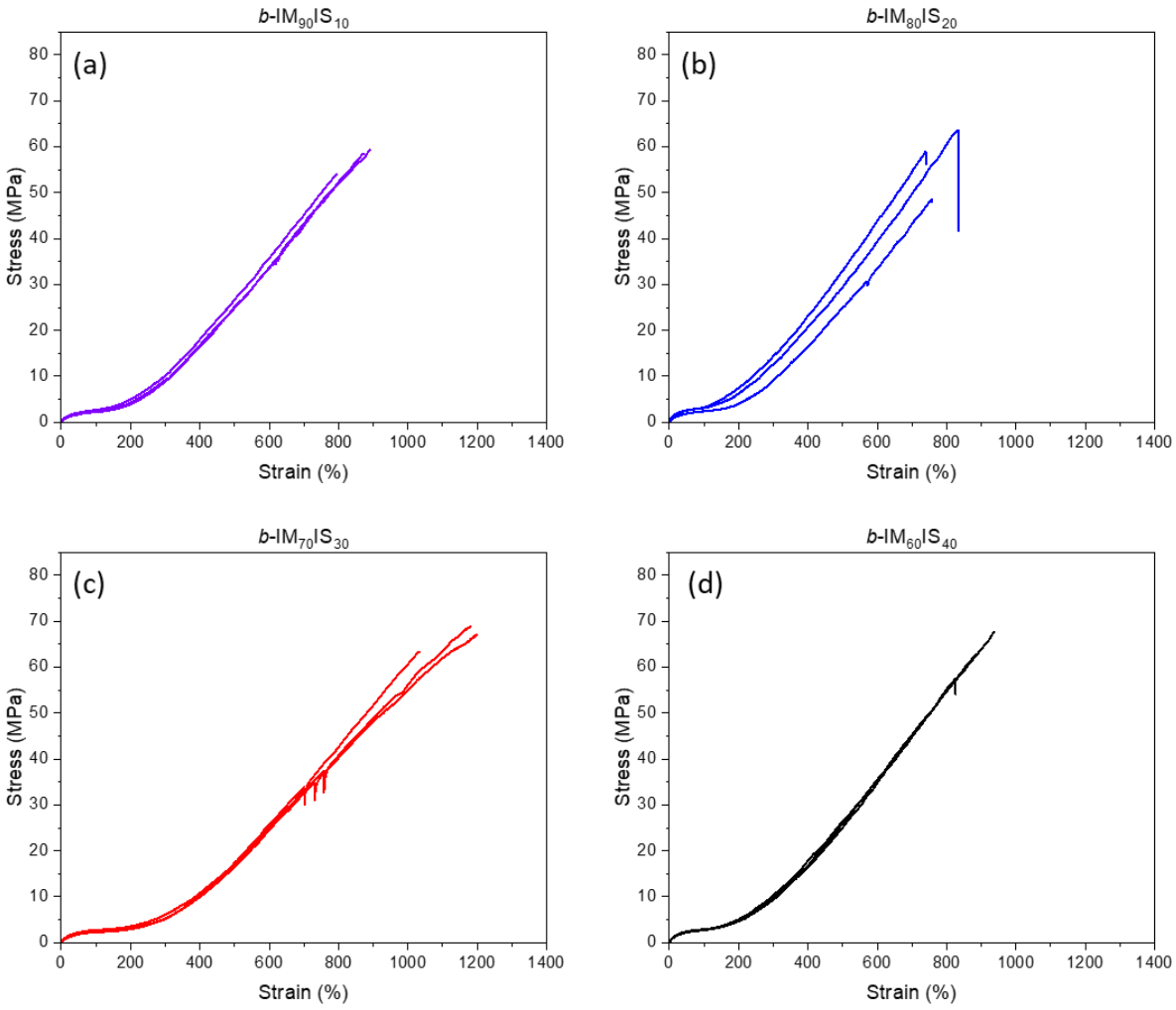

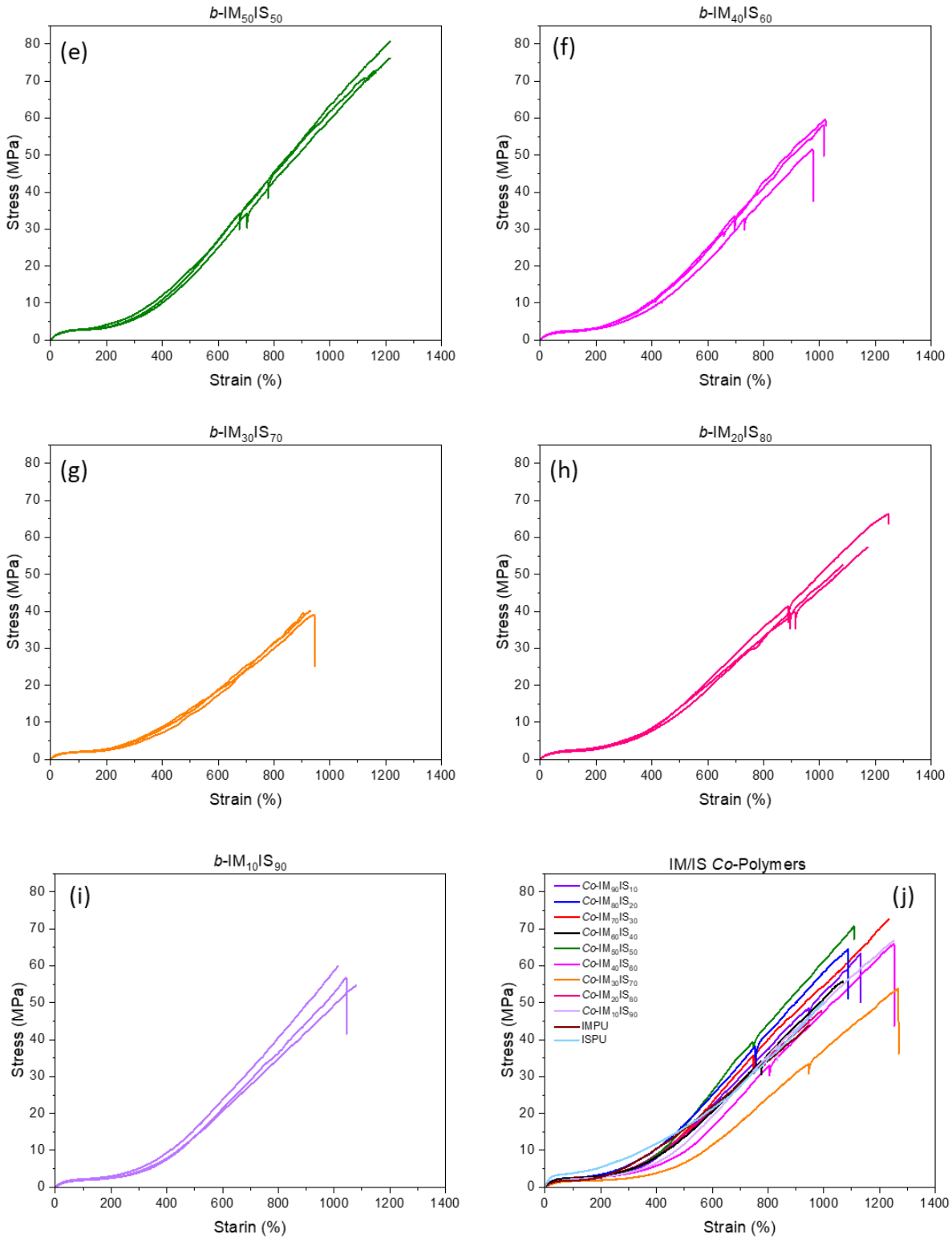

Figure 4.54 Stress vs strain curves of the blends at a strain rate of 10 mm·min^{-1} (a) b-$IM_{90}IS_{10}$ (b) b-$IM_{80}IS_{20}$ (c) b-$IM_{70}IS_{30}$ (d) b-$IM_{60}IS_{40}$ (e) b-$IM_{50}IS_{50}$ (f) b-$IM_{40}IS_{60}$ (g) b-$IM_{30}IS_{70}$ (h) b-$IM_{20}IS_{80}$ (i) b-$IM_{10}IS_{90}$ (j) All blends collated

Stress vs strain curves of the co-polymers

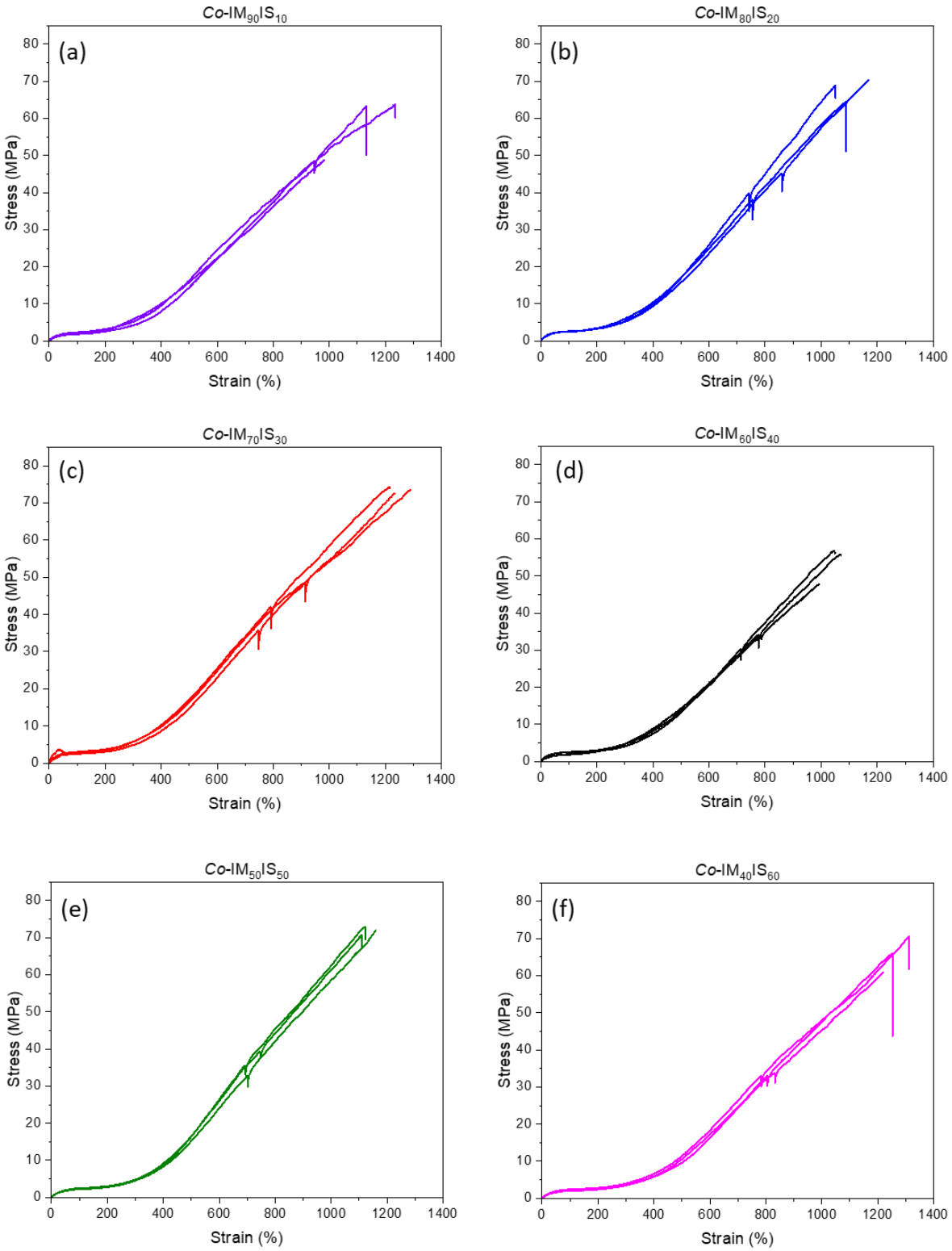

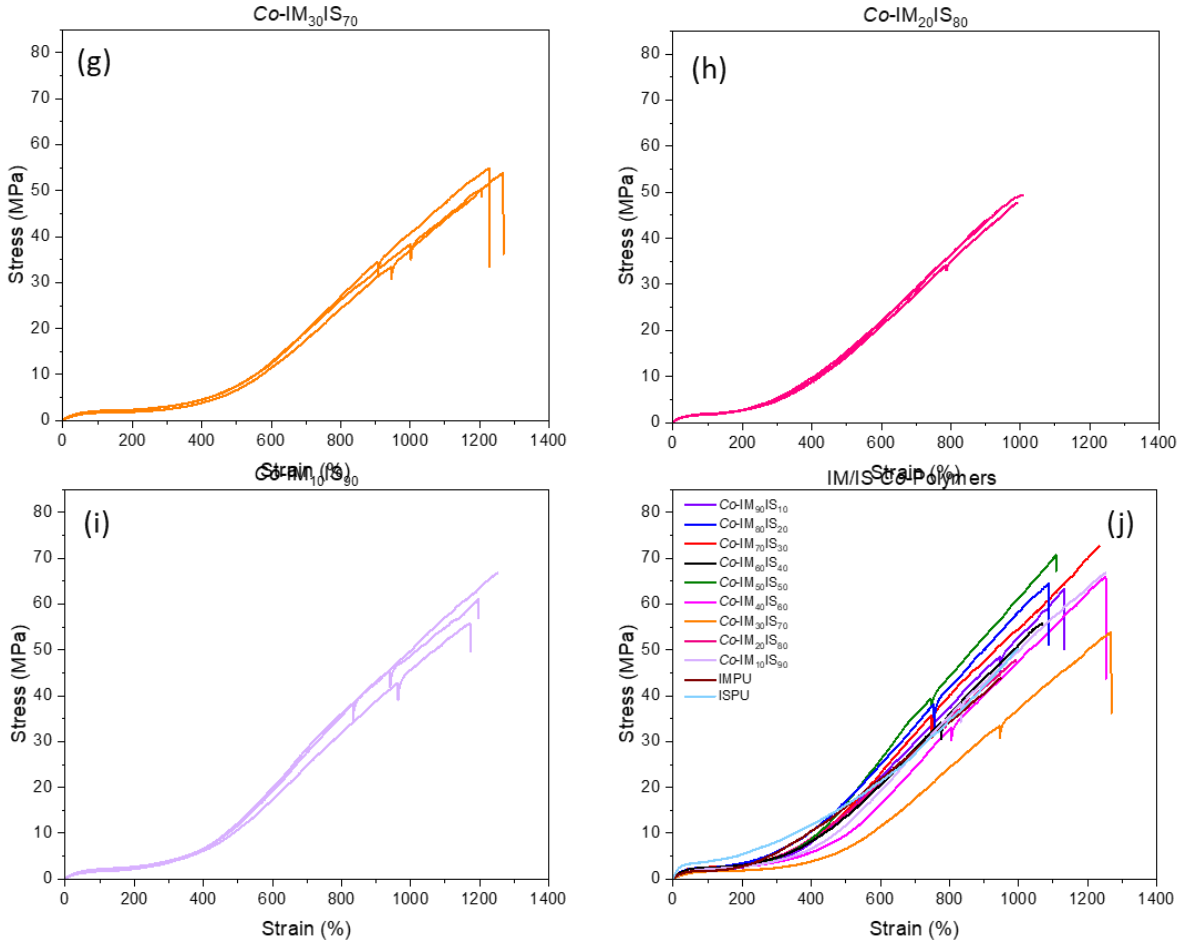

Figure 4.55 Stress vs strain curves of the co-polymers at a strain rate of 10 mm·min^{-1} (a) b-$IM_{90}IS_{10}$ (b) b-$IM_{80}IS_{20}$ (c) b-$IM_{70}IS_{30}$ (d) co-$IM_{60}IS_{40}$ (e) co-$IM_{50}IS_{50}$ (f) co-$IM_{40}IS_{60}$ (g) co-$IM_{30}IS_{70}$ (h) co-$IM_{20}IS_{80}$ (i) co-$IM_{10}IS_{90}$ (j) All co-polymers collated

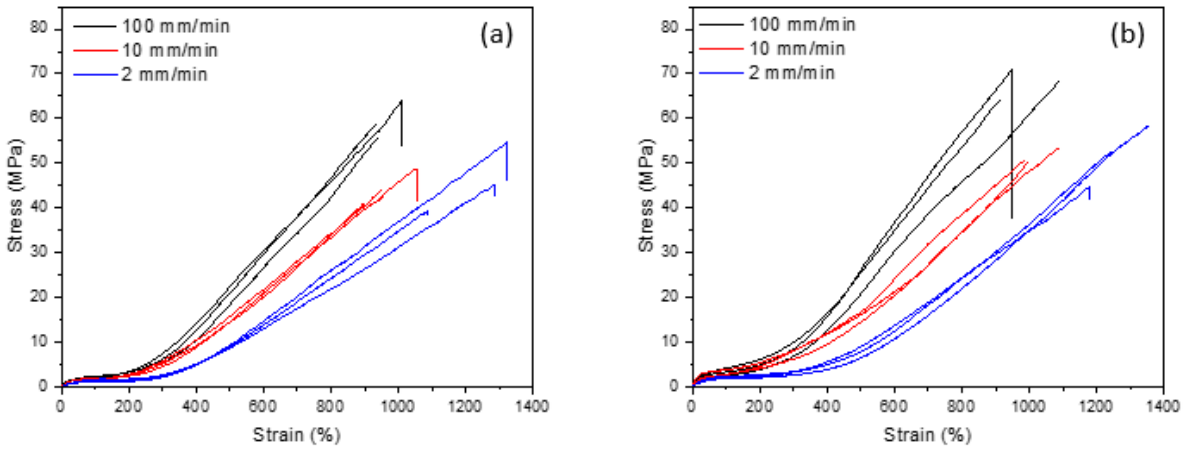

Figure 4.56 Stress vs strain curve of the homopolymers at a strain rate of 2 mm·min^{-1}, 10 mm·min^{-1} and 100 mm·min^{-1} (a) IMPU (b) ISPU

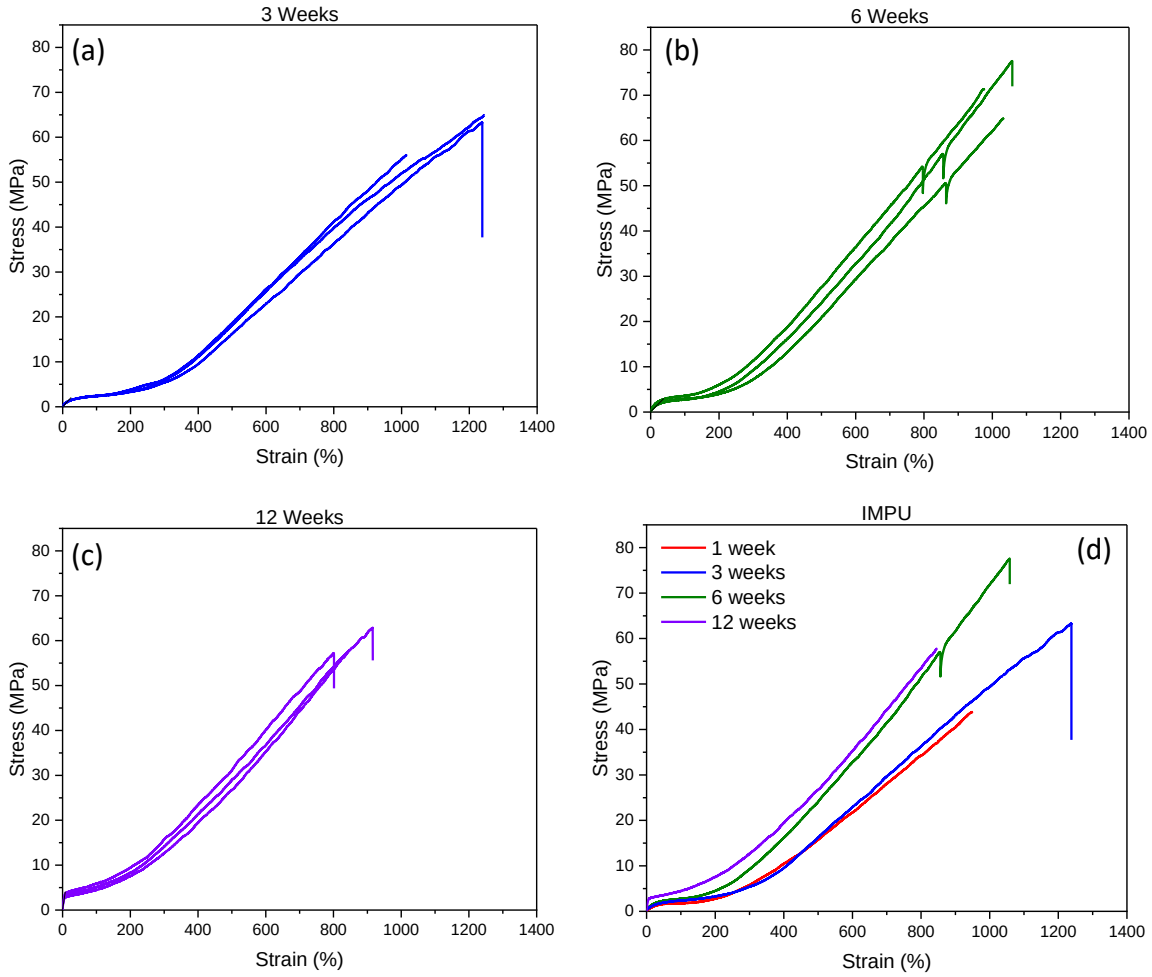

Figure 4.57 Stress vs strain curve of IMPU with a 22°C ageing time of (a) 3 weeks (b) 6 weeks (c) 12 weeks. (d) All aged samples collated

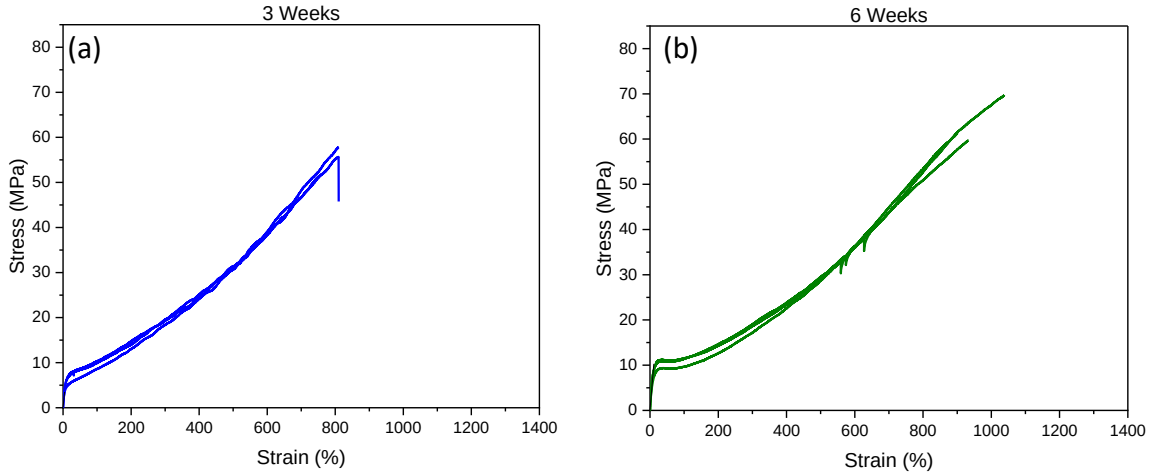

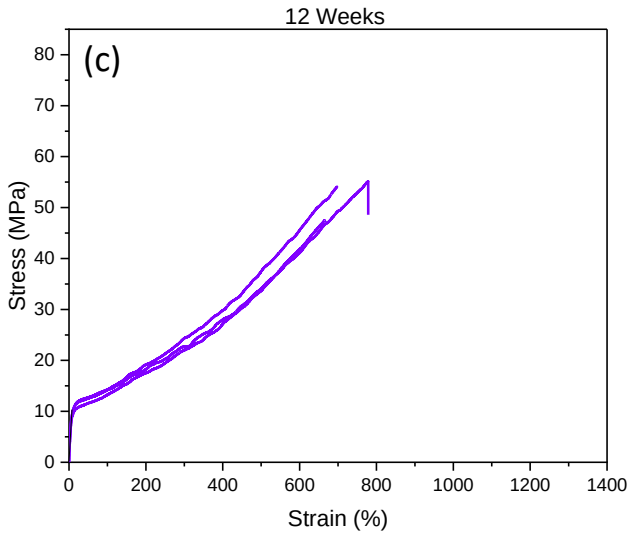

Figure 4.58 Stress vs strain curve of ISPU with a 22°C ageing time of (a) 3 weeks (b) 6 weeks (c) 12 weeks

Table 4.1 Summary data table of the homopolymers at a strain rate of 2, 10 and 100 mm·min^{-1}

	Strain rate (mm·min^{-1})	***E*^{a} (MPa)**	**U_T^{b} (MJ·m^3)**	**ε^{c} (%)**	**σ_b^{d} (MPa)**
IMPU	2	4.5 ± 0.6	222.07 ± 50.45	1285 ± 104	45.2 ± 6.4
	10	3.8 ± 0.21	165.65 ± 28.44	966 ± 65	45.0 ± 3.0
	100	5.7 ± 0.9	207.94 ± 27.90	940 ± 34	58.8 ± 3.4
ISPU	2	4.5 ± 0.6	198.51 ± 90.13	1245 ± 71	52.6 ± 5.5
	10	6.1 ± 0.33	208.95 ± 14.79	1024 ± 45	51.0 ± 1.0
	100	7.7 ± 1.8	266.98 ± 27.13	949 ± 76	68.4 ± 2.8

(a) Young's modulus (b) Tensile toughness (c) Strain at break (d) Stress at break. All uncertainties are presented as the standard deviation of n = 3 samples.

Table 4.2 Summary data table of the aged homopolymers after 1, 3, 6 and 12 weeks at 25 °C

	Age (Weeks)	E^a (MPa)	U_T^b (MJ·m³)	ε^c (%)	σ_b^d (MPa)	σ_y^e (MPa)
IMPU	1	3.80 ± 0.2	165.65 ± 28.44	966 ± 65	44.4 ± 3.3	-
	3	6.2 ± 0.1	328.13 ± 54.54	1239 ± 107	63.2 ± 3.9	-
	6	6.8 ± 1.9	287.02 ± 23.72	1033 ± 32	71.4 ± 5.1	-
	12	38.8 ± 4.0	204.98 ± 24.51	846 ± 47	57.8 ± 2.5	-
ISPU	1	6.1 ± 0.3	208.95 ± 14.79	1024 ± 45	51.4 ± 1.4	-
	3	65.9 ± 1.6	214.64 ± 9.98	813 ± 17	55.4 ± 2.0	-
	6	91.9 ± 12.9	281.15 ± 37.08	937 ± 58	61.3 ± 4.3	10.9 ± 0.3
	12	109.5 ± 0.3	200.81 ± 24.70	698 ± 47	54.1 ± 3.3	11.7 ± 0.5

(a) Young's modulus (b) Tensile toughness (c) Strain at break (d) Stress at break (e) Stress at yield. All uncertainties are presented as the standard deviation of n = 3 samples.

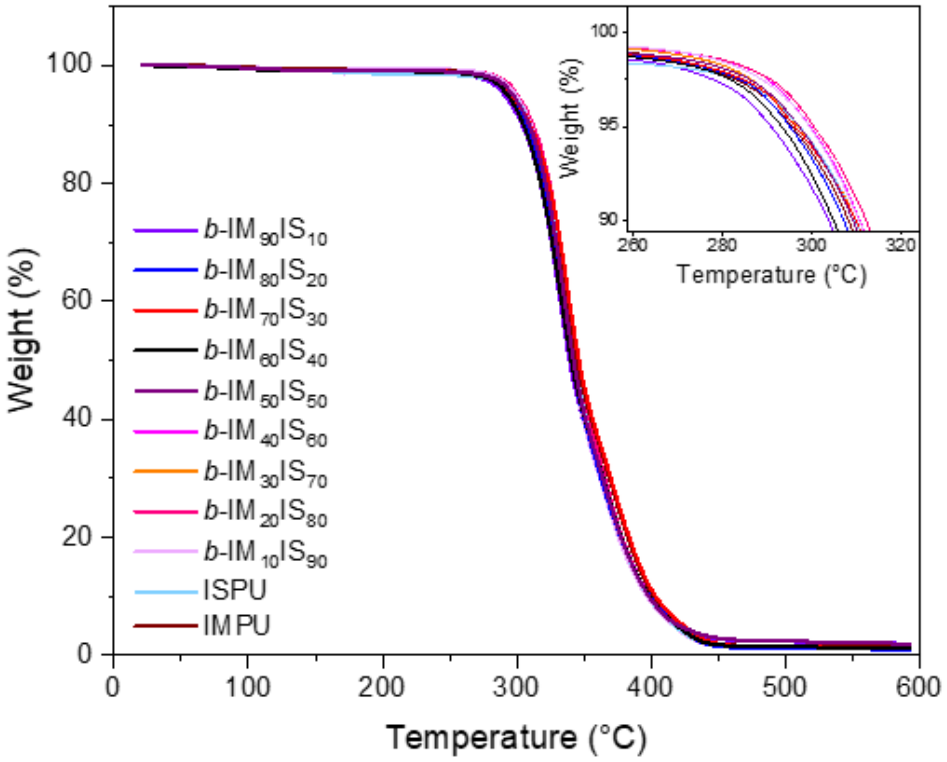

Figure 4.59 Thermogravimetric analysis of the homopolymers and blends from 0 - 600 °C at a heating rate of 10 °C·min^{-1}

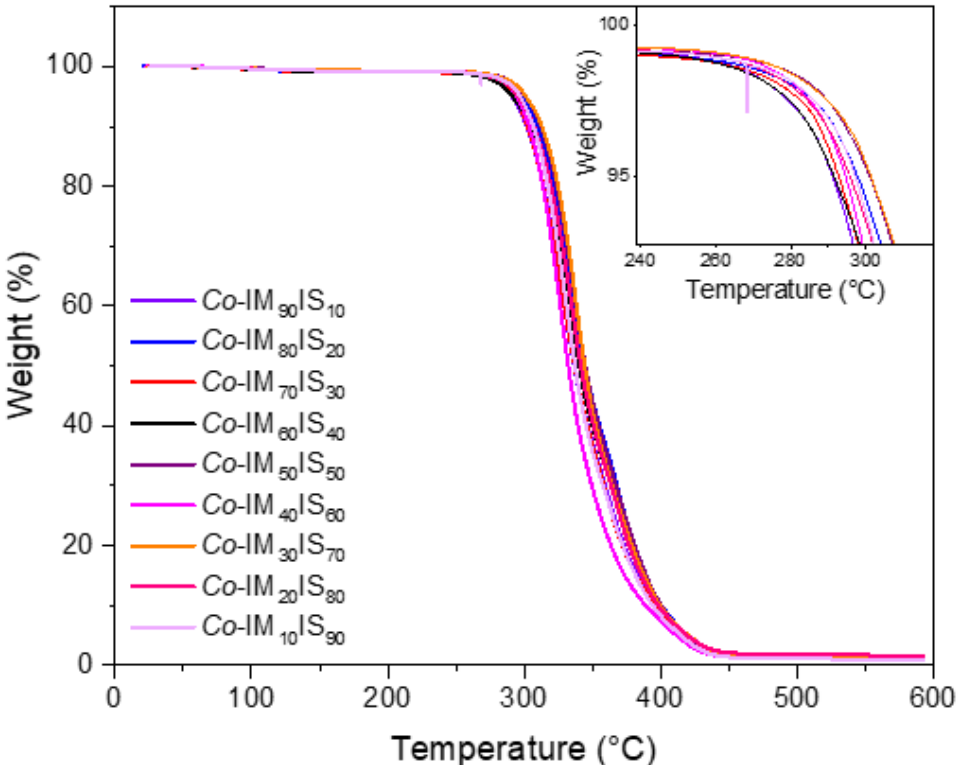

Figure 4.60 Thermogravimetric analysis of the co-polymers from 0 - 600 °C at a heating rate of 10 °C·min^{-1}

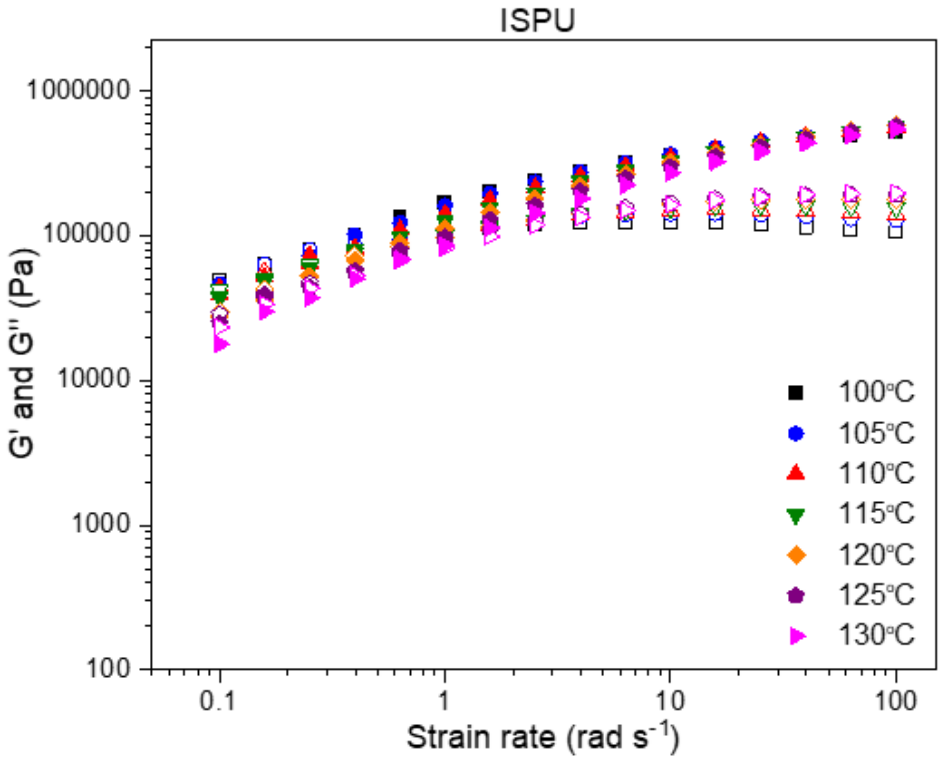

Figure 4.61 ISPU storage and loss modulus plot of a frequency sweep between 100 °C and 130 °C. Storage modulus (G') block colours, loss modulus (G'') hollow colours

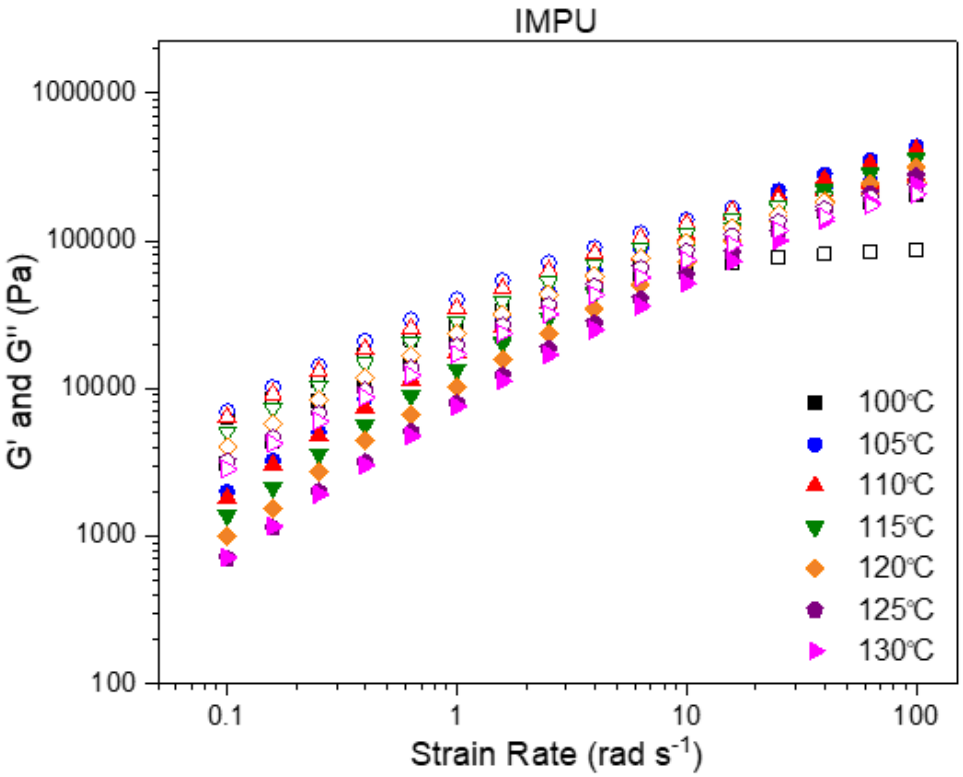

Figure 4.62 IMPU storage and loss modulus plot of a frequency sweep between 100 °C and 130 °C. Storage modulus (G') block colours, loss modulus (G'') hollow colours

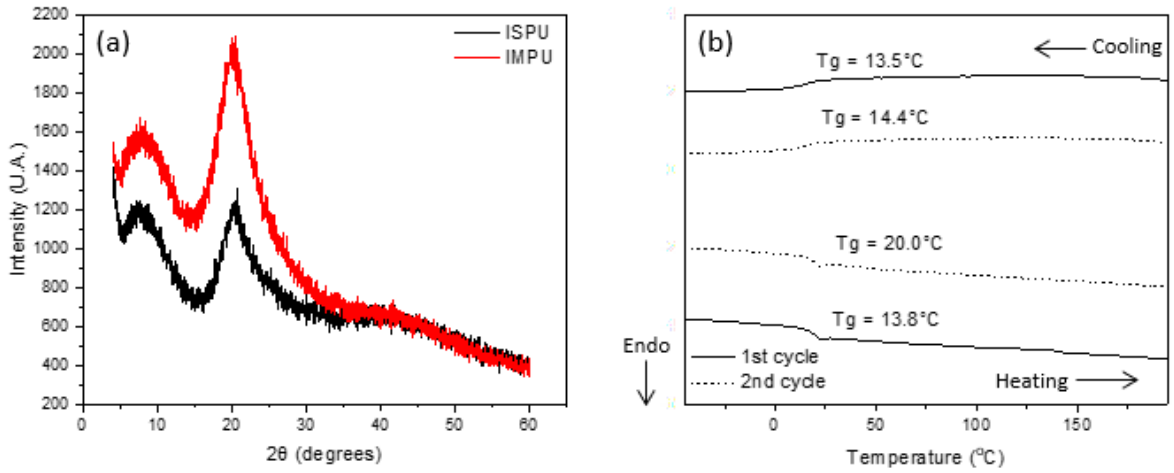

Figure 4.63 (a) WAX intensity profiles of IMPU and ISPU samples after 6 weeks of ageing. (b) Differential scanning calorimetry of the first and second heating cycle of 6-week aged ISPU at a heating rate of 10 °C·min^{-1}

Table 4.3 Summary data table of the homopolymers and their blends

	Molecular Weight Mw (kDa)	**Đ$_M$**	***E*^{a} (MPa)**	***U*$_T^b$ (MJ·m^3)**	**ε^c (%)**	**σ_b^d (MPa)**	**T$_g^e$ (°C)**	**T$_d^f$ (°C)**	**Degradation rate in 1M NaOH (Days)**
b-IM$_{90}$IS$_{10}$	126	23	3.62 ± 0.43	192.67 ± 17.90	853 ± 42	57.2 ± 2.3	17	282	42
b-IM$_{80}$IS$_{20}$	127	21	5.93 ± 1.04	175.11 ± 30.03	773 ± 44	57.0 ± 6.3	13	287	63
b-IM$_{70}$IS$_{30}$	89	14	4.37 ± 0.28	301.84 ± 41.50	1138 ± 74	66.4 ± 2.3	22	287	77
b-IM$_{60}$IS$_{40}$	115	20	6.24 ± 0.45	220.48 ± 27.58	888 ± 46	63.0 ± 4.2	20	281	91
b-IM$_{50}$IS$_{50}$	114	11	5.41 ± 0.16	369.61 ± 16.88	1199 ± 25	76.4 ± 3.4	22	288	98
b-IM$_{40}$IS$_{60}$	104	13	4.76 ± 0.14	214.03 ± 21.48	1005 ± 19	56.3 ± 3.6	22	286	98
b-IM$_{30}$IS$_{70}$	120	20	4.62 ± 0.48	133.36 ± 7.59	926 ± 16	39.5 ± 0.5	19	283	84
b-IM$_{20}$IS$_{80}$	180	10	5.35 ± 0.33	268.58 ± 48.40	1168 ± 67	58.7 ± 5.7	22	288	77
b-IM$_{10}$IS$_{90}$	178	30	4.92 ± 0.35	216.52 ± 4.00	1045 ± 27	57.1 ± 2.1	19	286	98
IMPU	125	12	3.80 ± 0.21	165.65 ± 28.44	966 ± 65	44.5 ± 3.3	22	286	91
ISPU	158	31	6.09 ± 0.33	208.95 ± 14.79	1024 ± 45	51.4 ± 1.4	16	287	112

(a) Young's modulus (b) Tensile toughness (c) Strain at break (d) Stress at break (e) Glass transition temperature taken from the second heating cycle (f) Decomposition temperature. All uncertainties are presented as the standard deviation of n = 3 samples.

Table 4.4 Summary data table of the homopolymers and their copolymers

	Molecular Weight Mw (kDa)	**$Đ_M$**	***E*[a] (MPa)**	**U_T[b] (MJ·m^3)**	**ε[c] (%)**	**σ_b[d] (MPa)**	**T_g[e] (°C)**	**T_d[f] (°C)**	**Degradation rate in 1M NaOH (Days)**
Co-$IM_{90}IS_{10}$	136	11.3	4.60 ± 0.60	268.32 ± 63.34	1132 ± 104	63.3 ± 7.0	23	282	42
Co-$IM_{80}IS_{20}$	179	16.8	5.15 ± 0.05	272.49 ± 23.38	1088 ± 50	69.9 ± 2.5	23	288	42
Co-$IM_{70}IS_{30}$	98	10.3	5.35 ± 1.24	366.01 ± 19.53	1234 ± 31	73.5 ± 0.7	21	285	35
Co-$IM_{60}IS_{40}$	97	12.3	4.12 ± 0.70	217.32 ± 19.93	1045 ± 32	56.0 ± 4.0	21	281	42
Co-$IM_{50}IS_{50}$	87	14.2	3.99 ± 0.17	311.16 ± 8.42	1122 ± 21	71.9 ± 0.9	20	289	52
Co-$IM_{40}IS_{60}$	88	12.1	4.44 ± 0.37	304.62 ± 32.69	1252 ± 39	66.0 ± 4.0	21	285	35
Co-$IM_{30}IS_{70}$	104	7.8	3.34 ± 0.45	241.13 ± 10.46	1229 ± 26	53.9 ± 2.0	20	291	84
Co-$IM_{20}IS_{80}$	104	12.6	3.49 ± 0.07	178.43 ± 11.12	992 ± 25	47.7 ± 1.0	21	286	70
Co-$IM_{10}IS_{90}$	115	19.1	3.62 ± 0.42	285.40 ± 31.14	1197 ± 33	61.0 ± 4.5	22	289	84
IMPU	125	12	3.80 ± 0.21	165.65 ± 28.44	966 ± 65	44.5 ± 3.3	22	286	91
ISPU	158	31	6.09 ± 0.33	208.95 ± 14.79	1024 ± 45	51.4 ± 1.4	16	287	112

(a) Young's modulus (b) Tensile toughness (c) Strain at break (d) Stress at break (e) Glass transition temperature taken from the second heating cycle (f) Decomposition temperature. All uncertainties are presented as the standard deviation of n = 3 samples.

Chapter 5

Conclusion

5.1 Conclusion and future work

The first section of this thesis aimed to develop a simple solvent-free and low-temperature polyolefin depolymerisation procedure targeting the incorporation of oxygenated functional groups. For this purpose, chapter 2 investigated the synthesis of dual solvent-catalyst DES accommodating known oxidative metals for the aerobic oxidation of model polyolefin squalane and LDPE. The synergy between the HBD:HBA of the DES was probed to establish their thermal stability and catalytic efficiencies, allowing for the fine-tuning of activity. Acetamide and octadecanamide-based DES posed an overestimation of their real-life thermal stability and thus their subsequent inappropriateness for long-duration experiments while choline chloride-based DES proved sufficiently stable. $[ChCl]_2[CoCl_2{\cdot}6H_2O]_3$ and $[ChCl]_2[MnCl_2{\cdot}4H_2O]$ DES were found to be the most effective at oxidising squalane with 37% and 32% squalane conversion after 14 days respectively, however, owing to the heterogeneous reaction of the DES and LDPE a phase transfer catalyst was necessary to facilitate the oxidation of LDPE. $[ChCl]_2[CoCl_2{\cdot}6H_2O]_3$ revealed a dependence on polymer topology, selectively depolymerisation LDPE M_n = 1,500 Da after 112 days and post-consumer LDPE to M_n = 3,000 Da after 100 days while under equivalent conditions HDPE remained unchanged. On the other hand, $[ChCl]_2[MnCl_2{\cdot}4H_2O]$ showed a greater proclivity for HDPE depolymerisation with 83% of its original M_n lost after 100 days. At the moment, there is no known method for the selective removal/depolymerisation of LDPE from mixed polyolefin waste, thus this chapter provides a potential starting point to bridge that technological gap while also providing alternative strategies towards unselective polyolefin depolymerisation.

As a continuation of Chapter 2, Chapter 3 investigated the accelerated DES-catalysed depolymerisation of LDPE and HDPE following two approaches. Firstly, using organic peroxides as radical initiators. Increased radical density accelerated the molecular weight loss

of both polyolefin topologies while also allowing the operating temperature to be lowered. Exploring potential peroxides found that low polarity alkyl substituents on the radical species made for better compatibility with the non-polar polyolefin. The recoverability of the DES revealed little change in its catalytic activity after two depolymerisation cycles, thus the DES has application in consecutive catalytic cycles.

Secondly, reactions were performed under oxygen in place of air to maximise the presence of potential reactive oxygen species and lower the activation energy for hydrogen abstraction. Moreover, the rate of depolymerisation of LDPE and HDPE was accelerated with evidence of increased chain scission events and loss of VOCs. Oxygen reactions exposed less of a dependence on the polymer crystallinity, creating a more uniform degradation of crystalline and amorphous regions. The influence of contaminants within post-consumer LDPE revealed that dyes cause divergent carbonyl index profiles, signifying varying levels of oxidation, nevertheless, clear post-consumer LDPE successfully depolymerised. The up-cycling of the oxidised LDPE and HDPE into stronger adhesives revealed a greater shear strength than their unmodified counterparts, although more work is required to target specific functional group content and therefore potential adhesive strength. Future studies involved in the project would require the identification of the VOC released to better understand the reaction mechanism as well as a larger scope into potential HBD, HBA, and peroxides. Overall, these two chapters provide a starting point for the solvent-free and low-temperature polyolefin depolymerisation, with the DES not only providing a dual solvent-catalyst system, elevating the need for traditional organic solvents but also their easily tuneable composition allowing access to an array of potential chemistries.

The second focus of this thesis, in Chapter 4, aimed to explore the influence of stereoisomerism on the mechanical performance and degradation kinetics of high-performance alternating strong thermoplastics based on renewability-sourced isohexides. Thiol-ene “click” polymerisation

formed isomannide and isosorbide polyurethane elastomers whose chemical similarity enabled co-polymerisation and physical blending. Ageing of ISPU revealed “plastic”-like characteristics while remaining amorphous, such behaviour is usually only accessible via the more challenging to synthesise semi-crystalline IIPU. Comparable mechanical properties were observed between the co-polymers, blends and homopolymers, however, divergent hydrolytic degradation profiles revealed that the rate of degradation can be decoupled from their mechanical properties. Although further investigation is required into the reasoning behind the divergent degradation profiles this work provides a starting point for the fine manipulation of polymer properties based on stereoisomerism.

The future progression for the polyolefin depolymerisation project would be to perform ultraviolet-visible spectroscopy (UV-Vis) on the DES before, during, and after the reaction. Cobalt and manganese chloride salts have distinctive colours depending on the oxidation state of the metal; therefore, it may be possible to determine changes in the oxidation state of the metal and thus identify the catalytically active species. Headspace gas chromatography-mass spectroscopy (GC/MS) will be a beneficial technique to run on the depolymerisations as the loss of VOCs is evident, however, with the current practices the VOCs are unable to be collected and thus identified. Identifying the VOCs may lead to a better understanding of the mechanism.

Future work on the sugar-based polyurethane project will involve investigating the divergent hydrolytic degradation rates. This investigation will be aided by techniques such as molecular dynamics to identify inconsistencies in the polymer morphology, GPC to corroborate the differing degradation rates, and NMR spectroscopy to gain a better understanding of the potential degradation products.